CHEMISTRY

DESIGNER NANOPARTICLES TO DETECT AND TREAT DISEASE

Lynn Samuelson

Dissertation under the direction of Professor Darryl J. Bornhop

Conjugation of targeting, imaging and drug molecules to nanoparticles has been a developing area of interest over the last 10-15 years. Although great strides have been made, characterization and activity of functionalized nanoparticles is still incomplete. More work needs to be done to allow generalized predictions to be made about the impact of size, amount loading and the best synthetic approaches to utilize nanoparticles to their fullest potential.

Imaging agents such as fluorophors and chelated metals have been attached to the surface of dendrimers and studied as profusion or targeted imaging agents. One important target, the translocator protein (TSPO, formerly named peripheral benzodiazepine or PBR), has not been targeted with a nanoparticle. The translocator protein is a mitochondrial membrane protein that spans the lipid bi-layer and mediates cholesterol transport across the mitochondrial membrane. Two cell lines that have high expression of TSPO are MDA-MB-231 human breast cancer and C6 rat glioma cell. The first portion of this dissertation describes the

synthesis, characterization and imaging capabilities of a TSPO targeted dendrimer with fluorescence, MRI and EM capabilities.

Matrix metalloproteinases (MMPs) are another target for substantiating the role of nanoparticles in biology. MMPs are a class of zinc dependant enzymes that have been found to degrade the extra cellular matrix. Several MMPs have been discovered and studied, but MMPs 2, 7 and 9 are most interesting for their high expression associated with the proliferation in certain types of tumor cells[1-2]. Although pharmacological inhibitors have been unsuccessful in treating MMP associated cancers, other approaches utilizing the enzymes have been successful. For example, small peptide sequences that are selectively cleaved by a specific MMP(s) have been developed and used in molecularly activated fluorescence probes and prodrug. The second portion of this dissertation describes the incorporation of dendrons to develop MMP-9 activated delivery of doxorubicin or paclitaxel to cancer cells.

DESIGNER NANOPARTICLES TO DETECT AND TREAT DISEASE

By

Lynn Samuelson

Dissertation

Submitted to the Faculty of the

Graduate School of Vanderbilt University

in partial fulfillment of the requirements

for the degree of

DOCTOR OF PHILOSOPHY

in

Chemistry

December, 2009

Nashville, Tennessee

Approved by:

Darryl J. Bornhop

Lynn Matrisian

Brian O. Bachmann

Gary Sulikowski

To my Grandma, Verda Louise Samuelson,

The first woman in my family to get a degree in science

ACKNOWLEDGEMENTS

Through the course of my graduate career I have several people to thank. First and foremost I need to thank my advisor, Dr. Darryl Bornhop, without your support and encouragement I would never have gone back to graduate school. My committee members, Dr. Lynn Matrisian, Dr. Brian Bachmann and Dr. Gary Sulikowski, have also played an integral role in my education through their direction and teaching and for that, many thanks. Dr. Oliver McIntrye, although not officially on my committee has been an invaluable resource in directing and teaching me. I look forward to working with you in the future.

The million things that colleagues do for each other did not go unnoticed in the last five years. With that I am very grateful to have worked with such wonderful people. To that I am thankful for all the members of the Bornhop laboratory that I have had the pleasure of working with. In particular I would like to thank, Dr. Mingfeng Bai, Dr. Bernard Anderson, Madeline Dukes whom have all contributed to the research projects presented here in some form. The remainder of the Bornhop laboratory members present during my time here have been a pleasure to work with as well. Amanda, Carly, Ereny, Travis, Charles, Shelby, and Stephen thank you for everything you have done. Last, but not least, I have worked with some very talented undergraduates: Kristin Cederquist, Sarah Smith, Sara Haviland, Jordan were all a pleasure to

have in the laboratory. Jonathan Casey and Colette Hunt (whom worked with me personally) are two very talented undergaduates whom working with was a pleasure. I wish all the past and present laboratory members the best of luck in the future.

Randy Scherer, a student in Dr. Matrisian's laboratory, has been a fabulous collaborator and great colleague to work with. Thank you for all your help, in particular over the last few months when the favors have not always been returned. Thank you to all the other members of the Matrisian laboratory who have provided knowledge and support throughout my time here. In particular thank you to Ian McFadden, for help with some of my final experiments.

I would like to thank all my friends and family who have been overwhelming supportive and understanding during my time here. Thank you for being supporting me during the difficult times, helping me during the busy time and always being ready to celebrate during the joyful times. In particular, my parents, John and Nancy, you have always been supportive of my dreams, encouraged me to do my best and loved me no matter what. To Bernie, you are the love of my life. Everything you have done for me is to long to list, but without your love and support, graduate school would have been impossible.

TABLE OF CONTENTS

Appendix

LIST OF FIGURES

LIST OF TABLES

LIST OF SCHEMES

CHAPTER I

BACKGROUND AND INTRODUCTION

1.1 Dissertation Overview

Nanoparticles that target, image and deliver therapeutics to disease through non-toxic and non-immunogenic processes have been a major goal of interdisciplinary research in the last 10-15 years. The exponential development of imaging methods and instrumentation, nanoparticles and discovery of molecular targets has opened numerous options for improving diagnostic imaging, drug delivery and efficacy monitoring. One area lagging behind in the quest for ideal agents in imaging and therapeutic efficacy quantification is the development of “smart” molecules designed for specific diseases and targets. Although great strides have been made in creating new nanoparticles, their functionalization and subsequent chemical and biological characterization remains a challenge. Determining which combination(s) of targeting modalities, imaging agents and therapeutics is most effective is another factor that must be addressed when developing smart agents. Also, more work needs to be done to allow generalized predictions to be made about the impact of size, loading amount and the best synthetic approaches so that nanoparticles can be utilized to their fullest potential. In the work I present for my dissertation, both imaging and therapeutic applications of dendrimeric structures were studied. First, as shown in Chapter 1, I developed a TSPO targeted dual-modality imaging agent

from a PAMAM dendrimer backbone. Second (Chapter 2), with the knowledge about the synthesis and characterization of dendrimeric scaffolds learned from the PAMAM project, I designed a new modular system of dendrimer based multifunctional nanoparticles and developed the therapeutic piece of that system, which incorporated two different drugs and two different peptides. Finally (Chapters 3, 4 & 5) the efficacy of these systems were evaluated *in vitro* (Chapters 3, 4, & 5) and finally the results are discussed based on their contribution to the overall modular system and their future use in this project (Chapter 6).

1.2 Molecular Imaging (MI)

Molecular Imaging (MI) is the process of detecting and studying specific molecules (genes, proteins, etc.) *in vivo* through the use of molecular probes, detection technologies and/or imaging strategies [3-5]. MI is used in magnetic resonance (MR), optical imaging, X-ray, ultrasound and with radionuclides to detect and study disease [3-4]. Each of these techniques has advantages and disadvantages as highlighted in Table 1.1. Expansion of the currently available imaging agents (both dendrimeric and non-dendrimeric) is essential in further detecting disease, understanding biology and treating disease. MI is in its infancy as a clinical tool with fluorodeoxy glucose positron emission tomography (FDG PET) being widely practiced, but has experienced an exponential growth as a research tool and has the potential to transform medicine. Yet for MI to be used in personalized medicine improvements are needed to the chemistry of the

Table 1.1: Summary of various imaging techniques available.

Imaging Technique	Portion of EM Radiation Spectrum Used in Image	Spatial Resolution	Depth	Temporal Resolution	Sensitivity	Cost	Advantages	Disadvantages
Positron Emission Tomography (PET)	γ-rays	1 - 2 mm	no limit	10 sec to minutes	10^{-11} to 10^{-12} mole/L	$$$$	High sensitivity, unlimited depth, isotopes substitute naturally occuring atoms, quantitative translational research	Cyclotron needed, nontrivial chemistry relatively low spatial resolution, ionizing radiation, expensive
Single Photon Emission Computed Tomography (SPECT)	γ-rays	1 - 2 mm	no limit	minutes	10^{-10} to 10^{-11} mole/L	$$$	Many probes available, multiple reporter imaging, adaptable to clinic	Relatively low spatial resolution, ionizing radiation, expensive
Magnetic Resonance Imaging (MRI)	Radiowaves	10 - 100 μm	no limit	minutes to hours	10^{-3} to 10^{-5} mole/L	$$$$	Highest spatial resolution, combines morphological and functional imaging	Relatively low sensitivity, long scan and post-processing time, may need mass quantity of probe
Optical Bioluminescence	Visible light	3 - 5 mm	1 - 2 cm	seconds to minutes	10^{-15} to 10^{-17} mole/L	$$	Highest sensitivity, quick, easy, low-cost, relatively high-throughput, lack of ionizing radiation	Low spatial resolution, relatively surface-weighted, limited translational research, limited depth
Optical Fluorescence Imaging	Visible light or near infrared	2 - 3 mm	< 1 cm	seconds to minutes	10^{-9} to 10^{-12} mole/L	$ - $$	High sensitivity, quick, easy, low-cost, multiple reporter imaging, lack of radiation, relatively high-throughput, real-time monitoring	Relatively low spatial resolution, surface-weighted, limited depth

agents to be uses for MI and targeted intervention. One avenue to improving MI and molecularly targeted therapy is through the use of dendrimeric scaffolds. However, most MI studies performed with dendrimers have utilized commercially available chemistries such as PAMAM™ and DAB™ (PPI) [6-8] rather than more unique structures with controllable functionalities.

Dendrimers have been most often been used in MI as MRI contrast agents. Based on the same principles as nuclear magnetic resonance (NMR) spectroscopy, MRI measures the relaxation rate of the hydrogen nuclei of water to realign with an applied magnetic field following a radiofrequency pulse. Two types of signal can be observed: T1 (longitudinal relaxation, return of the net magnetization to its maximum length in the direction of the magnetic field) and T2 (spin-spin relaxation, occurs when the spins in the high and low energy state exchange energy but do not loose energy to the surrounding lattice) relaxation. Signal from T1 relaxation corresponds to the energy released as the water molecules realign with the magnetic field; while, T2 relaxation relates to the precession of the spin vector about the plane perpendicular to the ground state and is affected by the mobility of the water molecule (protons). MR signals are obtained from the differences in relaxation of water molecules that are rapidly exchanging with the inner and outer sphere orbitals of an inorganic molecule or atom. Profusion agents used in development of better MI techniques and instrumentation, such as Gd chelated DOTA (1,4,7,10-Tetraazacyclododecane-1,4,7,10-tetraacetic acid) and DTPA (Diethylenetriamine- N,N,N',N',N''-pentaacetic acid, N,N-Bis(2-(bis-(carboxymethyl)amino)ethyl)-glycine pentetic

acid) increase MR contrast when chelating a paramagnetic ion such as Gd^{3+}, which changes the relaxation time of associated water molecules due to the coordination of the water molecule with the gadolinium ion. Contrast agents with multiple paramagnetic particles increase the differences in relaxation times between water molecules which are exchanging coordination with a metal (typically gadolinium) and those which are not. Since macromolecules rotate slower than small molecules, the rate of exchange is slower in larger molecules, producing longer T2 relaxations. The most commonly studied dendrimer MR agents are PAMAM™ dendrimers surface functionalized with Gd-DOTA or Gd-DTPA [9].

Optical Imaging techniques using fluorescence or bioluminescence have been reported [3-5, 10] for MI. Molecules that absorb and emit light in the near infrared (NIR) range of the spectrum (650-900 nm) are ideal for biological applications because in this region of the electromagnetic spectrum, tissue relatively transparent with low light scatter and absorption by water and hemoglobin. Numerous small organic dyes have been developed have desirable optical characteristics, with some being commercially available. Among these are indocyaninie green (ICG), IRDye800CW (LI-Cor), and Alexaflur680 (Molecular Probes). Several of these dyes have been conjugated to molecular targets and used to study disease both *in vitro and in vivo*[10].

Multivalent NIR fluorescence is difficult to accomplish by attaching multiple organic dyes to a backbone as with MRI due to self-quenching of the fluorophors. This quenching, caused by small stoke shifts (eg. significant overlap between the

absorption and emission spectra), has been utilized to make fluorescent switches [11-13]. In reported switches, several dyes are attached to a polymer backbone via a peptide linker which diminishes the fluorescence signal due to a high local concentration. After the peptide is proteolytically cleaved the dyes are released, activating fluorescence [12-14]. Forester resonance energy transfer (FRET) is another method used to make biochemical switches where quenching dye pairs are attached in close proximity (20-60Å) such that one is cleaved through a biological process (i.e. proteolytically, or through another biological process) inducing fluorescence [15-16]. A biochemical fluorescent switch can be made into a targeted imaging agent by making the cleavage process specific for a single biological event. This approach provides the advantage of targeting (and thus being able to study) a specific biological molecule or event.

Development of clinically relevant agents to image disease or biological processes is essential in MI. These chemistries generally contain two functionalities or components: a targeting moiety (ligand, protein, antibody, etc.) to provide selectivity and a signaling modality (fluorophor, MR agent, radioligand, etc.) to produce a signal [17-20]. Recently, multimeric imaging agents, in which several imaging and/or targeting agents are covalently attached to a biologically compatible backbone, have been developed [21-24].

Increasing the signal to background for detecting diseased tissues can be accomplished by numerous strategies so that the diseased tissues can be easily detected. Targeting can be accomplished with a molecule which will bind a receptor (small organic ligand, protein, antibody, etc.) or through the use of a

protease as in the fluorescent switch described above. Several proteins and enzymes have been identified as good targets for both therapeutics and imaging agents; including: vascular endothelial growth factor (VEGF), matrix metalloproteinases (MMP), translocator protein (TSPO), δ2-dopamine, and somatostatin-2[3]. These proteins and enzymes are typically overexpressed in diseased tissue (compared to normal), so in theory when these agents are delivered they target or label diseased cells with enhanced selectively. The Bornhop group has developed a number of MI agent that target TSPO [25-30].

Targeting can be accomplished with a molecule which will bind a receptor (small organic ligand, protein, antibody, etc.) or through the use of a protease as in the fluorescent switch described above. Several receptors have been identified as good targets for both therapeutics and imaging agents. Most of the receptors are up-regulated in diseased tissue compared to normal tissue.

1.3 Translocator Protein (TSPO)

TSPO is a mitochondrial membrane protein that spans the lipid bi-layer and mediates cholesterol transport across the mitochondrial membrane (Figure 1.1). Expression of TSPO is important in processes such as steroidogenesis and apoptosis. Although TSPO is ubiquitous, it is expressed more in steroid-producing cells such as testis, ovarian, placenta and brain [31-32]. TSPO has been shown to be a good target for molecular imaging because it has been found to be over expressed in diseased cells and there are several small molecules known to bind the protein (Figure 1.2). The ^{11}C, ^{3}H and ^{18}F analogs of several TSPO

binding ligands have previously been used in PET for *in vivo* imaging and to study TSPO activity [33-35]. Although these ligands are powerful imaging

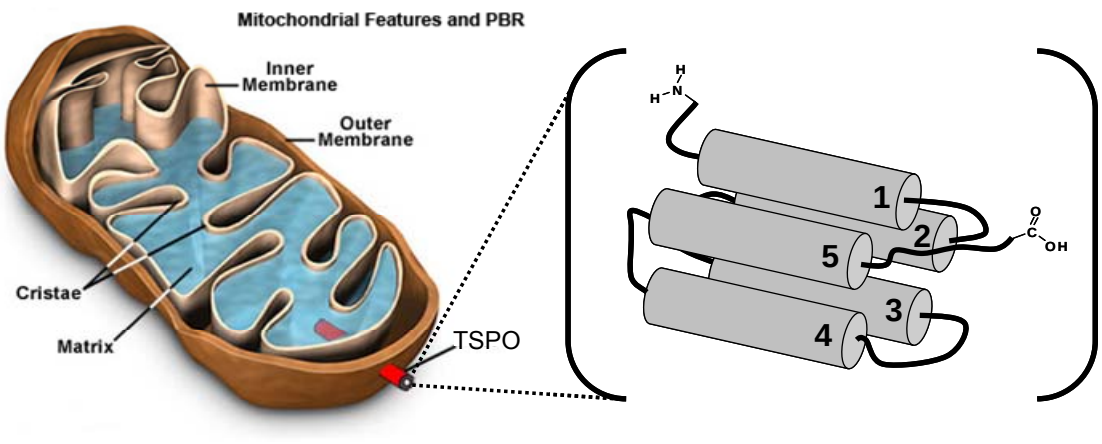

Figure 1.1. TSPO's structure and location in the mitochondrial membrane.

agents, they are limited by complex and expensive synthesis, short half lives and low resolution. Figure 1.2 displays several of the known, high affinity TSPO ligands: Alpidem, Ro5-4864, PK11195, FGIN-1, DAA1106, DAA1097 and SSR180575. Although PET analogs have been made of all these compounds, there are few examples of conjugating these ligands to non-radioactive imaging agents. Conjugation of these ligands to imaging modalities requires additional chemistry which can lower the binding affinity for TSPO. A derivative of PK11195 has been synthesized to provide a conjugable analog, ClPhIQ (Figure 1.3). In the process of synthesizing the amine terminated molecule with a six

carbon linker, another conjugable form of PK11195 was produced, the carboxylic acid derivative (ClPhIQ Acid) [36-37].

The development of ClPhIQ (ostensibly a conjugable form of a TSPO ligand) has facilitated the construction and evaluation of many new targeted imaging agents (ClPhIQ-molecular imaging agent). For example by appending organic fluorophors, lanthanide chelates both optical and MR imaging has been shown to be possible and by using a copper chelate for PET becomes an imaging option (Figure 1.3) [36]. Also, ClPhIQ has been attached to derivatives of the well known

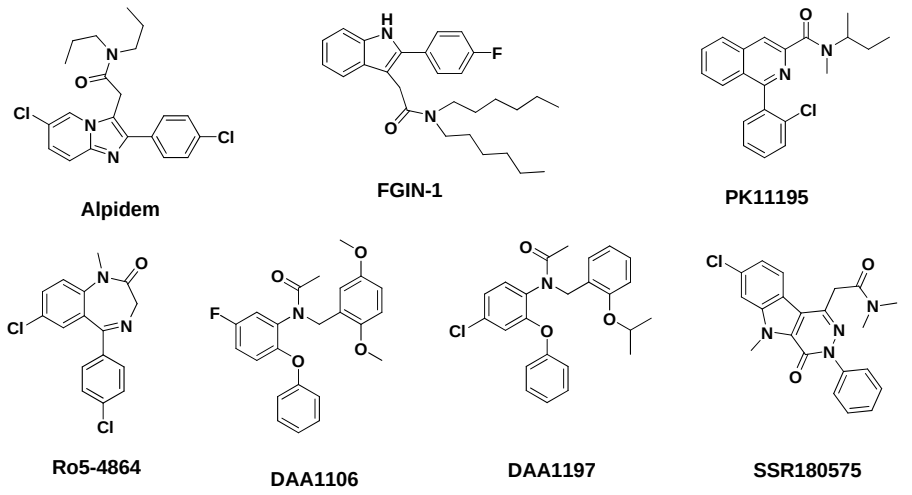

Figure 1.2. High affinity TSPO ligands.

metal chelate 1,4,7,10-tetraazacyclododecane (cyclen) which can lead to a unique optical agent, MR or even a PET imaging agents. The fluorescence analog used for optical imaging synthesized in the Bornhop laboratory contains

an antenna for light harvesting and two phosphonate esters for metal chelation[38]. Europium was then chelated to the macrocycle giving the desired compound. The cyclen derivative DO3A was also used to chelate Gd^{3+} (for MRI) and ^{64}Cu (for PET). Preliminary *in vitro* and *in vivo* experiments have shown that these MI agents target disease[26, 39-40]. Although the monomeric agents are extremely useful and have shown great utility, only one imaging agent can be attached to a single TSPO ligand, thus limiting limited because they contain a single imaging agent and a single targeting ligand.

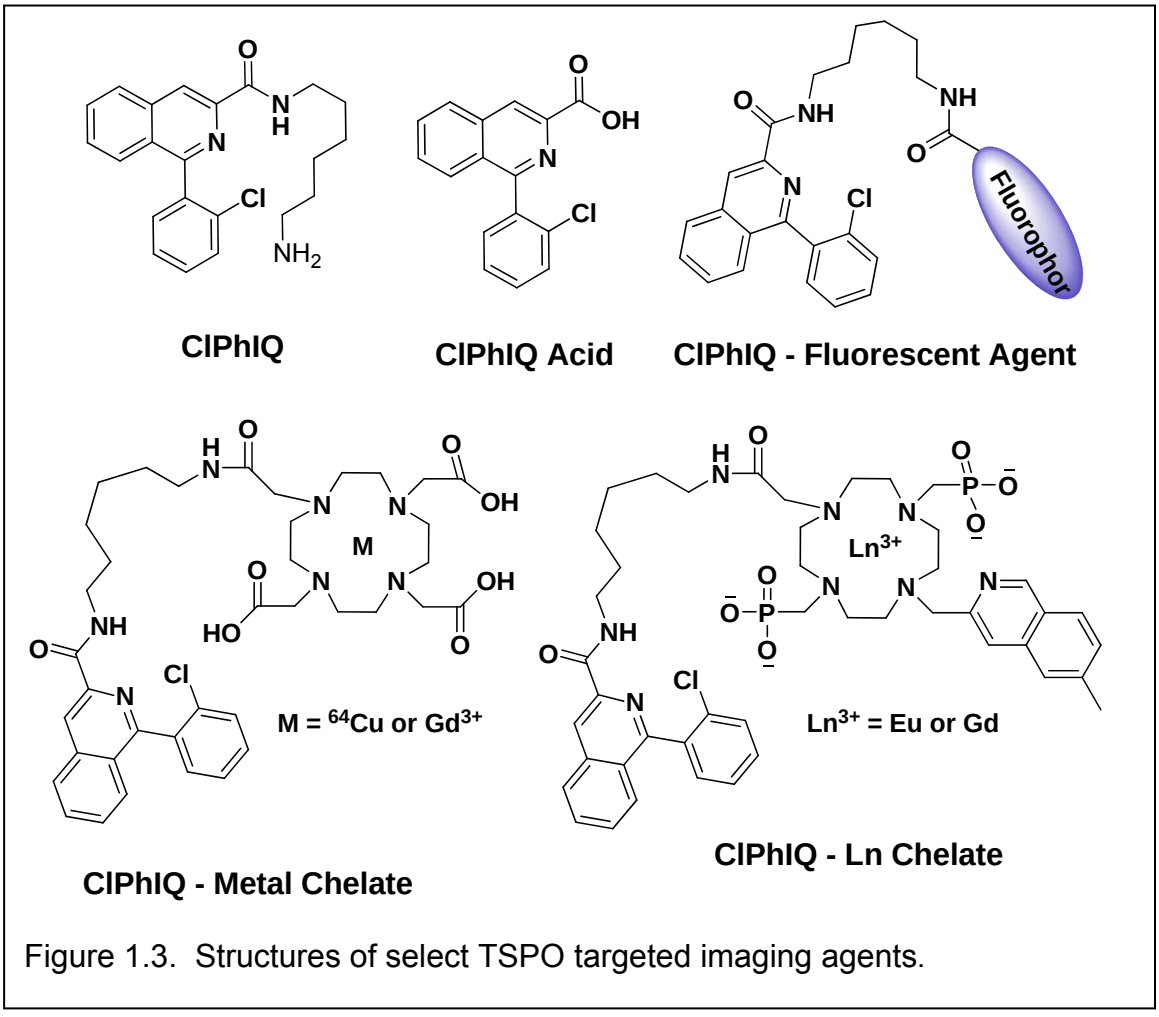

Figure 1.3. Structures of select TSPO targeted imaging agents.

While bi-functional agents described above are valuable, the ability to couple multiple ligands together could afford large increases in binding (improving targeting); incorporation of multiple imaging agents and can lead to increased signal. The potential for multi-modal imaging or monitoring the delivery of therapeutics can not be realized with traditional targeted imaging agents, but can be with nanoparticles.

1.4 Nanoparticals

Nanoparticle development has exploded in the last couple of decades. With nearly as many different nanoparticle structures as there are uses. A few of

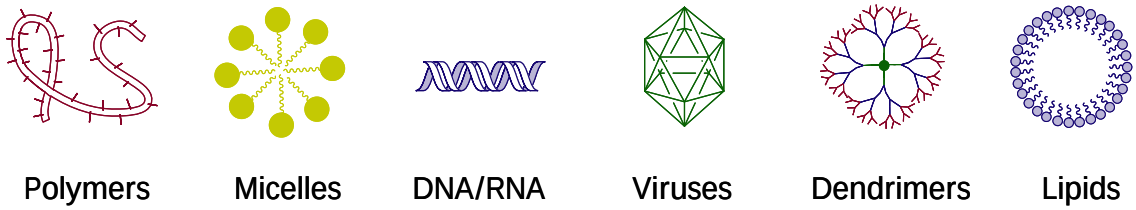

Figure 1.4 Representaions of select nanoparticle structures.

the most commonly studied nanoparticles are polymers, micelles, dendrimers, viruses, DNA/RNA, lipids, drug nanocrystals, ceramic-based, albumin, nanoemulsions, nanogels, metal oxides, proteins, liposomes, quantum dots, gold nanoparticles, carbon nanotubes, nanowires, as well as various hybrid systems such as metal cored dendrimers. Some of these systems are graphically

represented in Figure 1.4. Each of these systems has a variety of different chemical structures which have strengths and weaknesses as shown in Table 1.2[41-46].

Polymers offer the advantages of being easily synthesized, water-soluble, nontoxic, biodegradable, conjugable and can be in surface modified (i.e. pegylated). Furthermore, they can accumulate and be retained in tumor tissue (EPR effect). However, since some polymer structures are easily degraded *in vivo*, they can produce undesirable metabolites, do not easily encapsulate molecules and have undefined architecture in solution[42-43, 47]. Micells are suitable carriers for water-insoluble drugs, biocompatible, self-assembling and biodegradable; however, have limited stability, may require surfactant concentrations of 20% or higher, and can be immunogenic with growing diversity in amino acids [42-43, 47]. Dendrimers can be tuned for improved solubility and biodristrubution, contain high structural and chemical homogeneity, are easily functionalized, can have high ligand density, controlled degradation and multifunctionality. If not careful a positive charge on the dendrimer surface may lead to toxicity and immunogenicity[42-43, 47]. As a final example of strengths and weaknesses in nanoparticles, liposomes are amphiphilic, biocompatible, easily modified and have targeting potential, but the preparation steps have to be carefully controlled in order to achieve reproducible properties such as size and entrapment efficiency[42-43, 47].

The major two uses of nanoparticles in biotechnology are imaging and therapeutic delivery. Some systems are simple and contain multiple copies of a

Table 1.2 Characteristics of some Nanoparticles for Imaging and Therapy

Nanoparticle	Advantages	Disadvantages
Liposomes	1) Amphiphilic 2) Biocompatible 3) Easily modified 4) Targeting Potential	1) Careful synthetic control required for reproducibility
Polymers	1) Water-soluble 2) nontoxic 3) Biodegradable	1) May produce undesirable metabolites
Micelles	1) Carries water-insoluble drugs 2) Biocompatible 3) Self-assembling 4) Biodegradable	1) Limited stability 2) Possible toxic monomers 3) Possible immune response 4) May produce undesirable metabolites 5) May require 20% surfactant
Dendrimers	1) Biodistribution can be tuned 2) High structural homogeneity 3) Easily functionalized 4) High ligand density 5) Controlled degradation 6) Multifunctional	1) Positive charge may be toxic 2) Immunogenicity
Viral Nanoparticles	1) Bioconjugable 2) Multivalent 3) Targeted 4) Multifunctional 5) Defined geometry 6) Uniform	1) Genetic Alteration 2) May require additional regulatory oversight 3) Liposomes and Dendrimers may be better
Carbon Nanotubes	1) Water-soluble 2) Biocompatible through chemical modification (organic functionalization) 3) Multifunctional	1) Solublility issues 2) Toxicity problems

single imaging or drug molecule while other nanoparticles are more complex. Nanoparticles have properties optimal for incorporating multiple signatures or functions by the incorporation of multiple imaging modalities, drugs, targeting molecules, solubilizing molecules, etc. into a single particle. To date very few examples of more than two modalities have been reported, however the field is rapidly moving in this direction[43, 46].

Nanoparticles have been applied to every modality of molecular imaging including: light microscopy, optical microscopy, photoacoustic imaging, X-ray, computed tomography X-ray, PET, SPECT, and MRI[48-49]. MRI is currently one of the most benefitted modalities from nanoparticles. Due to its low sensitivity, the molecular structures of nanoparticles can increase signal in the MRI to near PET or SPECT resolution. This is accomplished with additional Gd^{3+} ions as well as through altering the T1 and T2 relaxations time due to the increased size (and thus slower rotation) of the nanoparticle[48]. Other examples of nanoparticles for imaging include hybrid nanoparticles such as quantum dots with PEG polymers attached to the surface. These QD-PEG hybrids have been conjugated with ^{18}F labeled RGD peptides for improved PET imaging and targeting ability as well as having a fluorescence signal[49].

Nanoparticle aided therapeutic delivery has been extensively studied with agents being used daily in the clinic [50]. Nanocarrier systems offer the advantage of fewer doses, improved delivery by protecting metabolically fragile molecules, increased drug efficacy and shorted patient recovery time[51-53]. Patient comfort is also increased with nanoparticle delivery systems due to their ability to delivery

drugs to the desired site, leaving healthy tissues unaffected and reducing or eliminating off target (systemic) toxicity[54]. One use of nanoparticles in drug delivery is the development of smart polymers. These polymers are designed to degrade in acidic conditions, delivering their therapeutic load to specific cells or parts of the cell. For example, Murphy et. al. reported poly(acrylic) polymers that disrupt red blood cell (RBC) membranes and distribute their drug specifically into the cytosol[46, 55].

1.5 Prodrugs

Drug therapy has long been used as one of the major methods for treatment of disease. The diagnosis of a new disease leads rapidly to the search for therapeutic treatments that cure, improve the quality of life or lengthen the life (for life threatening diseases) for patients with the disease. Classic drugs suffer from many shortcomings including: high toxicity, instability, inefficient solubility, undesirable methods of introduction, poor pharmacodynamics, non-specificity and bad smell and taste[56-58]. Drug research involves more than drug discovery, but also researching 1) methods to discover drugs quicker (i.e. high throughput screening), 2) properties that improve drug absorption, distribution, metabolism and excretion (ADME) and 3) reducing systemic toxicity and improving therapeutic efficacy[56,58]. One method for improving the ADME properties, reduce systemic toxicity and improve efficacy of therapeutic agents is through the development of prodrugs. Prodrugs are inactive derivatives of the parent drug molecule which becomes activated either by enzymes or under spontaneous

conditions. Prodrugs incorporate pieces that are designed to improve delivery of a drug to the active site by manipulating the physiochemical properties of the system in such a way that the lipophilicity, permeability, stability and/or tissue specificity of the active drug is modified[56, 59].

Several approaches to release of active drug from the prodrug have been explored, including enzyme activation or cleavage, intramolecularly activated and changes in chemical properties. Activation by enzyme cleavage is the most common type of prodrug and typically accomplished with ester, carbamate or amide linkages which can be hydrolyzed by caroxyesterases (ubiquitous in tissue) or other enzymes (for specificity)[60]. Intramolecularly activated prodrugs occur through cyclization reactions which either cyclize to form the active drug or are released as a leaving group in the cyclization reaction. A third kind of intramolecularly activate prodrug is referred to as a two step reaction in which the drug is released after cyclization that was initiated by enzyme activation.

Enzyme-mediated cancer imaging and therapy (EMCIT) has been utilized to deliver drugs and imaging agent to solid tumors specifically. Coupling of chemotherapy agents to polymers has provided better drug solubility, stability, specificity and controlled release. Other strategies in which doxorubicin (DOX) was coupled to an enzyme selective cleavable peptide and released solely in the tumor environment have show success in animal studies[61]. Cyclization of precursors to form benzoxazolones is anexample of prodrug cyclization that results in the active drug. With these drugs, alcohol and carbamate functionalities are ortho to each other on a benzyl ring. Upon activation, the

alcohol attacks the carbonyl followed by loss of a leaving group to provide the benzoxazolone therapeutic agent[58].

1.6 Dendrimers

Dendrimers are spherical macromolecules, developed simultaneously in the laboratories of Newkome [62] and Tomalia [63-66] in the mid 1980's, which contain an inner core followed by successive layers of branching. As dendrimers become larger (higher generations), the diameter and number of terminal groups increase exponentially. The spherical architecture of dendrimers and ease of synthesis is an attractive alternative to linear polymers leading to numerous applications of dendrimers and modifications to dendrimers [23, 67]. The most widely used dendrimers are polyamido amine (PAMAM™) dendrimers (Figure 1.5). The PAMAM™ dendrimer consists of an ethylene diamine (or ammonia) inner core with branching amide and amine linkages separated by two carbons. PAMAM™ dendrimers are attractive scaffolds because they are physically robust, water soluble and commercially available with amines (full generation), esters (half generation) or alcohols at the termini.

Although PAMAM™ dendrimers are attractive scaffolds for biological applications; there are some inherent weaknesses in the structure and synthesis of these molecules. PAMAM™ dendrimers are synthesized by a divergent method, which begins with a central core and builds towards the periphery by adding successive layers to form higher generations (Figure 1.6). Divergent

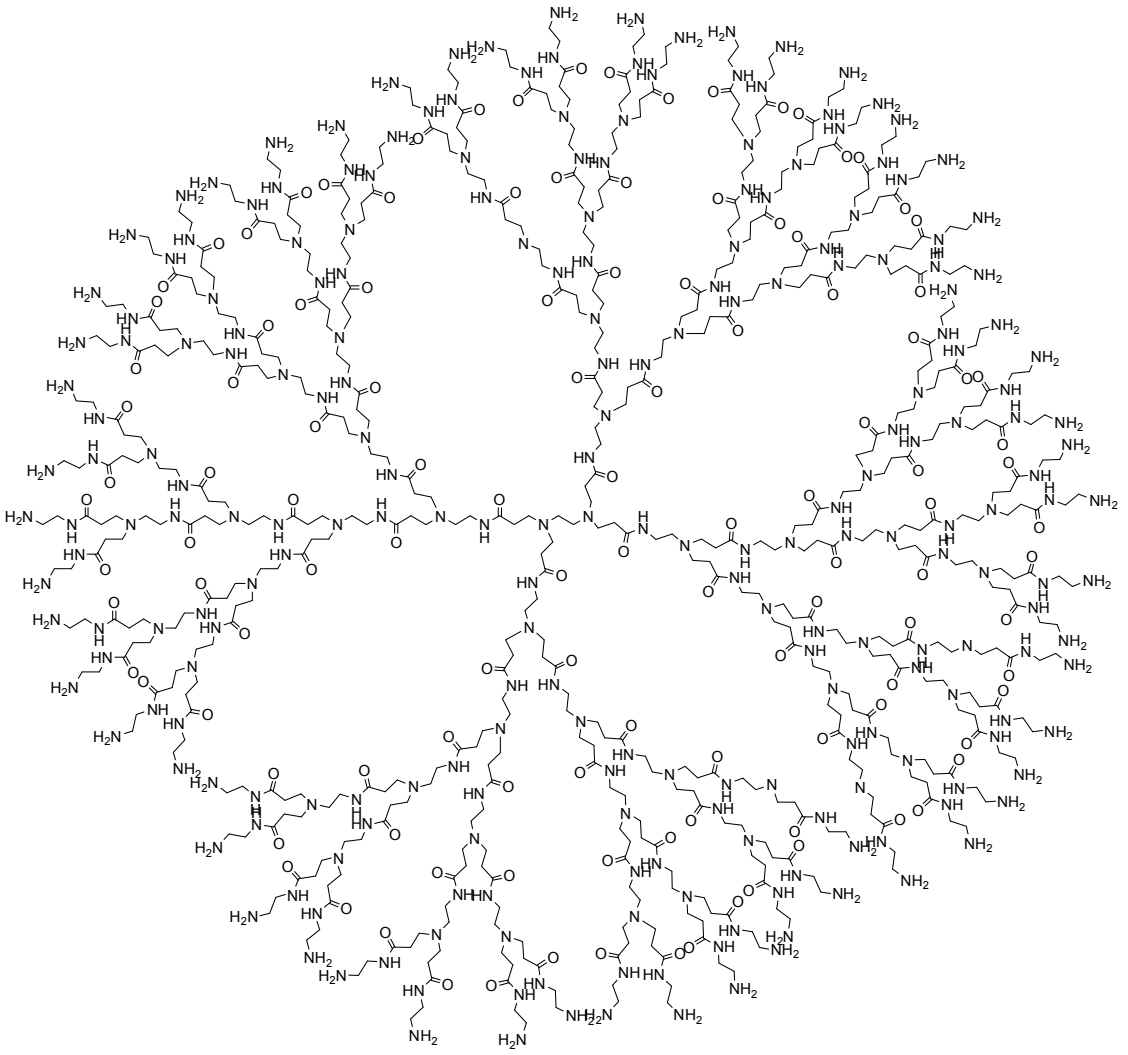

Figure 1.5 Fourth generation PAMAM dendrimer

synthesis consists of performing a few reactions iteratively to obtain higher generations. Although divergent synthesis allows for rapid production of high generation dendrimers, the products have imperfections caused by incomplete and side reactions, becoming more frequent in successive generations. The surface of traditional divergent dendrimers is uniform, limiting control over

functional group locations. In general each functional group will be randomly distributed over the surface, with other conformations unobtainable [68].

An alternative approach to the divergent preparation of dendrimers is through convergent synthesis; which consists of synthesizing dendrons or “arms” of the dendrimer first, followed by attaching them (dendrons) to a central core to form the final structure (Figure 1.7). Convergent synthesis of dendrimers consists of a variety of different reactions and is more labor intensive, but generally produces

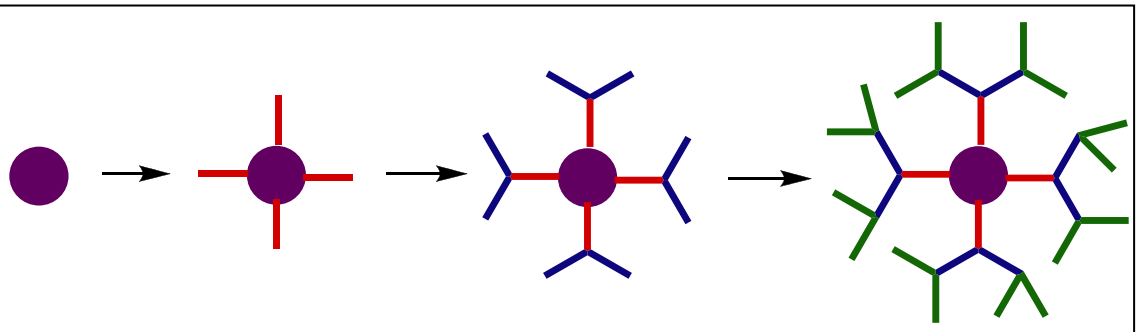

Figure 1.6 Schematic representation of divergent dendrimer synthesis

more homogeneous molecules. By changing a few synthetic steps, the core, middle or periphery of the dendron can be adjusted so that the final structure contains sections with different functionality. With convergent synthesis, the locations of functional groups can be controlled and modified as needed expanding applicability. However, convergent synthesis is more costly and time consuming.

Surface functionalized dendrimers are created by attaching ligands, etc. to the reactive terminal endgroups [68]. Numerous agents have been functionalized onto the surface of dendrimers, including: therapeutic agents[69-81], targeting moieties (peptide, proteins, antibodies and small molecules)[70, 76-78, 80, 82-87],

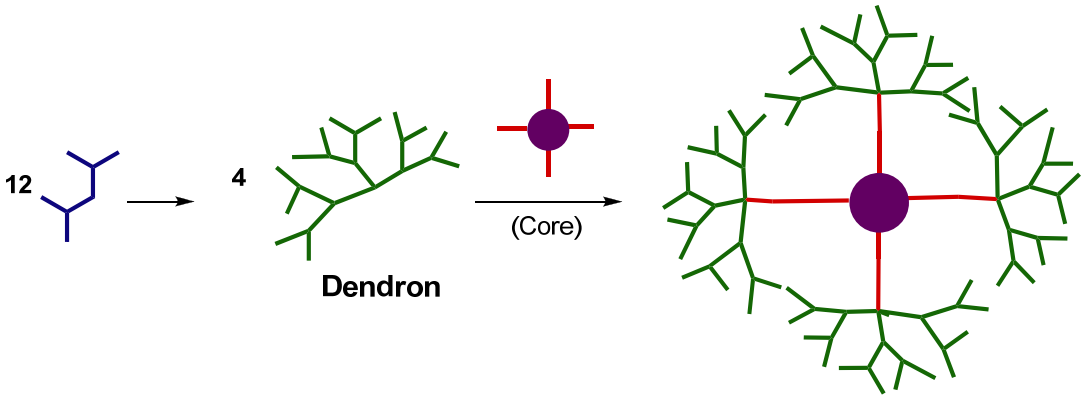

Figure 1.7 Schematic representation of convergent dendrimer synthesis

imaging agents (fluorescent compounds, chelated metals, sensors, radioligands[80, 88-92], solubilizing agents (PEG)[69], and carbohydrates[68, 85, 93-96], amongst others. Dendrimers can be functionalized homogeneously or heterogeneously. Homogenous functionalization is characterized by the entire periphery of the dendrimer being functionalized with the same functional group. A perfect example of homogenous functionalization is the first use of dendrimers for use as MRI probes. In these studies, PAMAM dendrimers were completely functionalized with DTPA or DO3A chelated Gd^{3+} [91, 97-98]. Heterogeneous

functionalized dendrimers contain two or more different functional groups on the surface. Heterogeneous functionalization can be either random or controlled (through the manipulation of the terminal groups). One example of heterogeneous functionalization comes from the Baker group which has synthesized a series of heterogeneously functionalized dendrimers that contain folate for targeting, fluorescent dyes for imaging and various therapeutics for disease elimination[78, 99-102].

Dendrimers have been used to encapsulate molecules for imaging, drug delivery, studying ionic properties, and much more[103]. One dendrimer design of hydrophobic interiors with hydrophilic exteriors makes dendrimers ideal for non-covalently incorporating drug molecules, while other dendrimer structures are perfect for encapsulating metals. Metals inside a dendrimer structure have been used as catalysts, for PET, SPECT, MRI, fluorescence and CT imaging[86, 104-107], for photodynamic therapeutic[108-109] and for light harvesting agents[110-111].

The convergent approach to synthesizing dendrimers can be used to make dendrons with differing functionalities (either orthogonal protecting groups, or pre-functionalized) which can be attached to a core in a "**mix and match**" fashion to provide a variety of dendrimers. This chemistry is highly tunable, allowing for rapid re-routing if the dendrimer does not prove biologically compatible. The **"mix and match"** dendrimers being developed in Chapters 2-5 are capable of: 1) Therapeutic delivery targeted to the site of disease; 2) a biochemical switch capable of monitoring both the cleaved dendrimer location and therapeutic delivery; 3) solubility agents for tuning the molecule; and 4) a

locator beacon for following the molecule from the site of injection. Presented here are studies using PAMAM™ dendrimers to demonstrate that multi-modal, targeted imaging agents can be synthesized to improve the current capabilities of imaging agents. Following the data obtained with PAMAM™ dendrimers, convergent dendrons which can be attached pre or post functionalization to provide "**mix and match**" functional nanoparticles containing imaging agents, therapeutics, sensors, solubility enhancers or any number of other modalities are possible.

1.7 Characterization of Dendrimers

The unique properties and structures of both surface functionalized and encapsulated dendrimers, as well as the diversity of research on dendrimers is reflected in the number of methods for characterizing the various characteristics of dendrimers. These methods include: atomic force microscopy (AFM), scanning tunneling microscopy (STM), optical tweezers (OTW), dynamic static light scattering (DLS and SLS), gel electrophoresis (GE), ethidium bromide intercalation assay (EBIA), fluorescent dye intercalation assay (FLIA), zeta potential (ZP), isothermal titration calorimetry (ITC), circular and linear dichroism (CD and LD), melting profiles (MeltP), differential scanning calorimetry (DSC), fluorescence quenching (FLQ), electron paramagnetic resonance (EPR), synchrotron X-ray diffraction (SXRD), cross-polarized microscopy (CPM), stopped-flow fluorescence and circular dichroism (SFF, SCD), fourier-transform infrared (FTIR) spectroscopy, small angle X-ray scattering (SAXS), optical

microscopy (OM), molecular simulations (M-S), nuclear magnetic resonance (NMR), UV-vis, matrix assisted laser desorption ionization mass spectrometry (MALDI-TOF MS), fluorescence, elemental analysis, gel permeation chromatography (GPC), size exclusion chromatography (SEC), reverse phase HPLC, and potentiometric titration[95, 100-101, 107, 112-116]. Even with the vast number of methods, characterizing dendrimers is not always trivial as many of these characterization methods only work due to specific properties of the dendrimer. In particular when working with heterogeneously functionalized dendrimers it is often difficult to determine that the different moieties are attached and to quantify how many of each are present.

1.8 Dendrimers as Imaging Agents

MRI dendrimer imaging agents have progressed over the last decade from blood pool agents containing several Gd^{3+} ions to targeted contrast enhancing agents. The original MRI dendrimer agents were based on the simple design to increase the signal. This was done by increasing the number of ions per molecule and by capitalizing on slower rotation of the large macromolecule thus decreasing the rate of exchange of water. Recently, targeted MRI dendrimers have been reported with polysaccharides, oligopeptides, proteins, antibodies, oligo-nucleotides, folic acid and biotin-avidin [117-118].

While building MRI agents has been the focus of most dendrimeric research efforts, the use of metals such as ^{111}In or ^{153}Gd radiotracers have been incorporated into scaffolds for PET imaging[86]. Also, several examples of

fluorescence imaging *in vitro* and small animal *in vivo* imaging have been reported[45, 89, 119], including a dual-modality MRI-fluorescence probe[118]. In further research, dendrimers have been used to develop fluorescent sensors based on quenching dye pairs[14-16, 120].

1.9 Dendrimers as Therapeutics

Several delivery mechanisms utilizing dendrimers have been developed using dendrimers, including conjugating or encapsulating drugs, photodynamic therapy, boron neutron capture therapy and photothermal therapy[121]. Drugs encapsulated into dendrimers have been shown to exhibit an increase in solubility and toxicity, compared to unloaded dendrimers. The type of dendrimer scaffold employed uses effects of encapsulation and delivery that are not always intuitive. For example, hydrophobic cores are not always necessary for encapsulation of hydrophobic drugs such as the encapsulation of paclitaxel into poly(glycerol) dendrimers, which is not fully understood[121].

Therapeutics that are covalently attached to dendrimers are generally incorporated with a method of detachment to reactivate the therapeutic; while some drug molecules are designed to remain toxic while still attached to the dendrimer. Various drugs have been attached to dendrimers including methotrexate, paclitaxel, doxorubicin, cis-platnin, and ibuprofen[86, 121-122]. These therapeutic dendrimers have been found to have lower systemic toxicity and give higher accumulation in solid tumors with slower release profiles[86]. Furthermore,

the dendrimer scaffold also plays a role in the delivery and therapeutic efficacy of the drug[121].

Photodynamic therapy relies on activation via light (visible or NIR) and has been enhanced by the incorporation of multiple porphyrin sensititizers (needed for therapy) and 5-aminolaevulinic acid (ALA, needed for tumor uptake and selectivity)[122] into a dendrimer. In Boron neutron capture therapy, ^{10}B is irradiated with low-energy thermal neutrons to produce high energy α-particles and ^{7}Li nuclei. Given that the α-particles pathlength is only 10 μm, the toxicity of the α-particles are limited to the cells containing ^{10}B. PAMAM dendrimers have been utilized to deliver large doses of ^{10}B to diseased tissue via targeting moieties[121-123].

1.10 Matrix metalloproteinases (MMPs)

MMPs are zinc dependant proteases found to partake in tumor progression with their ability to degrade the basement membrane and components of the extracellular matrix [124]. Twenty four human MMPs have been discovered and studied, but MMPs 2, 7 and 9 are found to be expressed in high concentration and are associated with certain cell types in the tumor microenvironment including tumor cells, tumor associated fibroblasts, endothelial cells and various cells of the myeloid and lymphoid classes [1, 125-126].

MMP Inhibitors (MMPI) were developed to phase III clinical trials and found to fail as treatments. One reason for this potential failure is the complex role MMPs play in tumor development and metastasis. Current research

indicates that MMP9 contributes to the establishment and early survival of metastatic tumors, but have an ever-changing role at later stages of tumor development [127-128]. Thus introducing MMPIs during late stage metastatic development would not effectively eradicate the cancer. Another possibility that could explain the success of MMPIs in mouse models and not in clinical trials is the type of studies completed. The mouse models primarily used in preclinical MMPIs studies were xenograft models[126, 128]. Recently, more complex genetic models have been developed because these models more accurately mimic the multistage progression of tumor progression and thus they better represent human tumors.

1.11 Matrix Metaloproteinase 9 (MMP9)

Gelatinase B, also known as MMP9, plays an important role in tumor metastasis. MMP9, a type IV collagenase, has been found to be a prognostic indicator in breast cancer patients[2]. This protease is important in degrading the basement membrane of tumors, which is a key role in tumor metastasis. Interestingly, MMP9 is not found exclusively in tumor cells, but also in inflammatory cells that surround the tumor environment [126]. Studies have shown MMP9 contributes to tumor metastasis and early development by degrading the basement membrane and promoting angiogenesis at the metastatic site among other mechanisms[2]. Subsequently, MMP9 has not been shown to have an effect on growth of the tumor following establishment of tumors in the lung[124].

1.12 MMP9 Cleavable Peptides

Several small peptide sequences that are selectively cleaved by a specific MMP(s) have been developed. These selectively cleavable peptides have been used in molecularly activated fluorescence molecular probes[14-16, 19, 129]. Pro-drugs using an MMP cleavable peptide have also been created by attaching the peptide to doxorubicin (DOX), auristatins or CBI-TMI[130]. The peptide was cleaved between the Gly-Leu bond in the presence of the enzyme, followed by a cascade reaction to liberate the active drug from the remaining amino acids [61]. Studies have also shown that a few amino acids attached to DOX do not significantly affect the efficacy of the chemotherapeutic [131]. The sequence AVRWLLTA has been shown to be cleaved by MMP9 and MMP2, however at very different rates. MMP9 cleaves AVRWLLTA more rapidly, making it capable of being used to specifically target MMP9.

1.13 MMP9 Associated Cell Lines

Although specific mouse models are ideal to mimic human tumor progression, *in vitro* studies are useful in deciphering mechanisms and effect of perturbation of the system. For cell studies, it is helpful to have both null and positive expressing cell lines. One positive expressing cell line for MMP9 is derived from the mouse mammary tumor virus–driven polyoma viral oncogene (MMTV-PyVT) transgenic mouse model. The MMTV-driven polyoma virus middle T antigen transgenic mouse, developed by Muller and colleagues in 1992 [51], is routinely used in the Matrisian laboratory for studies of breast cancer

metastasis to the lung. MMTV-PyVT animals develop multifocal mammary gland tumors that can affect all 10 glands with an average latency of 34 ± 6 days in females. Metastatic disease to the lung occurs in 100% of animals. A recent study has demonstrated that PyVT tumors develop through 4 distinct stages that are comparable to human disease both morphologically and by expression of biomarkers, indicating that this is a very relevant model for human breast cancer[132]. The Matrisian laboratory isolated and characterized a series of cell lines from a single primary tumor in an MMTV-PyVT FVB mouse. A highly aggressive PyVT antigen/E-cadherin-positive cell strain, now referred to as PyVT1, formed compact, rapidly growing unifocal tumors in the mammary fat pad of syngeneic FVB mice with a morphology consistent with the poorly differentiated component within MMTV-PyVT mammary tumors, and form colonies in the lung within 5 weeks when injected via the tail vein[126]. These cells have been labeled with Luciferase using the modified retroviral vector pMSCV for *in vivo* imaging (PyVT-R221A-luc)[126].

Two further cell lines, derived from Lewis Lung Carcinomas (LLC), have been developed with MMP9 positive and null versions. The LLC-RSV and LLC-MMP9 have undetectable and high levels of MMP9 respectively. These cells were made from LLC cells by incorporating an empty vector (LLC-RSV) and an MMP9 vector (LLC-MMP9) into the cells. A fourth cell line that is useful in studying therapeutic effects *in vitro* is the MDA-MB-231 human breast cancer cell line. Although this cell line is not specifically linked to MMP9, it is the benchmark cell line for translation into human tumor behavior. By using all four cell lines, a

comprehensive estimation of which molecules will be best to move forward into *in vivo* experiments can be established.

1.14 Doxorubicin (DOX)

A major challenge in drug development is selectively delivering a therapeutic dose to the site of disease. Targeted delivery will ideally result in the reduction of systemic activity, increased therapeutic index and increased efficacy of the drug. For example, many cancer drugs are limited as a therapeutic due to cardiotoxicity and myelosuppression, however modifications to the molecule have resulted in a compound that is activated in the tumor [131].

DOX, an anthracycline chemotherapeutic agent, is effective for treatment of acute leukemia, malignant lymphomas and solid tumors (including small cell lung carcinoma). Toxicity of DOX is caused by effecting ribosomal RNA precursor synthesis and DNA synthesis [133]. Unfortunately, the drug is also known for its systemic toxicity, primarily cardio toxicity and myelosuppression and becoming resistant to the cancer cells[134] which limit the use of DOX for treating malignant disease. Several attempts have been undertaken to make a prodrug form of DOX. These include attaching small protease cleavable peptide chains to the terminal amine[134-135], dangling DOX off of nanoparticles [43], and structure modification[133]. Although some modifications have proven to inactivate DOX, others have been shown to retain activity and still other modifications are debated as to whether the activity remains as will be discussed in Chapter 3.

1.15 Paclitaxel (PXL)

Paclitaxel (Taxol™) is one of the most prescribed chemotherapeutic agents currently in use, primarily being used to treat breast, lung, ovarian and head and neck malignancies[136-137]. Isolated from the bark of the Pacific Yew tree, paclitaxel super stabilizes microtubules by binding to the hydrophobic pocket within the central domain of the polymerized microtubule[138]. The mechanism of action of other microtubule inhibitors, such as colchicine or vica alkaloids, is to bind the dimers and prevent polymerization that assembles the microtubules. However, paclitaxel bound microtubules enhance polymerization so much that polymerization can occur without GTP present and depolymerization is resistant to Ca^{2+}, cold temperatures and dilution. The mechanism of paclitaxel action is concentration dependent; at high concentrations paclitaxel increases polymer mass and induces microtubule bundle formation in interphase cells while at low concentrations paclitaxel suppresses microtubule dynamics without altering polymer mass[137]. Two disadvantages of paclitaxel are the development of resistance and hypersensitivity. Resistance is believed to be caused by either hypostable microtubules that shift the equilibrium towards the dimer rather than the polymer[137, 139-140] or an equilibrium that shifts the dynamics of the microtubules toward being more dynamic rather than rigid [137, 141-143]. The problem of hypersensitivity is believed to be caused by the solvent emulsion used to administer paclitaxel rather than the drug itself. Due to poor solubility, paclitaxel is often administered in Cremophor EL, a caster oil emulsion, but has recently

been administered as an albumin bound molecule, nab-paclitaxel[144-145]. Albumin non-covalently binds paclitaxel and transports it into the tumor environment, providing an increased concentration of paclitaxel in the tumor environment. Overall, albumin bound paclitaxel is less hypersensitive, produces increased survival in patients, is better tolerated and is able to be given in higher doses[144]. Given the success of nab-paclitaxel other delivery mechanisms for paclitaxel are being developed, including the use of covalently bound paclitaxel [100].

CHAPTER II

PAMAM DENDRIMER AS AGENTS FOR TARGETING DISEASE

2.1 Background and Introduction

Development of clinically relevant molecular probes to image diseases or biological processes is essential for the advancement of personalized medicine. A variety of biomarkers specific to cancer and other diseases have been identified and used for therapy and/or imaging[10, 46, 80]. Proteins have been targeted using antibodies[146], complementary proteins[44], small molecules[29-30, 36], nanoparticles[147-149] and dendrimers[6, 80, 150]. Attachment of multiple and/or different species to a single dendrimer has produced a single molecule which targets, images and/or delivers a therapeutic dose to the site of disease[151-152]. The advantages of using dendrimers include a) multiple moieties or multiple copies of the targeting agent on a single particle, b) biocompatibility, c) size solubility and d) tunability. However the challenges of using dendrimers include, a) the difficulty in characterization of functionalized molecule, b) nonuniform distribution of the adduct(s), c) complexity in determining the optimum size and d) insuring that the targeting moiety retains activity after attachment to the dendrimer. It is clear that macromolecules will play an important role in personalized medicine; however, the current synthetic scaffolds are particularly ineffective in targeting *intra*-cellular receptors.

The translocator protein (TSPO, previously known as the peripheral-type benzodiazepine receptor or PBR), spans the mitochondrial membrane and has become an attractive receptor for therapeutics and targeted imaging[153]. TSPO is associated with a number of biological processes including cell proliferation, apoptosis, steroidogenesis, and immunomodulation, yet, its exact physiological role is still not fully defined[153-155]. Over expression of TSPO has been shown in numerous types of cancer including brain, breast, colorectal, prostate and ovarian cancers, as well as astrocytomas, hepatocellular and endometrial carcinomas[154]. Two well characterized cell lines with high TSPO expression are C6 Rat Glioma cells[35] and MDA-MB-231 human breast cancer cells[156]. Several small, high binding, selective molecules have been developed for TSPO and made into positron emission tomography (PET), magnetic resonance (MR) and optical imaging agents[157-158,28, 36, 159]. While attractive, macromolecules targeting TSPO have not been reported, possibly due to difficulty in internalizing large, synthetic molecules.

Dendrimers can be adapted to coupling technologies allowing them to be used with emerging targets, therapeutics and imaging strategies. Multiple attachment points can provide increased therapeutic efficacy, reduced drug side effects, increased signal to background for improved imaging detection limits. Methods of targeting include attaching several copies of a binding molecule (small molecules, peptides, proteins or antibodies) to the surface of the dendrimer to capitalize on polyvalency, or the enhanced permeability and retention (EPR) effect were tumor accumulation occurs due to the particle size

and the increased vasculature of the tumor[160-161]. Imaging with dendrimers is possible through the attachment of small molecule fluorophors (for optical), metal chelates (for fluorescence, MRI, PET and SPECT) or with a switch activated by a physiological process for enhanced tissue characterization[13, 162]. Dendrimers can serve as effective prodrug scaffolds with the drug molecules being attached through a linkage which activates the drug *in vivo* once they reach the delivery site. Cleavage from the scaffold can occur through a change in pH, enzyme reaction or slow degradation of the macromolecule[13].

While internalization of large nanoparticles through the cellular membrane has been shown; targeting of specific organelles has scarcely been reported[163-164]. Here I present the synthesis, characterization, cellular internalization and mitochondria labeling of a dendrimer nanoparticle. Although fluorescence is useful for *in vitro* studies of biological processes, *in vivo* and clinical analysis is difficult. In order to produce detectable *in vivo* signal, the fluorescence must be in the near infrared (NIR) region of the electromagnetic spectrum. An added complication with nanoparticles that use NIR dyes is the potential for fluorescence quenching at high local concentration of the dyes, limiting the number of dyes that can be attached per molecule. Metal chelates provide more imaging options (through being able to chelate different metals to the same chelate) for both clinical and academic arenas.

One research tool, electron microscopy (EM), has been used to probe many questions in biology[165-166]. Cellular organelles are visually distinguishable from each other in an EM image (resolution of 1-2 nm) while they are not in a

fluorescence image (resolution of 200 μm). Information related to specific cellular structures requires additional probes in fluorescence microscopy. Current techniques in EM include dosing and staining the samples post fixation to label the structure(s) and/or protein(s) of interest. Few reports of labeling live cells prior to fixation and EM imaging have been reported to date[167]. Labeling the cells before fixation offers the advantage of being able to directly study the effect a probe has on the biological system. Using dendrimers, targeting moieties, fluorescent dyes and electron dense metals incorporated into the same molecule it is demonstrated here that the ClPhIQ functionalized dendrimers enter the cell unperturbed and are imaged via fluorescence (live or fixed) and/or EM (fixed).

Here, the ability of PAMAMs as targeted, multi-modal imaging agents was substantiated through demonstrating the synthesis, characterization and biological utility of a TSPO targeted dendrimer. Binding studies demonstrate the affinity for TSPO was maintained. Studies with fluorescent cellular imaging show the potential of this agent to target high expressing TSPO cells. We further demonstrate that live cells can be labeled *in vitro* and subsequently imaged via thin section EM for TSPO specificity. The TSPO targeted dendrimers are useful for fluorescence, MRI and EM imaging because of their ability to enter cells under physiological conditions and label mitochondria specifically in diseased tissue. The combined body of work on the TSPO targeted dendrimers provides proof that PAMAM dendrimers can be used to target intracellular structures in living, diseased cells. The ability to deliver a dendrimer in an intracellular fashion to live, diseased cells will have an impact on both detection and treatment of

diseases. Highlighted in this chapter is a fourth generation (G(4)-PAMAM) dendrimer particle which targets an internal cellular receptor (TSPO) and binds that target by passing through the cellular membrane under normal physiological conditions and without the external perturbation of the cellular membrane can be prepared, characterized and imaged.

2.2 Synthesis of ClPhIQ-PAMAM-Liss

The TSPO targeted dendrimer was synthesized using 1-(2-chlorophenyl)isoquinoline-3-carboxylic acid (ClPhIQ Acid) a precursor of the conjugable TSPO targeted molecule previously reported[36]. ClPhIQ Acid

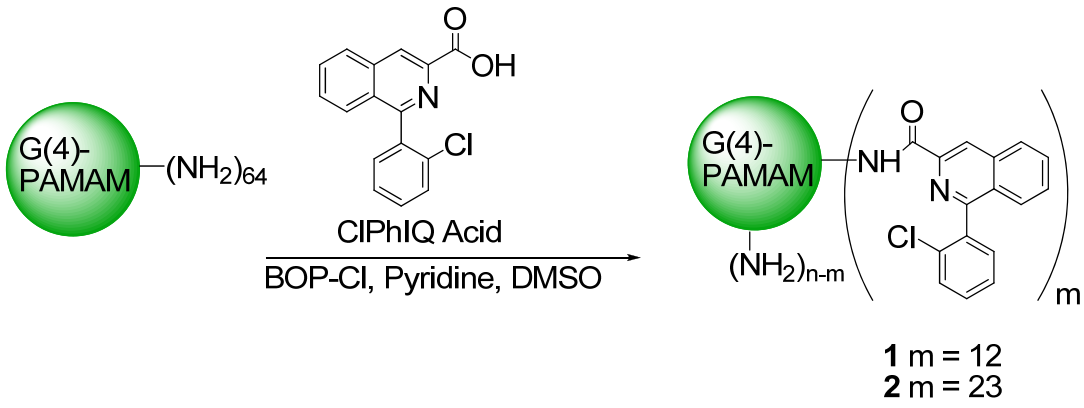

Scheme 2.1: Synthesis of ClPhIQ-PAMAM.

(Scheme 2.1) was activated with benzotriazol-1-yloxytris(dimethylamino)-phosphonium hexafluorophosphate (BOPCl), in pyridine and dimethyl sulphoxide

(DMSO) to a solution of G(4)-PAMAM dendrimer in DMSO. An average of 12 and 23 ClPhIQ Acids were attached by reacting G(4)-PAMAM dendrimer with 15 and 30 molar equivalents of the activated TSPO ligand respectively to obtain two ClPhIQ-PAMAM compounds, **1** and **2** (Scheme 2.1). Excess ClPhIQ Acid and coupling agent were removed by diafiltration with a molecular weight cut off (MWCO) of 5 kDa. Both ClPhIQ-PAMAM molecules were characterized with nuclear magnetic resonance (NMR) and matrix assisted laser desorption ionization time of flight mass spectrometry (MALDI-TOF-MS).

2.3 Characterization of ClPhIQ-PAMAM-Liss

The average number of TSPO ligands per dendrimer was estimated using NMR integrations. It was shown from proton NMR spectra of the PAMAM and ClPhIQ pieces individually that the aromatic proton signals are exclusively from the ClPhIQ Acids attached (7.0-7.9 ppm) to the particle (Figure 2.1); while the interior PAMAM methylenes are the only signal observed from 2-4 ppm (Figure 2.2) and the amides are found from 8.4-9 ppm (Figure 2.2). By calculation there are approximately 930 methylene protons in a G(4)-PAMAM dendrimer and 9 protons (all aromatic) per ClPhIQ Acid molecule. To determine the average number of ClPhIQ Acids per dendrimer, the integral from 7.0-8.2 was calibrated to 9 and the resulting integral from 2-4 ppm was divided into 930. As shown in Figure 2.3, we find 23 ClPhIQ Acids attached to the dendrimer when the dendrimer was reacted with 30 equivalents of ClPhIQ Acid. NMR spectra indicate that 12 ClPhIQ acids are attached when 15 equivalents of ligand are

reacted with the dendrimer (Figure 2.4). The amount of ClPhIQ that binds to the dendrimer nearly doubles (from 12 to 23) with doubling the amount of ClPhIQ in the reaction (from 15 to 30).

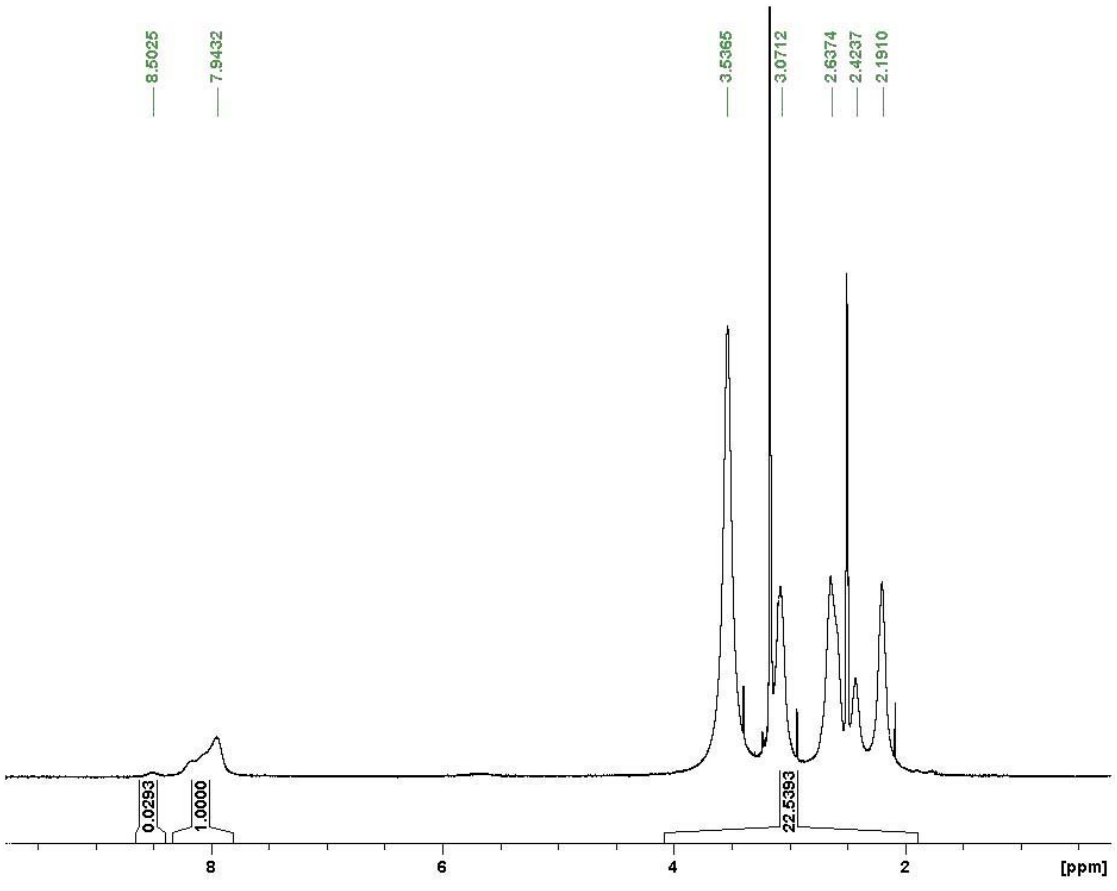

Figure 2.1. ^{1}H NMR of G(4)-PAMAM Dendrimer.

MALDI-TOF MS was also utilized to confirm the average number of ClPhIQ Acids attached to the dendrimer. First a MALDI-TOF spectrum was

acquired of the G(4)-PAMAM with the average molecular weight (MW) found to be 13,244 Daltons (Figure 2.5), significantly lower than the 14,215 Daltons of a G(4)-PAMAM without any of the widely reported structural defects[168]. These defects include incomplete reactions, making one arm of the dendrimer consistently a generation behind, and side reactions that stop the expansion of that branch of dendrimer altogether. The ClPhIQ-PAMAM (**1**) has an average MW of 16,513; and thus, by calculation has 12 ClPhIQ Acid molecules per PAMAM (Figure 2.6). This result is consistent with the NMR data; as was the number of ClPhIQ Acids per PAMAM for ClPhIQ-PAMAM (**2**) with 23 ClPhIQ ligands attached (Figure 2.7). Additionally, it was calculated that ClPhIQ-PAMAM, **2**, to have approximately 24 ClPhIQ Acids per PAMAM, consistent with NMR data.

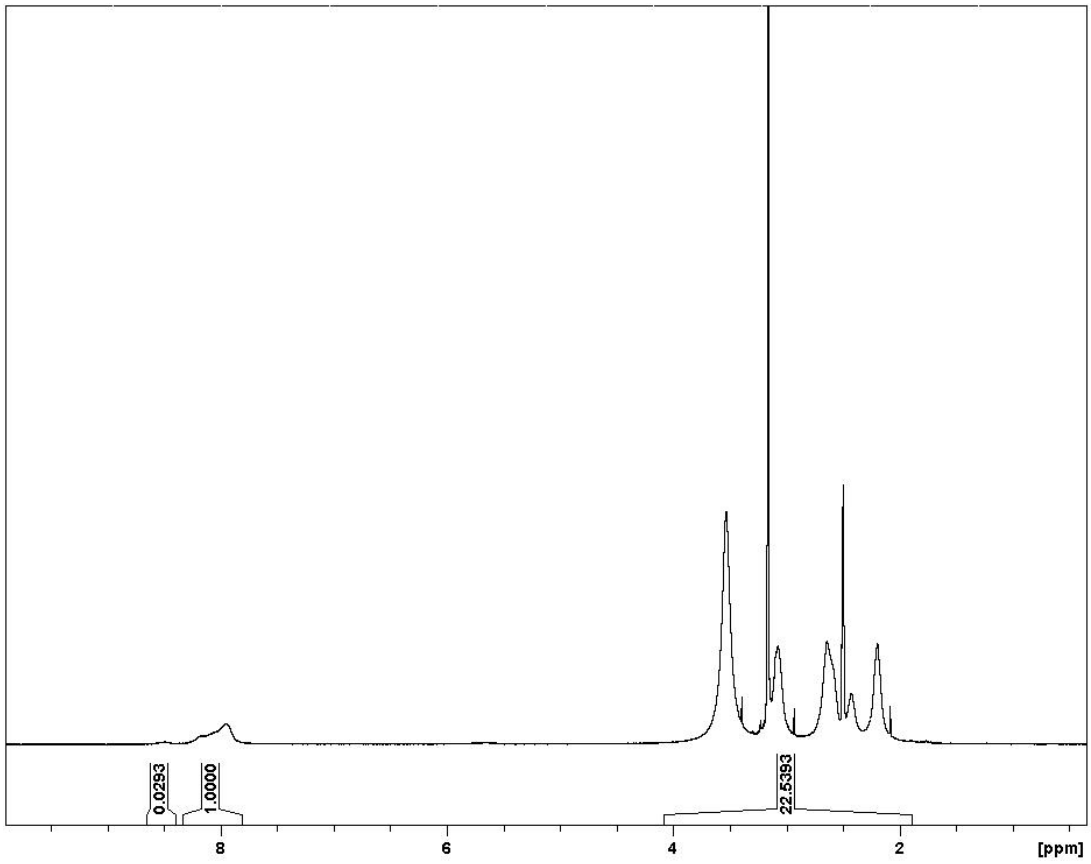

Figure 2.2: ^{1}H NMR of G(4)-PAMAM.

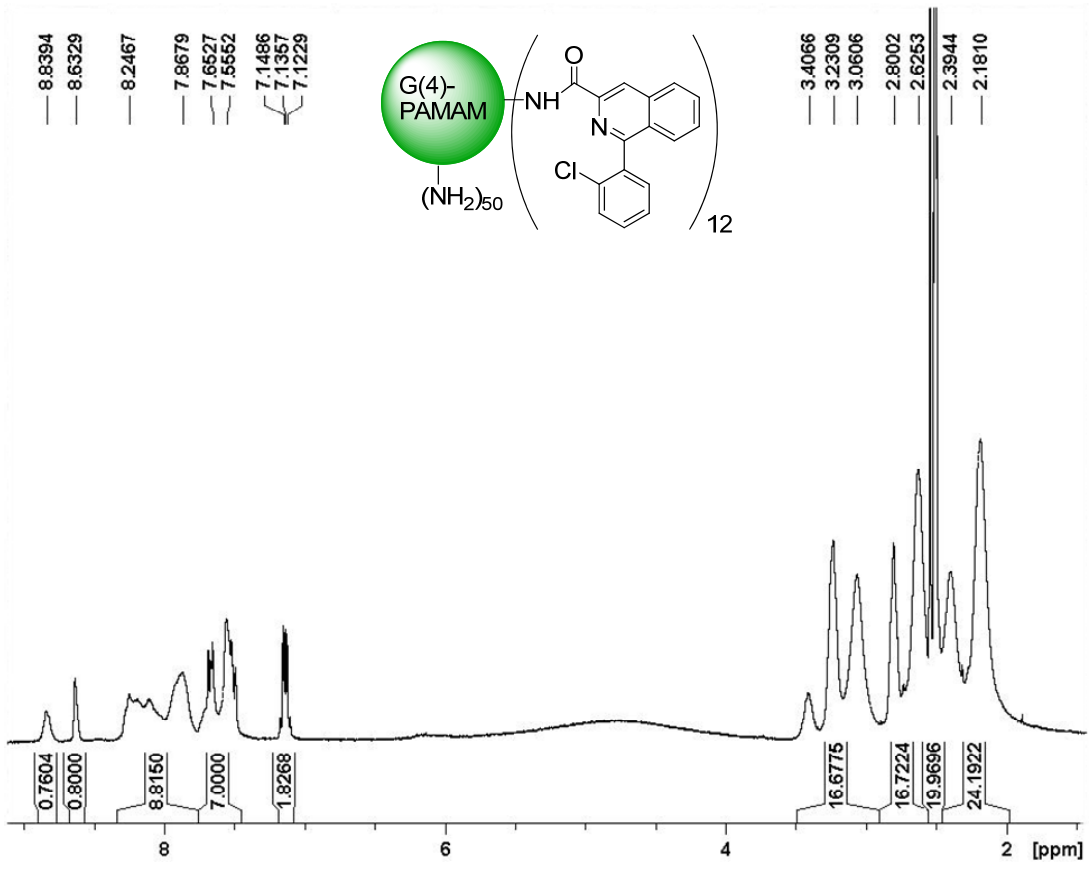

Figure 2.3: ^{1}H NMR of 23 ClPhIQ Acids attached to G(4)-PAMAM (ClPhIQ$_{23}$-PAMAM).

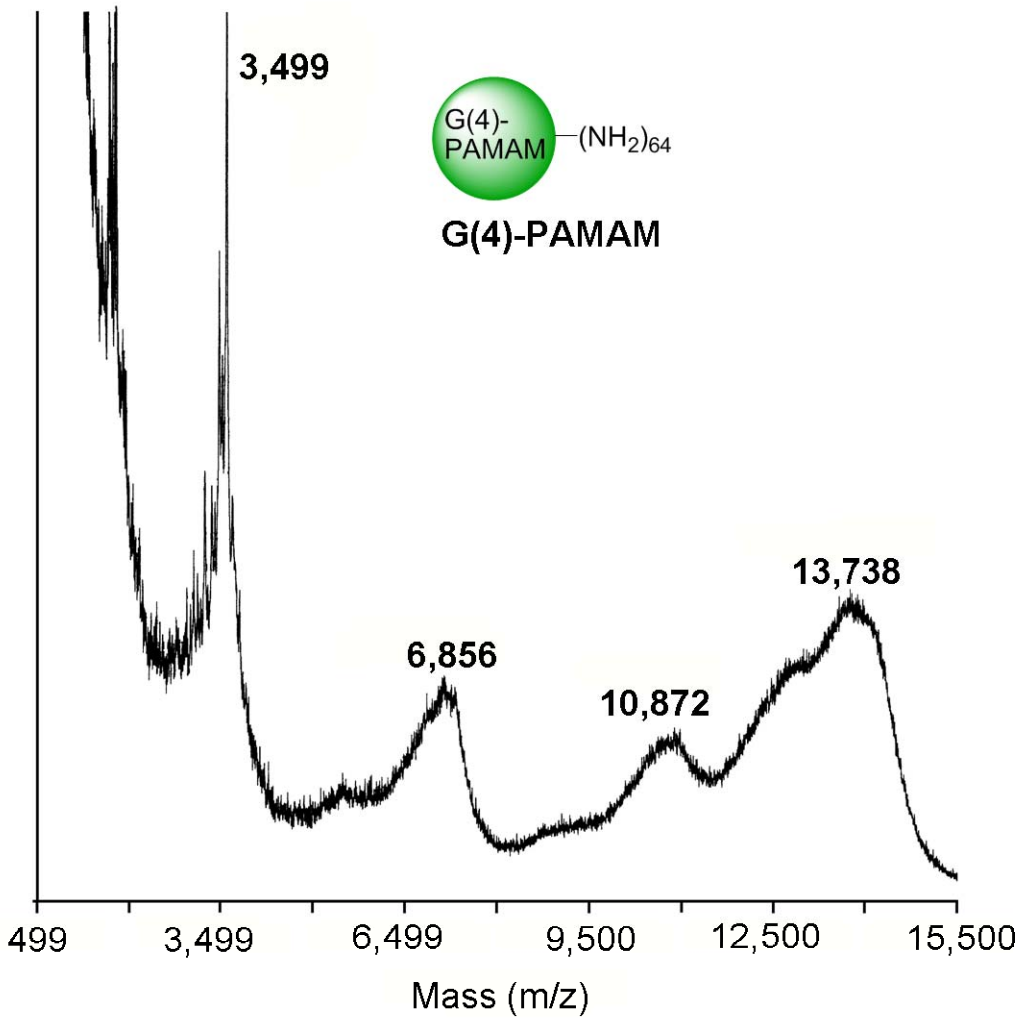

Figure 2.4: MALDI-TOF spectum of G(4)-PAMAM.

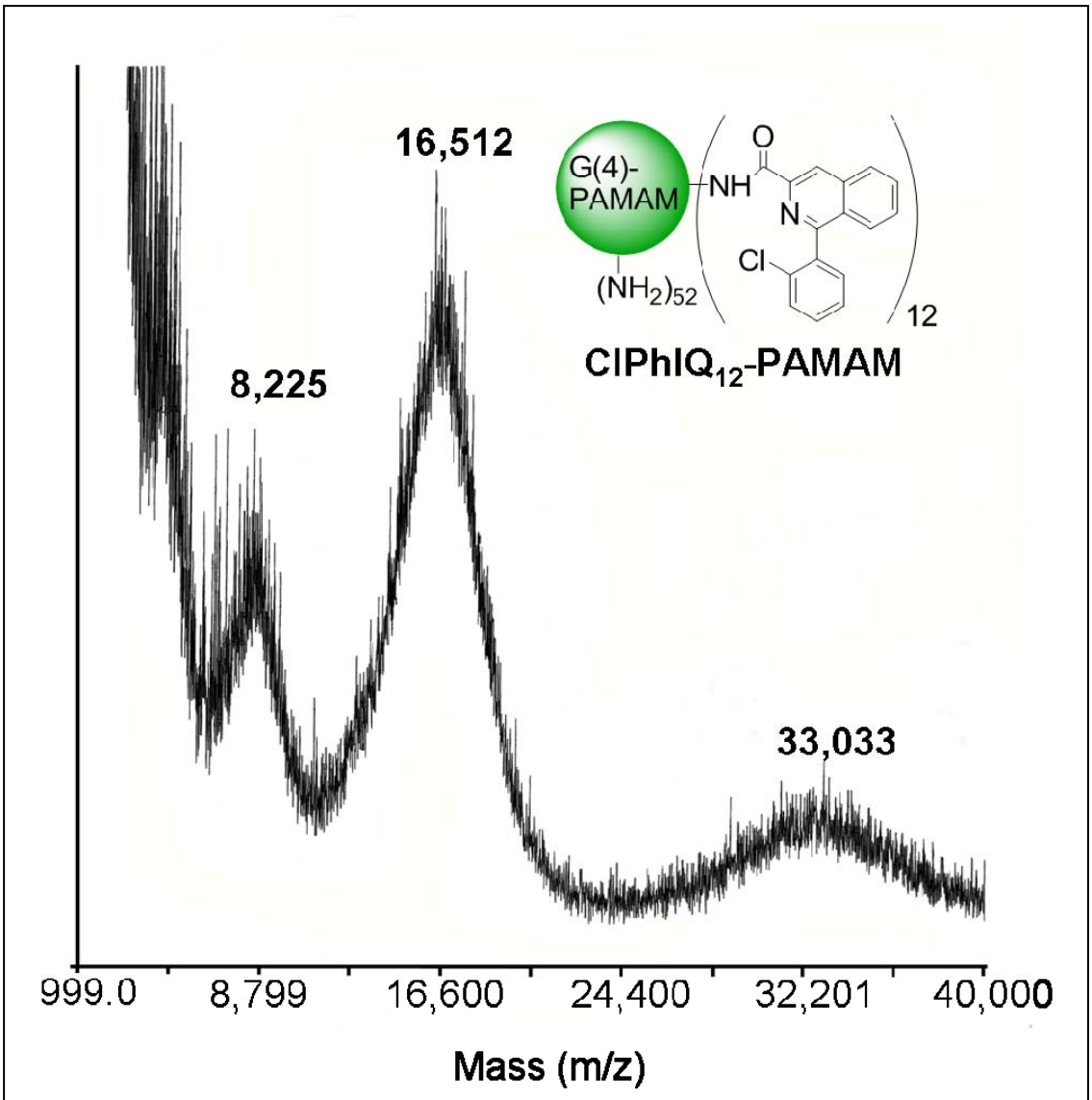

Figure 2.5. Characterization and determination of the average number of ClPhIQ per Dendrimer by MALDI-TOF MS. MALDI-TOF spectrum of $ClPhIQ_{12}$-PAMAM (**1**).

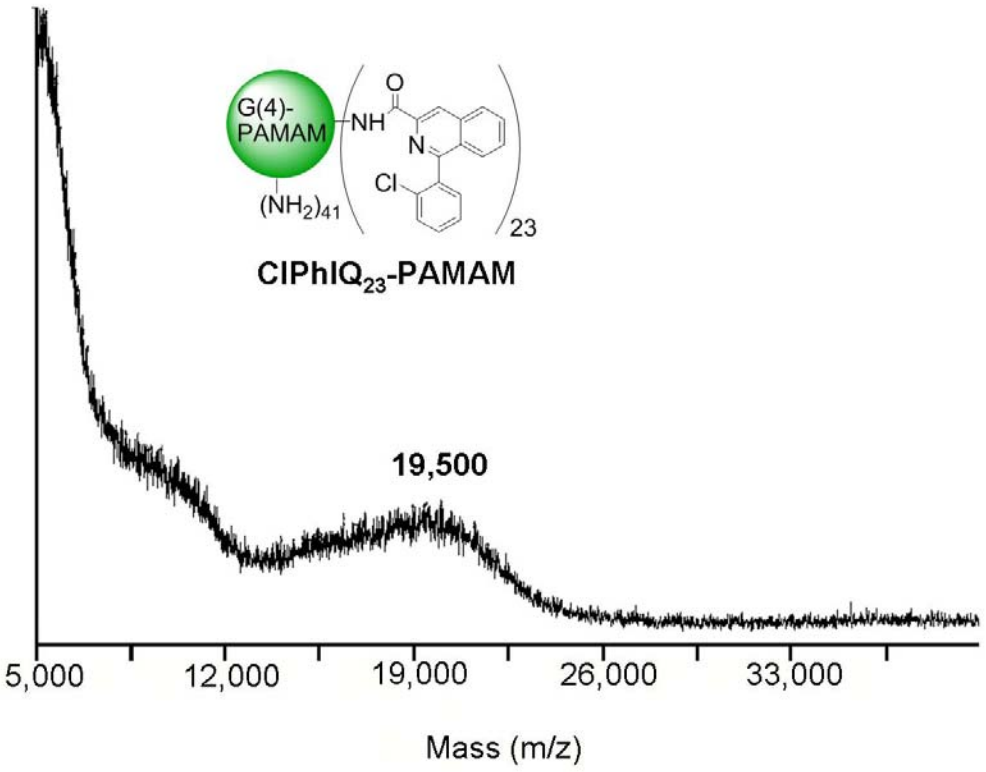

Figure 2.6. Characterization and determination of the average number of ClPhIQ per Dendrimer by MALDI-TOF MS. MALDI-TOF spectrum of $ClPhIQ_{23}$-PAMAM (**2**).

2.4 Synthesis of TSPO-PAMAM-Liss

After characterizing the ClPhIQ-PAMAM molecules with NMR and MALDI-TOF-MS, the dendrimer was further functionalized by reacting it with Lissamine rhodamine B sulfonyl chloride™ (Lissamine or Liss) in dimethyl formamide (DMF) overnight to give 1 or 2 Lissamine dyes per dendrimer (Scheme 2.2). The DMF was removed in vacuo and excess dye was removed by diafiltration (MWCO = 5,000) in water. UV-Vis and fluorescence were employed to characterize the optical imaging agent. Attaching the dye to the dendrimer produced a compound

with an absorbance maximum at 500 nm (versus 550 nm for free dye) and a slightly red shifted emission at 586 nm (versus 583 nm for free dye) as displayed in Figure 2.8. The broadening of the absorbance spectra is due to the large amount of ClPhIQ modalities attached and the PAMAM absorbing as high as 380 nm and the strong signal due to the large number of bonds absorbing; both broadening the UV-Vis spectrum. A control compound (PAMAM-Liss), the

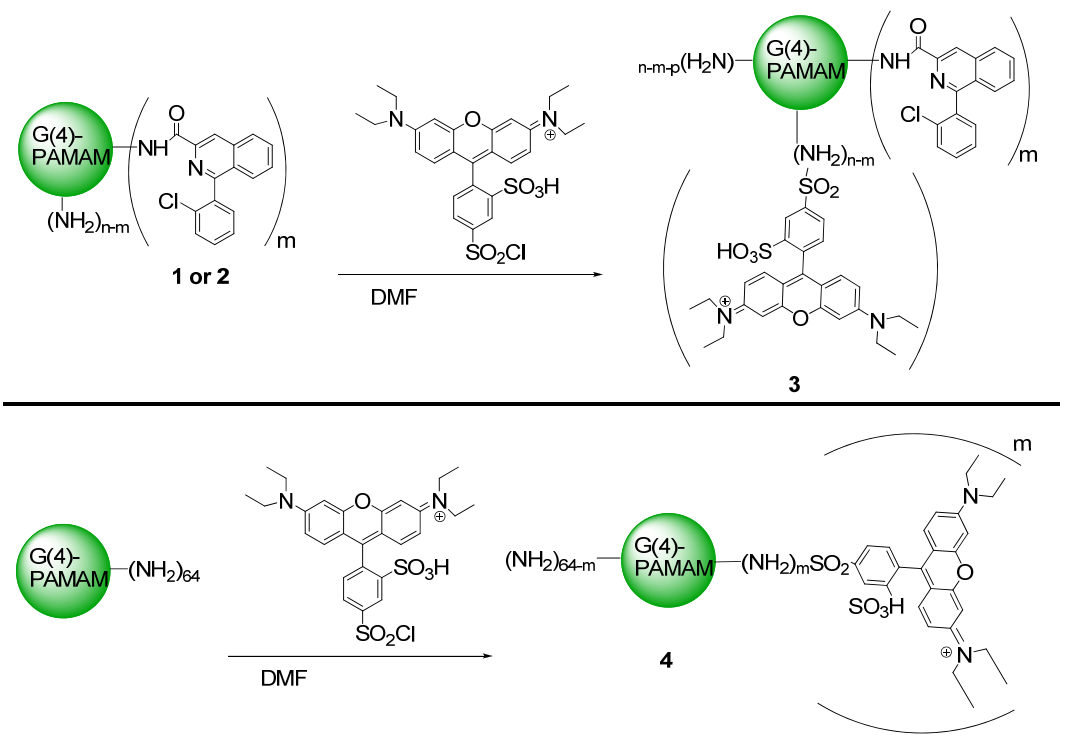

Scheme 2.2: Attachment of Lissamine dye to PAMAM.

agent absent of the targeting moiety, was synthesized similarly to the targeting agent by reacting G(4)-PAMAM dendrimer with Lissamine™ (Scheme 2.2). The

PAMAM-Liss (**4**) conjugate was also purified by diafiltration in which the first low molecular weight fraction was slightly pink (from dye) and subsequent washing resulted in lighter color until no color was present. A minimum of three colorless washing in the low molecular weight fraction was completed to provide pure ClPhIQ-PAMAM-Liss with no unreacted lissamine dye. A molecular weight difference for the PAMAM and PAMAM-Liss of 500 – 600 amu was observed in the MALDI-TOF MS spectrum, consistent with an average of 1 dye per dendrimer.

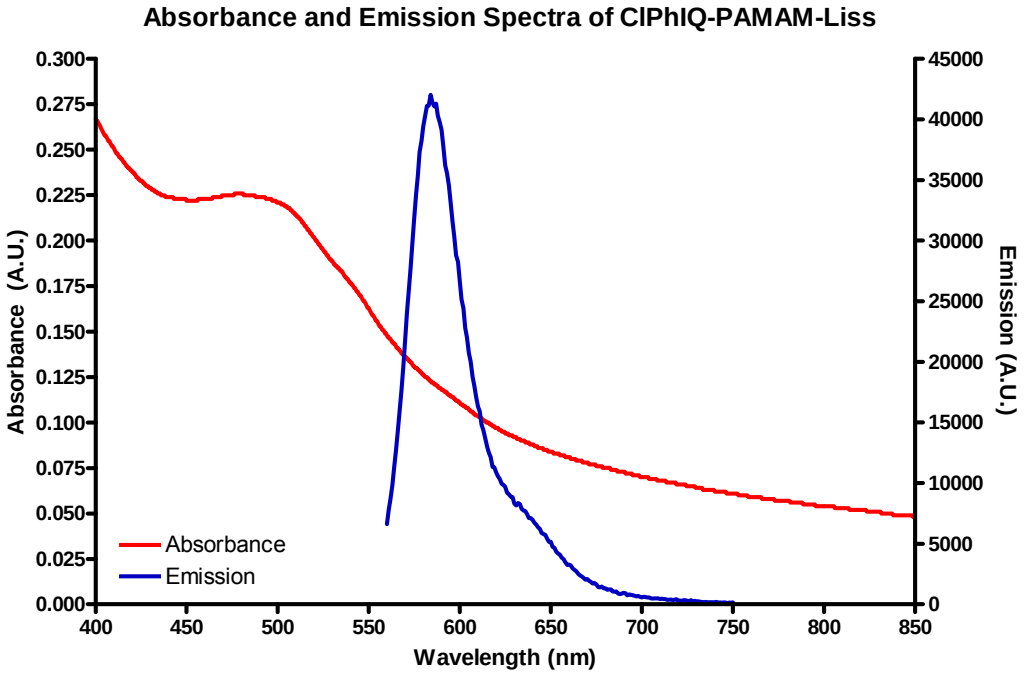

Figure 2.7. The absorbance and emission spectra of ClPhIQ-PAMAM-Liss.

2.5 Imaging of TSPO-PAMAM-Liss

To evaluate the biological activity of the imaging agent, C6 rat glioma cells, shown to express a high concentration of TSPO[169-170], were incubated with

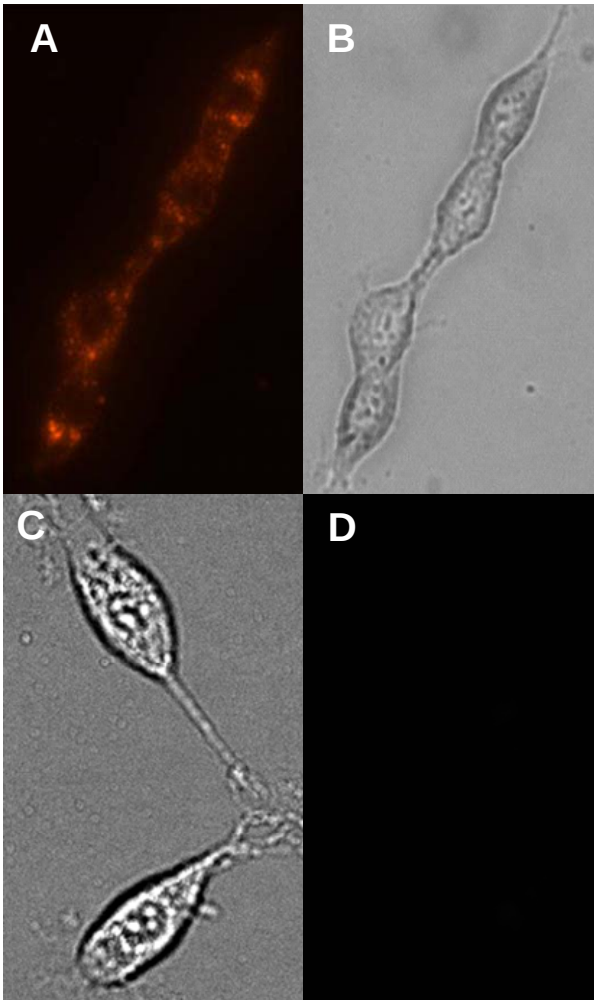

Figure 2.8. Live cell images of C6 rat glioma cells. Panal A: Red fluorescence of ClPhIQ-PAMAM-Liss (**3**) dosed cells; B: DIC image of ClPhIQ-PAMAM-Liss (**4**) dosed cells; C: DIC image of PAMAM-Liss dosed cells; D: Red Fluorescence image of PAMAM-Liss dosed cells.

ClPhIQ-PAMAM-Liss (**3**) or PAMAM-Liss (**4**) for 12 hours in collagen coated MatTek™ dishes and visualized by fluorescence microscopy. Live cell imaging was preformed immediately after rinsing the cells with PBS or saline to remove media and unbound or un-internalized imaging agent. A Nikon Eclipse TE2000-U fluorescence microscope (Lewisville, TX) equipped with Texas Red and FITC filter sets was employed for the *in-vitro* imaging. As shown in Figure 2.8, the ClPhIQ-PAMAM-Liss labels the cell, while the control (PAMAM-Liss) does not produce fluorescence. As another control, cells were incubated with Lissamine and again no fluorescence was observed. The imaging experiments were performed in triplicate with observations being consistent with respect to absorbance and fluorescence intensity and the absence of fluorescence in the controls. We hypothesize that the dendrimer with the TSPO binding ligand (ClPhIQ-PAMAM-Liss, **3**) produced bright, localized, cellular fluorescence due to its ability to pass through the cellular membrane and bind to the target protein TSPO (Figure 2.9). Since ClPhIQ Acid conjugated dye is known to bind TSPO, glioma cells overexpress TSPO and it is an organellular protein, we believe that the dendrimer labels the mitochondria by binding to TSPO. In the labeling experiment where the dendrimer without the targeting ligand (compound **4**) was used, no fluorescence was found in the cell at exposure times as long as 5 seconds. Taken together these results indicate that the ClPhIQ moiety is necessary for cellular uptake of the dendrimer at labeling concentrations of 1 μM and equilibration times of 6-12 hours.

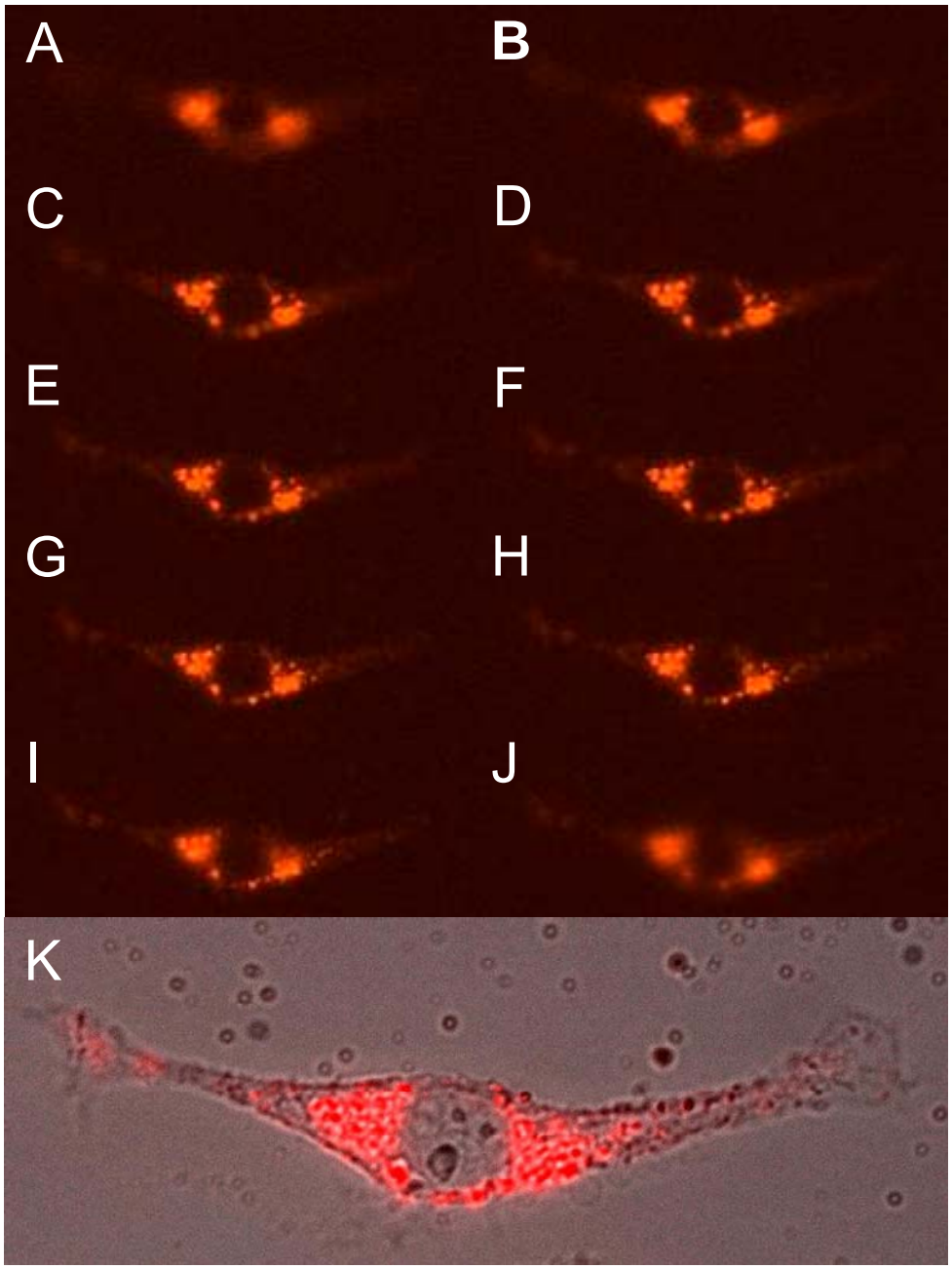

Figure 2.9. Selected montage of red fluorescence images of ClPhIQ-PAMAM-Liss (**4**) dosed cells from the z series. Panel A: slice 10; B: slice 15; C: slice 20; D: slice 21; E slice 22; F: slice 23; G: slice 24, H: slice 325; I: slice 30; J: slice 35; K: DIC Fluorescence overlay.

To further confirm that the agent was intracellular, a series of z stacked images (pseudo-confocal) were obtained allowing different regions of the cells to be viewed (Figure 2.10). These z stacked images were accomplished by changing the lens position incrementally, moving the focal planes of the microscope through cells and collecting the images by viewing fluorescence. In the center focal planes there is a dark hole, consistent with the nucleus as shown in the fluorescence-DIC overlay (Figure 2.10 panel K). This observation suggests that the agent undergoes internalization, passive or active, and does not just label the membrane due to lipophilic nature of the ClPhIQ moiety. Since only a small amount of out-of-focus light is observed in the membrane slices of the z stacked images, labeling of the membrane appears to be negligible. Furthermore, fluorescence signal is observed through the cell to the entire nuclear membrane, but not in the nucleus, indicating uptake of the dendrimer by the cells but not the nucleus. Previously reported small molecule agents have not labeled the nucleus, even though low concentrations of TSPO are present there[28]. The reported macromolecular agent behaved as expected and targeted the mitochondria and was not up-taken into the nucleus as indicated in Figure 2.10.

To further explore that ClPhIQ-PAMAM-Liss was targeting the mitochondria, a co-incubation experiment was preformed. This was accomplished by first incubating C6 rat glioma cells with ClPhIQ-PAMAM-Liss as described above for the live cellular imaging, followed by fixation using paraformaldehyde, and then treatment of the cells with Mitotracker Green™

(MTG) according to the manufacturer's guidelines. The cells were then imaged using a Texas Red filter set to interrogate the Lissamine (red) fluorescence and a FITC filter set to detect the MTG (green) fluorescence. Figure 2.11 shows C6 rat glioma cells incubated with either ClPhIQ-PAMAM-Liss or the control, PAMAM-

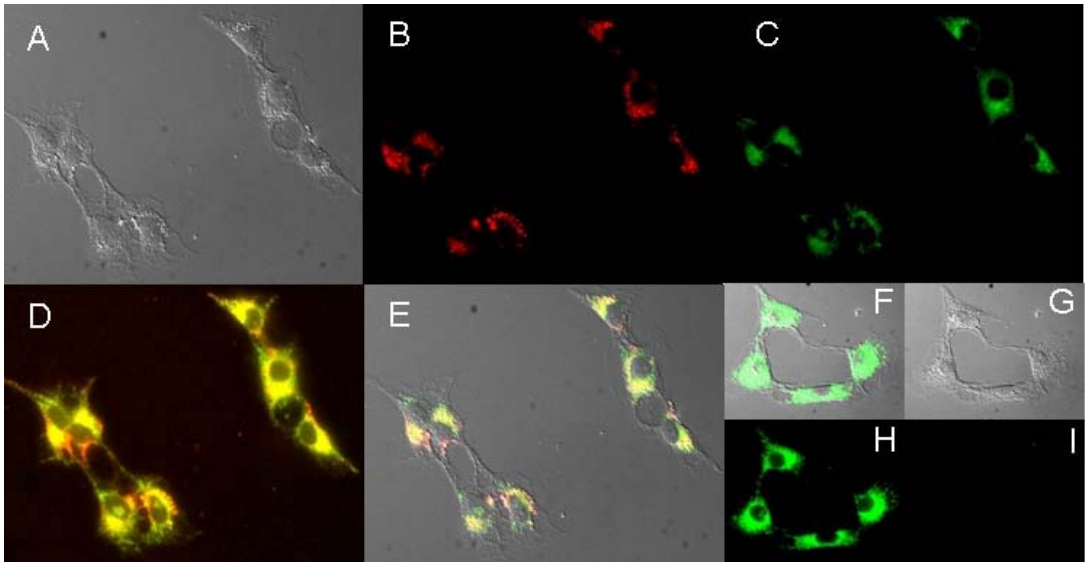

Figure 2.10. Fluorescence Images of fixed C6 rat glioma cells. Panal A: DIC of $ClPhIQ_{23}$-PAMAM-Liss (**2**) and MTG dosed cells; B: Red fluorescence of $ClPhIQ_{23}$-PAMAM-Liss (**2**) and MTG dosed cells; C: Green fluorescence of $ClPhIQ_{23}$-PAMAM-Liss (**2**) and MTG dosed cells; D: Red and Green fluorescence overlay of $ClPhIQ_{23}$-PAMAM-Liss (**2**) and MTG dosed cells; E: DIC, Red and Green fluorescence overlay of $ClPhIQ_{23}$-PAMAM-Liss (**2**) and MTG dosed cells; F: DIC, Red and Green Fluorescence overlay of PAMAM-Liss (**4**)and MTG dosed cells; G: DIC of PAMAM-Liss (**4**) and MTG dosed cells; H: Green fluorescence of PAMAM-Liss and MTG dosed cells; and I: Red fluorescence of PAMAM-Liss (**4**) and MTG dosed cells.

Liss. The DIC images in Figure 2.11A and 2.11G are present to indicate the location of the cells relative to fluorescence signal of ClPhIQ-PAMAM-Liss

(Figure 2.11A) and PAMAM-Liss dosed cells (Figure 2.11G). Fluorescence from the imaging agent is displayed in red (Figure 2.11B) and fluorescence from the MTG as green (Figure 2.11C). As demonstrated above with live cell imaging, the ClPhIQ-PAMAM-Liss (**2**) agent labels the fixed cells principally perinuclear (Figure 2.11B). The MTG labels the mitochondria of cells, as shown by numerous investigators[171-172], particularly when used in low concentrations as those employed here (25nM). MTG was used in low concentration (25 nM) to ensure that it primarily labeled only the mitochondria. More careful interrogation of the fluorescence signals allow an insight about where the species are within the cell. Figure 2.11 panels D and E display co-registration of ClPhIQ-PAMAM-Liss (**2**) and MTG with yellow indicating areas of overlap while red and green indicate areas where ClPhIQ-PAMAM-Liss (**2**) (red) and MTG (green) are not coincident. It is encouraging to see that most of the red and green converge to yellow, indicating that the majority of ClPhIQ-PAMAM-Liss (**2**) is in the same location of the cell as the MTG. This good co-localization is further evidence that ClPhIQ-PAMAM-Liss (**2**) is labeling the mitochondria and not other parts of the cell. As demonstrated in Figure 2.11 panels F – I and in the live cell imaging (Figure 2.9), fluorescence from the dendrimer is only detected if ClPhIQ Acid is incorporated into the dendrimer. In other words, images from cells inoculated with the control agent (PAMAM-Liss) exhibit no fluorescence (Figure 2.11I). MTG fluorescence was not affected (Figure 2.11C, F&H) by the presence or absence of dendrimer agent and the cellular membrane was not perturbed by non-physiological chemical or physical processes prior to or during the incubation

with ClPhIQ-PAMAM-Liss. Excess imaging agent was removed prior to fixation in all experiments. Taken together, the fluorescence images in Figure 2.11 indicate that the ClPhIQ-PAMAM-Liss is targeting the mitochondria and that the ClPhIQ ligand is necessary for this mitochondrial labeling to occur. The z stacked images and co-incubation experimental results indicate that the imaging agent is internalized into the cell through normal cellular functions. Although no quantitative binding studies were performed, the agent binds with high enough affinity to remain in the cell after fixation, washing and treatment with MTG.

Further evidence of the utility of ClPhIQ-PAMAM-Liss (**2**) was demonstrated by labeling MDA-MB-231 human breast cancer cells, an aggressive human cancer cell line. Like the C6 rat glioma cells, the MDA-MB-231 human breast cancer cells have been shown to over express TSPO [156]. The cells were incubated with ClPhIQ-PAMAM-Liss (**2**) following the same procedures as with the C6 rat glioma cells, fixed and treated with MTG for co-registration investigations. The individual red and green fluorescence of ClPhIQ-PAMAM-Liss (**2**) and MTG respectively in fixed MDA-MB-231 cells is demonstrated in panels A and C of Figure 2.12; while, panels E and F show the lack of red fluorescence in the PAMAM-Liss treated cells. Association between the red and green (shown in yellow) is evident in the overlays of panels B and D indicating co-localization of the ClPhIQ-PAMAM-Liss (**2**) and MTG. These additional results represent further evidence that ClPhIQ-PAMAM-Liss (**2**) is able to label TSPO rich mitochondria in cancer cells.

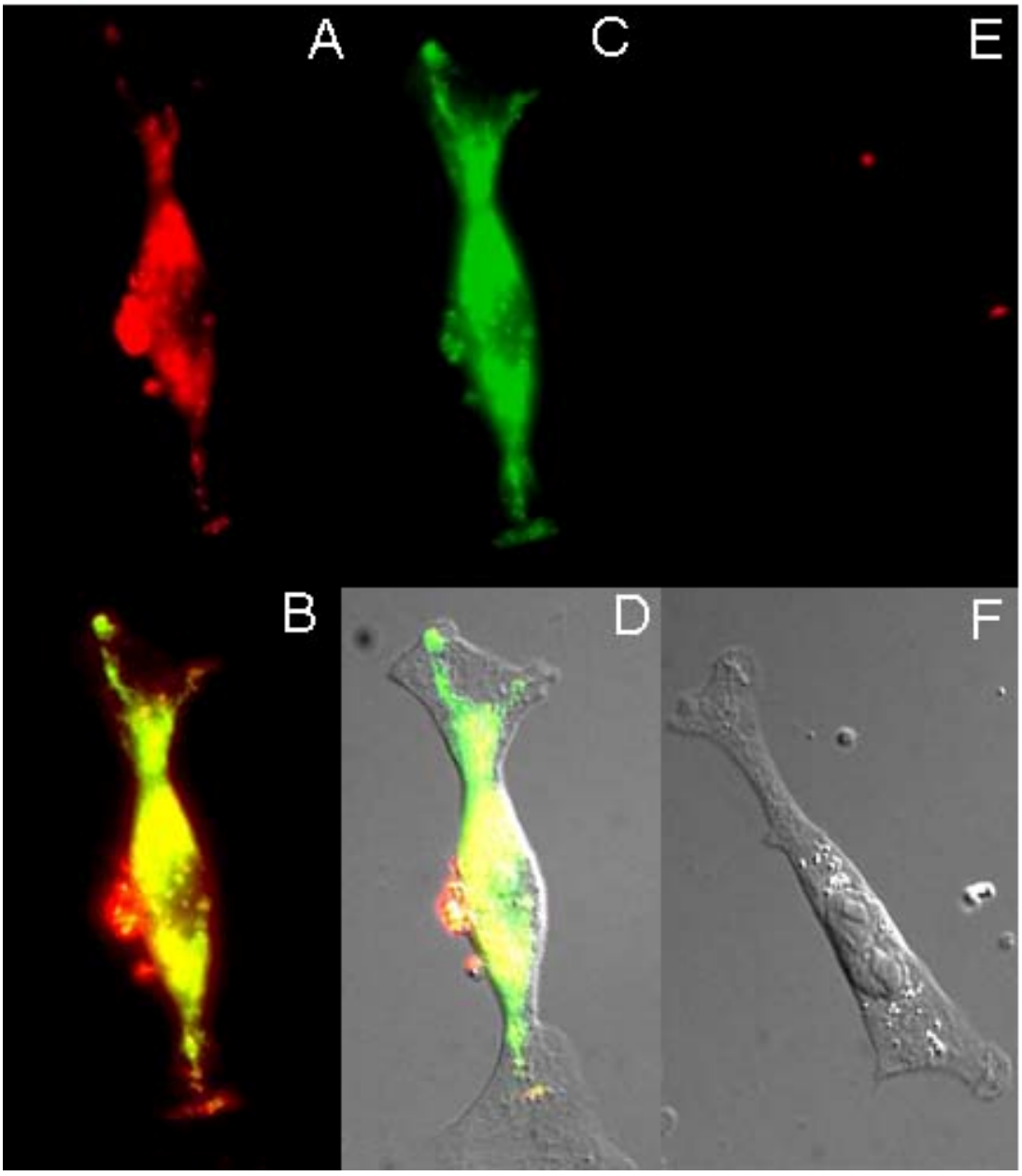

Figure 2.11. Microscope images of MDA-MB-231 cells. Panal A: Red fluorescence of ClPhIQ$_{23}$-PAMAM-Liss (**2**) and MTG dosed cells; B: Red and Green Fluorescence overlay of ClPhIQ$_{23}$-PAMAM-Liss (**2**) and MTG dosed cells; C: Green fluorescence of ClPhIQ$_{23}$-PAMAM-Liss (**2**) and MTG dosed cells; D:Red and Green Fluorescence and DIC overlay of ClPhIQ$_{23}$-PAMAM-Liss (**2**) and MTG dosed cells; E: Red fluorescence of PAMAM-Liss (**4**) dosed cells; F: DIC image of PAMAM-Liss (**4**) dosed cells.

2.6 Synthesis and Characterization of ClPhIQ-PAMAM-Gd-Liss

The ClPhIQ-PAMAM-Liss-Gd dendrimer was synthesized starting with ClPhIQ-PAMAM and reacting 1,4,7,10-Tetraazacyclododecane-1,4,7-tris(t-butyl acetate)-10-succinimidyl acetate (tri-T-butyl-DO3A-NHS) in DMSO to give ClPhIQ-PAMAM-tBuDO3A (**5**). Unreacted tri-T-butyl-DO3A-NHS and other low molecular weight byproducts were removed by diafiltration with a 5 kDa. MWCO. NMR and MALDI-TOF MS were used to characterize the number of tri-T-butyl-DO3A molecules attached to the dendrimer. The integration of the t-butyl methyl peak at 1.4 ppm was compared to the aromatic protons from the ClPhIQ ligands attached to the dendrimer to determine the ratio of TSPO ligand (as characterized above) to the metal chelate. Typically, reacting a dendrimer with 23 ClPhIQ ligands with 30 equivalents of tri-T-butyl-DO3A resulted in an

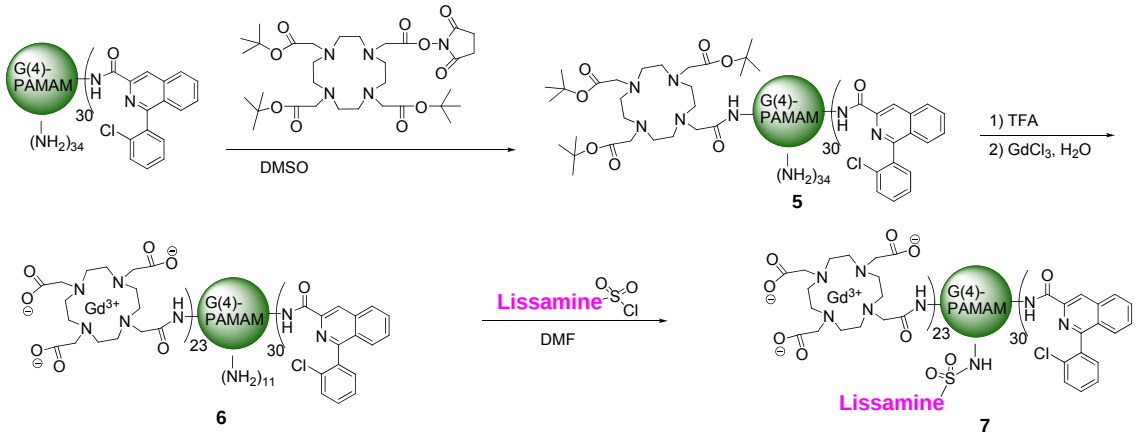

Scheme 2.3: Synthesis of G(4)-PAMAM TSPO targeted MRI and Fluorescence agent.

average attachment of 23 metal chelates per dendrimer. Next, in two steps, the t-butyl groups were removed by treatment with trifluoroacetic acid (TFA) and the resulting carboxylates on the DO3A were chelated with gadolinium by reaction with gadolinium trichloride in water. Characterization with NMR (pre-chelation) and MALDI-TOF MS (pre and post chelation) verified the desired reactions were completed. The MALDI-TOF MS of ClPhIQ-PAMAM-DO3A prior to chelation displays and average mass of 26,500 amu (Figure 2.13). This is consistent with the attachment of 18 chelates per PAMAM.

Finally, Lissamine was reacted with dendrimer **2** in DMF to produce a TSPO targeted molecule with dual imaging modalities (MR and Fluorescence). The fluorophore attachment was observed through characterization with MALDI-

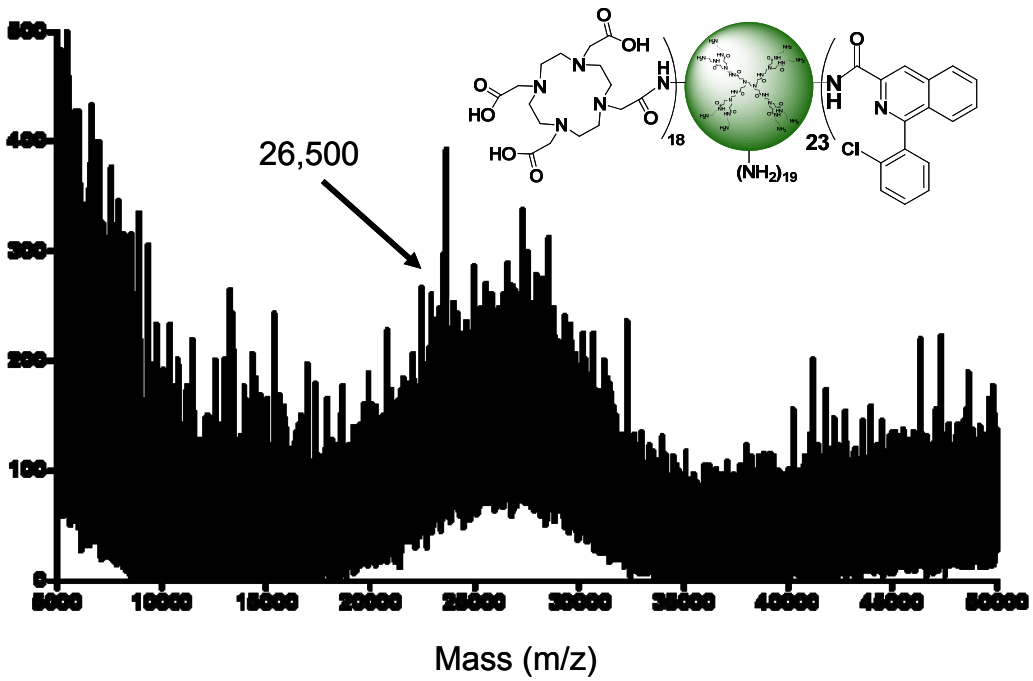

Figure 2.12. MALDI-TOF Spectrum of ClPhIQ-PAMAM-DO3A.

TOF MS (31,000 a.m.u.), UV-Vis (max absorbance at 551 nm) and fluorescence (ex. 551 nm, em. 586 nm) spectroscopy. As a control molecule, PAMAM-Gd was synthesized as described with ClPhIQ-PAMAM-Gd (**6**), by stating with unfunctionalized G(4)-PAMAM.

2.7 Fluorescence Imaging of ClPhIQ-PAMAM-Gd-Liss

Cellular internalization studies were first accomplished with fluorescence microscopy. Both MDA-MB-231 and C6 rat glioma cells were imaged with ClPhIQ-PAMAM-Gd-Liss. Fluorescence microscopy images were taken on a Nikon Eclipse TE2000-U fluorescence microscope (Lewisville, TX) equipped with Texas Red and FITC filter sets. The fluorescence samples were prepared by incubating the dendrimer with either C6 rat glioma or MDA-MB-231 human breast cancer cells for 6-18 hours in microscopy bottomed MatTek™ dishes, followed by removal of excess imaging agent by 3 - 4 washings with saline. In the first experiment, MDA-MB-231 cells were imaged live. As seen in Figure 2.14, the TSPO targeted imaging agent labels MDA-MB-231 cells. The overlay of the fluorescence and DIC images indicate that the imaging agent is perinuclear (Figure 2.14, panels A & B); as expected since TSPO is primarily located on the mitochondria. No perturbation of the cellular membrane was performed, indicating that the imaging agent is labeling the mitochondria via normal biological processes. A series of Z-stacked images (data not shown) show fluorescence from the dendrimer in the cell on several planes and not solely on

the cell surface. The control compound, PAMAM-Liss (**4**), did not label the cells at higher fluorescence integration times and higher concentrations of molecule (Figure 2.14, panels C & D). As with the ClPhIQ-PAMAM-Liss (**4**) molecule, the indication is that the ClPhIQ moiety is necessary for the labeling and internalization of the imaging agent into the cell.

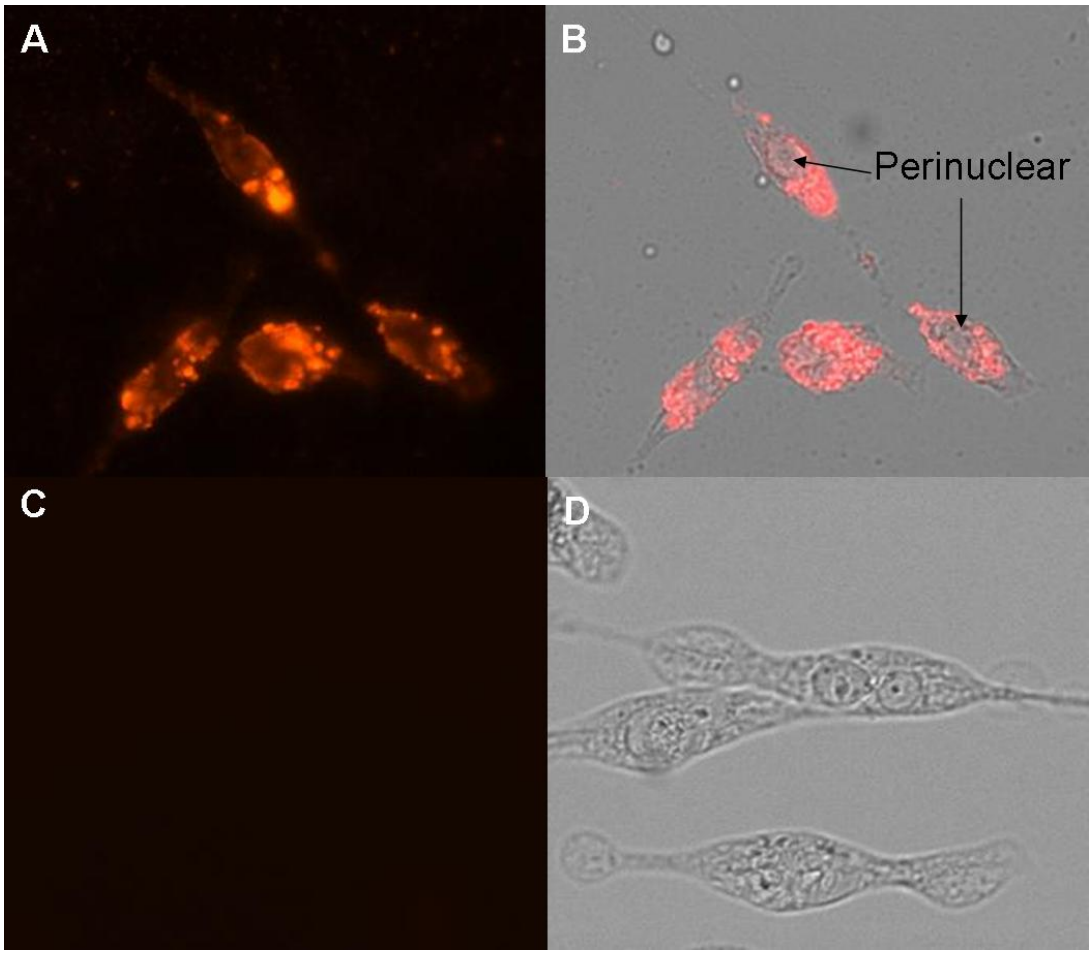

Figure 2.13. Cellular images of MDA-MB-231 cells dosed with ClPhIQ-PAMAM-Gd-Liss (**7**) and PAMAM-Liss. Panel A: Red Fluorescence image of ClPhIQ-PAMAM-Gd-Liss (**7**); Panal B: DIC and Red Fluorescence overlay of ClPhIQ-PAMAM-Gd-Liss (**7**); Panal C: Red Fluorescence image of PAMAM-Liss (**4**); Panal D: DIC image of PAMAM-Liss (**4**).

Further cellular fluorescence studies were completed in C6 rat glioma cells with commercially available Mitotracker Green™ (MTG). The cellular labeling was completed using the procedure described for the MDA-MB-231 cells, but after incubation, the cells were fixed with 4% para-formaldehyde and treated with 25 nM MTG immediately before imaging. MTG is a commercially available small molecule known to label mitochondria and has fluorescence properties (ex. 490 nm & em 516 nm) complementary to ClPhIQ-PAMAM-Gd-Liss (**7**) and our microscope. The ClPhIQ-PAMAM-Gd-Liss (**7**) was imaged using a Texas Red filter set while the MTG was imaged with a FITC filter set. Fluorescence bleeding was tested with cell plates that were dosed with either MTG or ClPhIQ-PAMAM-Liss-Gd (**7**) and imaged using both filter sets. No signal bleed-through was seen for either molecule when images with the improper filter set.

In Figure 2.15 panel A displays the MTG (FITC filters) fluorescence and panel B displays the ChPhIQ-PAMAM-Liss-Gd (**7**) (Texas Red filters) fluorescence in C6 rat glioma cells. Figure 2.15, Panel C is an overlay of panels A & B; coincident fluorescence from the MTG and the fluorescence from the ClPhIQ-PAMAM-Liss-Gd (**7**) appear yellow and non-coincident fluorescence is red (ClPhIQ-PAMAM-Liss-Gd) (**7**) or green (MTG). Very little green or red is seen and yellow dominates the image. The co-incubation evidence suggests that the ClPhIQ-PAMAM-Liss-Gd (**7**) and MTG are located in the same intracellular location as seen with the ClPhIQ-PAMAM-Liss (**2**). Since TSPO is found on the mitochondria and MTG is designed to bind mitochondria, this observation suggests that ClPhIQ-PAMAM-Liss-Gd (**7**) is binding to the

mitochondria. Since the ClPhIQ-PAMAM-Gd-Liss (**4**) was shown to bind TSPO, which is located on the mitochondrial membrane; mitochondria labeling was expected as confirmed in the fluorescence images. The culmination of all the fluorescence data provides strong evidence that the ClPhIQ-PAMAM molecules are internalized into cells by normal biological processes and bind to the

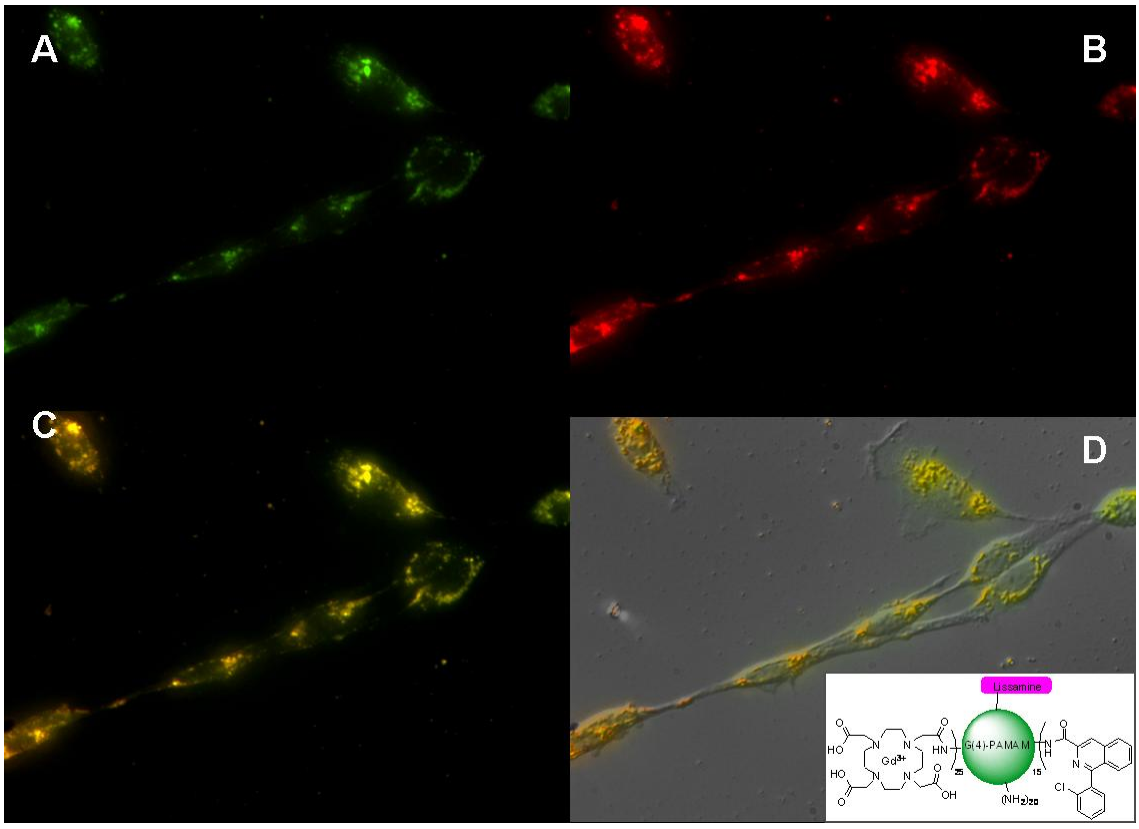

Figure 2.14: Cellular co-localization in C6 Rat Glioma cells and co-incubation with Mitotraker Green. Panel A: Fluorescence of MTG. Panel B: Fluorescence of ClPhIQ-PAMAM-Gd-Liss (**7**). Panel C: Fluorescence overlay of MTG and ClPhIQ-PAMAM-Gd-Liss (**7**) fluorescence. Yellow indicates co-registration. Panel D: The fluorescence overlay of MTG and ClPhIQ-PAMAM-Gd-Liss (**7**) onto the DIC image.

mitochondria. To further examine the utility of the ClPhIQ-PAMAM molecules binding affinity to TSPO, T1 and T2 relaxation (for Gd^{3+} containing molecules) and EM studies were completed.

2.8 Binding studies of ClPhIQ-PAMAM-Gd to TSPO

A radioligand binding study of the ClPhIQ-PAMAM-Gd (**6)** was completed by Mingfeng Bai performing a competition assay using the tritiated ligand [^{3}H]PK11195 as the competitor. The [^{3}H]PK11195 ligand was used because it has the most similar structure to ClPhIQ. PK11195 is the best previously characterized ligand[27-28, 36] to compete with ClPhIQ binding. Displacement

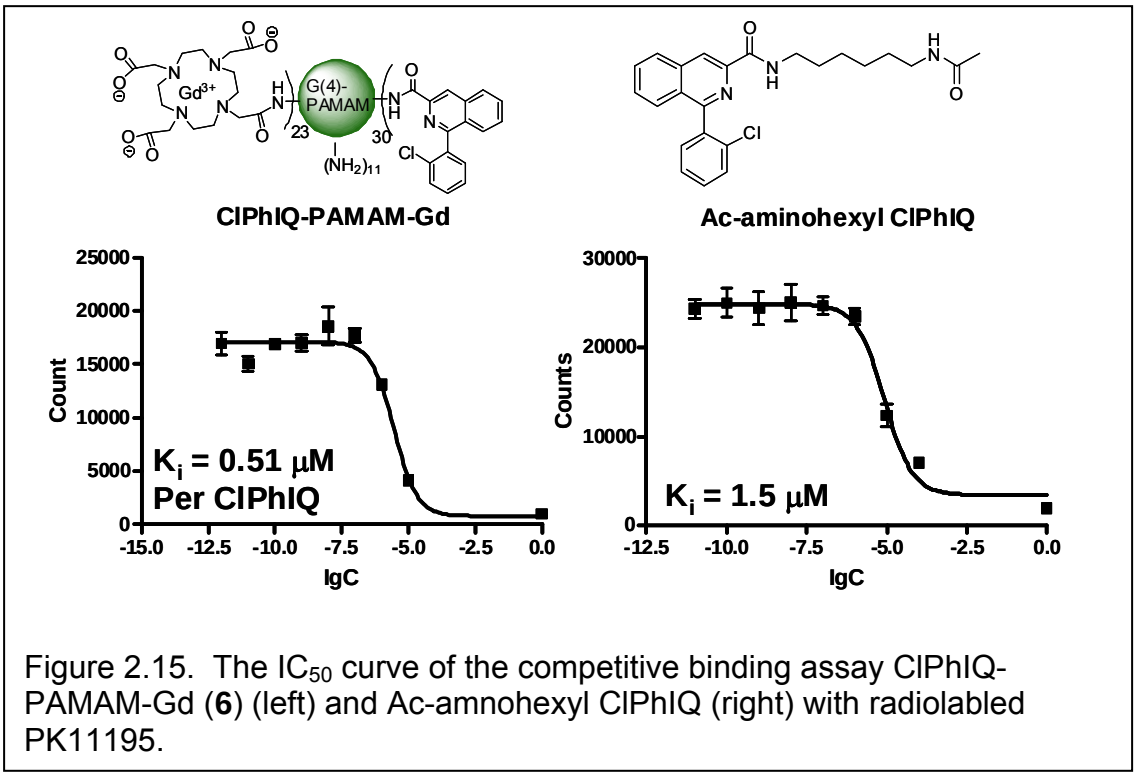

Figure 2.15. The IC_{50} curve of the competitive binding assay ClPhIQ-PAMAM-Gd (**6**) (left) and Ac-amnohexyl ClPhIQ (right) with radiolabled PK11195.

studies using increasing concentrations of ClPhIQ-PAMAM-Gd (**6**) were performed in the presence of 15 nM [^{3}H]PK11195 to obtain the IC_{50} curve (Figure 2.15). Radiobinding assays were also performed on an acetate capped aminohexyl ClPhIQ (Ac-aminohexyl ClPhIQ) compound. The ClPhIQ-PAMAM-Gd was found to have a K_i of 510 nM per ClPhIQ ligand while the Ac-aminohexyl ClPhIQ has a binding affinity of 1.5 μM. These results indicate that having several molecules attached to a dendrimer improves the binding capabilities of ClPhIQ 3 fold.

2.9 MR studies of ClPhIQ-PAMAM-Gd

Having Gd^{3+} chelated to the TSPO targeted dendrimer allows for two new imaging methods to be utilized: MRI and EM. Previous studies have found increased rates of relaxation in both T1 and T2 experiments using nanoparticles,

Table 2.1 Relaxivities of PAMAM-Gd compounds.

Compound	T1 Relaxation per Gd^{3+} ($mM^{-1}s^{-1}$)	T1 Relaxation per PAMAM ($mM^{-1}s^{-1}$)	T2 Relaxation per Gd^{3+} ($mM^{-1}s^{-1}$)	T2 Relaxation per PAMAM ($mM^{-1}s^{-1}$)
Magnevist™	4.8±0.044	-	5.6±0.13	-
PAMAM-Gd	7.8±0.65	180	7.7±0.27	177
ClPhIQ-PAMAM-Gd (**6**)	7.7±0.76	177	8.0±1.2	184
ClPhIQ-PAMAM-Gd-Liss (**7**)	4.0±1.04	92	3.8±0.40	87

including dendrimers [91, 98, 117]. To explore the utility of ClPhIQ-PAMAM-Gd (**6**) and ClPhIQ-PAMAM-Liss-Gd (**7**) and MRI agents, T1 and T2 relaxivities were determined. The TSPO targeted dendrimer was tested for its ability to increase relaxation of water molecules compared to Magnevist™ using a Maran 0.5T NMR scanner. Samples were diluted to five different concentrations in Gd^{3+} with saline and placed in disposable NMR/MR tubes. The T1 and T2 relaxation rates of each sample were measured three times per sample. The samples were cooled between trials to ensure consistent temperature. The ClPhIQ-PAMAM-Gd (**6**), ClPhIQ-PAMAM-Gd-Liss (**7**), PAMAM-Gd and Magnevist were all measured at five concentrations (20 – 100 μM in Gd). Table 2.1 provides the relaxation rates for each of these molecules.

The T1 relaxivitiy of PAMAM-Gd and ClPhIQ-PAMAM-Gd (**6**) is greater than that of Magnevist™ by a factor 1.6 on per Gd^{3+} or by 37 on a per molecule basis. The ClPhIQ-PAMAM-Gd-Liss (**7**) has a lower relaxivity than Magnevist™ per Gd^{3+}. The difference between ClPhIQ-PAMAM-Gd (**6**) and ClPhIQ-PAMAM-Liss-Gd (**7**) is the presence of 1-2 dyes attached to the dendrimer.

T2 relaxivity was not increased as significantly as with T1 but was still 1.4 and 33 times better than Magnevist™ on average based on a per molecule and per Gd^{3+} ion basis respectively. These values are consistent with recently published PAMAM-Gd molecules when the amount of Gd^{3+} and generation of the dendrimer are taken into account[98]. Again, the relaxation rate of ClPhIQ-PAMAM-Liss-Gd (**7**) was lower than the other samples, even Magnevist™.

Lissamine is a zwitter ion and charged molecules have been shown to reduce relaxivity, this is most likely the cause of the reduced relaxivity. In order to test the charged molecule theory on the PAMAM system, a series of dye and Gd^{3+} functionalized PAMAM molecules were synthesized and T1 and T2 relaxivities were acquired. The four reactions completed were 1) Cy5.5 attachment to PAMAM-Gd; 2) Lissamine attachment to PAMAM-Gd; 3) PAMAM-Gd reacted under the conditions of dye conjugation without dye present and 4) Gd chelated to PAMAM-Liss. The T1 and T2 results are all lower with dye attached to the scaffold than without dye attached (Table 2.2). Although Cy5.5™ does not affect the relaxivity as much as Lissamine in either T1 or T2, the rates are still faster than without the dye: 5.56 versus 7.33 for T1 and 5.95 versus 7.19 for T2. Liss-

Table 2.2 Relaxation rates of Dye-PAMAM-Gd compounds obtained on a Maran 0.5T NMR scanner.

Compound	T1 Relaxation per Gd^{3+} ($mM^{-1}s^{-1}$)	T1 Relaxation per PAMAM ($mM^{-1}s^{-1}$)	T2 Relaxation per Gd^{3+} ($mM^{-1}s^{-1}$)	T2 Relaxation per PAMAM ($mM^{-1}s^{-1}$)
Magnevist™	4.8±0.044	-	5.6±0.13	-
Cy5.5-PAMAM-Gd	5.56±0.10	128	5.95±0.17	137
Liss-PAMAM-Gd (Gd attached first)	4.34±0.24	100	4.04±0.33	93
PAMAM-Gd (reacted under dye conjugation conditions)	7.33±0.25	169	7.19±0.18	165
Liss-PAMAM-Gd (Liss attached first)	5.83±0.79	134	6.10±0.86	140

PAMAM-Gd (T1 = 4.34 and T2 = 4.04) has relaxation rates close to ClPhIQ-PAMAM-Liss-Gd (T1= 4.0 and T2 = 3.8) suggesting that the extra crowding associated with the ClPhIQ ligand with more attached to the dendrimer does not effect the relaxation rate. By reacting PAMAM-Gd under the reaction conditions (stirred the compound with DMF), and having the molecule maintain the relaxation rate prove that the reaction conditions do not effect the integrity of Gd^{3+} to the dendrimer or otherwise change the molecule. Interestingly, the order of addition does affect the relaxivities since Lissamine conjugated to the dendrimer first has slower relaxation rates than Gd added first. Overall, the relaxation experiments confirm 1) increased relaxivities present with PAMAM-Gd compounds compared to Magnevist™; 2) the ClPhIQ ligand does not significantly effect the relaxation of the Gd ions; 3) the zwitterionic dyes do effect the relaxation rates of the PAMAM-Gd molecule; 4) the effect of the dyes on the PAMAM-Gd is dependent on which dye is used and the order of attachment to PAMAM and 5) PAMAM-Gd is stable to the dye conjugating conditions.

2.10 Summary of EM studies

An added advantage of having electron dense metal ions directly incorporated into the dendrimer allows the molecule to produce contrast in a transmission electron microscope (TEM) independent of heavy metal staining. Since the gadolinium dendrimers were shown via fluorescence to label mitochondria on cells overexpressing TSPO, EM experiments were performed by Dr. Bernard Anderson. High TSPO concentration C6 rat glioma cells were plated

in 4 cm cellular culture dishes, dosed with ClPhIQ-PAMAM-Gd (**6**) and prepared for EM as described in the experimental section. The cells were free of any lead or uranium salts, which are commonly employed for improved contrast of organelles in biological samples[173]. A set of cells not dosed with ClPhIQ-PAMAM-Gd served as the control. Figure 2.16 illustrates typical TEM images of C6 cells labeled with ClPhIQ-PAMAM-Gd and unlabeled control. The differences between the labeled and control cells at 2,650X magnification are apparent as numerous individual mitochondria in the labeled sample (Figure 2.16A) have enhanced contrast over the surrounding cellular area whereas little contrast difference is visible between the mitochondria and the intracellar material in the control sample (Figure 2.16D). Magnification of the mitochondrial regions by 7650X and 25,000X for both samples further illustrates their differences (Figure 2.16 B, C, E & F). The mitochondria for those cells treated with ClPhIQ-PAMAM-Gd (**6**) have become very dark compared to control.

The enhanced contrast of ClPhIQ-PAMAM-Gd (**6**) treated cells compared to control cells was initially attributed to the accumulation of the high-Z, electron dense Gd^{3+} chelated to the dendrimer. The elemental composition of these electron dense regions was analyzed using Energy Dispersive X-ray Analysis (EDX), and it was determined that the enhanced contrast of the mitochondria was due to osmium and not gadolinium. It was concluded that osmium tetroxide, a strong oxidizer, used in the EM sample preparation as a secondary fixative,[174] reacted with receptor-bound ClPhIQ-PAMAM-Gd (**6**) forming large, polymeric osmium structures. Osmium tetroxide is known to coordinate nitrogen, (ClPhIQ-

PAMAM-Gd has ~238 nitrogens) and oxidize the surrounding material[175] creating areas of increased contrast anywhere there is a build-up of dendrimer. Although this data suggests osmium causes the increase in mitochondrial

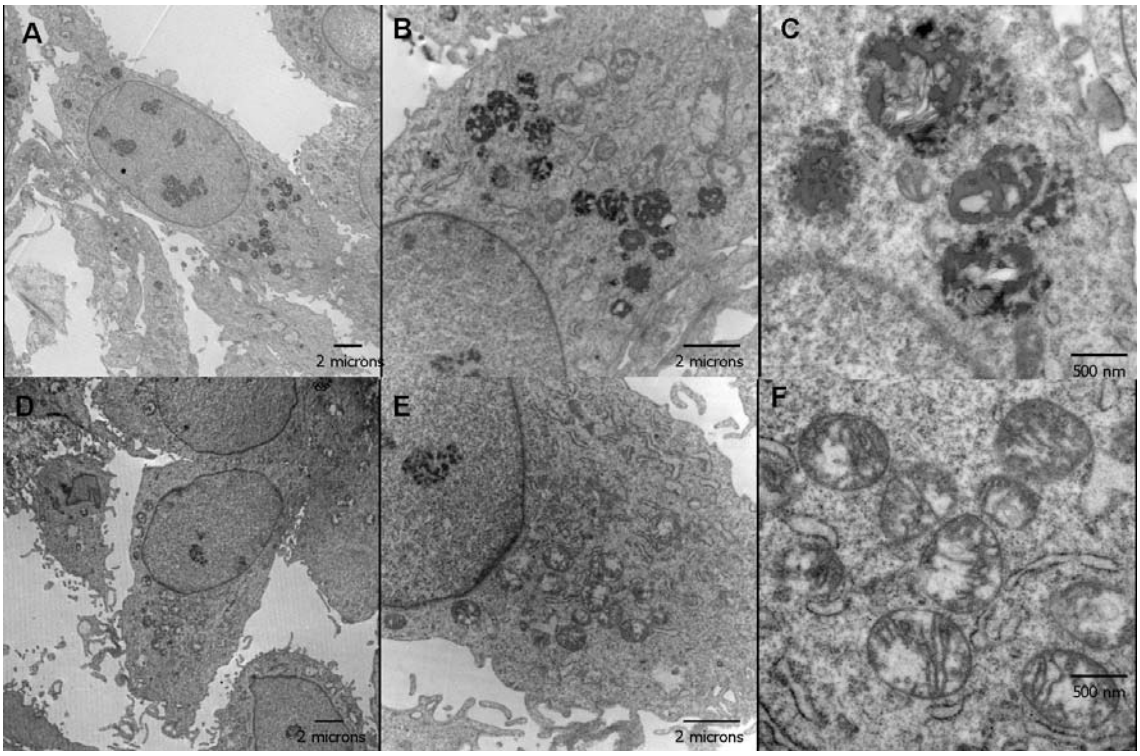

Figure 2.16. TEM images of ClPhIQ-PAMAM-Gd dosed (A-C) and undosed cells (D-F). A: ClPhIQ-PAMAM-Gd dosed cell at 2650x magnification. B: ClPhIQ-PAMAM-Gd dosed cells at 7100x magnification. C: ClPhIQ-PAMAM-Gd dosed cell at 25,000x magnification. D: Undosed cell at 2650x magnification. E: Undosed cell at 7100x magnification. F: Undosed cell at 25,000x

contrast and not Gd^{3+}, further experiments provided evidence that osmium reacted with the dendrimer. Plus, the control cells without dendrimer did not have

the increased contrast on the mitochondria. The collective data indicate that the ClPhIQ-PAMAM molecules target the mitochondria.

2.11 Conclusions

The work described in this chapter expanded on previous work completed in the Bornhop laboratory to synthesize new imaging agents that target TSPO. The previous agents were exclusively small molecules that could incorporate only a single imaging agent per ligand. Incorporating dendrimers as scaffolds for TSPO targeting has allowed expansion to dual-modality imaging and for EM experiments to be performed.

First, a TSPO targeted imaging agent was synthesized using a G(4)-PAMAM backbone, ClPhIQ acid and Lissamine™ (ClPhIQ-PAMAM-Liss, **3**). Second, the imaging agent was characterized with MALDI-TOF-MS and NMR and third imaged in C6 rat glioma and MDA-MB-231 human breast cancer cells. To our knowledge this is the first example of a TSPO-targeted dendrimer and among the few dendrimeric compounds that are internalized into the cell under normal physiological conditions. Cellular experiments demonstrate the ability for a large, synthetic molecule (conjugated PAMAM) to be internalized into the cell and target a specific protein (TSPO). Overall, this first set of imaging agents based on ClPhIQ-PAMAM moves the research a step closer to understanding biological events at the molecular level and ultimately enabling personalized medicine. Co-localization of the ClPhIQ-PAMAM-Liss and MTG indicates that the compound binds to the mitochondria.

The second half of this project focused on the synthesis of a dual-imaging TSPO targeted dendrimer. The original ClPhIQ-PAMAM-Liss was expanded to include a Gd^{3+} ion that can be utilized for MRI or EM studies. The ClPhIQ, Gd^{3+} and Lissamine functionalized dendrimers were then found to label cells with high TSPO concentrations analogous to the ClPhIQ-PAMAM-Liss (**3**) molecule. As with the ClPhIQ-PAMAM-Liss (**3**), the ClPhIQ-PAMAM-Gd-Liss (**7**) was found to only label the cells if the ClPhIQ ligand was attached to the dendrimer. Again, the cells were labeled perinuclear, not found in the membranes and entered the cell without perturbing the membrane. Co-incubation of ClPhIQ-PAMAM-Gd-Liss (**7**) with MTG yielded significant overlap between the mitochondrial binding dye (MTG) and the dendrimer indicating that the TSPO targeted dendrimer was on the mitochondria. ClPhIQ-PAMAM-Gd (**6**) was shown to bind to TSPO with a 510 nM binding affinity in a radiobinding study completed by Mingfeng Bai. These molecules also provide increased relaxation compared to Magnevist™. Due to the Gd^{3+} loaded within the dendrimer, EM studies were performed by Dr. Bernard Anderson. EM studies confirmed that the ClPhIQ-PAMAM compounds are labeling the mitochondria by only producing contrast on mitochondria of cells dosed with ClPhIQ-PAMAM-Gd (**6**). Through developing TSPO targeted dendrimers, the fields of dendrimer functionalization, characterization of functionalized dendrimer products, fluorescence and MRI imaging, TSPO targeting and biological EM have been advanced.

2.11 Experimental Procedures

General Methods:

G(4)-PAMAM™ dendrimer in a 10% w/w solution of methanol was purchased from Fischer Scientific and pipetted into a pre-weighed vial immediately before use. The methanol was evaporated under a stream of $Ar_{(g)}$ and the resulting viscous oil was dissolved in water, frozen and lyophilized to give a fluffy white powder. The mass of the dendrimer was determined by re-weighing the vial and calculating the mass difference. 1-(2-chlorophenyl)isoquinoline-3-carboxylic acid ClPhIQ Acid was synthesized in our laboratory as previously reported[36-37]. All 1,4,7,10-Tetraazacyclododecane-1,4,7,10-tetraacetic acid (DOTA) and DOTA derivatives were purchased form Macrocyclics and used as arrived. All other chemicals were purchased from Fischer Scientific and used as is unless otherwise indicated.

MALDI-TOF MS were obtained on a PerSeptive Biosystems Voyager-DE STR mass spectrometer. Freshly recrystalized trans-indole acrylic acid (IAA) was used as the matrix in a 10 mg/mL solution of DMSO. The plate was spotted with 1 μL of a 10:1 solution of matrix to analyte. NMR spectra were obtained on a 400 MHz Bruker AV-400 instrument with a 5 mm Z-gradient broadband inverse probe. NMR spectra were obtained in d6-dimethyl sulphoxide. UV-vis spectra were obtained on a Shimadzu 1700 UV-vis spectrophotometer. Fluorescence spectra were obtained using a ISS PCI spectrofluorometer at room temperature. MR relaxivities were obtained using a Maran 0.5T NMR scanner.

ClPhIQ-G(4)-PAMAM™ (1):

First, ClPhIQ Acid (152.9 mg, 540 μmoles) and benzotriazol-1-yloxytris(dimethylamino)-phosphonium hexafluorophosphate (BOPCl, 288.1 mg, 651 μmoles) were dissolved in 2 mL of DMSO each. Triethyl amine (Et_3N, 100 μL) was added to the ClPhIQ Acid solution. The BOPCl solution was added to the ClPhIQ Acid solution. The mixture was stirred for 5-10 minutes (sometimes a change from clear to bright orange would occur) and was then added to a stirred solution of G(4)-PAMAM™ dendrimer (252.2 mg, 18 nmoles) in DMSO (5 mL). The reaction was stirred at room temperature overnight. Unreacted ClPhIQ Acid was removed by diluting the solution 4 fold with water and placing the solution in an Amicon Centrifugation molecular weight filter (molecular weight cut off = 5 kDa.) and concentrating the solution to approximately 500 μL via centrifuging at 3000 revolutions/minute (1419 x g) for 1 hour. The solution was diluted and re-concentrated three times with water to wash any unreacted materials away. Finally, the solution was lyophilized to give 441.2 mg (100 % yield) of a slightly yellow powder. The same procedure was followed for synthesizing the (ClPhIQ)12-PAMAM using fewer equivalents of ClPhIQ Acid and BOPCl. ClPhIQ30-G(4)-PAMAM: MALDI-TOF MS 19,500 a.m.u. ^1H NMR (300 MHz, $CDCl_3$) δ 8.8 (1H, s), 8.6 (1H, s), 8.2-8.5 (5H, m), 7.5-8.0 (9H, multi), 2.9 (3H, bs) and 3.1-3.5 (28H, m) ppm.

ClPhIQ-G(4)-PAMAM™-Lissamine (2):

G(4)-PAMAM™ (9 mg, 400 nmoles) with or without ClPhIQ Acid was dissolved in 2 mL of dimethylformamide (DMF). Next, 23 μL of a 17.3 mM solution of lissamine sulphonyl chloride™ was added to the stirred dendrimer solution. The reaction was stirred overnight followed by purification in Amicon Centrifugation filters as described above and lyophilized to give 5.6 mg (61% yield) of a pink fluffy solid. The presence of the fluorophor was confirmed with UV-vis (max absorbance at 551 nm) and Fluorescence (ex 551 nm, em. 586 nm) spectroscopies. Specific conditions and yields provided above were for $ClPhIQ_{23}$-G(4)-PAMAM, but UV-vis and fluorescence spectra were identical for $ClPhIQ_{12}$-PAMAM and PAMAM-Liss.

ClPhIQ-G(4)-PAMAM™-DOTA^{t}Bu (3):

ClPhIQ-G(4)-PAMAM™ (202 mg, 9 μmoles) and DOTA^{t}Bu (179 mg, 97 μmols) were dissolved in 2 and 1 mL of DMSO respectively. The 1,4,7,10-Tetraazacyclododecane-1,4,7-tris(t-butyl acetate)-10-acetic acid mono(N-hydroxysuccinimide ester) (DOTA^{t}Bu-NHS) solution was added dropwise to a stirring solution of ClPhIQ-G(4)-PAMAM™ over a 10 minute period. The reaction was stirred overnight and purified with the Amicon Centrifugation filters (5kDa. MWCO) following the procedure used for ClPhIQ-G(4)-PAMAM™ purification and lyophilized to give 163.2 mg (100% yield) of ClPhIQ-G(4)-PAMAM™-DOTAtBu. The molecular weight was determined using MALDI-TOF MS to be

31,000 a.m.u. ^{1}H NMR (300 MHz, $CDCl_3$) δ 8.8 (1H, s), 8.6 (1H, s), 8.2-8.5 (20H, m), 7.5-8.0 (9H, multi), 2.9 (3H, bs) and 3.1-3.5 (208H, m), 1.4 (108, s) ppm.

ClPhIQ-G(4)-PAMAM™-DOTA (4):

ClPhIQ-G(4)-PAMAM™-DOTAtBu (256.0 mg, 9 μmoles) was dissolved in 3 mL of neat trifluoroacetic acid (TFA) and stirred overnight. The solution was diluted 10 fold with water and purified with Amicon Centrifugation filters (5kDa. MWCO) following the procedure used for ClPhIQ-G(4)-PAMAM™ purification and lyophilized to give 120 mg (100% yield). The molecular weight was determined using MALDI-TOF MS to be 27,000. ^{1}H NMR (300 MHz, $CDCl_3$) δ 8.8 (1H, s), 8.6 (1H, s), 8.2-8.5 (5H, m), 7.5-8.0 (20H, multi), 2.9 (3H, bs) and 3.1-3.5 (73H, m) ppm.

ClPhIQ-G(4)-PAMAM™-DOTA-Lissamine (5):

ClPhIQ-G(4)-PAMAM™-DOTA (4.8 mg, 148 nmoles) was dissolved in 1 mL of dimethylformamide (DMF). Next, 12.8 μL of a 17.3 mM solution of lissamine rhodamine B sulfonyl chloride™ (221 nmoles) was added to the stirred dendrimer solution. The reaction was stirred overnight followed by purification in Amicon Centrifugation filters (5kDa. MWCO) as described above and lyophilized to give 2.8 mg (57% yield) of a pink fluffy solid. The presence of the fluorophor was confirmed with UV-vis (max absorbance at 551 nm) and Fluorescence (ex 551 nm, em. 586 nm) spectroscopies.

ClPhIQ-G(4)-PAMAM™-DOTAGd^{3+}(6):

ClPhIQ-G(4)-PAMAM™-DO3A (22 mg, 679 nmoles) was dissolved in water. Next, 1 mL of a 9.1 mg/mL solution of $GdCl_3$ (9.1 mg, 25 μmoles) was added to the dendrimer solution. The reaction was stirred at room temperature for 24 hours and purified with Amicon Centrifugation filters (5kDa. MWCO) following the procedure used for ClPhIQ-G(4)-PAMAM™ purification and lyophilized to give 24.7 mg (100% yield). The molecular weight was determined using MALDI-TOF MS to be 30,500 Da.

ClPhIQ-G(4)-PAMAM™-DOTAGd^{3+}-Lissamine (7):

ClPhIQ-G(4)-PAMAM™-DOTAGd^{3+} (5.3 mg, 145 nmoles) was dissolved in 1 mL of dimethylformamide (DMF). Next, 12.7 μL of a 17.3 mM solution of lissamine rhodamine B sulfonyl chloride™ (220 nmoles) was added to the stirred dendrimer solution. The reaction was stirred overnight followed by purification in Amicon Centrifugation filters (5kDa. MWCO) as described above and lyophilized to give 3.7 mg (69% yield) of a pink fluffy solid. The presence of the fluorophor was confirmed with UV-vis (max absorbance at 551 nm) and Fluorescence (ex 551 nm, em. 586 nm) spectroscopies.

G(4)-PAMAM™-Lissamine:

G(4)-PAMAM™ dendrimer (5.5 mg, 393 nmoles) was dissolved in 3 mL of DMF and 22 μL of 17.3 mM lissamine rhodamine B sulfonyl chloride™ in DMF was added to the stirred dendrimer solution. The reaction was stirred overnight

followed by purification in Amicon Centrifugation filters (5kDa. MWCO) as described above and lyophilized to give 4.0 mg (70% yield) of a fluffy pink solid.

Cell Internalization Experiments

G(4)-PAMAM™-Lissamine derivatives: Either 20,000 C6 rat glioma or 40,000 MDA-MB-231 breast cancer cells were plated into collagen coated glass bottom microscopy (MatTeck™) dishes and allowed to grow for two days in cell media. After two days, the cells had good morphology and were attached, however were not confluent. G(4)-PAMAM™-Lissamine compounds (with or without other moieties) were diluted to 1 μM with media from a 10 mg/mL stock solution in DMSO. The media over the cells was replaced with the media containing the fluorophor and incubated for 6-12 hours. The media was then poured off and the cells were carefully rinsed 3-4 times with Dulbecco's Phosphate Buffered Saline (DPBS). The cells were imaged live. Both white light and fluorescence pictures were obtained.

For fixed cells, the rinsed cells were incubated at room temperature for 30 minutes with a 4% Para formaldehyde solution. The cells were carefully washed 4 times with DPBS and stored under DPBS at 4 °C until imaged (not longer than 1 week, typically overnight). Immediately before imaging, the fixed cells were incubated with a 25 nM solution of mitotracker green (MTG) for 10 minutes. Excess MTG was removed by 4 washings with DPBS and the cells were imaged.

Radiobinding Assay:

To complete this assay, C6 rat glioma cells (cultured in Dulbecco's modified Eagle medium (DMEM)-F12 medium (Gibco/Invitrogen) supplemented with 0 5% FBS and 2.5% horse serum (HS) at 3.7% CO_2) were scraped from 150 mm culture dishes into 5 mL of phosphate buffered saline (PBS), dispersed by trituration, and centrifuged at 500 x*g* for 15 min. Cell pellets were resuspended in PBS and assayed to determine protein concentration. The binding studies with [^{3}H]PK11195 on 30 μg of protein from cell suspensions were performed as previously described [176]. The data was analyzed using PRISM software (vs 4.0, GraphPad, Inc., San Diego, CA). In PRISM, the one binding site competition assay wizard was used, which incorporates the equation: Y=Bottom + (Top-Bottom)/(1^10(X-LogEC_{50})). For the ClPhIQ-PAMAM-Gd dendrimer, the IC50 was found to be 510 nM on a per ClPhIQ ligand basis with a goodness to fit error of 0.9394.

Preparation of TEM Samples:

C6 cells were plated in a 4 cm culture dish, allowed to propagate to near 75% confluency and treated with a 32 μM ClPhIQ-PAMAM-Gd solution in Dulbecco's Modified Eagle Medium. After incubation at 37 °C for 10 hours, the C6 cells were then washed three times with a 0.1 M solution of sodium cacodylate buffer to remove any extracellular ClPhIQ-PAMAM-Gd. The cells were subsequently fixed for one hour using a 4% paraformadehyde solution. The fixed cells were post-fixed using a 1% Osmium Tetroxide solution,

dehydrated using ethanol, pelletized and sliced into 80 nm thick sections. The sections were placed on a 300 mesh copper grid and imaged on a Phillips CM-12 Electron Microscope.

Relaxivity of Gd Dendrimers:

Samples were prepared at 5 concentrations (in Gd) from 1 μM to 1 mM, depending on the availability of sample. Pre-written pulse sequences were used to obtain the relaxation at each concentration for both T1 and T2 which varied the time intervale between the pluse and detecting the population that had relaxed. The data was graphed and fitted to a three parameter exponential rise to max curve to give the relaxation at each concnetration. Each sample was run 3 times with 15 minute intervals between trials. The relaxivity was determined by graphing the relaxation versus concentration and fit to a line. The slope of the line is the relaxivity.

CHAPTER III

ATTEMPTED DELIVERY OF DOX WITH MMP-9 TARGETED DENDRONS

3.1Introduction

Although there is a plethora of research being done in cancer, science still has left many questions about the cause, progression and best therapeutic strategy unanswered. Of the different angles being developed, “smart systems” are an imperative branch to be developed. These systems are usually based on a large MW scaffold and are designed to selectively target disease leaving healthy cells and tissue unaffected. Smart systems can be designed to also to image the location(s) of diseased tissues while subsequently delivering therapy [50, 121]. Although there are a few smart systems undergoing clinical trials [177], many opportunities exist toward improving clinical outcomes for cancer patients.

Matrix metalloproteinases (MMPs) represent an attractive target for smart system approaches to treating and diagnosing cancer. Specific MMPs have been associated with the microenvironment of tumors and are found in increasing levels of concentration through all stages of tumor progression, making them good targets for prodrug therapy. In addition, several short peptide sequences have been identified that are cleaved selectively by a specific MMP or specific groups of MMPs. One such sequence, AVRWLLTA, is known to be cleaved by MMP9 between the tryptophan and leucine residues with good selectivity[178]. Although pharmacological inhibitors have been unsuccessful in

treating MMP associated cancers, other non-inhibitor approaches utilizing MMP enzymes as targets have been successful[120, 179-180]. The goal of this part of the project is to develop a modular system for therapeutic, efficacy monitoring, molecule tracking and tenability based on a dendrimeric scaffold. The modular system will be explored by making an MMP-9 cleavable peptide for therapeutic delivery to the primary tumor site of cancerous tissue as well as micrometastatic lesions while leaving healthy tissue unaffected by the drug.

The development of improved scaffolds for imaging and drug delivery is being extensively investigated. Scaffolds allowing the attachment of a variety of different modalities to a single nanoparticle for targeting, imaging, drug delivery and controlling circulation time have been reported; however no modular systems in which pieces of nanoparticles can be synthesized individually and "**mix and matched**" together have been reported. One challenge with this type of system is characterization of both the precursor scaffolds and the functionalized product. The modular system being developed here includes the therapeutic (as described in this and the following chapter), a beacon for monitoring MMP cleavage, a tracer for monitoring the location of the scaffold before and after cleavage and room for one more modality. The fourth modality could be an agent to increase circulation time (such as PEG), target specific tumor receptors (small molecule ligands, antibodies, proteins, etc.), or a second therapeutic as well as a number of other agents.

In this chapter I report the synthesis and characterization of a prodrug component of a modular system based on polyester backbones. The prodrug

contains the doxorubicin (DOX), modified for attachment and an MMP9 cleavable peptide for inactivation of the drug until released. The DOX was then attached to a dendron scaffold and chemical characterization of the molecule was completed to determine the exact number of drug molecules per dendron. Finally, preliminary cellular studies were performed which indicate this DOX-peptide-Dendron is not a viable candidate to move forward into animals or for combination with the other pieces of the modular system. The goal of this part of the project (Chapters 3, 4 & 5) is to develop a MMP-9 cleavable peptide to deliver therapy to the primary tumor site of cancerous tissue as well as micrometastatic lesions while leaving healthy tissue unaffected by the drug.

3.2 Synthesis of H_2N-Gly-Dendron

In the construction of the MMP-9 cleavable peptide-dendron scaffold, Boc-Gly (2-(tert-butoxycarbonylamino)acetic acid) was first attached to the dendron (**8**, 2-

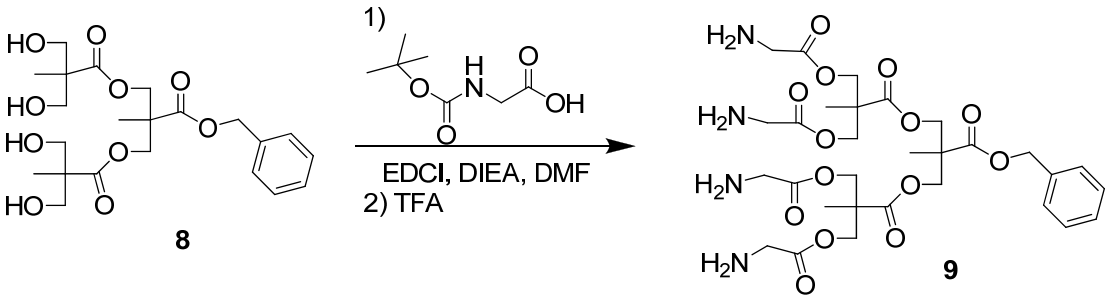

Scheme 3.1. Synthesis of H_2N-Gly-Dendron. 2-(benzyloxycarbonyl)-2-methylpropane-1,3-diyl bis(3-hydroxy-2-(hydroxymethyl)-2-methylpropanoate) (H_2N-Gly-Dendron, **9**).

(benzyloxycarbonyl)-2-methylpropane-1,3-diyl bis(3-hydroxy-2-(hydroxymethyl)-2-methylpropanoate) reported by Hult et. al.[181] for easier conjugation of the peptide since primary amines are more reactive than alcohols. This was accomplished by reacting dendron **8** with excess Boc-Gly using 1-ethyl-3-(3'-

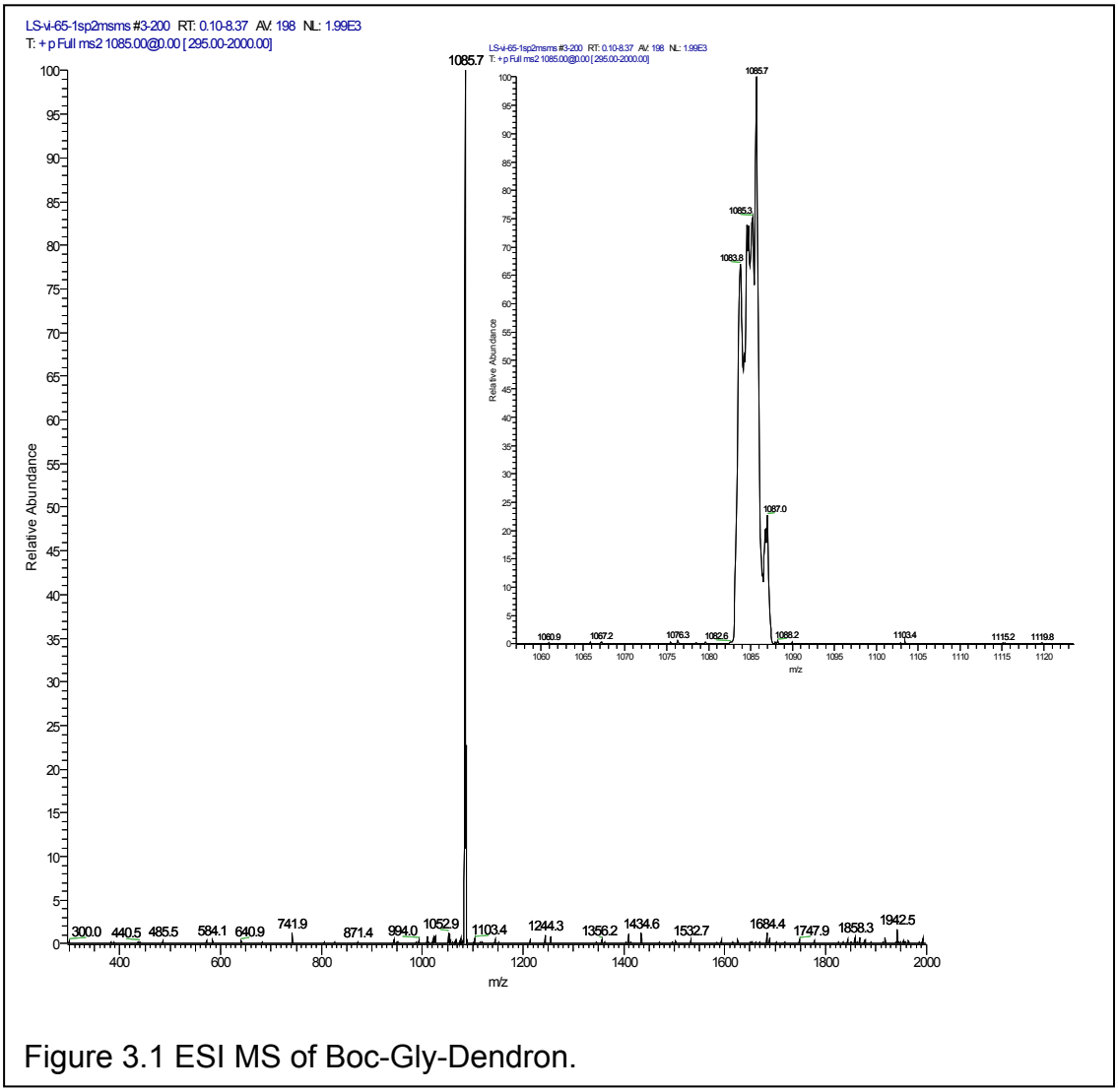

Figure 3.1 ESI MS of Boc-Gly-Dendron.

dimethylaminopropyl)carbodiimide (EDCI) as the coupling agent and diisoproplyethyl amine (DIEA) in dimethyl formamide (DMF) under anhydrous conditions. The crude product was purified with the Biotage SP1™ system (silica gel with a hexane/ethylacetate gradient) to give Boc-Gly-Dendron (2-(benzyloxycarbonyl)-2-methylpropane-1,3-diyl bis[3-(2-amino acetate)-2-((2-amino acetate)-methyl)-2-methylpropanoate) in 31% yield. The Boc-Gly-Dendron was characterized with both ^{1}H NMR and ESI^{+} MS. The MS gave the product ion peak at 1,085 (Figure 3.1). The NMR provided all the expected peaks, including carbamate NHs at 8.0, aromatic benzyl peaks at 7.3, benzyl CH_2 peak at 5.2, Gly and interior dendron methylenes from 3.7-4.4 and methyl peaks from the Boc protecting groups and dendron interior (Figure 3.2). There was also a small amount of DMF still present in the product even after extensive concentration and chromatography as seen at 2.9 ppm in the NMR.

The Boc groups were removed with TFA, either neat or in 50% methylene chloride, to give H_2N-Gly-Dendron (**9**, 2-(benzyloxycarbonyl)-2-methylpropane-1,3-diyl bis[3-(2-amino acetate)-2-((2-amino acetate)-methyl)-2-methylpropanoate). The H_2N-Gly-Dendron was characterized with MS and NMR. The MS provided the expected product ion peak at 685.40 (Figure 3.3). Extensive NMR characterization studies were performed, including ^{1}H, HSQC (^{1}H-^{13}C) and HMBC (^{1}H-^{13}C) spectra to obtain the exact assignments of each

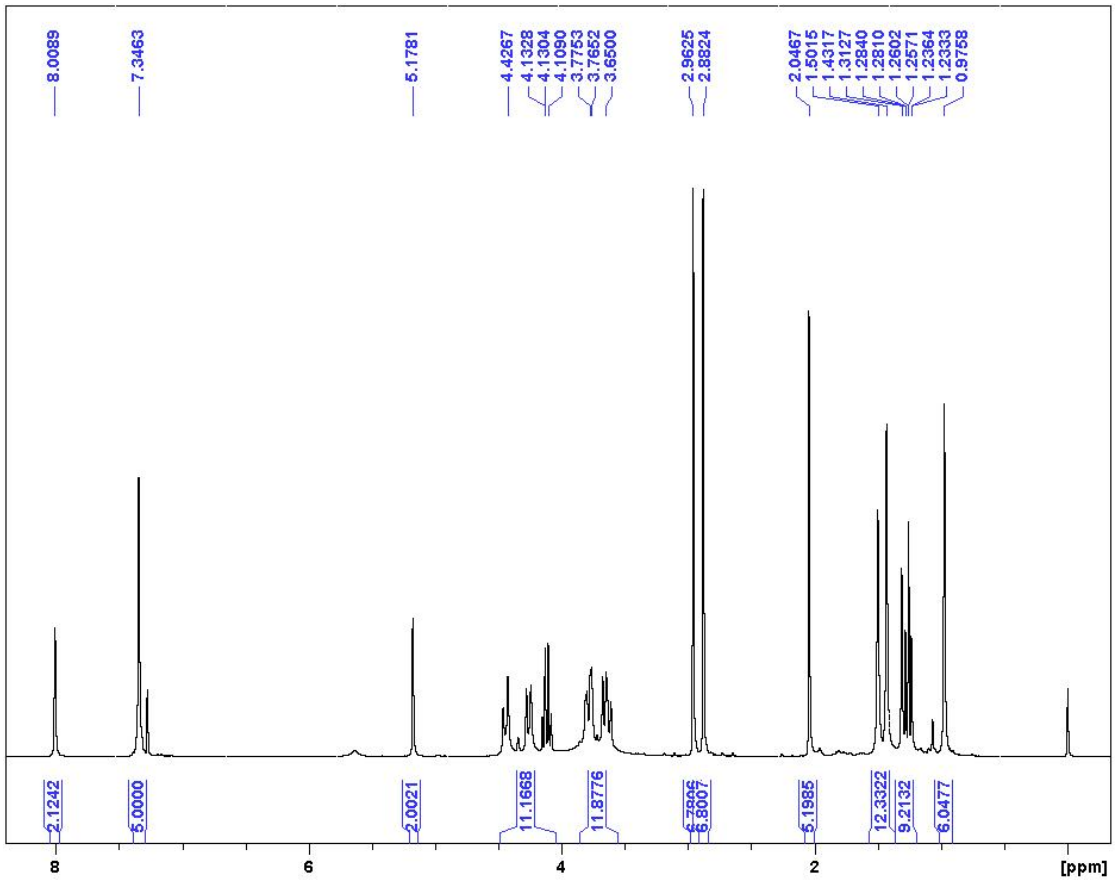

Figure 3.2 NMR of Boc-Gly-Dendron.

peak for later evaluation after Fmoc-[Ahx]-AVRWLLTA-[Ahx] was coupled to H_2N-Gly-Dendron (**9**). The proton peaks were mostly assigned using the proton NMRs (Figure 3.4) of the starting materials and confirmed with the HSQC and HMBC spectra (Figures 3.5 and 3.6). Again, the ^1H NMR provided the expected peaks at 8.5 (amines), 7.3 (Aromatic Benzyl protons), 6.3 (Benzyl methylene), 4.3 (interior dendron methylenes), 3.8 (Gly methylenes) and 1.2 (interior dendron methyls). The Gly methylene peak was confirmed by looking at the HSQC and HMBC data where HSQC shows protons coupled to carbon by 1 bond (proton

directly bonded to that carbon) and HMBC shows protons coupled by 2 bonds (the proton is coupled to the carbon alpha to it). In the HSQC

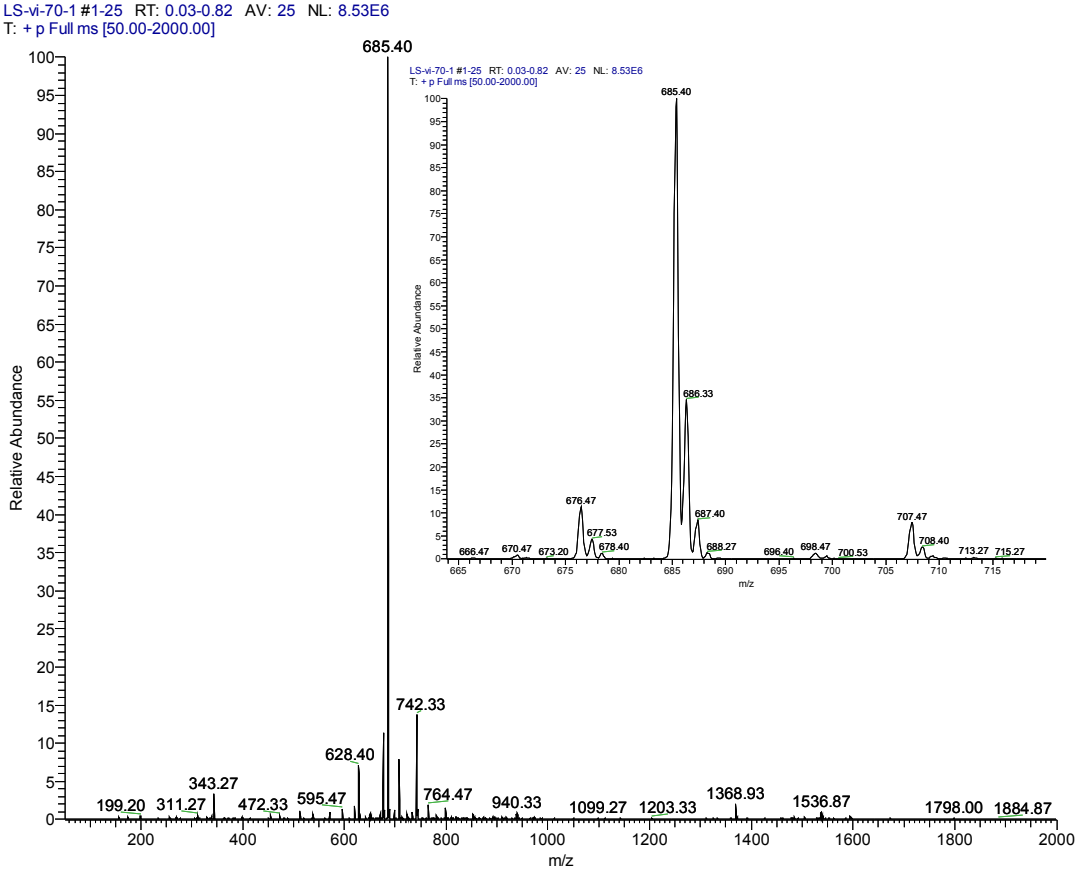

Figure 3.3. ESI MS of H_2N-Gly-Dendron.

spectra, the peak at 3.8 ppm is coupled to the carbon at 40 ppm, indicating that the carbon at 40 ppm is the glycine methylene carbon. The ester carbonyl between the glycine and dendron scaffold was assigned as 168 pmm because in the HMBC, 3.8 ppm is coupled with 168 ppm (Figure 3.6). These assignments

were used later to determine whether the peptide (Fmoc-[Ahx]-AVRWLLTA-[Ahx]) was attached to the H_2N-Gly-Dendron scaffold.

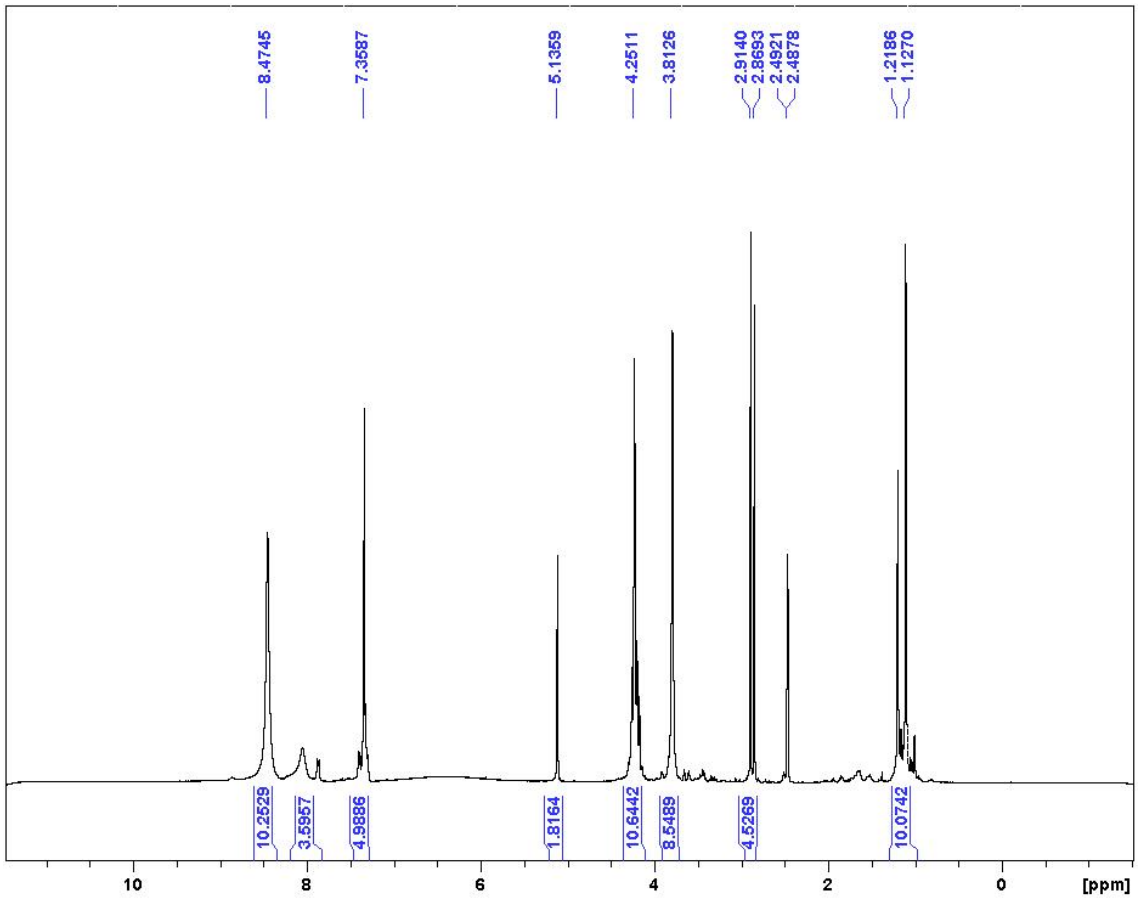

Figure 3.4. ^{1}H NMR data of H_2N-Gly-Dendron.

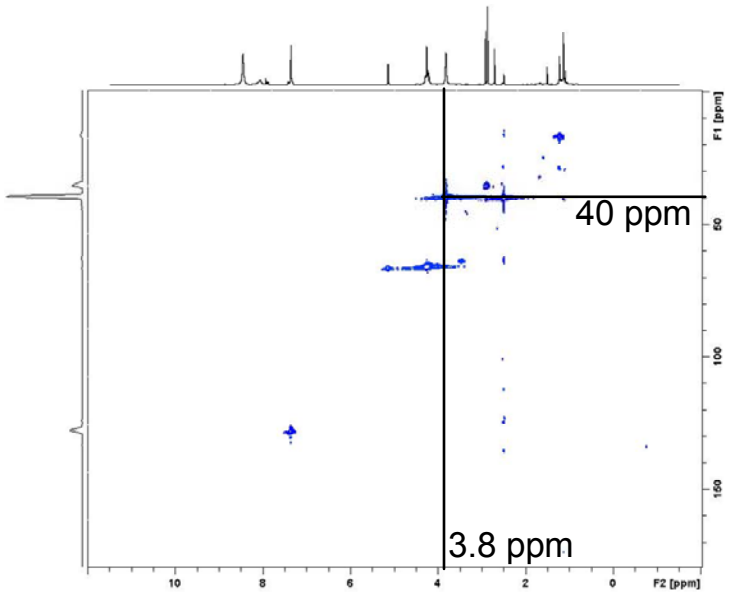

Figure 3.5 HSQC of H_2N-Gly-Dendron.

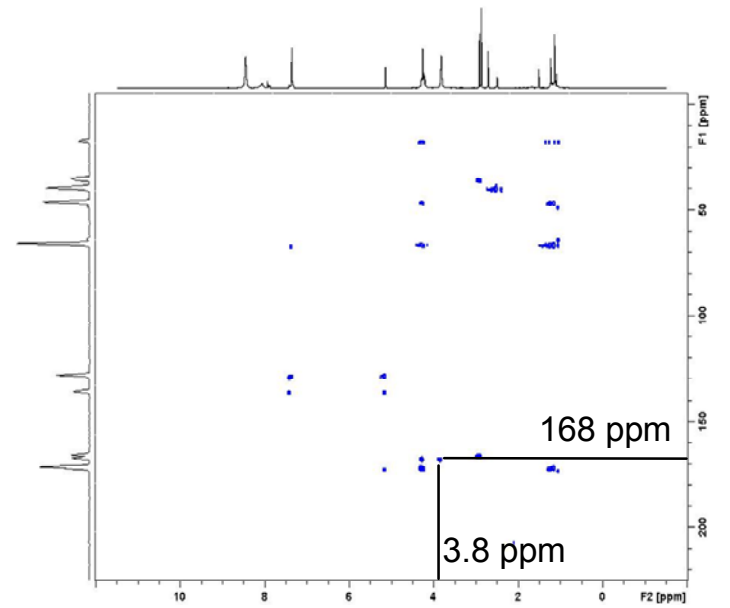

Figure 3.6 HMBC NMR spectra of H_2N-Gly-Dendron (**9**).

3.3 Synthesis and Characterization of Fmoc-Pep-dendron

The peptide sequence AVRWLLTA has been shown by Chen et. al. to be cleaved specifically by MMP9 [178]. Therefore, this sequence was chosen to be used in constructing an MMP9 cleavable therapeutic scaffold. The peptide was attached to the dendron by activating the carboxylic acid of Fmoc-[Ahx]-AVRWLLTA-[Ahx] with 1-ethyl-3-(3'-dimethylaminopropyl)carbodiimide (EDCI)

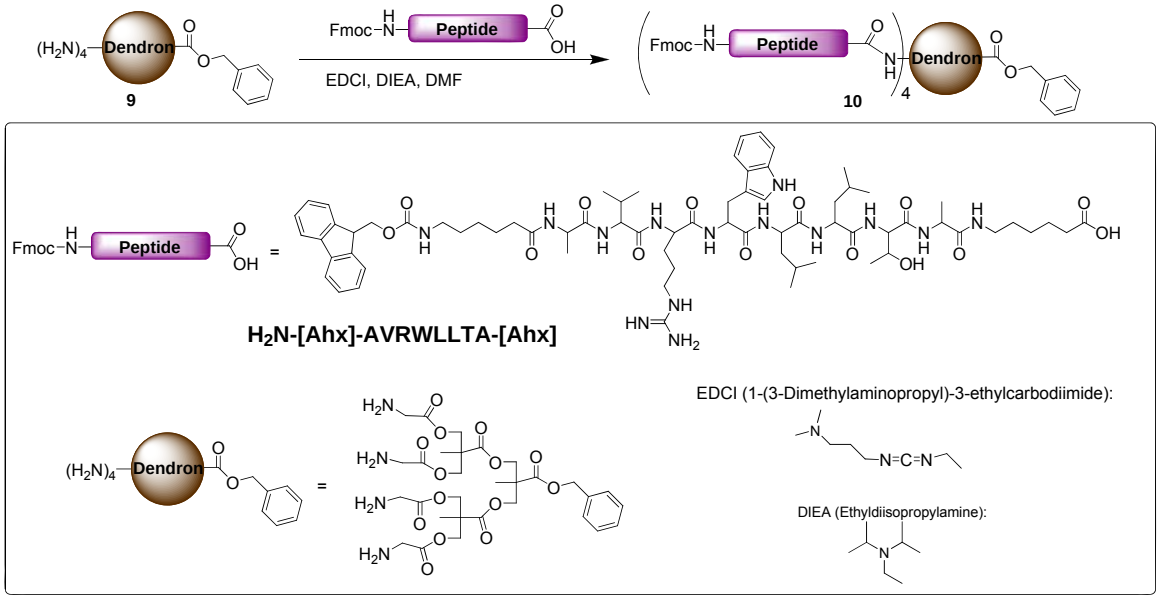

Scheme 3.2. Conjugation between the Gly-Dendron and Fmoc-[Ahx]-AVRWLLTA-[Ahx]

and N,N-Diisopropylethylamine (DIEA) in anhydrous DMF under $Ar_{(g)}$ for 30 minutes. After activation of the peptide, H_2N-Gly-Dendron (**9**) in anhydrous DMF was added to the reaction. The reaction was stirred until complete (by HPLC)

and then concentrated and purified with high pressure liquid chromatography (HPLC) to give Fmoc-Pep-Dendron (**10**).

The reaction was monitored by HPLC using a BioBasic 120 SEC column. Initially a reverse phase C18 column was used, but deciphering what new peaks were generated throughout the course of the reaction were was impossible without another means of characterization. At the time no MALDI-TOF MS conditions could be found to give product ion peaks, making identification by MS impossible as well. With SEC the peaks elute in order of relative size; providing a starting point for characterizing the product(s) from small molecular weight biproducts. As shown in Figure 3.7, the dendron (black) is eluted at 21 minutes (**E**) and the Fmoc-[Ahx]-AVRWLLTA-[Ahx] peptide spiked with EDCI (blue) at 19 minutes (**D**). The coupling reaction (red) gives several peaks at 14 (**A**), 16 (**B**), 18 (**C**), 19 (**D**, shoulder), 23 (**F**) and 28 (**G**) minutes. The reaction was purified by collecting the peaks off the HPLC and concentrating each individually. By the nature of SEC chromatography, peaks **A**, **B** and **C** at 14, 16 and 18 minutes respectively in the reaction trace are larger molecules than any of the components in the reaction mixture. Peak **D** in the trace is the peptide and the shoulder of one of the peaks in the reaction. For characterization purposes, the shoulder in the reaction trace (Figure 3.7, red) was carefully separated from peak **C** by collecting 3 fractions: **C**, **C** & **D,** and **D.** The ESI^+ MS of this shoulder (peak **D**) is consistent with that of the peptide. Peaks **A**, **B** and **C** were expected to be conjugation products, given that larger molecules elute earlier in SEC. No side

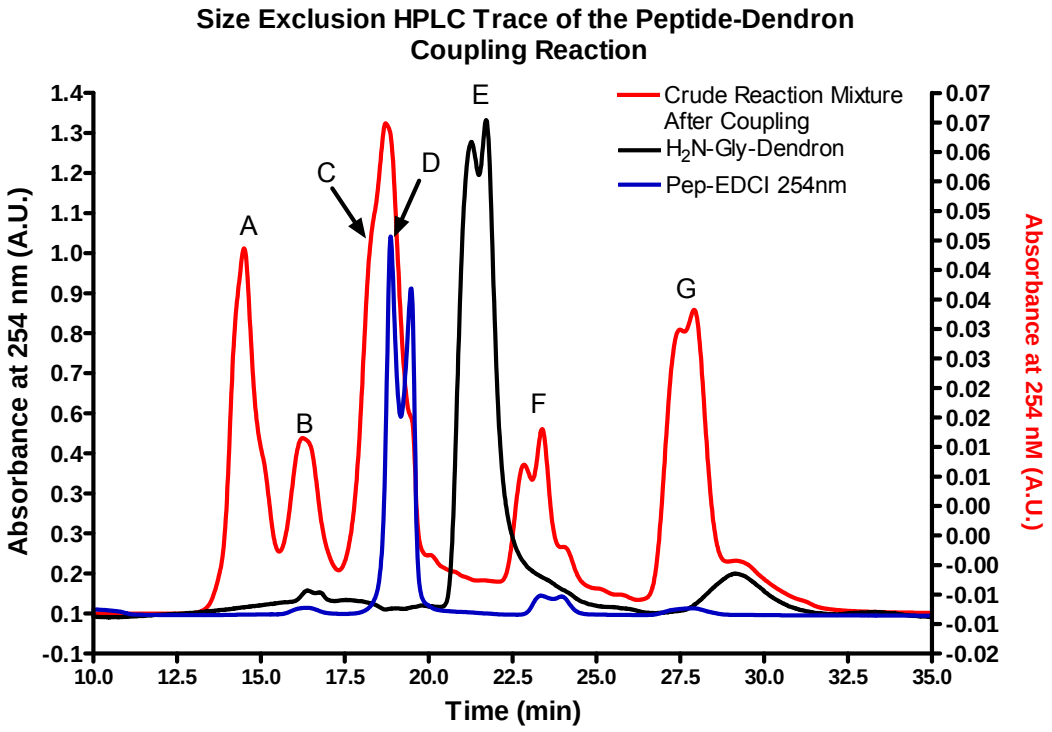

Figure 3.7. SEC Traces of Fmoc-[Ahx]-AVRWLLTA-[Ahx] with EDCI (Blue), Gly-Dendron (black) and the coupling reaction between the two components

reactions that produce larger molecules were expected, but to be sure peaks **A**, **B** and **C** were further characterized to determine coupling efficacy.

Although SEC provided evidence that the coupling occurred, this was not strong enough evidence for peptide attachment, nor did it provide information about how many peptides had been attached to each dendron. Since initial attempts at MALDI-TOF MS failed, two other methods were developed to characterize the coupling reaction and to determine the number of peptides attached to each dendron. Peak **A** was characterized for the formation of the

bond between the carboxyl terminal of the peptide(s) and the primary amine(s) of the dendron using 2 dimensional (2D) NMR techniques. Then peaks **A**, **B**, **C** and **D** were analyzed with a ninhydrin assay for quantifying the amine content [16], leading to the number of peptides attached to the dendron.

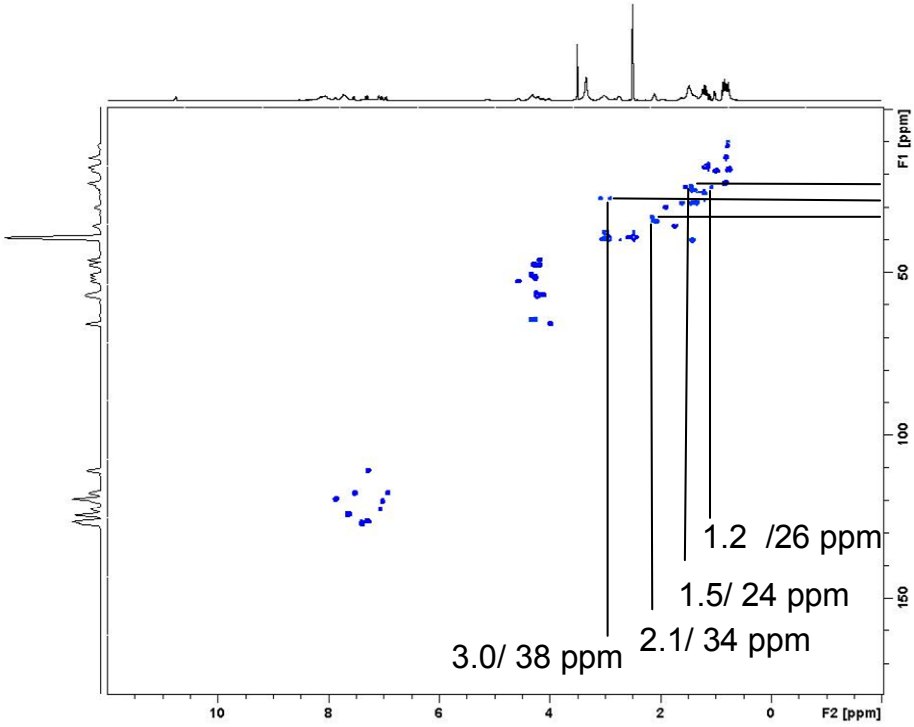

Figure 3.8. HSQC NMR of Fmoc-[Ahx]-AVRWLLTA-[Ahx].

The NMR experiments were meant to determine that a bond formed between the carboxylic acid of the Fmoc-[Ahx]-AVRWLLTA-[Ahx] peptide and the amine(s) on the dendron. To obtain the needed information, ^{1}H, HSQC (Figure 3.8) and HMBC (Figure 3.9) NMRs from the individual pieces (dendron and

Fmoc-[Ahx]-AVRWLLTA-[Ahx]) were assigned. The Fmoc-[Ahx]-AVRWLLTA-[Ahx] peptide peaks were assigned by finding the five carbon methylene chains present at either end of the peptide (Ahx groups). The specific proton and

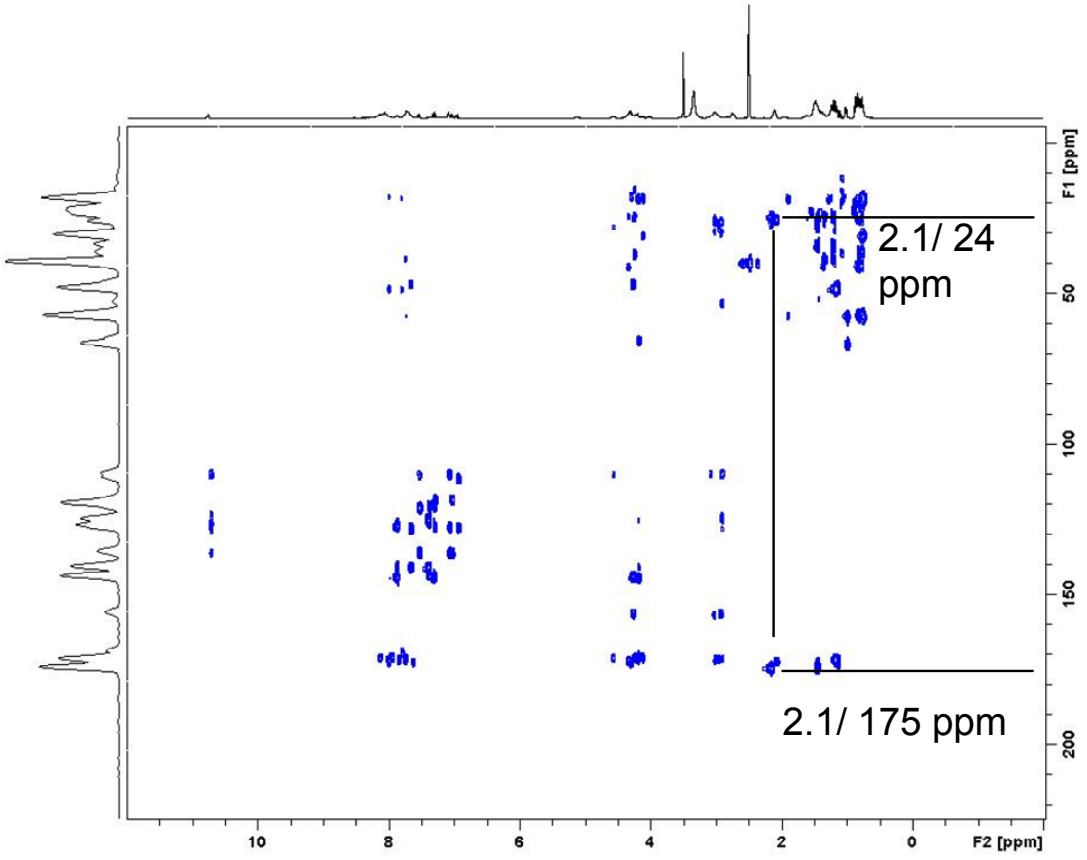

Figure 3.9 HMBC NMR of Fmoc-[Ahx]-AVRWLLTA-[Ahx].

carbon signals for the carboxy terminal methylene chain were assigned by locating the carboxylic acid carbon at 175 ppm. Then the HMBC and HSQC

spectra were assigned by working from the peak at 2.1 ppm that was coupled to 175 ppm in the HMBC spectra, therefore 2.1 ppm was assigned as

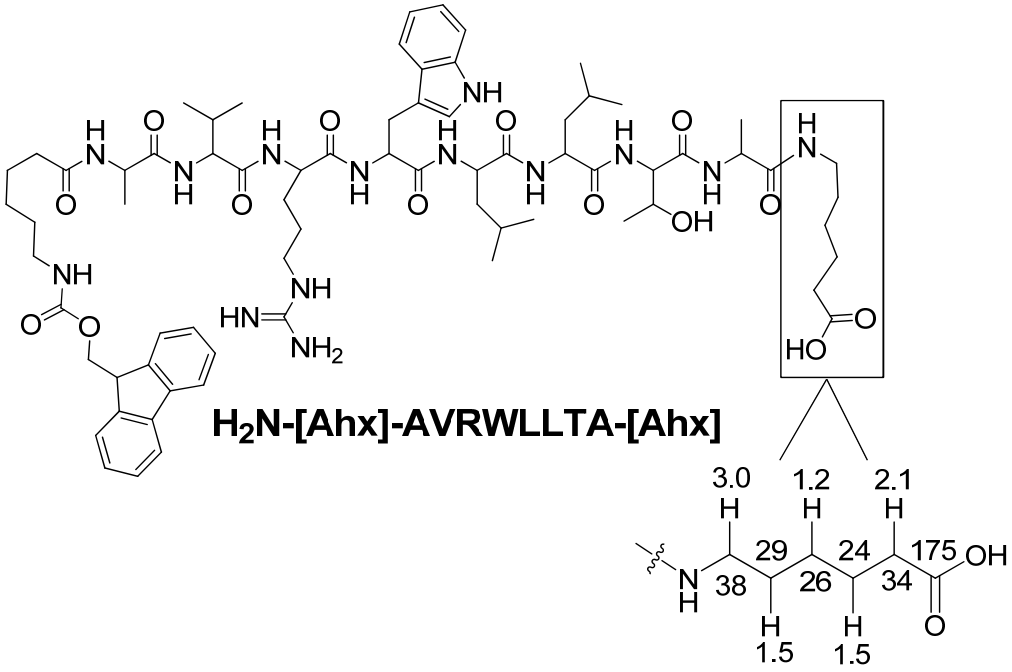

Figure 3.10 Proton and carbon assignments from the proton, HSQC and HMBC NMR spectra

the methylene protons alpha the carboxylic acid terminus. HSQC indicated that the carbon peak at 34 ppm was the carbon alpha to the carboxylic acid by association with the 2.1 ppm ^{1}H peak. The peak at 2.1 ppm was coupled to both 175 and 24 ppm in the HMBC spectra. Thus, the peak at 24 ppm was assigned to the carbon in the beta position from the carboxylic acid. HSQC then provided the coupling signal between 24 ppm and 1.5 ppm to indicate that the ^{1}H peaks at

1.5 ppm were on the beta carbon. The remaining peaks were assigned using these techniques. The peak assignments are shown in Figure 3.10.

To determine coupling between Fmoc-[Ahx]-AVRWLLTA-[Ahx] and H_2N-Gly-Dendron (**10**), HMBC NMR was used to prove that the methylene proton of the glycine methylene (3.8 ppm) on the H_2N-Gly-Dendron is coupled to the carbonyl carbon (173 ppm) on the peptide. Further confirmation that the carbon at 173 ppm was the carboxylic acid carbon from the peptide came from the peak between 173 ppm and 2.1 ppm (the methylene protons on the peptide chain). An HSQC was also used to monitor any shifts in the proton and carbon spectra that occurred due to coupling (Figures 3.8, 3.9 and 3.11). Fortunately, the peak at 3.8 ppm did not shift significantly nor did any other proton peak shift to overlap this methylene. This system is a rare example for using NMR to determine coupling, since often with larger synthetic products peaks overlap too much to be assigned.

Since no information regarding the coupling efficiency was obtained with NMR, a ninhydrin assay to quantify the concentration of the primary amines in each sample was completed. The primary amine concentration was then used to back calculate the number of peptides attached to the dendron. Ninhydrin assay was performed by reacting samples with a DMSO ninhydrin standard in boiling water for 10 minutes followed by cooling and addition of ethanol. A series of standard leucine samples from 10 nM to 1 mM were reacted along with known

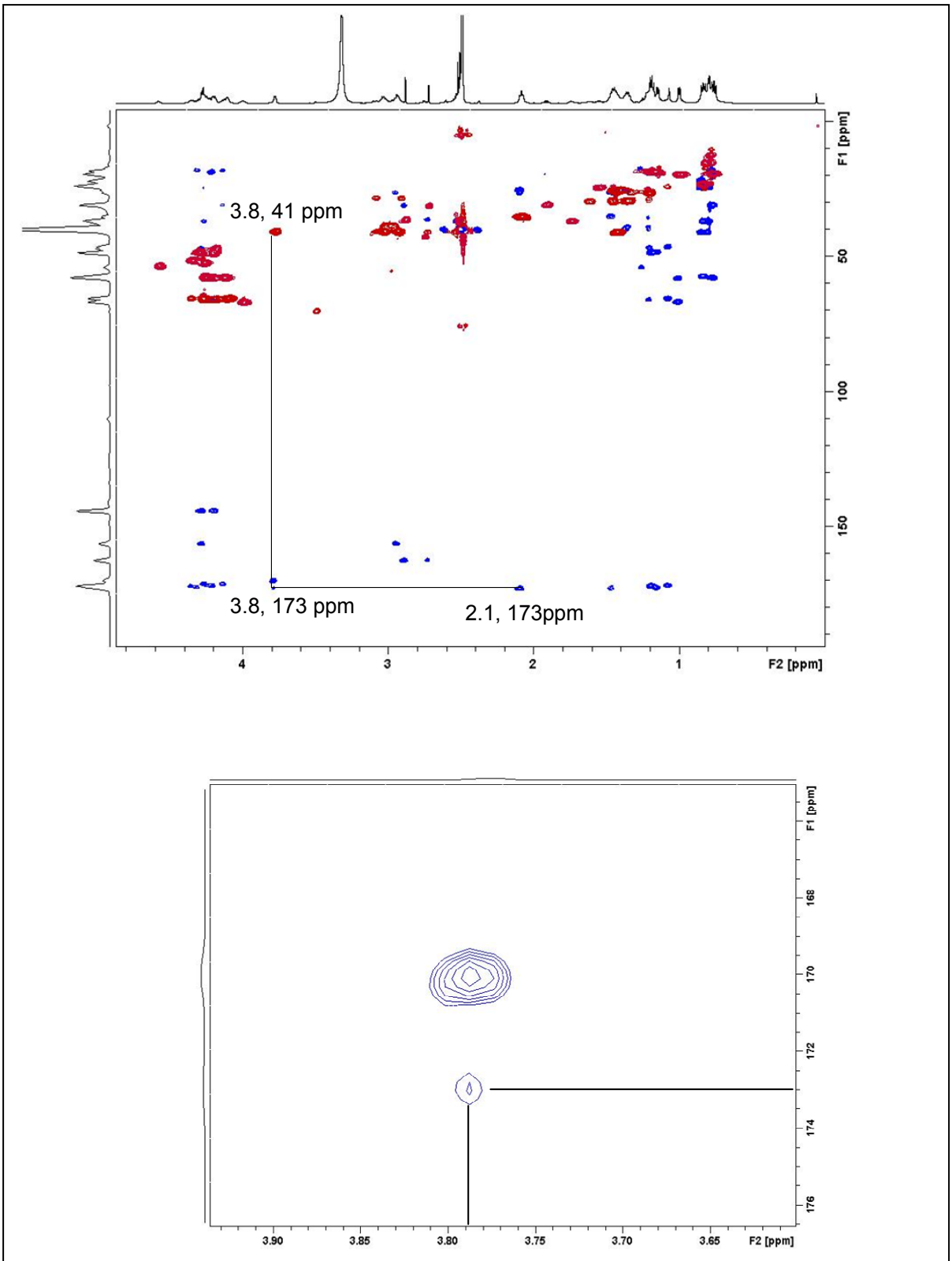

Figure 3.11. The HMBC (blue) and HSQC (red) NMR spectra of FmocPep-Dendron (**10**). Top: full spectra; Bottom: zoom in of the peak at 3.8 and 173 ppm.

samples like the peptide and the Gly-Dendron and the unknown samples (peaks eluted from the SEC column) at 0.1 mg/mL. The amine concentration of each sample was determined from the linear relationship of the leucine standards. All four primary amines on the dendron reacted with the ninhydrin while the peptide did not react significantly with the ninhydrin, as expected since no primary amines are present. To determine the number of free amines present in the unknown samples, the amine concentration of 1, 2, 3, and 4 peptides attached to the dendron were calculated. These concentrations were then compared with the concentration of amine determined by the assay. As shown in Figure 3.12,

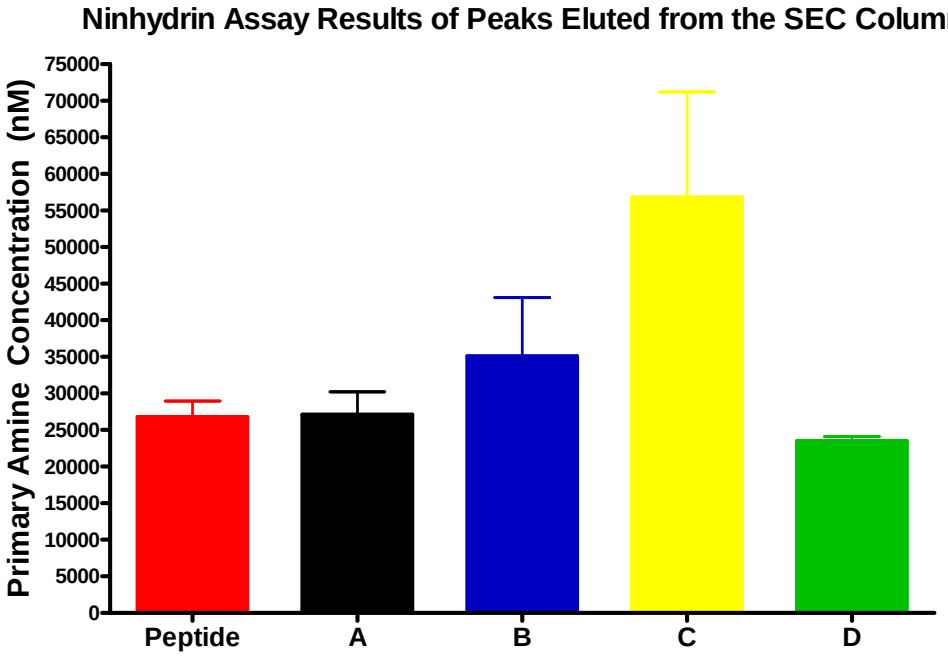

Figure 3.12. Concentration of peaks A-D eluted from the SEC column as determined by the ninhydrin assay.

peak **A** has the same amount of primary amine as the peptide, which was normalized to zero. A steadily increasing amount of primary amine is found from peak **A** to peak **C** followed by the concentration dropping radically from peaks **C** to **D**. Table 3.1 presents calculated concentrations of amine and presents the expected concentration for each anticipated coupling product (1, 2, 3 or 4 peptides attached) as well as the concentrations of amine compared to the peptide. All samples were normalized to the peptide. As can be seen in Table 3.1, peaks **A** and **D** have no primary amines indicating they are either peptide or 4 peptides attached to the dendron, since these are the two possible products

Table 3.1. Concentration of primary amine in the coupled product and the calculated concentration for each theoretical product.

Compound	Calculated Concentration	Peak	Concentration
Fmoc-[Ahx]-AVRWLLTA-[Ahx]	0 uM		
4 peptides attached	0 uM	A	0 uM
3 Peptides Attached	21 uM	B	21 uM
2 Peptides Attached	59 uM	C	77 uM
1 Peptide Attached	147 uM	D	0 uM

without any primary amines. Peak **B** is 21 μM in amine, equivalent with 3 peptides attached to the amine. Peak **C** is 77 μM in amine, about half way between 2 and 1 peptides attached to the dendron. Based on the SEC, NMR and quantitative ninhydrin data it was concluded that Peak **A** has 4 peptides

attached to the dendron, peak **B** has 3 peptides attached; peak **C** is a mixture of 1 and 2 peptides attached; and peak D is unreacted peptide.

After several MALDI-TOF MS conditions were attempted, including varying the matrix, the concentration of matrix, the concentration of analyte, the matrix to analyte ratio and the settings on the instrument, only a peak at 1,471 could be obtained. The MW 1,471 was found to be consistent with breakage of the ester bond between the Gly and dendron, indicating coupling. Occasionally, the breakage of an interior dendron ester bond was also observed. These MALDI-TOF results gave no information about how many peptides were attached to each dendron. Finally, MALDI-TOF conditions were discovered that provided the expected MW ion. To obtain spectra of intact molecules, the samples were dissolved in 80 -90% Tricine Buffer and 10 - 20% methanol, then mixed 10:1 with alpha-cyano-4-hydroxycinnamic acid (CHCA) in 50:50 acetonitrile/water with 0.05% TFA and spotted on the MALDI plate. The MALID-TOF MS of peak **A** is shown in Figure 3.13. The MW ion peak is at 6,167. The peak at 4,733 is consistent with 1 peptide fragmenting between the Gly and the dendron. Since the Gly was initially attached to the dendron, this indicates that it is a fragment and not incomplete coupling. Also, SEC confirmed that only 1 peak (consistent with 4 peptides attached) was present. The fragment at 2,735 is consistent with 2 peptides fragmenting at the ester bond in the interior dendron portion and 1 peptide fragmenting between the valine and arginine residues. Finally, the peak at 1,471 correlates to the Fmoc-Pep-Gly peak that was seen in many of the

previously attempted MALDI spectra indicating coupling between the peptide and the dendron.

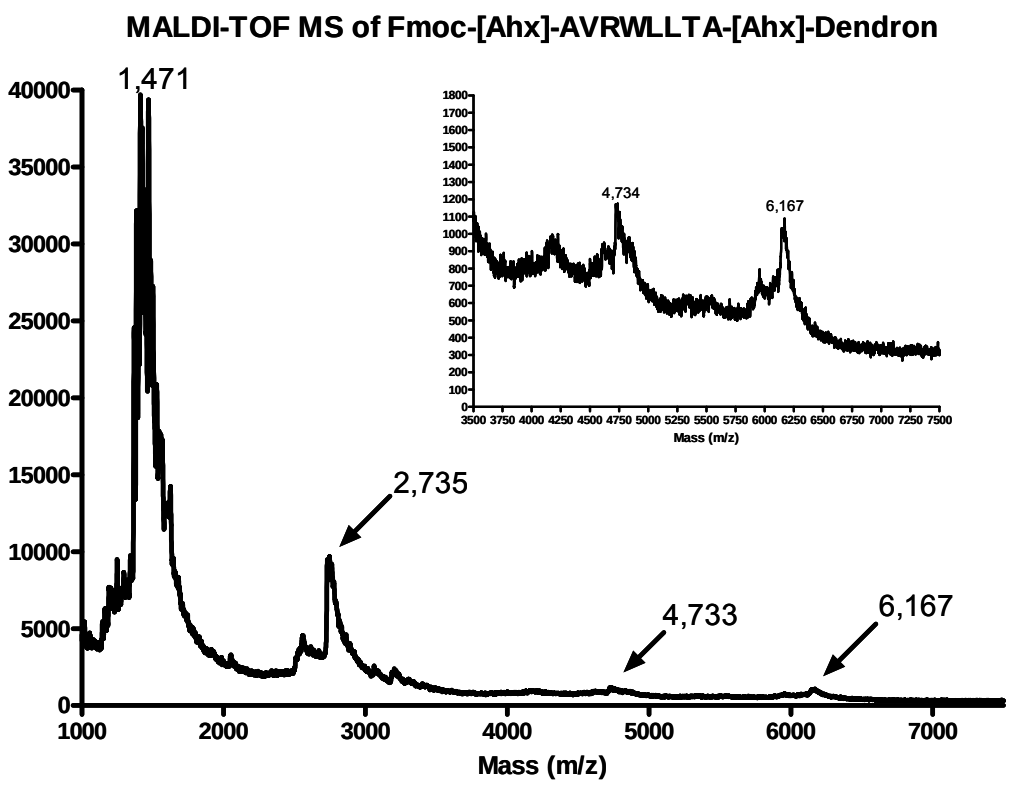

Figure 3.13. MALDI-TOF MS of Fmoc-Pep-Dendron (**10**).

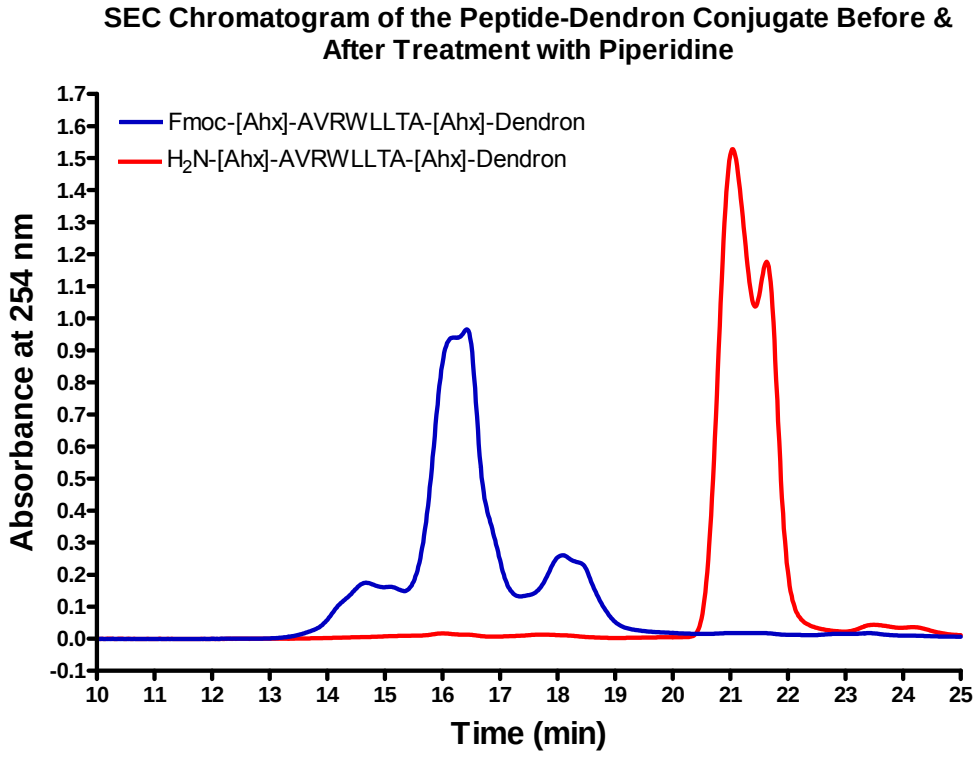

Figure 3.14. SEC traces before and after treatment with piperidine to remove the Fmoc groups.

3.4 Synthesis of DOX-Pep-Dendron

In order to attach doxorubicin (DOX) to the peptide-dendron conjugate, the DOX first had to be modified to contain a carboxylic acid. This was accomplished by reacting the DOX with glutaric anhydride (Scheme 3.3), producing 5-((2S,3S,4S,6R)-3-hydroxy-2-methyl-6-((1S,3S)-3,5,12-trihydroxy-3-(2-hydroxyacetyl)-10-methoxy-6,11-dioxo-1,2,3,4,6,11-hexahydrotetracen-1-yloxy)tetrahydro-2H-pyran-4-ylamino)-5-oxopentanoic acid (**11**, DOX-COOH), a DOX with a linker off the amine that terminates in a carboxylic acid. Mass

spectrometry confirmed the product with MW peaks of 680 (DOX-COOH+Na^+) and 696 (DOX-COOH+K^+). The spectrum is shown in the experimental section.

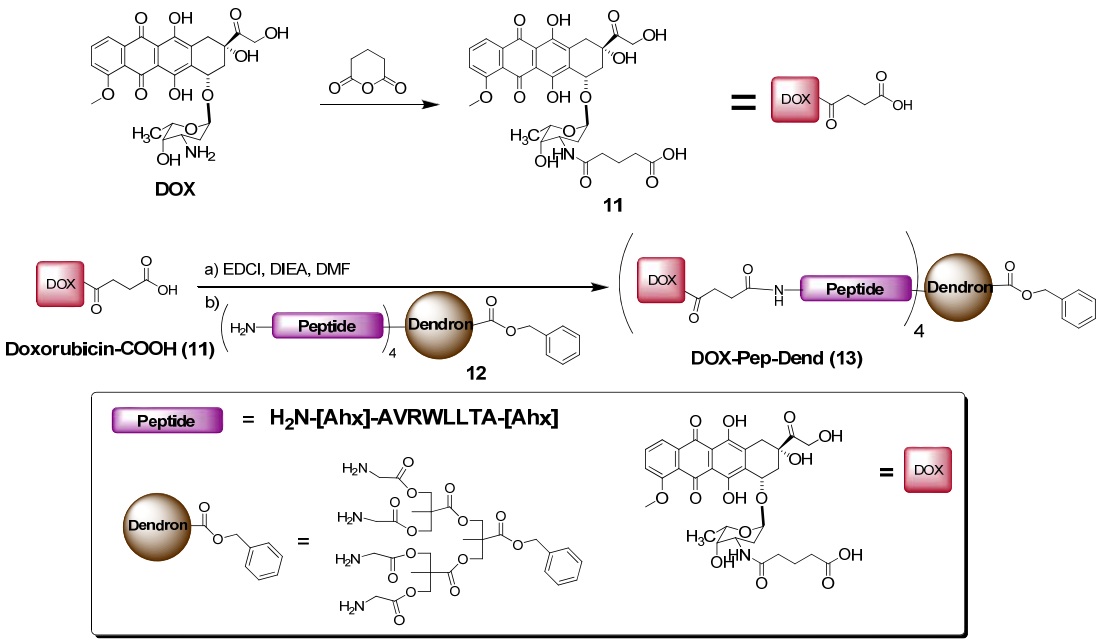

Scheme 3.3. Synthesis of DOX-Pep-Dendron (**13**).

DOX-COOH (**11**) was attached to the H_2N-Pep-Dendron via peptide coupling conditions as shown in Scheme 3.3. The DOX-COOH (**11**) was activated with EDCI in DMF with DIEA prior to addition to H_2N-Pep-Dendron in DMF. Typically, 6 - 8 equivalents of DOX-COOH were used per dendron to ensure complete coupling of all primary amines present. The reaction was followed with SEC by running the reaction within 5 minutes of the activated DOX-COOH (**11**) being added to the dendron and then often 2 and 4 hours followed by at least every 24

hours after the coupling reaction was started. The reaction was followed at 280 nm to track the H_2N-Pep-Dendron (**12**) and 500 nm to track the DOX. A new peak appeared at 18 minutes in both the 280 and 500 nm channels which is consistent with a coupling product. Once the SEC remained consistent, the reaction was concentrated and purified by SEC.

3.5 Characterization of DOX-Pep-Dendron

The DOX-Pep-Dendron was characterized with both SEC, MALDI-TOF MS and ninhydrin. Since DOX absorbs at 500 nm while the other components of the reaction do not, the product peak was located by monitoring the chromatogram at 500 nm for DOX-COOH (**11**) and 280 nm for H_2N-Pep-Dendron (**12**). As can be seen in Figure 3.15, the DOX-COOH (**11**) coupled H_2N-Pep-Dendron (**12**) elutes at 18 minutes while DOX-COOH (**11**) elutes at 24 minutes. Furthermore, the DOX-Pep-Dendron (**13**) peak elutes earlier than the H_2N-Pep-Dendron (**12**), indicating the creation of a larger molecule. However, the DOX-Pep-Dendron (**13**) elutes later than H_2N-Pep-Dendron (**12**). This is possibly due to a conformational change in the molecule from going to a hydrophobic end groups (DOX) form hydrophilic (NH_2) end groups. Since the SEC column is designed for peptides and proteins, which have a defined shape, it is possible that the less defined structures of H_2N-Pep-Dendron (**12**) and DOX-Pep-Dendron (**13**) could interact differently with the column packing beads and cause elution times to vary.

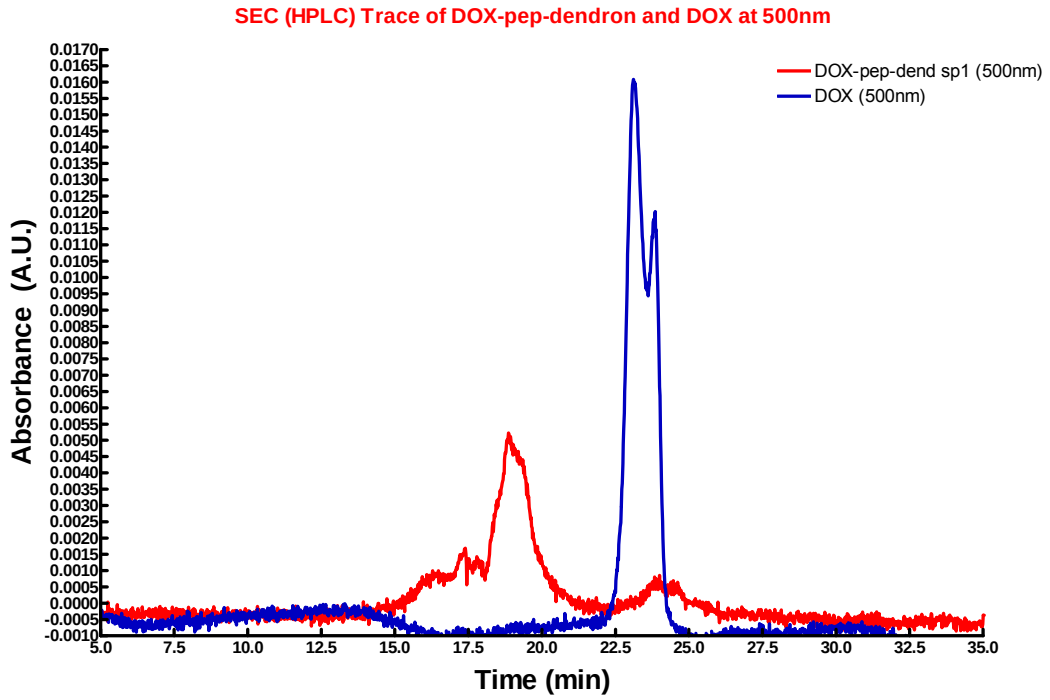

Figure 3.15. SEC traces of DOX-Pep-Dendron (**13**) and DOX-COOH (**11**)

To further show that the DOX-COOH attached to the H_2N-Pep-Dendron (**12**), MALDI-TOF MS was performed on the isolated product (Figure 3.16). Unfortunately, the product ion peak could not be detected, but a quadruply charged (m/z = 4) product ion peak was observed at 1,981 amu. Also, a peak at 1,380 amu was detected which is the DOX-[Ahx]-AVRWL fragment, indicating coupling of the DOX to the H_2N-Pep-Dendron scaffold. Extensive spotting on a TLC plated followed by staining with ninhydrin elicited no color change, indicating no primary amines present in the molecule. The culmination of these data

indicate that all four primary amines from H_2N-[Ahx]- AVRWLLTA-[Ahx]-Dendron (**12**) reacted with the DOX-COOH (**11**) to give a single product with a DOX-COOH (**11**) molecule attached to each amine on the H_2N-Pep-Dendron scaffold.

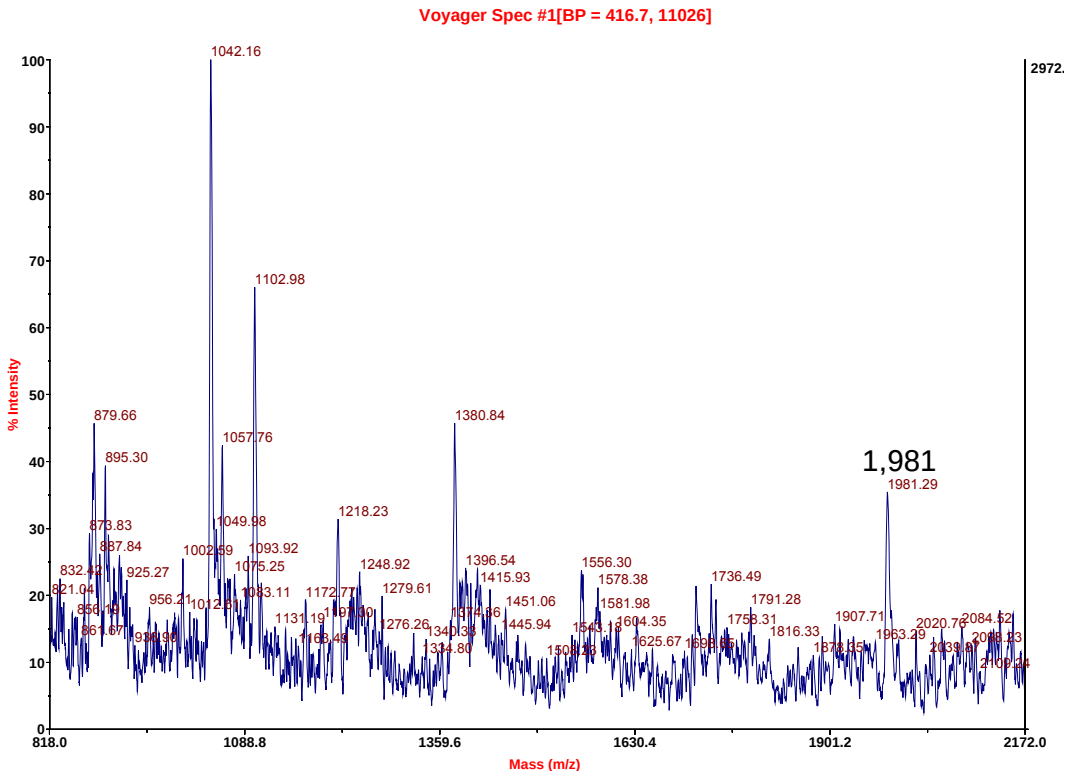

Figure 3.16. MALDI of DOX-Pep-Dendron.

3.6 Toxicity studies of DOX-Pep-Dendron

Once the synthesis of the DOX-Pep-Dendron was complete, cellular toxicity studies were done using PyVT-R221A-luc cells. These cells were developed from the MMTV-driven polyoma virus middle T antigen transgenic

mouse, developed by Muller and colleagues in 1992[132], which is routinely used in the Matrisian laboratory for studies of breast cancer metastasis to the lung. The MMTV-driven polyoma virus middle T antigen transgenic mouse is an improved model for studying breast to lung metastasis compared to previous models[126]. Furthermore, these tumors and the resulting cells express high levels of MMP9[124].

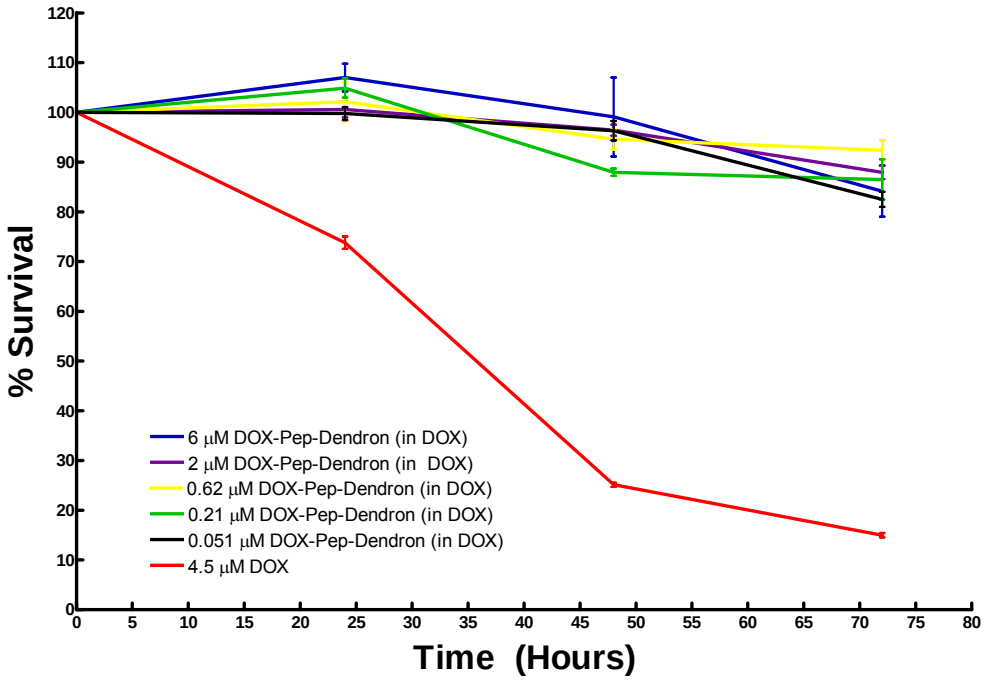

Figure 3.17. Toxicity of DOX-Pep-Dendron (**13**) in PyVT-R221A-Luc cells.

The toxicity studies were done by plating 40,000 cells into 24 well plates and allowing them to equilibrate for 24 hours. Three or four 24 well plates per

sample were prepared to obtain 3 - 4 time points. Cells were then treated media containing compound to be tested (Dose 1) and were incubated another 24 hours. After 24 hours, three of the replicates were redosed (Dose 2) while one plate was treated with trypsin to detach the cells and counted using the trypan blue method. This process was repeated until cells had 4 doses of drug over a 96 hour period. The first toxicity studies indicated the intact DOX-[Ahx]-AVRWLLTA-[Ahx}-Dendron (**13**) was not toxic to the PyVT-R221A-luc cells. Since the molecule was designed as a prodrug, this lack of toxicity was

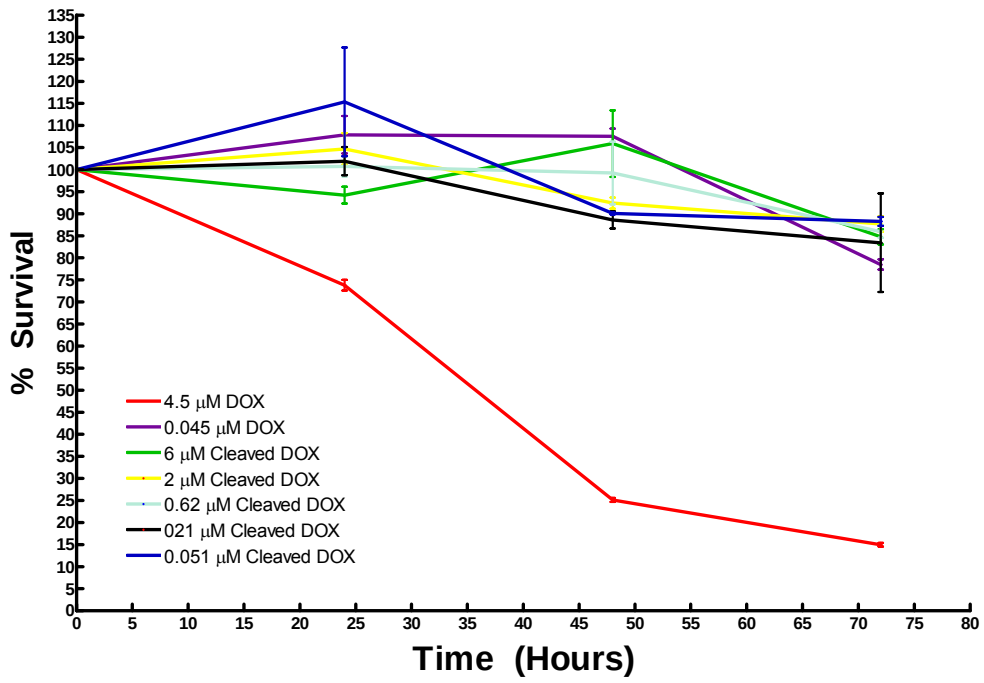

Figure 3.18. Toxicity curves of Cleaved DOX-Pep-Dendron (**13**).

anticipated. As seen in Figure 3.17, none of the concentrations of DOX-Pep-Dendron (6 μM to 51 nM in DOX) were toxic towards the cells. This was compared to a 4.5 μM solution of DOX, which is lethal to the cells.

Although the DOX-Pep-Dendron (**13**) digested with MMP9 to provide the cleaved product, DOX-[Ahx]-AVRW, was hypothesized to be toxic against PyVT-R221A-Luc cells, the compound was found to be non-toxic. As shown in Figure 3.18, the cleaved compound had no toxicity at the same concentrations (6 μM to 51 nM in DOX) as the intact DOX-Pep-Dendron (**13**), implying that the prodrug did not produce a toxic molecule when cleaved. Although, the inactivation of DOX was accomplished with the prodrug approach, it was not possible to reactivate the drug's activity. Although, the cleaved product, DOX-[Ahx]-AVRW, did not produce toxicity, the reason for this lack of toxicity was not completely understood. Any of a number of possible cleaved molecules could lead to the lack of toxicity of the cleaved prodrug. To narrow down the possibilities, the DOX-COOH molecule was tested for toxicity against the PyVT-R221A-Luc cells.

Further experiments revealed that the DOX-COOH (**11**) was not toxic at concentrations as high as 152 μM while DOX is toxic at concentrations as low as 184 nM in the PyVT-R221A-Luc cells. As shown in Figure 3.19, the DOX-COOH

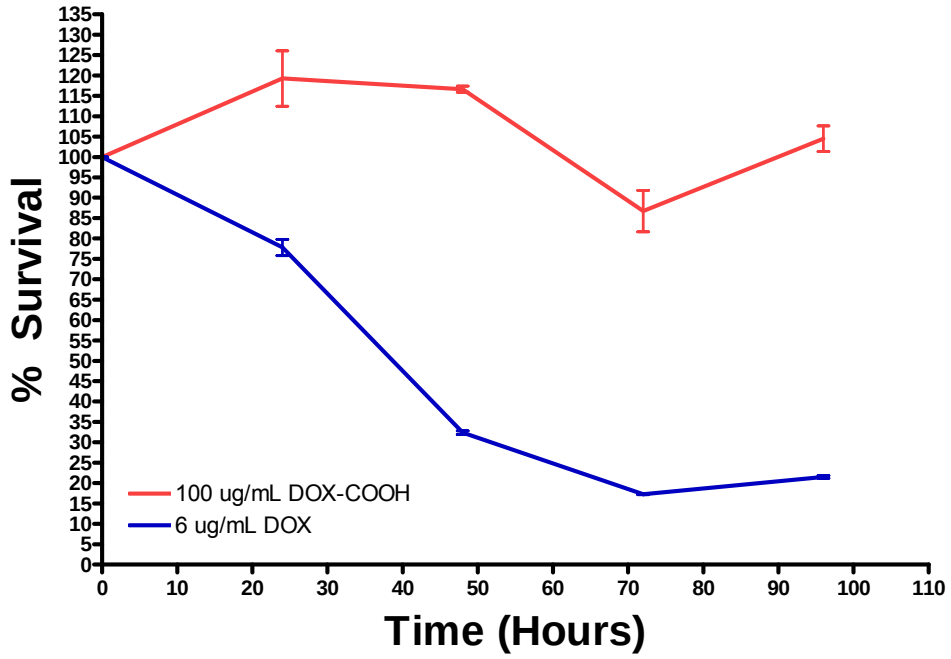

Figure 3.19. Toxicity of DOX-COOH (**11**) versus DOX.

(**11**) did not produce a toxic effect over 96 hours and 4 doses. With this data in hand, further investigation into the literature revealed that modification at the amine to form an amide and the specific glutaric acid modification used inactivates the toxic effects found in DOX[182-183]. In fact most modifications that did not leave an amine within close proximity of the DOX amine inactivated the DOX[131, 182-183].

3.7 Conclusions

In the process of attempting to create an MMP9 prodrug, that can be attached to a modular system for delivery and monitoring the drug *in vivo* many lessons were learned. The most important lesson that was learned was that not all coupling strategies produce the desired results. This knowledge was then moved forward into redesigning molecules using a different peptide (AVRWLL) and different coupling strategy between the DOX and the peptide. Major accomplishments highlighted in this chapter include, 1) the design and synthesis of the delivery system (H_2N-Gly-Dendron, **9**), 2) the conjugation of the dendron scaffold to MMP9 cleavable peptides and 3) cellular toxicity of the DOX conjugates. The major challenge in preparing an MMP9 cleavable peptide system was in characterizing the final compounds. First, attachment had to be proven and second how many groups attached needed to be determined. The Fmoc-Pep-Dendron coupling was easily accomplished with standard peptide coupling reagents, but finding the appropriated HPLC conditions proved more difficult. Ultimately this was accomplished by using a SEC column rather than a reverse phase C18 silica column. The SEC column provided the added advantage of giving the relative size of the starting materials compared to what was being formed. By seeing peaks elute earlier from the column compared to the peptide or the dendron it was possible to discern that coupling was taking place since larger molecules were being synthesized. Further characterization was performed using NMR, a ninhydrin assay for amines and MALDI-TOF MS.

All the data show that the peptide and dendron couple to completion (four peptides attach to each dendron).

After coupling the dendron and peptide, the first DOX derivative was attached to the MMP9 cleavable Fmoc-Pep-Dendron. This synthesis was accomplished by modifying the DOX with glutaric anhydride to provide a carboxylic acid off the amine and then coupling to the FmocPep-Dendron. Characterization was accomplished using SEC and MALDI-TOF MS. While, the DOX-Pep-Dendron construct was successfully constructed and found to be non-toxic when DOX was coupled to the scaffold it did not perform as a prodrug. In other words, the toxic effect of DOX could not be re-initiated once DOX was released from the scaffold by MMP digestion. After further investigation, it was found that the modified DOX (DOX-COOH, **11**) was not toxic to the cells at high concentrations (up to 152 μM) concentrations. Although some literature suggested that this modification was acceptable[131], upon further investigation two papers were found stating that this specific modification eliminated the toxicity of DOX[182-183]. Since the original strategy with DOX was unfruitful, the system was redesigned, based on the literature, to incorporate a new DOX coupling strategy[184].

3.8 Experimental Procedures

General Methods:

MDA-MB-231 cells were purchased from ATCC and cultured in DMEM, 10% FBS and gentamycin with 5% CO_2. PyVT-R221A-Luc cells were obtained

from the Matrisian laboratory and cultured in DMEM without L-glutamine, 10% FBS, gentamycin and puromycin with 5% CO_2. LLC-RSV and LLC-MMP9 cells were obtained from the Matrisian laboratory and cultured in DMEM, 10% FBS and gentamycin with 5% CO_2. The custom ordered peptides were purchased from Genscript™. The enzymes were purchased from Calbiochem. All other chemicals were purchased from Fisher Scientific or Aldrich Chemical companies and used as is unless otherwise indicated.

Ninhydrin Assay:

A stock solution of leucine was made to be approximately 10 mM in water, using a volumetric flask. A series of more dilute leucine standards were made from this original stock solution to cover the amine concentration range being examined. The products to be tested were dissolved in water at 0.1 mg/mL and pipetted (100 μl per sample) into individual microcentrifuge tubes. Next, 200 μl of ninhydrin reagent was added and the tubes were sealed and placed in boiling water for 10 minutes. The solutions were cooled to room temperature, 600 μl of ethanol was added and the samples were analyzed by looking at the absorbance at 562 nm. A graph of the absorbance intensity versus concentration was linear from mM to nM concentrations and used to determine the concentration of primary amine present in the sample.

5-(3-hydroxy-2-methyl-6-(3,5,12-trihydroxy-3-(2-hydroxyacetyl)-10-methoxy-6,11-dioxo-1,2,3,4,6,11-hexahydrotetracen-1-yl)tetrahydro-2H-pyran-4-ylamino)-5-oxopentanoic acid (DOX-COOH, 11)

Doxorubicin was stirred in DMF with glutaric anhydride overnight and purified by silica gel chromatography as synthesized previously[131]. ^{1}H NMR 400 MHz; δ 0.9779 (t, 2H), 1.55 (d, 2H), 1.69 (s, 4H), 1.76 (s,2H), 2.72 (s, 2H), 2.98 (s, 6H), 3.41 (bs, 7H), 6.63 (s, 4H), 7.27 (s, 1H), 7.37 (s, 1H), 7.47 (s, 1H), and 8.98 (s, 2H) ppm. ^{13}C NMR 125 MHz. δ 15.7 (CH_3), 21.7, 22.1, 25.2 (CH_2), 32.8 (CH_2), 33.1 (CH_2), 34.1 (CH_2), 36.3 (CH_2), 42.0, 43.5, 54.5 (C-N), 56.1 (CH_3-O), 60.2 (C-O), 65.5 (C-O), 68.3 (C-O), 69.8 (C-O), 72.3 (C-O), 90.3, 94.1 (Acetal), 114.2 (Ar), 116.2 (Ar), 118.2 (Ar), 120.2 (Ar), 121.4 (Ar), 158.3 (Ar), 158.5 (Ar), 158.7 (Ar), 158.8 (Ar), 159.0 (Ar), 171.4 (HNCO), 172.0 (COOH), and 174.7 (C=O) ppm. COSY correlations: 0.98 to 2.98, 1.55 to 1.76, 1.67 to 3.41, 1.67 to 2.98, 2.98 to 8.98 ppm.

2-(benzyloxycarbonyl)-2-methylpropane-1,3-diyl bis[3-(2-tert-butoxycarbonylamino acetate)-2-((2-tert-butoxycarbonylamino acetate)-methyl)-2-methylpropanoate) (Boc-Gly-Dendron):

All glassware used in the reaction was flame dried and cooled in a desiccator prior to use. The solvents were anhydrous and all solid materials were dried under vacuum for more than 3 hours prior to use and exposed to anhydrous Ar(g) gas upon breaking the vacuum seal. First, 2-(benzyloxycarbonyl)-2-methylpropane-1,3-diyl bis(3-hydroxy-2-(hydroxymethyl)-2-methylpropanoate) (1.1849g, 2.60 mmols), 2-(tert-butoxycarbonylamino)acetic

acid (Boc-Gly, 2.0277g, 11.6 mmols) and EDCI (2.4257g, 12.7 mmols) were dissolved in DMF individually and then mixed under Ag(g). Next, DIEA was added via syringe and the reaction was stirred overnight (16 hours). The reaction was concentrated under reduced pressure, dissolved in methylene chloride (100 mL) and washed with water (3 x 100 mL). The aqueous layers were combined and extracted with methylene chloride (3 x 100 mL). The organic layers were combined and TLC with 1:1 hexanes: ethyl acetate revealed 4 spots (Rf = 0.7, 0.38, 0.2, 0.12) after staining with potassium permanganate. The organic layers was dried with magnesium sulphate, filted and concentrated onto silica gel at reduced pressure. The product was purified on the Biotage SP1 system with a 40i column using a gradiant (100% hexanes to 100% ethyl acetate over 700 mL). The product was isolated as the second peak eluted (Rf = 0.38), and concentrated as a viscous yellow oil to yield 886.6 mg pure product (31%). MS $(ESI)^+$: 1107.5 Dalton $(M + Na)^+$; Calculated: 1107.48 Dalton ($C_{50}H_{76}N_4O_{22}Na$). ^1H NMR 400 MHz (*d*6-DMSO) δ 8.00 (s, 2H), 7.35 (s, 5H), 5.18 (s, 2H), 4.13 (m, 11H), 3.77 (dm, 12H), 2.96 (s, 6H), 2.88 (s, 7H), 2.05 (s, 5H), 1.50 (s, 6H), 1.43 (s, 6H), 1.26 (s, 9H), 0.98 (s, 6H) ppm.

2-(benzyloxycarbonyl)-2-methylpropane-1,3-diyl bis[3-(2-amino acetate)-2-((2-amino acetate)-methyl)-2-methylpropanoate) (H_2N-Gly-Dendron):

Boc-Gly-Dendron was dissolved in 1 mL of 1:1 methylene chloride to trifluoroacitic acid. The reaction was stirred overnight then concentrated under vacuum to provide an oil with a very slight yellow color. The product was used without further purification. MS $(ESI)^+$: 685.40 Dalton $(M + H)^+$; Calculated:

685.29 Dalton ($C_{30}H_{45}N_4O_{14}$). 1H NMR 400 MHz (*d*6-DMSO) δ 8.05 (bs, 4H), 7.36 (s, 5H), 5.14 (s, 2H), 4.25 (bs, 11H), 3.81 (bs, 9H), 1.22 (s, 3H), 1.13 (s, 6H) ppm.

Fmoc-Pep-Gly-Dendron:

All glassware used in the reaction was flame dried and cooled in a desiccator prior to use. The solvents were anhydrous and all solid materials were dried under vacuum for more than 3 hours prior to use and exposed to anhydrous Ar(g) gas upon breaking the vacuum seal. The peptide of sequence Fmoc-Pep-COOH (35.12 mg, 0.026 mmols) was dissolved in 3.5 mL DMF with 4A molecular sieves). Solutions of EDCI (20 mg/mL, 5.87 mg, 0.0306 mmols) and BOP (20 mg/mL, 13.5 mg, 0.0305 mmols) were made separately and added to the peptide solution followed by DIEA (10 μl. 0.109 mmols). The peptide solution was stirred for 30 minutes at room temperature before H_2N-Gly-Dendron (3.5 mg, 0.00511 mmols) was added to the reaction. The reaction was stirred under Ar(g) for 69 hours with SEC being completed after 0.3, 1.5, 21, 24, 44, 49 and 69 hours. The reaction was filtered and the filter cake with molecular sieves was washed with DMF. The filtrate was concentrated under reduced pressure to give a brown oil. The oil was dissolved in actetonitrile/water and purified by SEC to elute 6 fractions, which were concentrated and characterized individually. The first peak eluted provided 22.5 mg (72%) of $(Fmoc\text{-}Pep)_4$-Gly-Dendron. MADLI-TOF MS (CHCA) Found 6,167 Dalton (M + K)+; calculated 6,162 Dalton ($C_{314}H_{453}N_{60}O_{66}K$). SEC (55% 0.05% TFA in Acetonitrile/ 45% 0.065% TFA in

water) elution time 14 minutes. Ninhydrin assay (see procedure above): no primary amines present.

H_2N-Pep-Gly-Dendron:

Fmoc-Pep-Gly-Dendron (4.01 mg) was dissolved in 1 mL of DMF and injected onto the SEC column. Then 1 mL of piperidine was added followed by a second SEC injection (within 60 seconds). The reaction was stirred overnight, injected onto the SEC column, concentrated under vacuum. The oily product was dissolved in water and lyophilized overnight to give an extremely viscous yellow product. . MADLI-TOF MS (CHCA) Found 1,256 Dalton (Fragment: [Ahx]-AVRWLLTA-[Ahx]-Gly + K)$^+$; calculated 1,251 Dalton ($C_{58}H_{97}N_{15}O_{13}K$). SEC (55% 0.05% TFA in Acetonitrile/ 45% 0.065% TFA in water) elution time 21.5 minutes. Ninhydrin assay (see procedure above): 4 primary amines present.

5-((2S,3S,4S,6R)-3-hydroxy-2-methyl-6-((1S,3S)-3,5,12-trihydroxy-3-(2-hydroxyacetyl)-10-methoxy-6,11-dioxo-1,2,3,4,6,11-hexahydrotetracen-1-yloxy)tetrahydro-2H-pyran-4-ylamino)-5-oxopentanoic acid (DOX-COOH):

First, 2.33 mg (0.00402 mmols) of Doxorubicin ((8S,10S)-10-((2R,4S,5S,6S)-4-amino-5-hydroxy-6-methyltetrahydro-2H-pyran-2-yloxy)-6,8,11-trihydroxy-8-(2-hydroxyacetyl)-1-methoxy-7,8,9,10-tetrahydrotetracene-5,12-dione) was dissolved in 0.5 mL of pyridine. Then, glutaric anhydride (0.46 mg, 0.00403 mmols) was added. The reaction was covered with aluminum foil and stirred overnight. Solvent was removed under vacuum and the product was purified on the Biotage SP1™ system with a gradient from 100% methylene

chloride to 25% methanol. The product peak was concentrated to give 2.55 mg (96%). MADLI-TOF MS (CHCA) Found 680.39 Dalton $(M + Na)^+$ and 696.94 $(M+K)^+$ calculated 680.61 Dalton ($C_{32}H_{35}NO_{14}Na$) and 696.72 Dalton ($C_{32}H_{35}NO_{14}K$).

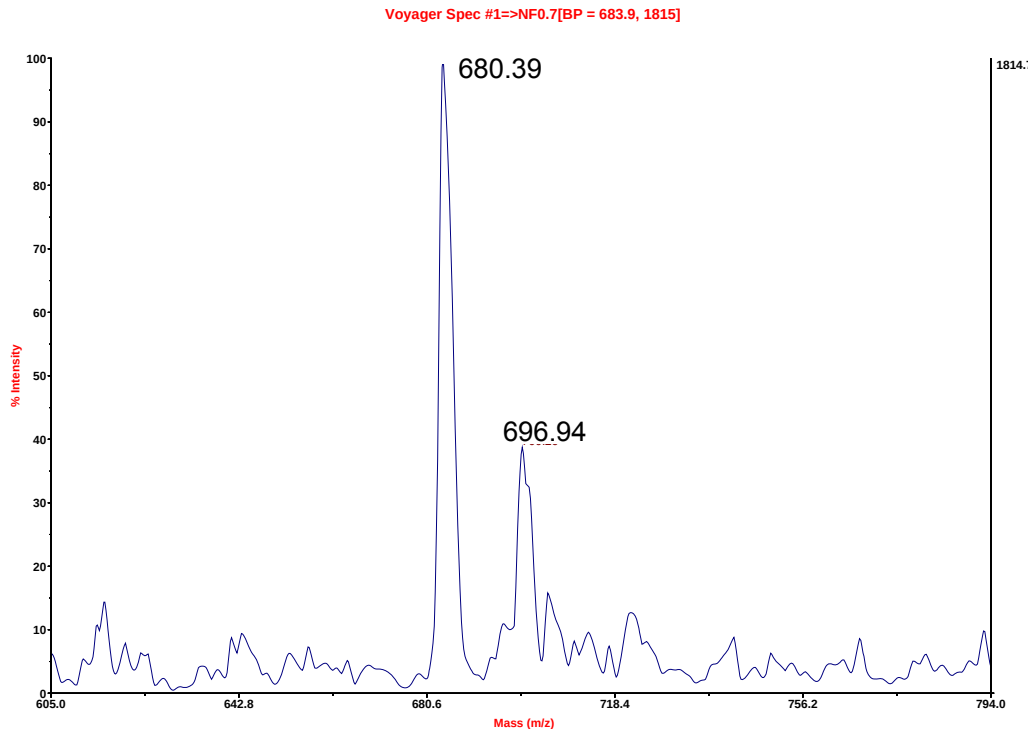

Figure 3.20. Mass Spectrometry of DOX-COOH.

DOX-Pep-Dendron:

All glassware used in the reaction was flame dried and cooled in a desiccator prior to use. The solvents were anhydrous and all solid materials were dried under vacuum for more than 3 hours prior to use and exposed to anhydrous Ar(g) gas upon breaking the vacuum seal. DOX-COOH (1.37 mg, 0.00209 mmols) was dissolve in anhydrous DMF and EDCI (0.7 mg, 0.00365 mmols) and DIEA (0.7 μl, 0.00765 mmols) were added. The reaction was stirred

for 30 minutes prior to the addition of H_2N-Pep-Gly-Dendron (1.37 mg, 0.000519 mmols) in 0.5 mL DMF. The reaction was stirred under $Ar_{(g)}$ until SEC indicated completion. SEC was completed after 5 minutes, 2, 6, 24, 27 and 48 hours. After 48 hours, not change had occurred since the 27 minute chromatogram. The reaction was concentrated under vacuum and purified with SEC chromatography to give 25 mg (79%) of DOX_4-Pep-Dendron. MADLI-TOF MS (CHCA) Found 1981 Dalton $(M+4K)^{+4}$; calculated 1,984 $(C_{81}H_{543}N64O_{110}K_4)/4$.

Cleavage of Peptide compounds with Enzymes:

The compound to be cleaved or tested for ability to cleave was dissolved in methanol at 10 mg/mL. Next, 100 μl of this solution was diluted with 900 μl of tricine buffer to make a 1 mg/mL solution. The solution was injected into the HPLC (C18 silica with 55% 0.05% TFA in Acetonitrile/ 45% 0.065% TFA in water) for a zero time point. Following HPLC, enzyme was added (either MMP9, MMP2 or Trypsin). The vials were incubated at 37 ^{o}C overnight. Again HPLC was used to determine what percentage of the sample had cleaved. For samples which produced solid, the solid was collected, dissolved in 100% methanol and injected into the HPLC. The samples were then characterized with ESI and MALDI-TOF MS to determine the cleavage products. The solid usually contained the cleaved product.

Toxicity studies

PyVT-R221A-Luc cells were cultured in glutamine free DMEM media supplemented with 10% FBS, 500 μg/mL gentamycin and puromycin. Cells were plated at 40,000 – 60,000 cells/mL into 24 well plates (0.5 mL/well) in their culture medium. A separate plated was used for each time point observed in the assay. Thus 4 time points meant that 4 plates were used. The cells were incubated overnight at 37 ^{o}C (usually 24 hours). After examination under the microscope to ensure the cells were attached and looked healthy, the media was aspirated off each well (taking care to not disrupt the cells) and replaced with media containing the drug/ compound of interest or a control compound. The drug and control solutions were made fresh just prior to use. The cells were incubated 24 hours and then either redosed with fresh drug-media solutions or the cells were trypsinized and counted using trypan blue. For typsinization, the media was removed by aspiration and each well was washed with 0.5 mL of DPBS. The DPBS was removed and each well was treated with 200 μl of trypsin. The plate was incubated for 10 - 15 minutes and then agitated, either with a shaker or by hand. Finally, 40 μl of trypan blue was added to each well (typically 4 wells at a time) and the cells were counted with a hemocytometer. The dosing and counting was continued for the remaining time points so that the cells were given fresh drug every 24 hours until counted.

CHAPTER IV

ALTERNATIVE STRATEGY FOR DOX DELIVERY THROUGH AN MMP9 CLEAVABLE PEPTIDE

4.1 Introduction

The modification of doxorubicin (DOX) at the amine to provide a carboxylic acid results in inactive drug. With this knowledge, investigations into alternative strategies for DOX delivery were explored. Since it was reported that Leu-DOX and Leu-Leu-DOX were toxic in HT1080 cells[185], a new prodrug that gave LL-DOX as the active drug was investigated. This was attempted by shortening the peptide sequence from [Ahx]-AVRWLLTA-[Ahx] to AVRWLL. Although AVRWLL has not been reported to be digested with MMP9, it is similar to the known cleavable sequence AVRWLLTA. The sequence AVRWLLTA is cleaved by MMP9 between the tryptophan and leucine residues[178]. The modified strategy leaves the [Ahx] groups off the peptide, shortening the sequence by two residues removing threonine and alanine (TA) attaches DOX to the carboxy terminus rather than the amine terminus of the peptide.

In this chapter, the peptide sequence AVRWLL was investigated as a potential MMP9 activated prodrug for cancer therapy. This was accomplished by 1) synthesizing L-DOX and LL-DOX, 2) testing L-DOX and LL-DOX for toxicity *in vitro*, 3) investigating the digestion of AVRWLL by MMP9, 4) synthesizing AVRWLL-DOX and Dendron-AVRWLL-DOX and 5) investigating the digestion and cytotoxicity of AVRWLL-DOX and Dendron-AVRWLL-DOX. It was

hypothesized that AVRWLL would be cleavage by MMP9 between the W and L residues because; the important recognition sequence was shown to be RWLL. It was anticipated that cleavage would not be as specific or rapid as the sequence AVRWLLTA but sill expected that the drug would be activated selectively in the tumor environment.

4.2 Cleavage of the Fmoc-AVRWLL with Trypsin and MMP9

The peptide, Fmoc-AVRWLL was treated with trypsin and MMP9 in separate vials to determine digestion efficacy. Trypsin was used as a positive control since it cleaves universally between arginine and tryptophan. The peptide was incubated at 37 ^{o}C with either trypsin or MMP9 overnight in 10% methanol in tricine buffer. Reverse phase HPLC (C18 silica with 0.065% TFA in water and 0.05% TFA in acetonitrile) was completed before the addition of enzyme and again after overnight incubation. Figure 4.1 highlights the HPLC results obtained from the cleavage products. As can be seen, the intact Fmoc-AVRWLL peptide elutes at 31 minutes while samples treated with enzyme have more peaks at different elution times. The sample treated with trypsin elutes four peaks at 25, 32, 34 and 36 minutes. The sample treated with MMP9 elutes at 32, 34 and 36 minutes with a small bump at 25 minutes. Since the peak at 31 minutes disappears after treatment with either enzyme digestion is occurring from trypsin and MMP9.

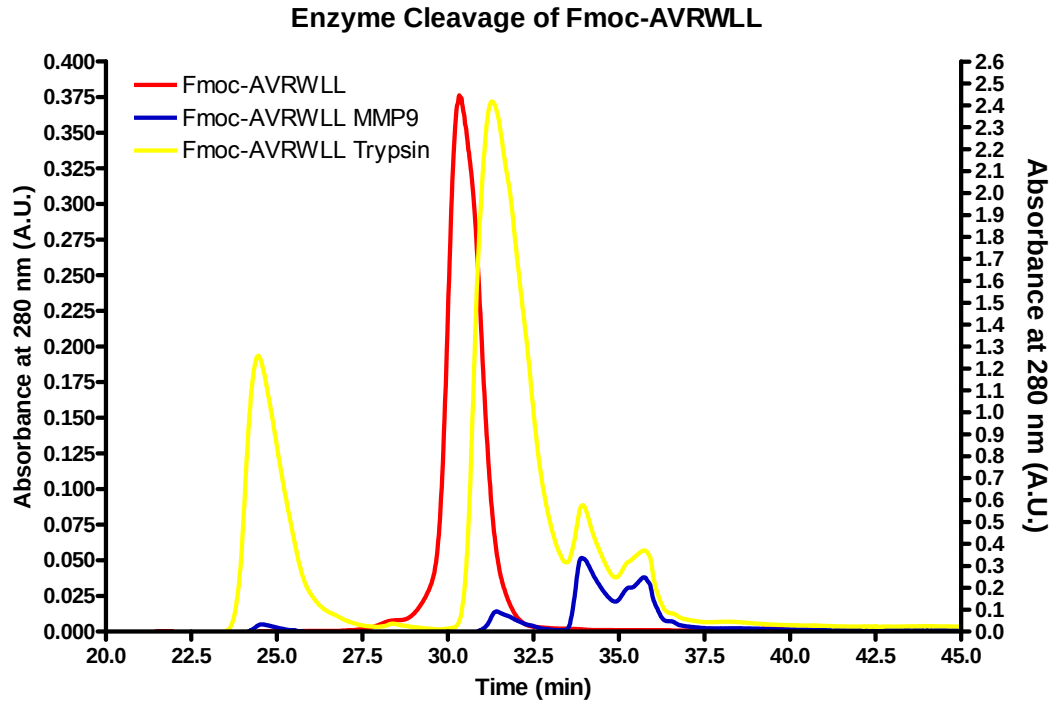

Figure 4.1. Enzyme digestion of Fmoc-AVRWLL. HPLC traces before

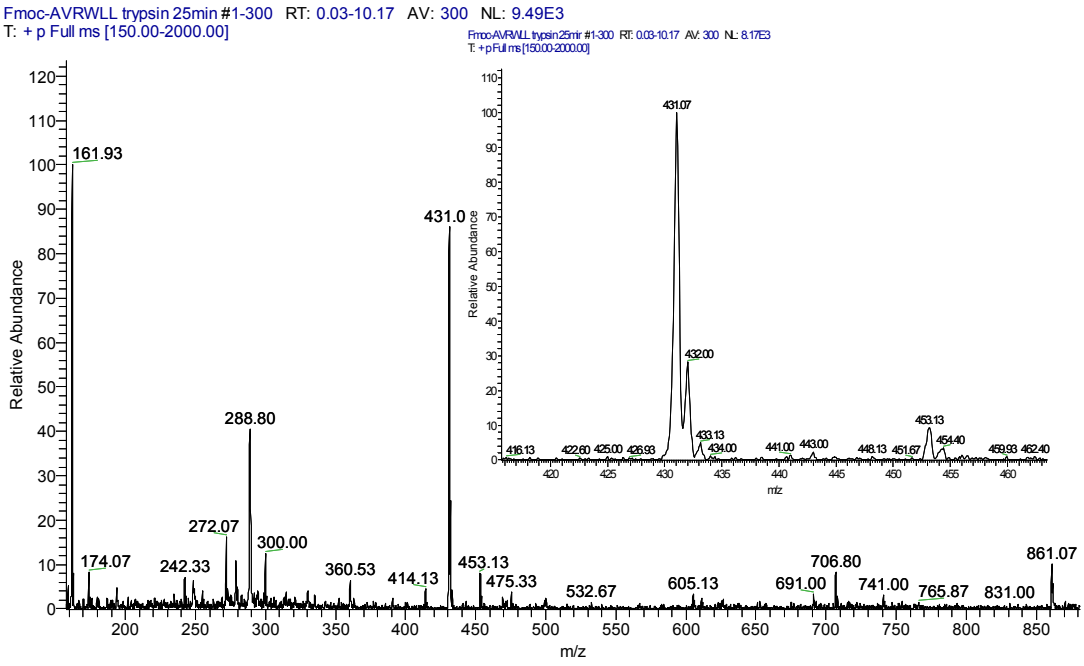

Figure 4.2. ESI MS of Fmoc-AVRWLL cleaved with trypsin. The peak at 431 is from the WLL cleaved product.

The cleavage of the Fmoc-AVRWLL peptide with trypsin and MMP9 was also characterized by collecting the peaks from the HPLC and performing ESI^+ MS on the samples. Trypsin treated Fmoc-AVRWLL provided the expected product, WLL, with a molecular weight of 431.07 amu at a 25 minute elution time from the column (Figure 4.2). When Fmoc-AVRWLL was treated with MMP9, a cleavage product was detected, but not the expected product. Peaks at 567 and 589 were detected at an elution time of 32 minutes as shown in Figure 4.3. This molecular weights are equivalent to protonated and sodiated RWLL-COOH. This product could be further degraded in the cellular or tumor environment to LL-DOX or L-DOX to become activated. The expected cleavage product of LL-COOH, with a molecular weight of 243, was barely detectable in the ESI^+ MS spectrum of the crude cleavage product solution as shown in Figure 4.3. Given that some cleavage is detected in the test tube and the microenvironment of a cell differs significantly from the test tube enough evidence was present to suggest that this peptide may cleave efficiently *in vitro* or *in vivo* to deliver a toxic dose of DOX selectively to cancerous tissue.

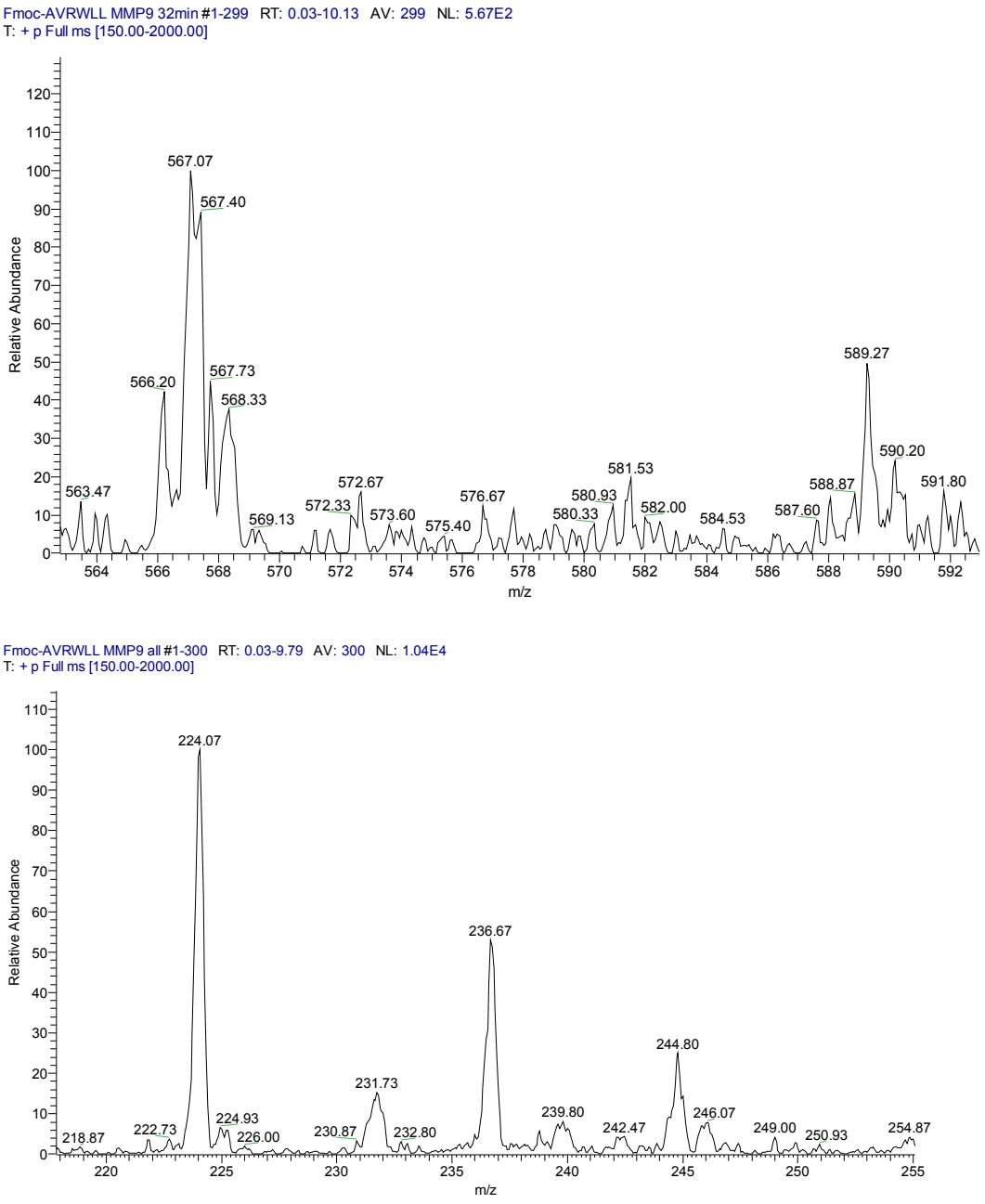

Figure 4.3. ESI MS of Fmoc-AVRWLL after digestion with MMP9. Top, product collected at 32 minutes. The peak at 567 is from unexpected product RWLL. Bottom: expected product LL (229) in the crude mixture.

4.3 Synthesis of Leu-DOX and Leu-Leu-DOX

Leu-DOX (**14**) and Leu-Leu-DOX (**16**) were synthesized using peptide coupling agents 1-ethyl-3-(3'-dimethylaminopropyl)carbodiimide (EDCI) and Benzotriazole-1-yl-oxy-tris-(dimethylamino)-phosphonium hexafluorophosphate (BOP). Leu-DOX was synthesized in two steps by first attaching DOX to BOC-Leu using EDCI and diisopropylethyl amine (DIEA) in dimethyl formamide (DMF)

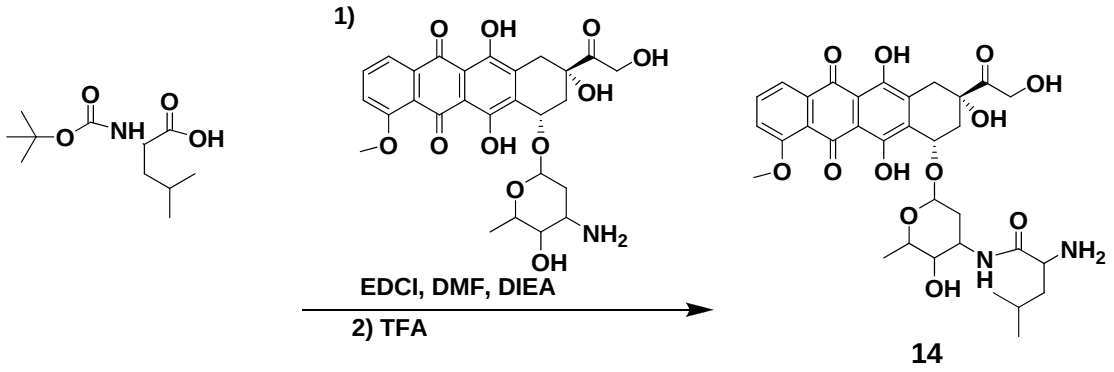

Scheme 4.1. Synthesis of Leu-DOX (**14**).

under anhydrous conditions followed by purification on the Biotage SP1™ system using a hexane/ethyl acetate gradient to give Boc-Leu-DOX. To complete the synthesis, the Boc-Leu-DOX was treated with TFA to remove the BOC protecting group and provide Leu-DOX (Scheme 4.1), which needed no further purification. Nuclear Magnetic Resonance (NMR) and mass spectrometry (MS) match the reported data[185].

Leu-Leu-DOX (**16**) was synthesized in three linear steps by first coupling BOC-Leu with Leu using BOP and DIEA in DMF under anhydrous conditions followed by purification on silica with the Biotage SP1™ system (methylene chloride to methanol gradient). Pure product **15** was then reacted with DOX using EDCI and DIEA in DMF under anhydrous conditions to obtain Boc-Leu-Leu-DOX after purification on the Biotage SP1™ system. Purification was accomplished by first running a gradient with hexanes/ ethyl acetate and then

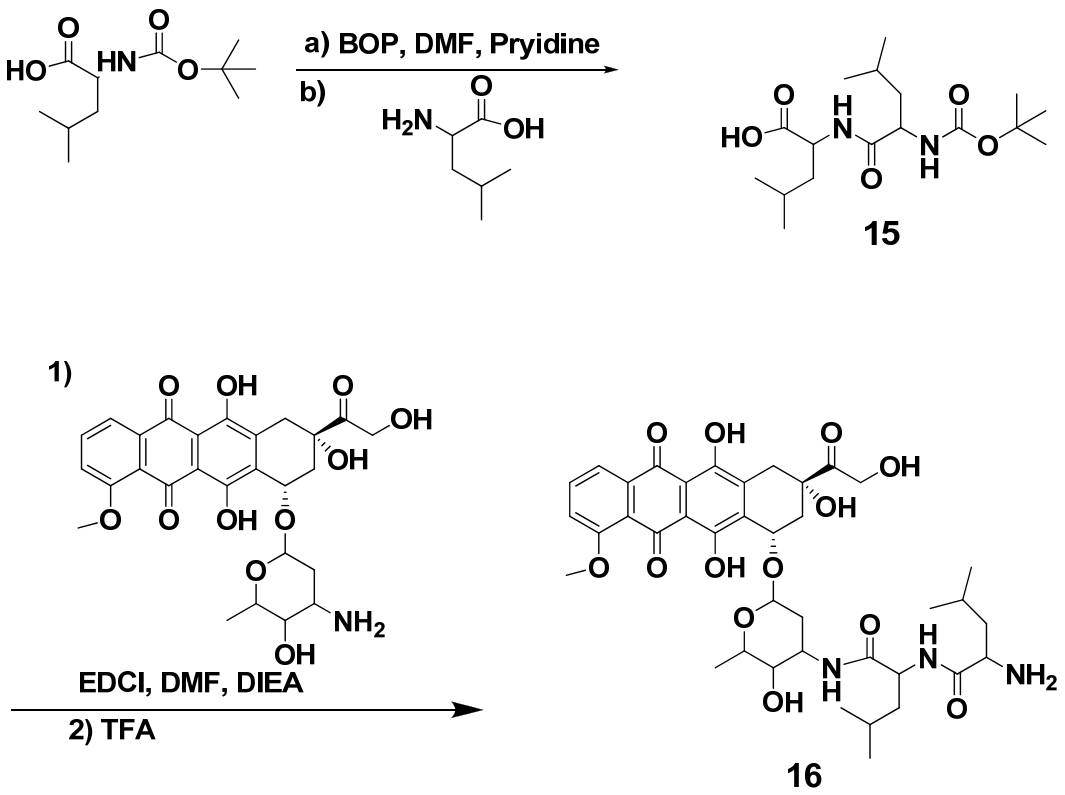

Scheme 4.2. Synthesis of LL-DOX (**16**).

rinsing the column with 0.1% ammonium hydroxide in methanol to elute the desired product. Finally, pure Boc-Leu-Leu-DOX was treated with TFA to give the desired Leu-Leu-DOX (**16**, Scheme 4.2); which was used without further purification. NMR and MS match the reported data[185]. With these compounds in hand, toxicity against PyVT-R221A-Luc cells was tested to determine efficacy of the cleaved products.

4.4 Cytotoxicity of L-DOX and LL-DOX

Toxicity assays were performed on the DOX drugs and prodrugs against PyVT-R221A-Luc cells by means of the trypan blue assay. Briefly, cells were plated into 24 well plates at a density of 50,000 cells/mL (0.5 mL/well). The cells were incubated overnight (20 – 24 hours) before the media was replaced with fresh media that contained the compounds to be tested, controls or untreated media. The cells were incubated another 24 hours prior to the first batch being detached, stained with trypan blue and counted with a hemocytometer. Further plates of cells were retreated and incubated another 24 hours. This process was repeated to obtain 3 or 4 time course points (24, 48, 72 and/or 96 hours) with 1 - 4 doses of drug. The number of total cells per well were calculated and then the percentage of live cells in the drug treated wells versus media (or DMSO) treated was calculated.

Over the dose course of DOX (Figure 4.4, top), the drug produces a toxic effect at all time points and concentrations. As expected, DOX becomes more toxic with increased dose concentration and incubation times. At 24 hours there

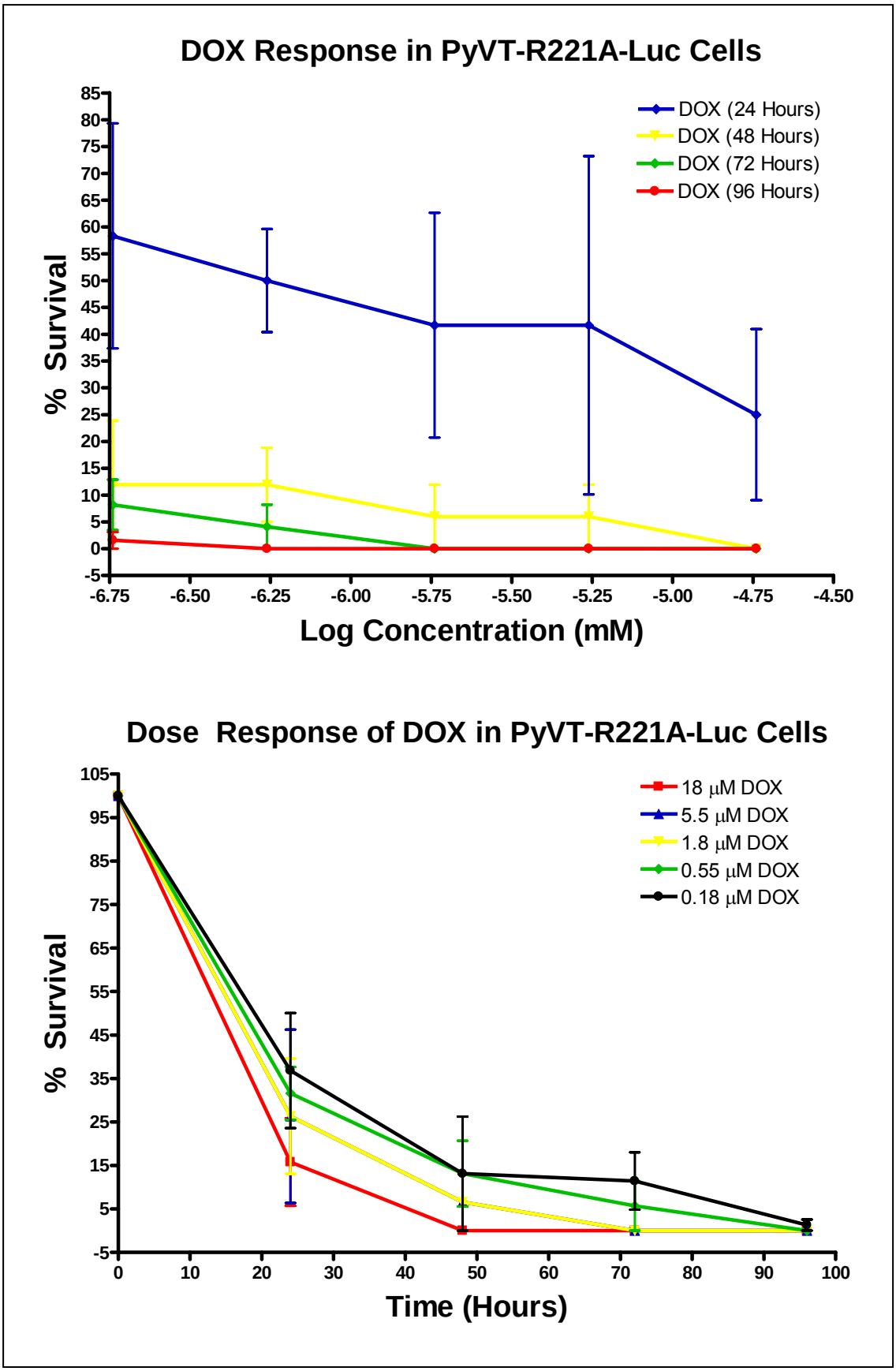
DOX Response in PyVT-R221A-Luc Cells
DOX (24 Hours)
DOX (48 Hours)
DOX (72 Hours)
DOX (96 Hours)
% Survival
85
80
75
70
65
60
55
50
45
40
35
30
25
20
15
10
5
0
-5
-6.75
-6.50
-6.25
-6.00
-5.75
-5.50
-5.25
-5.00
-4.75
-4.50
Log Concentration (mM)
Dose Response of DOX in PyVT-R221A-Luc Cells
18 μM DOX
5.5 μM DOX
1.8 μM DOX
0.55 μM DOX
0.18 μM DOX
% Survival
105
95
85
75
65
55
45
35
25
15
5
-5
0
10
20
30
40
50
60
70
80
90
100
Time (Hours)

is a 30 – 50% (depending on the drug dosing concentration) survival rate compared to control cells. At other time points there are lower survival rates at all concentrations tested. The assay plateaus above 1.8 mM doses, with no difference at 72 and 96 hours. Looking at the data from a different perspective, DOX has a toxic effect at all concentrations. This toxic affect increases over time (Figure 4.4 bottom) and the number of doses. Also, the toxic effect is indeed dose dependent as over time the toxicity increases as the dose increases.

L-DOX (**14**) compound, has been reported to have EC_{50} values of 6.7 μM in LNCa and 14.0 μM in DuPRO cells[131]. The cleavage product is also toxic to HT1080 cells[185]. Testing for dose response toxicity at high concentrations in the PyVT-R221A-Luc cell line was completed and compared to the LNCa and DuPRO cell lines. As with the DOX, the toxic effect increases over time, the number of doses and concentration. The 24 and 48 hour time points are equally as toxic for the lower concentrations tested (0.15 – 7.5 μM). As expected, two doses over 48 hours proves more toxic for concentrations of 15 and 23 μM, compared to the 24 hour (1 Dose) points. After 72 hours, a greater therapeutic efficacy is noticeable compared to 48 hours and 2 doses, but not as good as 96 hours and 4 doses. From the survival versus time course graphs, it is obvious that toxicity is dose dependent with 0.15 μM producing a cell reduction of 75% over the 96 hour time course (4 Doses), and 23 μM eradicating all the cells over the same time and dose period. The concentration tested is directly related to the efficacy of toxicity with higher concentrations producing greater cell death than lower concentrations. Overall, the L-DOX toxicity supports the data

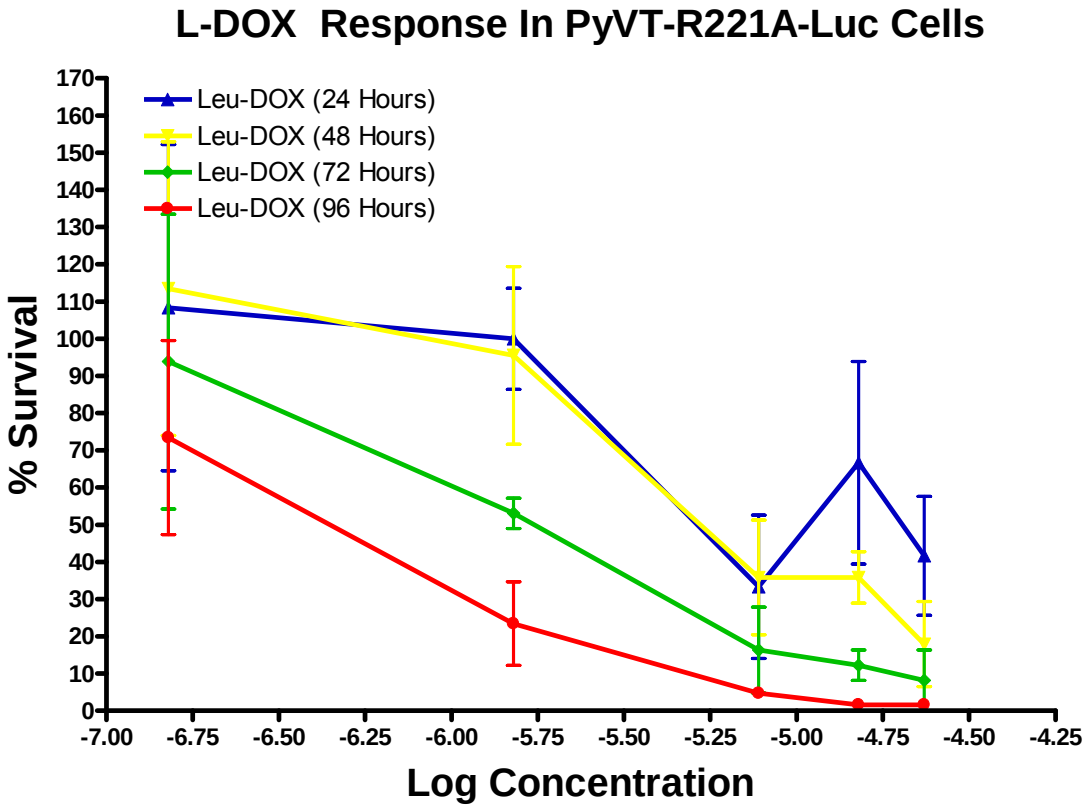

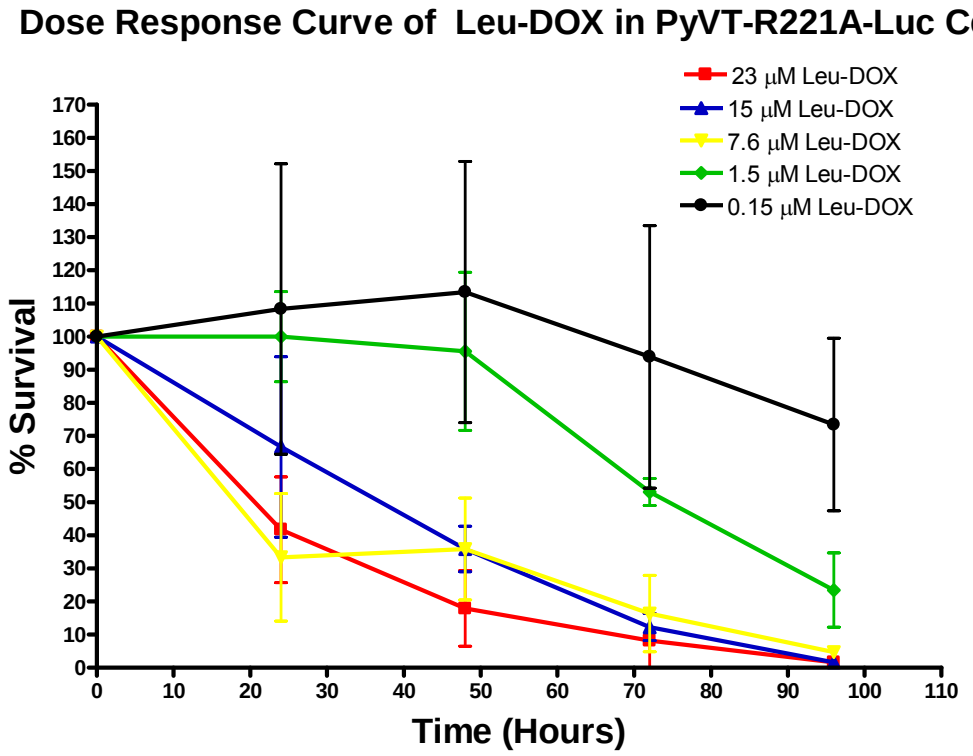

Figure 4.5. Cytotoxicity of L-DOX (**14**) against the PyVT-R221A-Luc cell line.

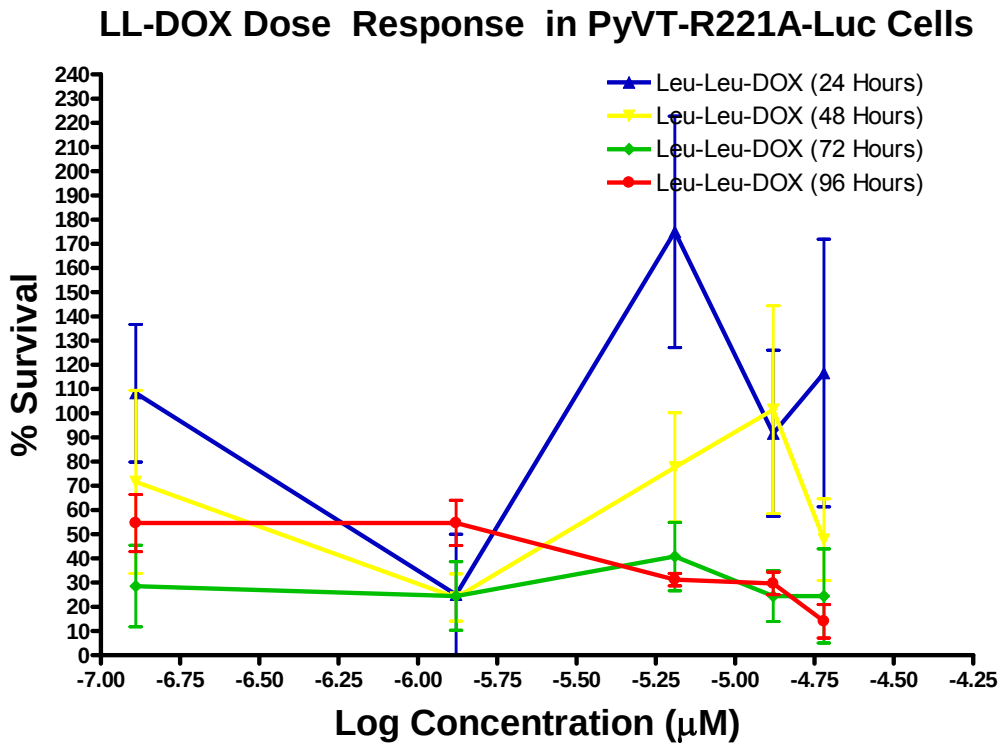

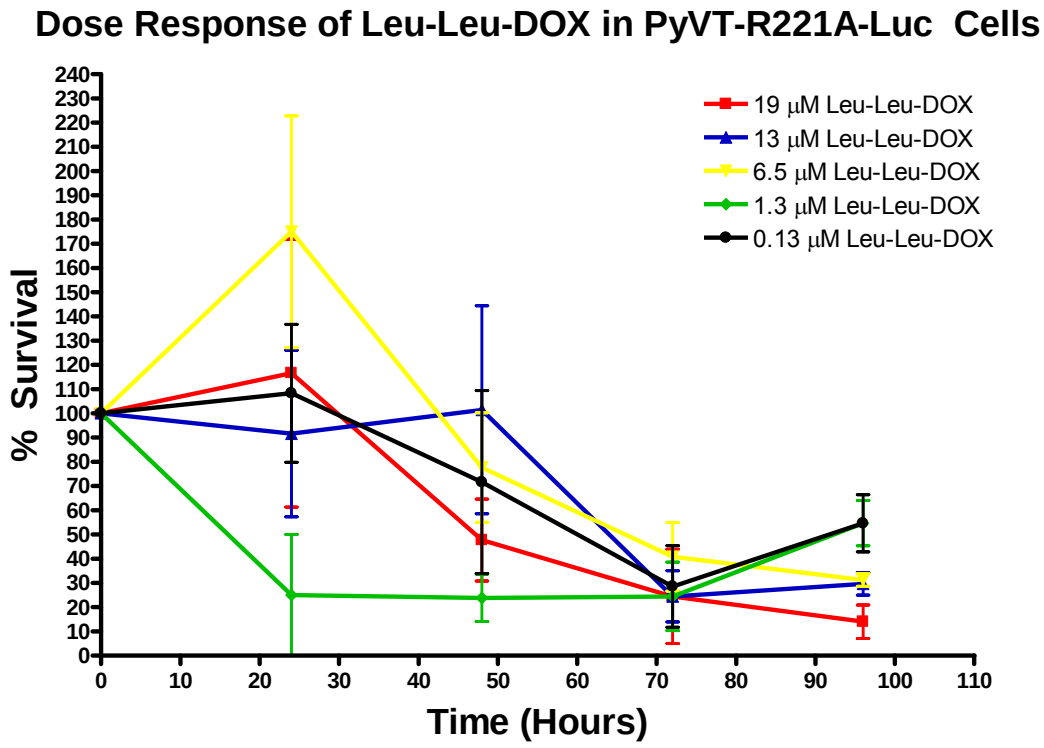

Figure 4.6. cytotoxicity of LL-DOX (**16**) against PyVT-R221A-Luc cell line. Top: Survival versus log concentration at 24, 48, 72 and 96 hours; Bottom: Survival versus time at different concentrations of drug.

demonstrated in the literature with the LNCa, DuPRO and HT1080 cell lines, but is not as effective against the PyVT-R221A-Luc cell line. The IC_{50} values for L-DOX in PyVT-R221A-Luc cells are 17.4, 12.0, 7.1 and 3.1 μM for 24, 48, 72 and 96 hours or 1, 2, 3 and 4 doses respectively (Table 4.1).

Third, a dose response over time was completed for LL-DOX (**16**), the expected cleavage product. Although not as pronounced as with the DOX and L-DOX (**14**), the same general trends are observed; the more doses, the higher the therapeutic efficacy. The 24 and 48 hour time points are less effective than the 72 and 96 hour time points if the 1.3 μM concentration value is disregarded. The the 72 and 96 hour treatments are approximately the same with the 72 hour time point being more effective at 0.13 and 1.3 μM, the 96 hour time point being better at 6.5 and 19 μM. When looking at the data from the perspective of survival versus time, the results look a little more variable. After 96 hours however, the anticipated order is maintained where the highest concentration (19 μM) is the most effective and the lowest concentration (0.13 μM) is the least effective with the remaining three concentrations falling into the expected order; the higher the concentration of drug, the higher the efficacy *in vitro*.

Table 4.1. IC_{50} values for DOX, L-DOX and LL-DOX.

Compound	IC50 (μM)
DOX	
24 Hours	5.5
48 Hours	NA
72 Hours	NA
96 Hours	NA
L-DOX	
24 Hours	17.4
48 Hours	12.0
72 Hours	7.1
96 Hours	3.1
LL-DOX	
24 Hours	NA
48 Hours	166.7
72 Hours	1.1
96 Hours	5.8

Using five concentrations for the toxicity curve allowed for initial IC_{50} values to be calculated. As shown in Table 4.1, the IC_{50} values are generally in the trend expected, however higher than optimal. For DOX, only the 24 hour time point could be calculated due to the high doses used. At more than 1 dose, the cells were completely wiped out, skewing the values to negative concentrations. The L-DOX provides the expected trend with higher concentrations needed to eliminate half the cells after 1 dose (24 hours) and decreasing concentrations after additional doses. The LL-DOX data does not fit the anticipated trend. The 24 hour survival versus log concentration data (1 dose) is not linear enough to calculate an IC_{50}. Furthermore, it appears that 3 doses (72 hours) is more efficacious than 4 doses (96 hours). Testing lower concentrations of DOX, L-DOX and LL-DOX would likely provide more consistent results.

4.5 Synthesis and Characterization of AVRWLL-DOX

First, AVRWLL-DOX was synthesized by coupling the DOX to the carboxyl termini of Fmoc-AVRWLL using EDCI and DIEA in DMF under anhydrous conditions for coupling (Scheme 4.3). The peptide was activated with EDCI prior to addition of DOX. The reaction was followed by reverse phase HPLC (C18 silica with 0.065% TFA in water and 0.05% TFA in acetonitrile) with chromatograms being ran prior to DOX addition, within 5 minutes of DOX addition and after 2 and 24 hours of DOX addition. Typically after 24 hours, the reaction was complete as shown by HPLC. After purification with preparatory

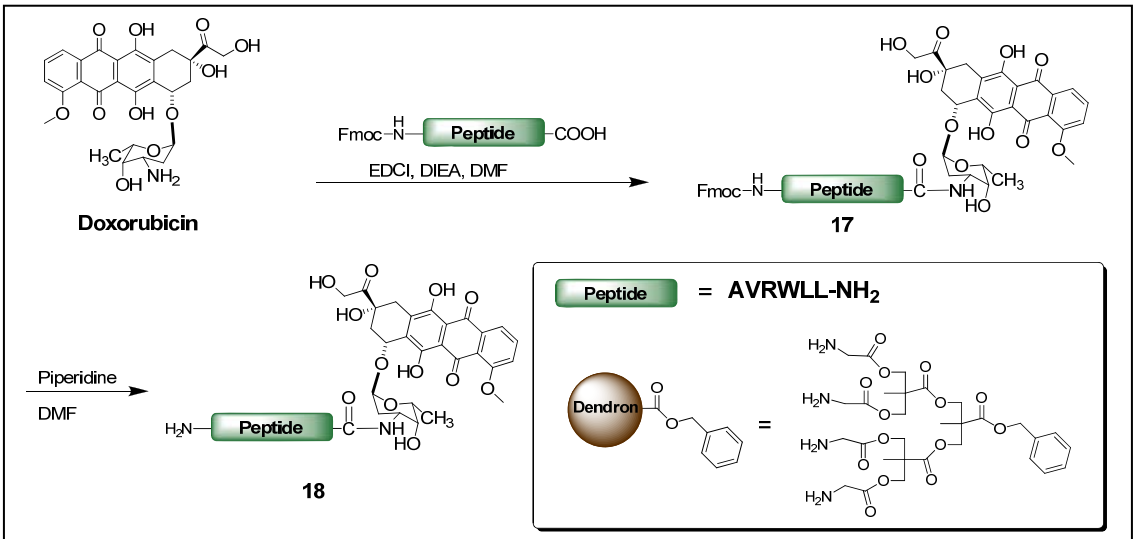

Scheme 4.3. Synthesis of AVRWLL-DOX (**18**).

HPLC, the product was characterized with ESI$^+$ MS to give the product ion peak at 1531.87 amu (Figure 4.4). The Fmoc protecting group was then removed using 50% piperidine in DMF. Deprotection of the Fmoc groups was confirmed by ninhydrin TLC where ninhydrin stains for primary amines. The starting material was not stained by ninhydrin, while the extensively concentrated and lyophilized product (removing all the piperidine) was stained, indicating that primary amines are present.

4.6 Synthesis and Characterization of Dendron-AVRWLL-DOX

To complete the synthesis of Dendron-AVRWLL-DOX (**20**), the H_2N-AVRWLL-DOX (**18**) was reacted with gultaric anhydride to provide a carboxylic acid for coupling to the dendron amines (Scheme 4.7). The HOOC-AVRWLL-DOX (**19**) product was purified with HPLC and coupling confirmation was completed with TLC using ninhydrin and bromo-cresol green stains. Ninhydring, which selectively stains primary amines stained the starting material, H_2N-AVRWLL-DOX, and did not stain the product, HOOC-AVRWLL-DOX. The product did stain with bromocresol green, a stain selective for carboxylic acids.

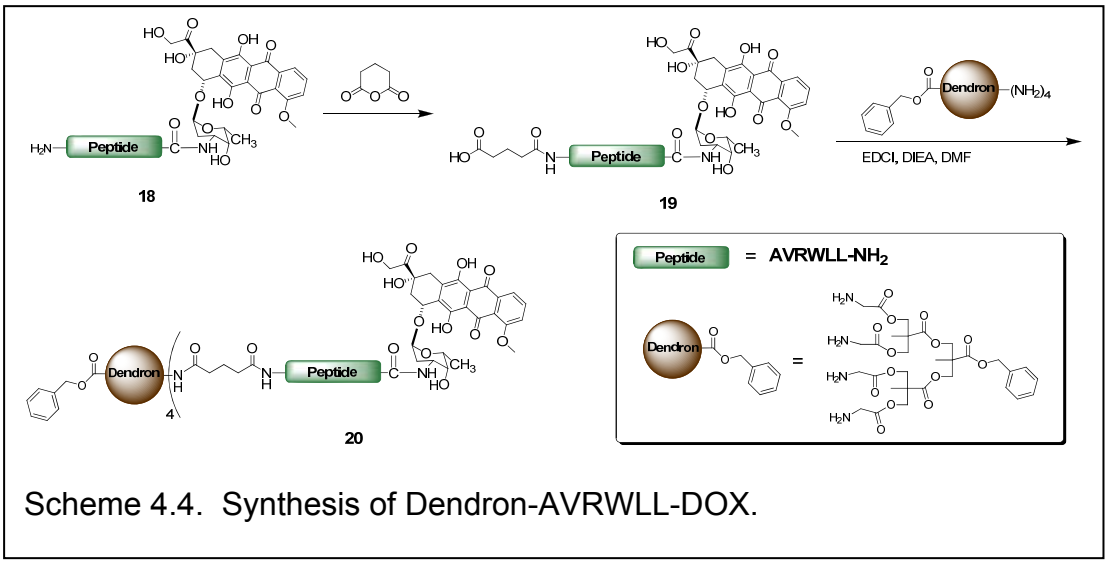

Scheme 4.4. Synthesis of Dendron-AVRWLL-DOX.

Finally, the COOH-AVRWLL-DOX (**19**) was coupled to the dendron by EDCI coupling. The HOOC-AVRWLL-DOX (**19**) was activated with EDCI in DIEA and

DMF and then added to a solution of dendron in DMF and stirred under anhydrous conditions until the reaction was complete as determined by HPLC. The reaction was purified with SEC to give a product with four peptide attached to each dendron. The pure product was characterized with MADLI-TOF MS. As seen in Figure 4.8, the MALDI-TOF spectrum does not provide an singularly

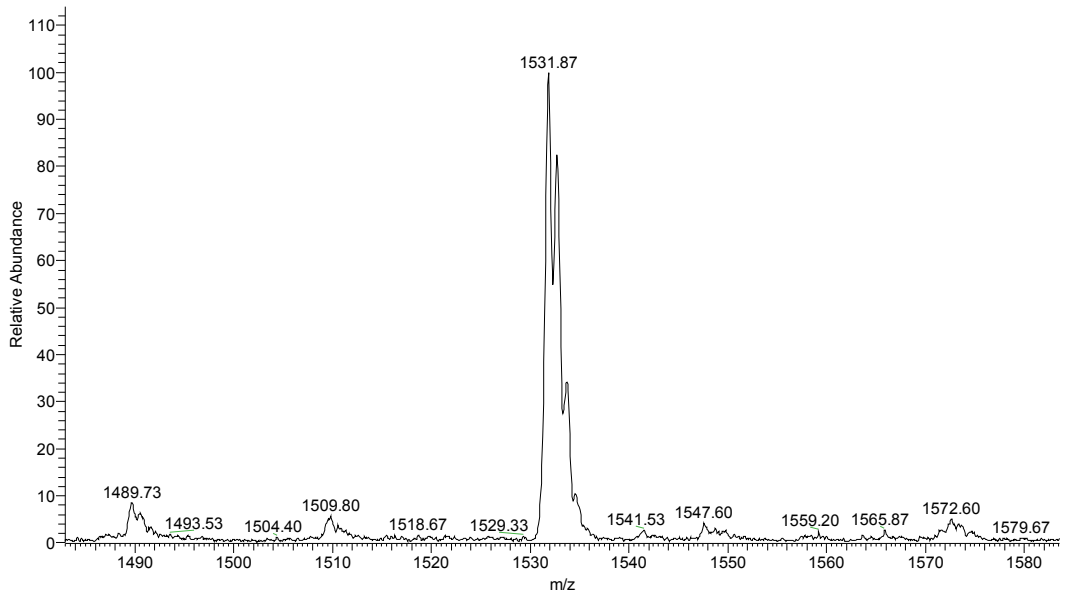

Figure 4.7. ESI MS of Fmoc-AVRWLL-DOX. The MW of 1531.87 indicates protonated Fmoc-AVRLL-DOX

charge molecular weight ion peak, but three key peaks that indicate coupling. The peak at 1,491 amu is from the dendron fragmenting at an interior ester bond, as seen in other peptide-dendron coupled products, and is equivalent to K^+O^-

$(CH_2)_3$-AVRWLL-DOX fragment. This fragment indicates coupling between the peptides and the dendron, but does not indicate the number of AVRWLL-DOX attached. The other two peaks are from m/z = 4 charged molecules. Ordinarily, quadruply charged molecular ions would not be expected; however, since each peptide contains an arginine residue, which could be protonated, makes this mass is observable. The peaks at 1,521 amu and 1,551 amu are both from quadruply charged product ion peaks. The mass of 1,521 is equivalent to the dendron with four AVRWLL-DOX (**18**) molecules attached and

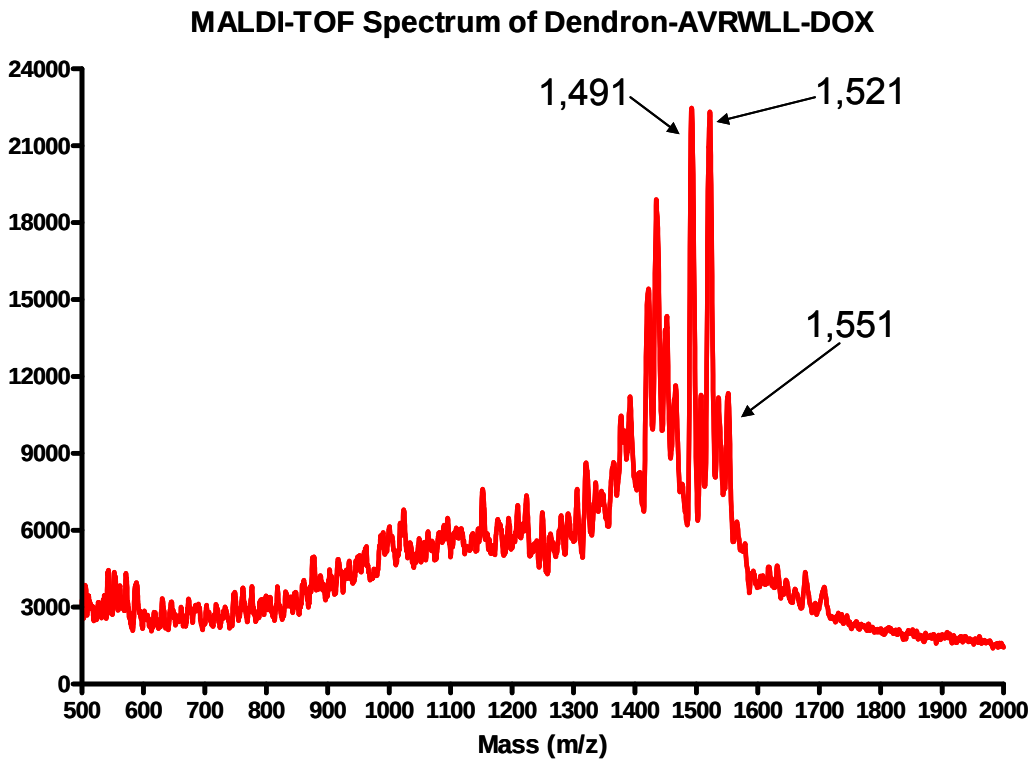

Figure 4.8. MALDI-TOF MS of Dendron-AVRWLL-DOX.

the benzyl group cleaved and the mass of 1,551 is equivalent to the quadruply charged molecule with four AVRWLL-DOX molecules attached to the dendron. With the Dendron-AVRWLL-DOX (**20**) and AVRWLL-DOX molecules on hand, cleavage and toxicity studies were completed.

4.7 Digestion of AVRWLL-DOX (**18**) and Dendron-AVRWLL-DOX (**20**)

The AVRWLL-DOX (**18**) and Dendron-AVRWLL-DOX (**20**) molecules were treated with MMP9 in the same manor as the Fmoc-AVRWLL peptide to determine if cleavage occurred (described in section 4.2). Unfortunately, no cleavage occurred. As shown in Figure 4.12, there is no difference in the MALDI-TOF spectra before and after enzyme digestion. Alternatively there was also no change in the HPLC chromatogram, which were low signal and resembled noise. The environment of the cell differs from the test tube and may produce a toxic effect in PyVT-R221A-Luc cells. To test this hypothesis, *in vitro* toxicity studies were performed.

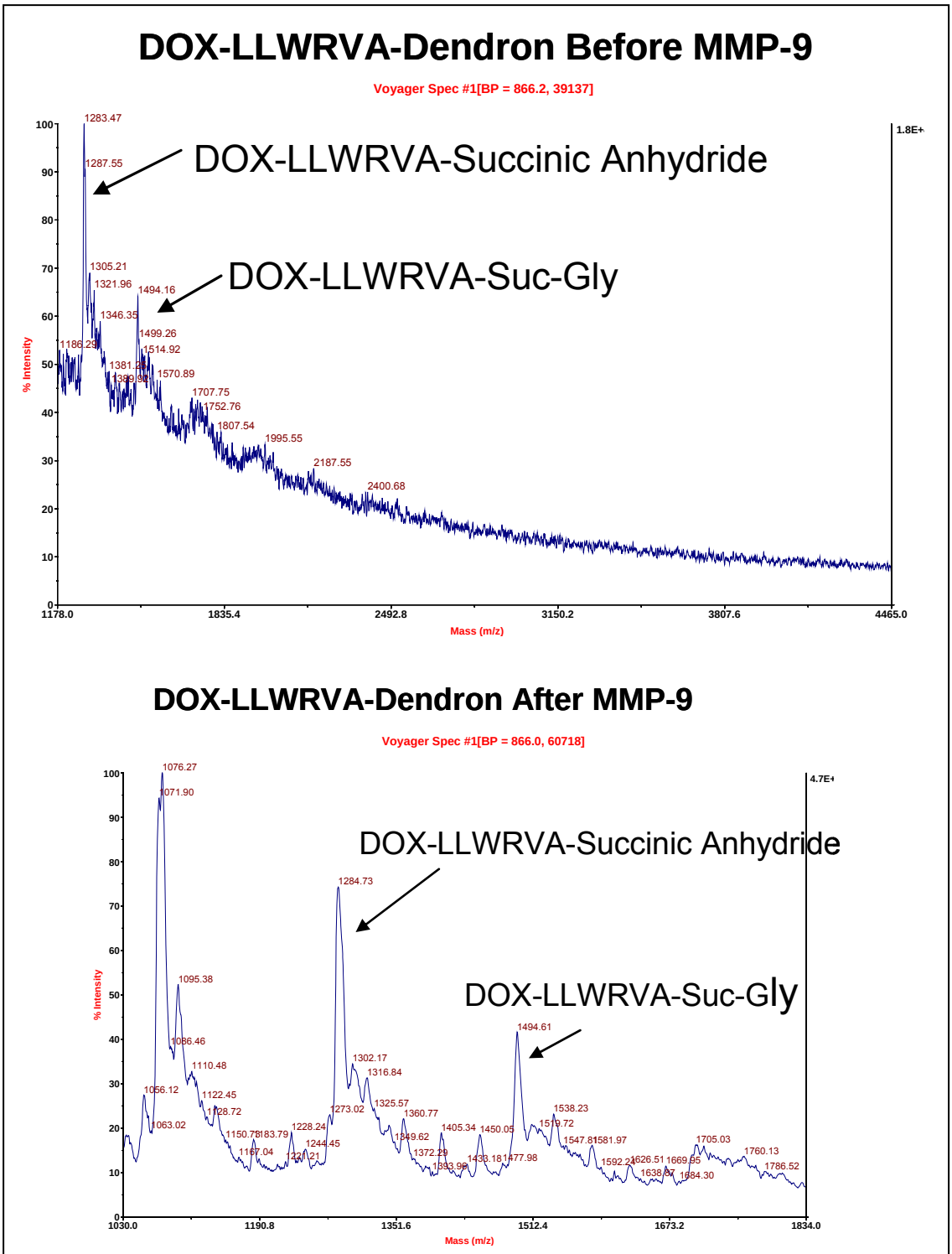

Figure 4.9. MMP9 digestion of Dendron-AVRWLL-DOX. MALDI-TOF spectra of Dendron-AVRWLL-DOX (**20**) before and after MMP9 Cleavage. Top: Dendron-AVRWLL-DOX before treatment with MMP9; Bottom: Dendron-AVRWLL-DOX (**20**) after treatment with MMP9.

4.8 Cytoxicity of AVRWLL-DOX (**18**) and Dendron-AVRWLL-DOX (**20**)

Curves over several high concentrations of DOX, L-DOX (**14**) and LL-DOX (**16**) were obtained prior to testing AVRWLL-DOX (**18**) and Dendron-AVRWLL-DOX (**20**), which were in limited quantities. When testing the AVRWLL-DOX (**18**)

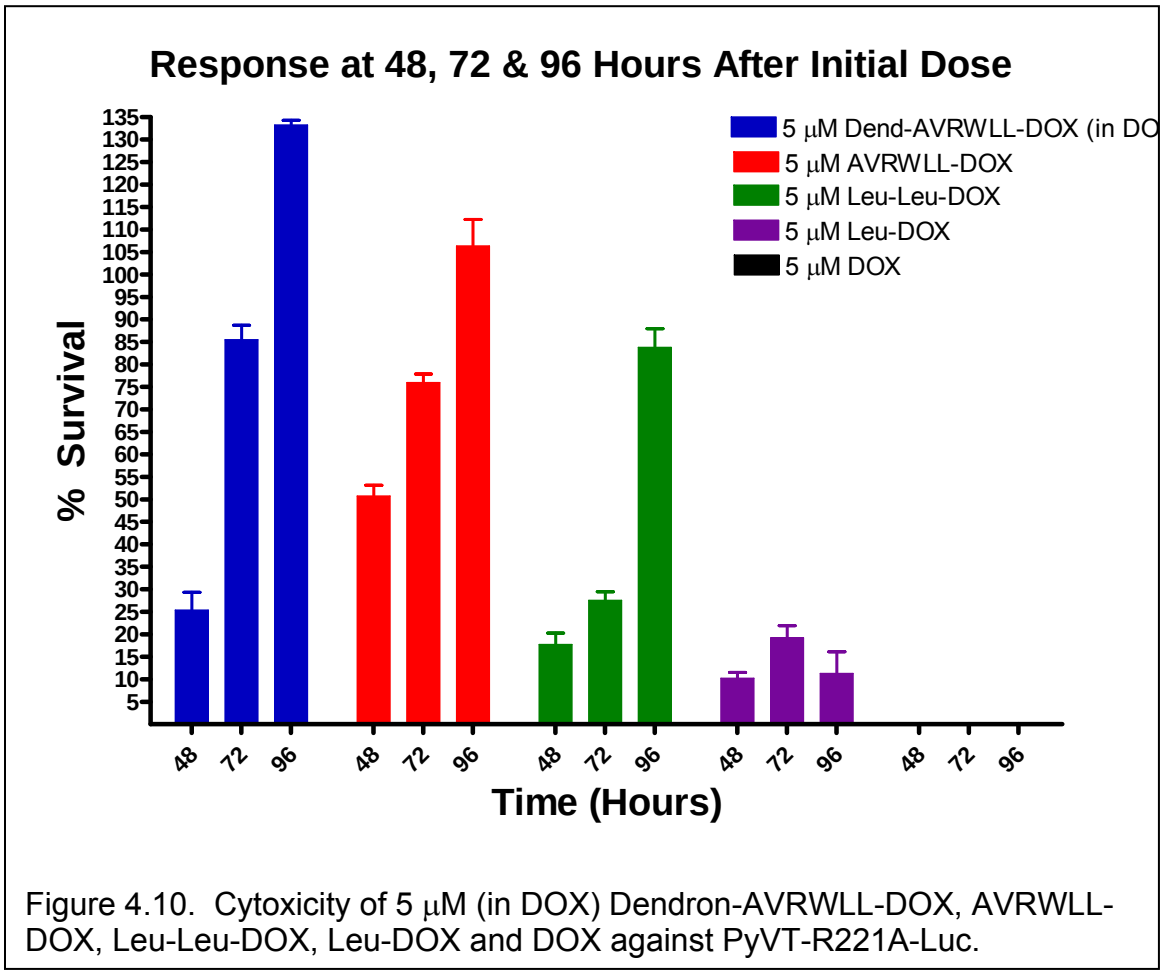

Figure 4.10. Cytoxicity of 5 μM (in DOX) Dendron-AVRWLL-DOX, AVRWLL-DOX, Leu-Leu-DOX, Leu-DOX and DOX against PyVT-R221A-Luc.

and Dendron-AVRWLL-DOX (**20**) compounds, DOX was used as a positive control while media and DMSO treated media were negative controls. The cells were also treated with L-DOX (**14**) and LL-DOX (**16**) to test the therapeutic efficacy of the expected cleavage products.

In the final toxicity experiment with the DOX prodrugs, the PyVT-R221A-Luc cells were treated with AVRWLL-DOX (**18**), Dendron-AVRWLL-DOX (**20**), LL-DOX (**16**), L-DOX (**14**) and DOX at 5 μM and 50 nM concentrations. The 5 μM dose was to high to compare the prodrugs to the positive controls and DOX because the cells were completely wiped out after 48 hours (Figure 4.13). The Leu-DOX (**14**) indicated a large amount of toxicity after 48 hours as well, but the cytotoxicity is lower after 72 and 96 hours. The remaining three compounds, Dendron-AVRWLL-DOX (**20**), AVRWLL-DOX (**18**) and Leu-Leu-DOX (**16**) followed the same pattern. After 48 hours, the toxicity of the drug was high compared to the DMSO controls; however, after 72 hours the toxic effect is only 15%. Once the cells were given four doses over 96 hours, the PyVT-R221A-Luc cells proliferate more than the media and DMSO treated controls. Leu-Leu-DOX (**16**) also proliferated from 48 to 72 hours and 72 to 96 hours. This pattern indicates that there is some toxicity initially of the drug(s), followed by loss of efficacy. Since the DOX and Leu-DOX (**14**) were so toxic after 48 hours, comparison of these compounds to the LL-DOX, AVRWLL-DOX and Dendron-AVRWLL-DOX was not possible at 5 μM concentrations. Although the exact reason for the cells becoming viable in the presence of DOX and the other

compounds tested is not known, one possibility is that a sub-population of DOX resistant cells proliferate after the non-resistant cells die.

In order to compare the effect of DOX and L-DOX with LL-DOX, AVRWLL-DOX and Dendron-AVRWLL-DOX against the PyVT-R221A-Luc cells, the assay was repeated using 50 nM concentrations of DOX and looking at 48 and 96 hour time points. The pattern of initial toxicity followed by recovery of the cells was more evident in the 50 nM assay. The 48 and 96 hour time points, produce the same pattern at 50 nM doses (Figure 4.11) as the 5 μM doses did (Figure 4.10). In the 50 nM dosed cells, the Dendron-AVRWLL-DOX (**20**) compound knocked the survival of the cells down to 40% after 48 hours and then recovered to 110% after 96 hours. The AVRWLL-DOX (**18**) had survival rates of 40 and 130% after 48 and 96 hours respectively. Leu-Leu-DOX (**16**), showed the same pattern but overall was more toxic, with survival rates of 30 and 80% after 48 and 96 hours respectively. Leu-DOX (**14**), which could not be compared well at the 5 μM dose had survival rates of 15 and 160% after 48 and 96 hours. This compound had the greatest change in survival between the two time points. Finally, even DOX has an increase in survival between the 48 and 96 hour time points at 50 nM concentrations with a difference from 8 to 51% respectively. One likely explanation is that there is a sub-population of cells growing that are resistant to DOX and DOX analogues. This sub-population then experiences a faster growth rate in the PyVT-R221A-Luc cells than the non-resistant cells. The assay was repeated to confirm the results. The initial assay curves that did not produce this

effect were grown from a different vial of cells, which could explain the discrepancy.

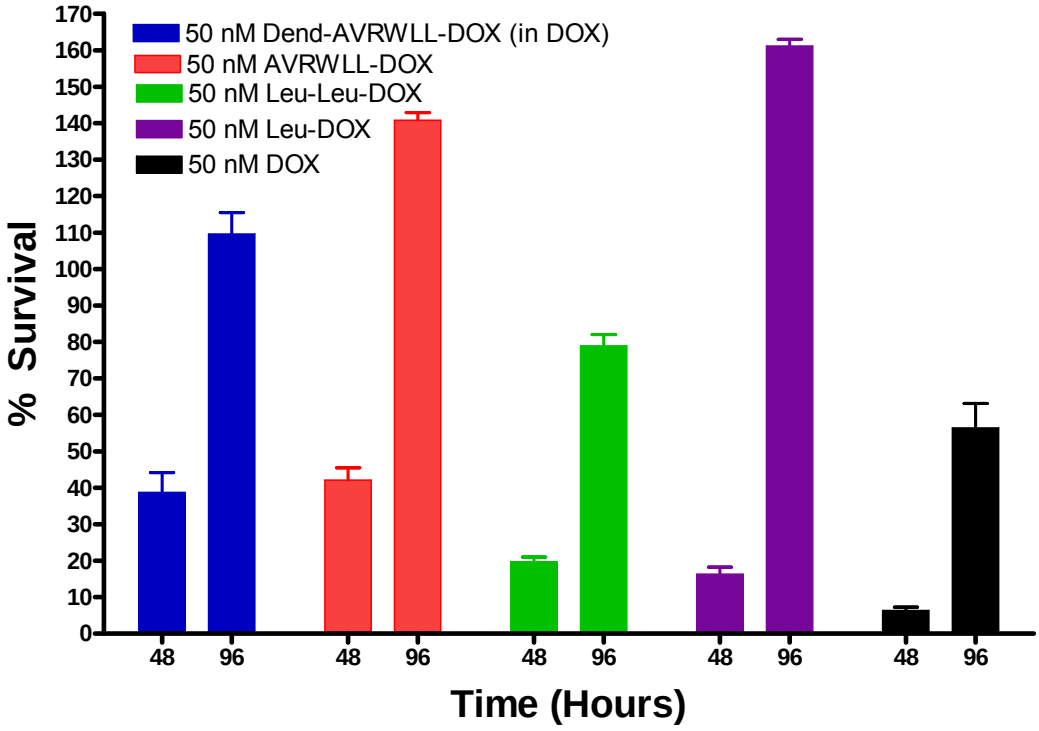

Figure 4.11. Cytoxicity of Dendron-AVRWLL-DOX, AVRWLL-DOX, Leu-Leu-DOX, Leu-DOX and DOX at against PyVT-R221A-Luc cells at 50 nM concentrations of DOX.

4.9 Conclusions

Since initial experiments with an MMP9 activatable DOX prodrug were unsuccessful; a new strategy was to used to reactivate DOX selectively in cancer cells. This new strategy utilized a different peptide that is similar to the reported sequence known to be cleaved by MMP9. The new sequence, AVRWLL, was

expected to be cleaved by MMP9 between the tryptophan and leucine residues like the original sequence, AVRWLLTA, is to provide cleavage product LL-DOX (**16**). The literature reports that L-DOX (**14**) is toxic in HT-1080, LNCa and DuPRO cell lines and there are reports of other amino acid DOX conjugates that are toxic to cancer cells with up to four amino acids attached[131, 185]. Construction of L-DOX (**14**) and LL-DOX (**16**) and the study of their toxicity in PyVT-R221A-Luc cells proved the cleavage product is toxic indicating that the prodrug could be reactivated. Even though the expected cleavage product did produce toxicity, there was little evidence that the new peptide was cleaved at a rate fast enough to produce toxic levels *in vitro*. If any digestion occurred with MMP9 the majority of the product was WLL-DOX and not LL-DOX, since HPLC and MS analysis indicated cleavage primarily between the alanine and tryptophan residues.

Amino acids conjugated to DOX had been shown to produce toxic effects in other cell lines and cleavage by enzymes other than MMP9 could occur *in vitro*. Two prodrugs, AVRWLL-DOX (**18**) and Dendron-AVRWLL-DOX (**20**), were synthesized and tested in PyVT-R221A-Luc cells. At 5 μM concentrations (in DOX), the LL-DOX and AVRWLL-DOX compounds are toxic to PyVT-R221A-Luc cells after 48 hours but not after all 96 hours. The L-DOX (**14**) and DOX controls are so toxic at 48 hours that all the cells are killed or no reproliferation is observed. At 50 nM, all the compounds (Dendron-AVRWLL-DOX (**20**), AVRWLL-DOX (**18**), LL-DOX (**16**), L-DOX (**14**) and DOX) are toxic at 48 hours and regrow to 80 – 160% of the control by 96 hours. The most likely explanation for this effect is that DOX sensitive cells are eliminated with the first two

treatments (24 and 48 hours) and then DOX resistant cells rapidly proliferate. Growth rates between the PyVT-R221A-Luc and DOX resistant PyVT-R221A-Luc cells may differ, resulting in the discrepancy between the number of cells in treated and untreated samples. Interestingly, the LL-DOX (**16**), L-DOX (**14**) and DOX do not show the same trend in earlier toxicity curve studies (Figures 4.7, 4.8 and 4.9). This could be due to inconsistencies in the cells from two different frozen vials or a transformation of the cells between the initial assay and the assay testing with the AVRWLL-DOX (**18**) and Dendron-AVRWLL-DOX (**20**) prodrugs.

4.10 Experimental Procedures

General Methods:

MDA-MB-231 cells were purchased from ATCC and cultured in Dulbeco's minimum essential medium (DMEM), 10% Fetal Bovine Serum (FBS) and gentamycin with 5% CO_2 at 37 ^{o}C. PyVT-R221A-Luc cells were obtained from the Matrisian laboratory and cultured in DMEM without L-glutamine, 10% FBS, gentamycin and puromycin with 5% CO_2 at 37 ^{o}C. LLC-RSV and LLC-MMP9 cells were obtained from the Matrisian laboratory and cultured in DMEM, 10% FBS and gentamycin with 5% CO_2. The custom ordered peptides were purchased from Genscript™ and tested for purity then used as arrived. The enzymes were purchased from Calbiochem. All other chemicals were purchased from Fisher Scientific or Aldrich Chemical companies and used as is unless otherwise indicated.

2-amino-N-(3-hydroxy-2-methyl-6-((1S,3S)-3,5,12-trihydroxy-3-(2-hydroxyacetyl)-10-methoxy-6,11-dioxo-1,2,3,4,6,11-hexahydrotetracen-1-yloxy)tetrahydro-2H-pyran-4-yl)-4-methylpentanamide (Leu-DOX, 14):

All glassware used in the reaction was flame dried and cooled in a desiccator prior to use. The solvents were anhydrous and all solid materials were dried under vacuum for at least 3 hours prior to use and exposed to anhydrous $Ar_{(g)}$ gas upon breaking the vacuum seal. Boc-Leu (10.66 mg, 0.046 mmoles) was stirred in DMF (2.5 mL) with EDCI (7.30 mg, 0.038 mmoles), BOP (20.54 mg, 0.046 mmoles) and DIEA (266 μL) for 30 minutes under $Ag_{(g)}$. Doxorubicin (10 mg, 0.017 mmols) in 0.5 mL DMF was added to the reaction. The reaction was stirred overnight then concentration in vacuo. The product was purified on the Biotage SP1™ system with silica gel. First a gradient from 100% hexanes to 100% ethyl acetate was used and then a second gradient of 100% ethyl acetate to 100% methanol was flushed through the column to elute pure Boc-Leu-DOX as the third product off the column. MS $(ESI)^+$: Found: 779.27 Dalton $(M + Na)^+$; Calculated: 779.78 Dalton ($C_{38}H_{48}N_2O_{14}Na$). NMR and MS spectra are in Appendix B.

The Boc-Leu-DOX was then stirred in neat TFA for 2 hours at room temperature and concentrated to give pure Leu-DOX (**14**). MS $(ESI)^+$: Found: 679.33 Dalton $(M + Na)^+$; Calculated: 679.67 Dalton ($C_{33}H_{40}N_2O_{12}Na$). NMR and MS spectra are in Appendix B.

2-amino-N-(1-(3-hydroxy-2-methyl-6-((1S,3S)-3,5,12-trihydroxy-3-(2-hydroxyacetyl)-10-methoxy-6,11-dioxo-1,2,3,4,6,11-hexahydrotetracen-1-yloxy)tetrahydro-2H-pyran-4-ylamino)-4-methyl-1-oxopentan-2-yl)-4-methylpentanamide (Leu-Leu-DOX, 16):

All glassware used in the reaction was flame dried and cooled in a desiccator prior to use. The solvents were anhydrous and all solid materials were dried under vacuum at least 3 hours prior to use and exposed to anhydrous $Ar_{(g)}$ gas upon breaking the vacuum seal. Boc-Leu (180.43 mg, 0.78 mmoles) was stirred with BOP (415.43 mg, 0.939 mmoles) and DIEA (250 μL) in DMF (5 mL) for 30 minutes. Leucine (124.61 mg, 0.950 mmols) in DMF (3 mL) was added to the reaction. The reaction was stirred overnight and concentrated in vacuo. The product was purified on the Biotage SP1™ system with a silica gel column and a gradient of 100% methylene chloride to 100% methanol to elute 4 peaks. The first peak eluted was 13.41 mg (5%) of Boc-Leu-Leu. MS $(ESI)^+$: Found: 367.13 Dalton $(M + Na)^+$; Calculated: 367.44 Dalton ($C_{17}H_{32}N_2O_5Na$). NMR and MS spectra are in Appendix B.

Boc-Leu-Leu (6 mg, 0.017 mmoles) was stirred with BOP (12.39 mg, 0.028 mmoles) and DIEA (5.6 μL, 0.61 mmoles) in DMF (0.8 mL) for 10 minutes. Doxorubicin (5 mg, 0.0086 mmoles) in DMF (0.3 mL) was added to the reaction. The reaction was stirred overnight and concentrated in vacuo. The product was purified on the Biotage SP1™ system with a silica gel column and a gradient of 100% methylene chloride to 100% methanol followed by rinsing with 1% ammonium hydroxide (3 column volumes) in methanol to elute 5 peaks. The last peak eluted was 7.5 mg (99%) of Boc-Leu-Leu-DOX. MS $(ESI)^+$: Found: 869.47

Dalton $(M + H)^+$; Calculated: 869.95 Dalton ($C_{44}H_{59}N_3O1_5Na$). NMR specta are in Appendix B.

The Boc-Leu-Leu-DOX was then treated with neat TFA for 2 hours at room temperature and concentrated to give pure Leu-Leu-DOX (**16**). MS $(ESI)^+$: Found: 679.33 Dalton $(M + Na)^+$; Calculated: 679.67 Dalton ($C_{33}H_{40}N_2O_{12}Na$). NMR spectra are in Appendix B.

2-(2-(2-aminopropanamido)-3-methylbutanamido)-5-guanidino-N-(1-(1-(1-(3-hydroxy-2-methyl-6-((1S,3S)-3,5,12-trihydroxy-3-(2-hydroxyacetyl)-10-methoxy-6,11-dioxo-1,2,3,4,6,11-hexahydrotetracen-1-yloxy)tetrahydro-2H-pyran-4-ylamino)-1-oxopentan-2-ylamino)-4-methyl-1-oxopentan-2-ylamino)-3-(1H-indol-3-yl)-1-oxopropan-2-yl)pentanamide compound with methane (1:1) (AVRWLL-DOX, 18):

All glassware used in the reaction was flame dried and cooled in a desiccator prior to use. The solvents were anhydrous and all solid materials were dried under vacuum for at least 3 hours prior to use and exposed to anhydrous $Ar_{(g)}$ gas upon breaking the vacuum seal. Fmoc-AVRWLL (6.99 mg, 0.0071 mmoles) was stirred with EDCI (1.5 mg, 0.0078 mmoles) and DIEA (50 μL) in DMF (1 mL) for 30 minutes. Doxorubicin (4.55 mg, 0.0078 mmols) in DMF (0.5 mL) was added to the reaction. The reaction was stirred overnight while being monitored with reverse phase HPLC (C18 silica with a gradient using 0.065% water and 0.05% Acetonitrile) after 100 minutes and 24 hours. The reaction was concentrated in vacuo and purified by prepatory (C18 silica with a gradient using 0.065% water and 0.05% Acetonitrile) HPLC to give pure Fmoc-AVRWLL-DOX. MS $(ESI)^+$: Found: 1531.87 Dalton $(M + Na)^+$; Calculated: 1531.69 Dalton ($C_{79}H_{100}N_{11}O_{19}Na$).

Fmoc-AVRWLL-DOX was treated with 1 mL piperidine in 1 mL DMF for 2 hours. The reaction was concentratated in vacuo and purified by prepatory HPLC (C18 silica with 0.065% water and 0.05% Acetonitrile) to give pure AVRWLL-DOX. MS (MALDI-TOF)$^{+}$: Found: 1283.31 Dalton $(M + H)^{+}$; Calculated: 1,284.45 Dalton ($C_{64}H_{89}N_{11}O_{11}$).

Dendron-AVRWLL-DOX (20):

AVRWLL-DOX (7.0 mg, 0.0055 mmols) was stirred with succinic anhydride (0.94 mg, 0.0094 mmols) in DMF (1.5 mL) overnight. The reaction was spotted on TLC plates to show that it was negative for primary amines (ninhydrin stain) and positive for carboxylic acid functional groups (bromo-cresol green stain). MS (MALDI-TOF)$^{+}$: Found: 1,384.32 Dalton $(M + H)^{+}$; Calculated: 1,384.53 Dalton ($C_{68}H_{93}N_{11}O_{20}$).

All glassware used in the reaction was flame dried and cooled in a desiccator prior to use. The solvents were anhydrous and all solid materials were dried under vacuum for at least 3 hours prior to use and exposed to anhydrous $Ar_{(g)}$ gas upon breaking the vacuum seal. The COOH-AVRWLL-DOX (3.85 mg, 0.0027 mmoles) product was stirred with EDCI (0.55 mg, 0.0029 mmoles) and DIEA (2 μL) in DMF (0.5 mL) for 30 minutes. Next, H_2N-Gly-Dendon (0.5 mg, 0.00073 mmoles) in DMF (0.5 mL) was added to the reaction. The reaction was stirred overnight while being monitored with SEC (0.065% water and 0.05% Acetonitrile). The reaction concentrated in vacuo and purified by SEC to give Dendon-AVRWLL-DOX. MS (MALDI-TOF)$^{+}$: Found: 1,549 Dalton $(M+4H)^{4+}$; Calculated: 1,549 Dalton ($C_{306}H_{408}N_{48}O_{90}Na$).

Cleavage of Peptide compounds with Enzymes:

The compound to be tested for ability to cleave was dissolved in methanol at 10 mg/mL. Next, 100 μl of this solution was diluted with 900 μl of tricine buffer to make a 1 mg/mL solution (10% methanol). A 20 μl sample was injected into the HPLC (C18 reverse phase silica with 55% 0.05% TFA in Acetonitrile/ 45% 0.065% TFA in water) for an undigested reference chromatogram. Following HPLC, enzyme was added (either MMP9, MMP2 or Trypsin) and the samples were incubated at 37 ^{o}C overnight. HPLC was repeated to determine the cleavage percentages (in any) of the sample. For samples in which a solid was precipitate formed, the solid was collected by centrifugation, dissolved in 100% methanol and an aliquot was injected into the HPLC. The samples were then characterized with ESI^{+} and MALDI-TOF MS to determine the cleavage products. The solid usually contained pure cleaved product.

Toxicity studies

Cells were plated at 40,000 – 60,000 cells/mL into 24 well plates (0.5 mL/well) in their culture medium. A separate plate was used for each time point observed in the assay. Thus 4 time points using 4 plates. The cells were incubated overnight at 37 ^{o}C (20 - 24 hours, usually 24 hours). After examination under the microscope to ensure the cells were attached and looked healthy, the media was aspirated off each well (taking care to not disrupt the cells) and replaced with media containing the drug, prodrug or a control compound. The

drug prodrug and control solutions were made fresh just prior to use. The cells were incubated 24 hours and then either redosed with fresh drug-media solutions or the cells were trypsinized and counted using trypan blue. For typsinization, the media was removed by aspiration and each well was washed with 0.5 mL of DPBS. The DPBS was removed by aspiration and each well was treated with 200 μl of trypsin. The plate was incubated at 37 ^{o}C and 5% CO_2 for 10 - 15 minutes and then agitated, either with a shaker or by hand. Finally, 40 μl of trypan blue was added to each well (typically 4 wells at a time) and the live cells (cells that did not stain with trypan blue) were counted with a hemocytometer. The dosing and counting was continued for the remaining time points so that the cells were given fresh drug every 24 hours until counted (either 72 and 96 hours after the initial dose).

CHAPTER V

FUNCTIONALIZATION OF PACLITAXEL TO A DENDRON THROUGH AN MMP-9 CLEAVABLE PEPTIDE

5.1 Introduction

Prodrugs as cancer therapeutics offer significant advantages over traditional chemotherapeutic drugs. Traditional chemotherapeutics are non-targeted and interact with all cells in the body. Given that chemo drugs interact with both cancerous and non-cancerous tissues, near maximum tolerated doses need to be administered to ensure efficacy. The systemic side effects of traditional chemotherapeutics include many minor symptoms such as vomiting and dizziness to potentially major problems such as increased myelotoxicity and cardiotoxicity. A common strategy to overcome these side effects and improve efficacy is to deliver the chemotherapeutic agent directly to diseased tissue via a prodrug. Prodrugs allow the therapeutic to remain latent until activated, which could be accomplished by a variety of chemical reactions which include enzymatic reactions such as proteolytic cleavage. Targeting prodrugs to tumor cells reduces interactions between the drug and non-cancerous cells and allows for delivery of more active drugs to the diseased tissue, increasing efficacy and decreasing systemic toxicity.

A variety of specific proteinases, including matrix metalloproteinases (MMPs), are found in the microenvironment of tumors and tumor metastases. MMPs present opportunities for prodrug therapy at the earliest stages of breast

cancer metastasis using nanotechnology rather than traditional pharmacological agent. Previous results indicate that MMP9 expression influences the earliest stages of implantation of breast cancer cells in the lung. There is epidemiological evidence that MMP9 is an indicator of poor prognosis for many cancers, including breast cancer[125]. Targeting MMP9 expression provides the ability to specifically identify and target micrometastatic lesions that may be present in breast cancer patients but are undetectable by current imaging technology.

Paclitaxel is an ideal drug for incorporation into a prodrug to treat breast cancer and micrometastatic lesions to the lung due to its current use for treating breast cancer. Several cancers other than breast cancer are also sensitive to PXL including: lung, ovarian and head and neck malignancies. Furthermore, the modification of PXL with succinic anhydride and subsequent conjugation to amine terminated dendrimers has been reported by Baker, et al[100]. The specific modification was shown to not significantly effect the toxicity of the native drug[101].

To deliver the therapeutic, dendrimers offer multiple advantages for use as molecular scaffolds for prodrugs, including 1) the ability to conjugate multiple drugs to a single molecule, 2) the ability to incorporate multiple elements for therapy, imaging, tracking and targeting and 3) tunable size and functionality. In the work presented here, a dendron is used as the scaffold for an MMP9 activated paclitaxel (PXL prodrug). The dendron can then be coupled to other dendrons of differing functionalities in a “mix and match” manner to synthesize multifunctional dendrimers. These dendrimers can be used to deliver therapeutics, monitor the location and efficacy of delivery (with a fluorescence

sensor), target micrometastatic lesions, track the dendrimer location and tune the bioavailability for optimal delivery and excretion. In this chapter, the conjugation of PXL to H_2N-Pep-Dendron is described, followed by the *in vitro* testing of this new prodrug for cytotoxicity versus several cell lines.

5.2 Synthesis and Characterization of PXL-Pep-Dendron (**22**)

To synthesize the MMP9 activated prodrug, paclitaxel was modified with succinic anhydride to provide a carboxylic acid linkage from the C2'OH as previously described by Baker, et. al.[101]. Next, the H_2N-Peptide-Dendron was

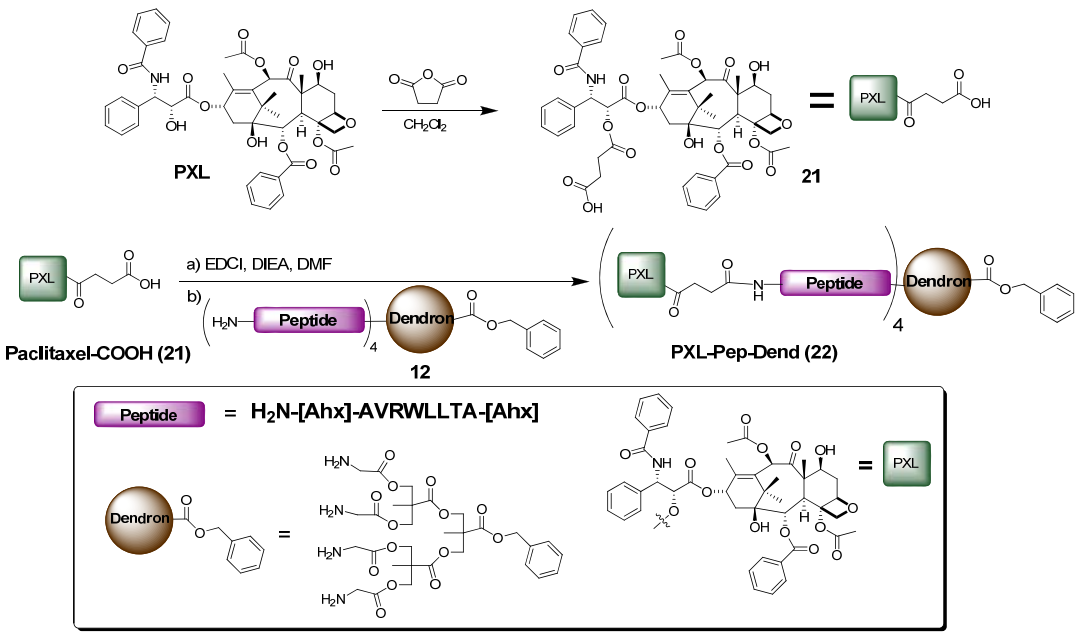

Scheme 5.1. Synthesis of PXLPep-Dendron.

coupled to PXL-COOH using (3-(dimethylamino)propyl)ethyl Carbodiimide Hydrochloride (EDCI) and diisopropyl-diethyl amine (DIEA) in anhydrous dimethyl formamide (DMF) followed by purification with size exclusion chromatography (SEC) as seen in Scheme 5.1.

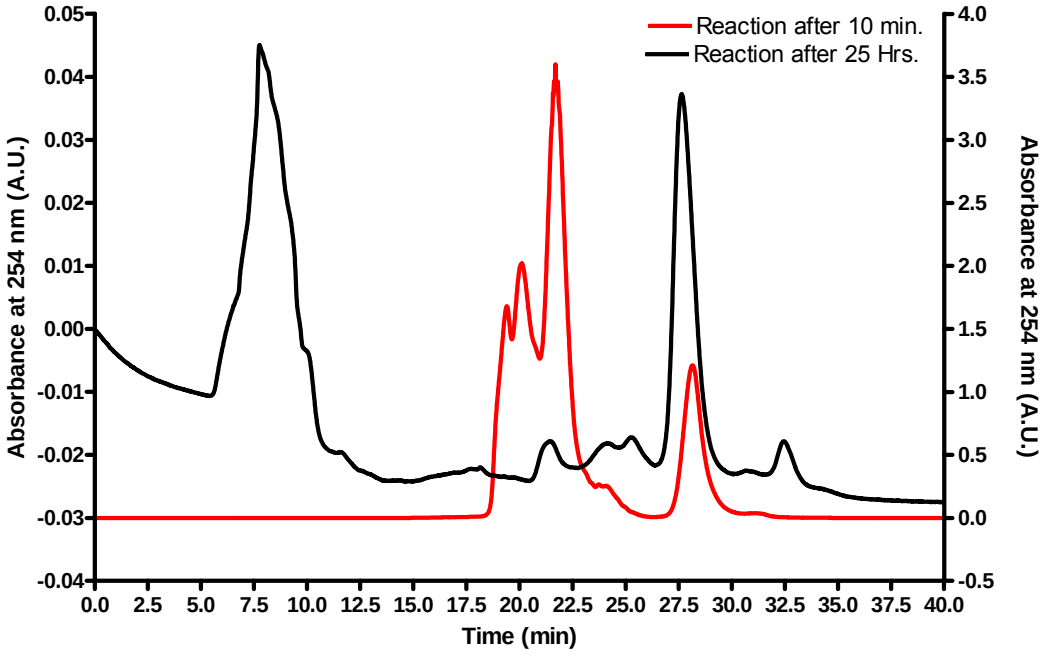

Figure 5.1. Reaction Progress of PXL coupling to the H_2N-Peptide-Dendron. SEC of H_2N-Pep-Dendron (**12**) and PXL-Pep-Dendron (**22**).

The reaction was followed using SEC to monitor the disappearance of H_2N-Pep-Dendron and the appearance of a new peak. As can be seen in Figure 5.1, the H_2N-Pep-Dendron (**12**) elutes at 21 minutes while after 25 hours of

reacting, the H_2N-Pep-Dendron peak disappears and a new peak at 7.7 minutes appears. Since the new peak elutes earlier than the H_2N-Pep-Dendron, indicates a larger molecule. The peak at 28 minutes is from the coupling agents and the byproducts of coupling. Thus its increased amplitude at 25 hours indicates the presence of more coupling byproducts. Further characterization of the coupled product was accomplished with MALDI-TOF MS. Among other MADLI-TOF fragments detected was the m/z = 4 mass at 4,409 amu for an intact PXL-Pep-Dendron (**22**) (Figure 5.2).

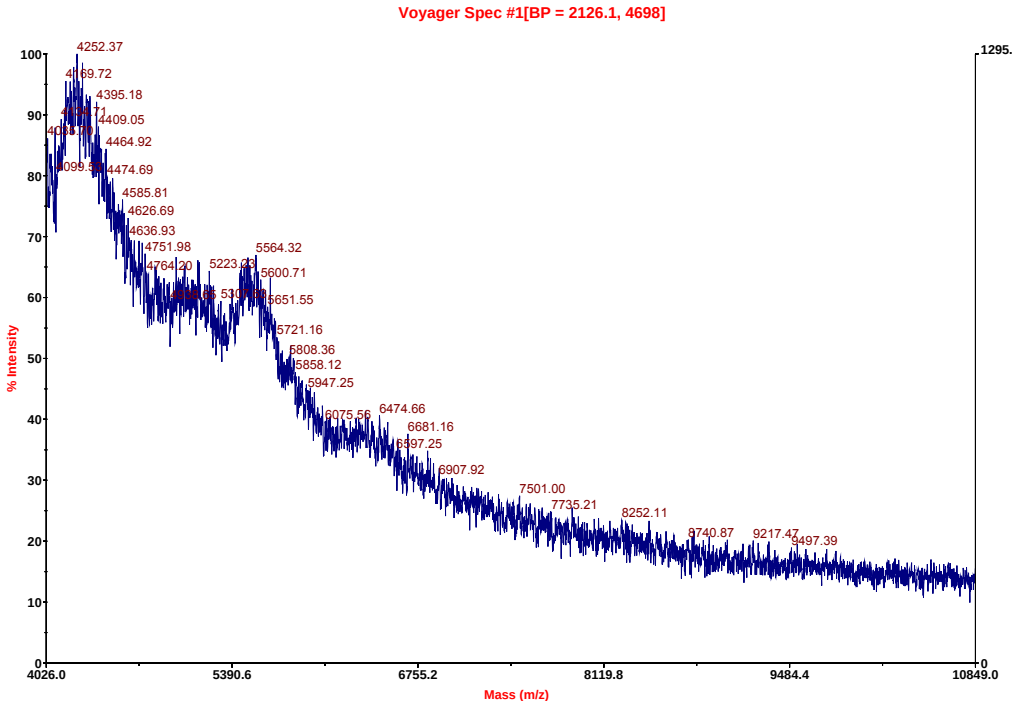

Figure 5.2. MALDI-TOF MS of PXL-Pep-Dendron. The 5,564 peak corresponds to the PXL-Pep-Dendron fragment after loss of two PXL-[Ahx]-AVRWL groups.

5.3 Cleavage of Fmoc-Pep-Dendron (**11**) & PXL-Pep-Dendron (**22**) with MMP9

Although the sequence AVRWLLTA has been previously reported to be cleaved selectively by MMP9 [178], cleavage of several copies of that sequence on a dendron has not been established. The samples were treated with active MMP9 and analyzed for both the expected products and unreacted starting material using HPLC and MALDI-TOF-MS. First, Fmoc-Pep-Dendron was digested with MMP9. As seen in the HPLC spectra (reverse phase, C18 silica with a gradient from 0.065% water to 0.05% acetonitrile) in Figure 5.3, Fmoc-Pep-Dendron is cleaved into two main components and at least one minor component. Mass spectrometry (MALDI-TOF) further confirming the proteolytic cleavage shows expected cleavage peaks at 2,731 and 888 amu (Figure 5.3 Bottom) of Fmoc-Pep-Dendron. The peak at 2,731 amu is equivalent to (LLTA-[Ahx])$_4$-Dendron, one of the expected cleavage peak. The peak at 888 amu is from the other expected product, Fmoc-[Ahx]-AVRW. The remaining two identical peaks in the MS may result from further fragmentation of the digested dendron to (A-[Ahx])$_4$-Dendron (1,469 amu) and Gly-Dendron (684 amu), likely arising from the analysis by MALDI-TOF MS.

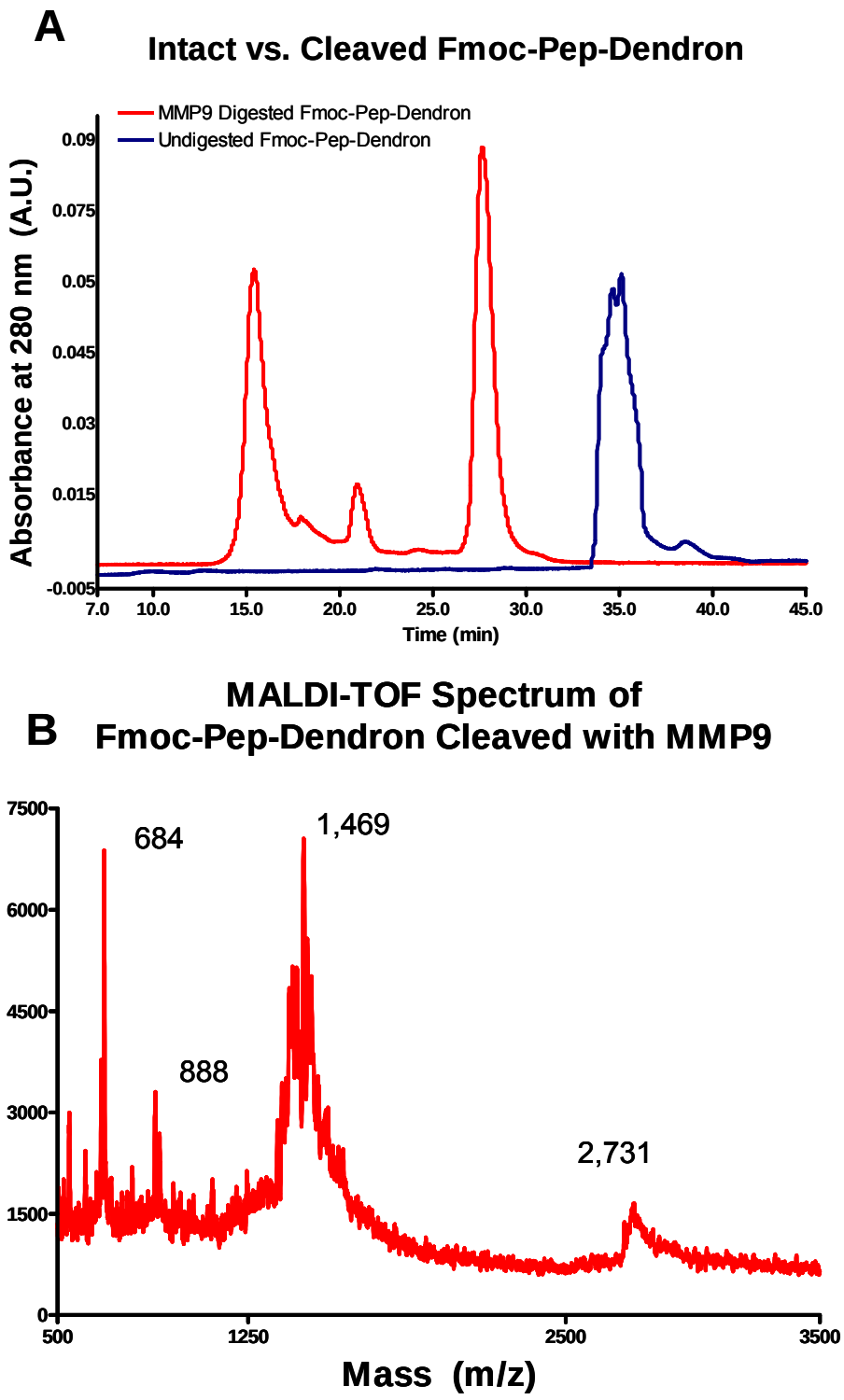

Figure 5.3. Digestion of Fmoc-Pep-Dendron (**11**) with MMP9. Chromatography before and after cleavage with MMP9 (Top) MALDI-TOF MS after cleavage with MMP9 (Bottom).

In Figure 5.4, the results of MMP9 treatment with PXL-Pep-Dendron are highlighted. Before HPLC or MALDI-TOF MS it was evident that digestion occurred due to the formation of a significant amount of precipitate. This precipitate was pelleted in the centrifuge, purified by washing twice with water followed by pelleting. The precipitate was then dissolved in DMSO for HPLC and MALDI-TOF MS analysis. The HPLC trace before and after treatment with MMP9 (reverse phase C18 column with 0.1% triethyl amine in acetonitrile and water; gradient from 45 – 100% acetonitrile) indicates digestion occurred. The intact product elutes as a peak at 10.5 minutes while the cleaved product elutes at 8.5 minutes. Solubility likely plays a role in the shape of the chromatogram of the digested product. The cleaved product provided the expected cleavage peak PXL-[Ahx]-AVRW (1,545 amu) as well as further fragmentation products at 1,319 amu (PXL-[Ahx]-AVR) and 1,108 amu PXL-[Ahx]-A (Figure 5.3 Bottom) in the MALDI-TOF spectra. From the MALDI-TOF MS data it can be concluded that MMP9 at least cleaves the peptide between the tryptophan and argenine residues are PXL-[Ahx]-AVR and PXL-[Ahx]-A or from further proteolytic cleavage of the initial PXL-[Ahx]-AVRW product. The two smaller products detected in the MS, corresponding with PXL-[Ahx]-AVR and PXL-[Ahx]-A, could be a result of fragmenting in the MALDI-TOF MS instrument.

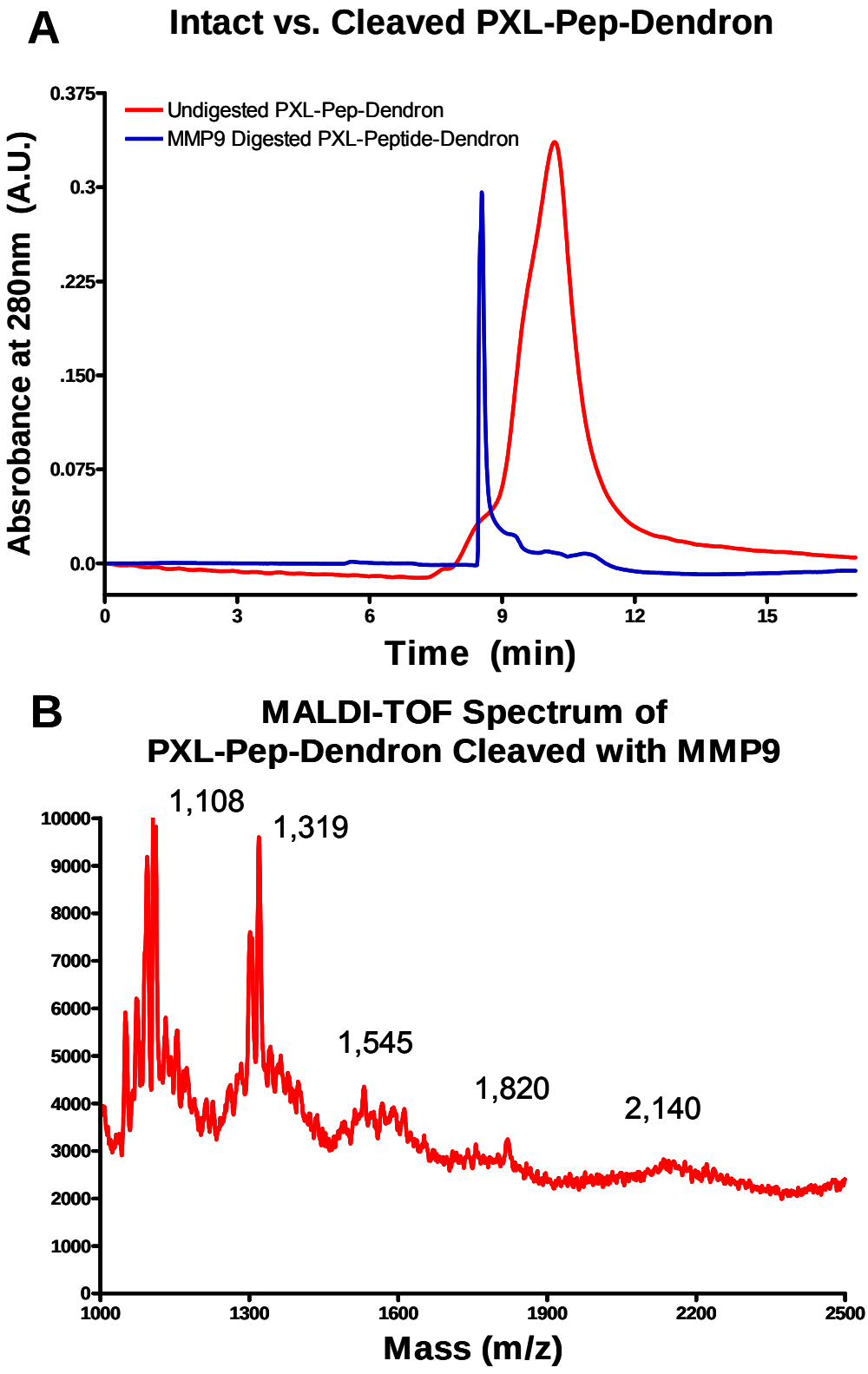

Figure 5.4. Digestion of PXL-Peptide-Dendron (**22**) with MMP9. Chromatography before and after cleavage with MMP9 (Top) and MALDI-TOF MS after cleavage with MMP9 (Bottom).

5.4 Cellular Toxicity Studies of PXL-Pep-Dendron (**22**)

After the synthesis and confirmation of MMP9 cleavage, PXL-Pep-Dendron (**22**) was tested for cytotoxicity against PyVT-R221A-Luc, MDA-MB-231, LLC-RSV and LLC-MMP9 cells. The PyVT-R221A-Luc and LLC-MMP9

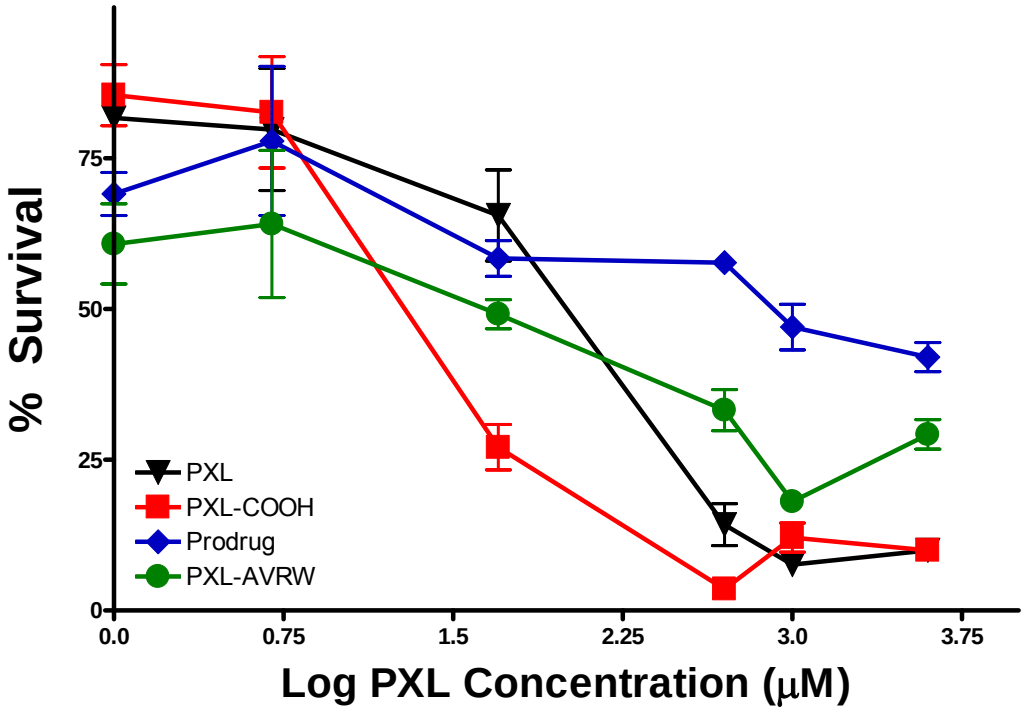

Figure 5.5 Dose dependent cytotoxicity of paclitaxel compounds in PyVT-R221A-Luc cells (high MMP9 expression) of Paclitaxel (PXL, triangles), modified Paclitaxel (PXL-COOH, squares), Paclitaxel Prodrug (PXL-Pep-Dendron, diamonds) and cleaved Paclitaxel Prodrug (PXL-AVRW, circles) after 72 hours.

cells are MMP9 expressing cell lines, while MDA-MB-231 and LLC-RSV do not express detectable MMP9 in culture (MMP9 negative lines). Initially, PyVT-R221A-Luc cells were studied in preparation for *in vivo* studies in the MMTV-PyVT mouse model, the parent model from which the PyVT-R221A-Luc cell line was derived. Due to this pairing with the mouse model, the majority of cytotoxicity studies were performed with the PyVT-R221A-Luc cell line. A human breast cancer cellular line, MDA-MB-231, was also investigated for confirmation of activity in a clinically relevant cell line. Although, MDA-MB-231 cells express insignificant amounts of MMP9, the cytoxicity data provided insight into the prodrug efficacy in humans. The remaining two cell lines, LLC-RSV and LLC-MMP9, serve as MMP9 negative and positive cell lines respectively, but are otherwise identical[124]. The MMP9 positive and negative cell lines were used to access the role of MMP9 for prodrug activation *in vitro*.

The results of the initial toxicity studies using PyVT-R221A-Luc cells were encouraging as the intact prodrug (PXL-Pep-Dendron) is significantly less toxic than the MMP9 cleaved product or paclitaxel (Figure 5.5) as determined by the t-test (analysis is Appendix A). As expected, all paclitaxel compounds produce concentration-dependent cytotoxicity (Figure 5.5). At the lower concentrations tested (1 and 5 nM in PXL), the number of viable cells after 3 days treatment is 60% - 80%, with the prodrug and digested prodrug being slightly more toxic than PXL or PXL-COOH. At higher concentrations, the drugs are more toxic to the PyVT-R221A-Luc cells, with the native PXL and modified (PXL-COOH) paclitaxel compounds being the most toxic. By definition, a prodrug should not produce

toxicity until activated. It was found that the cells are only 50 % viable at high concentrations of PXL-Pep-Dendron in the PyVT-R221A-Luc cells. Given that the PyVT-R221A-Luc cells produce large concentrations of MMP9; peptide cleavage, releasing PXL-AVRW, likely occurs *in vitro* delivery a toxic dose of drug to the cells.

Through the course of multiple doses over time, the cytotoxic effects are also increased. For example, the MMP9 cleaved product (PXL-AVRW) is only slightly toxic after 1 or 2 doses (24 and 48 hours) while after 3 or 4 doses (72 and

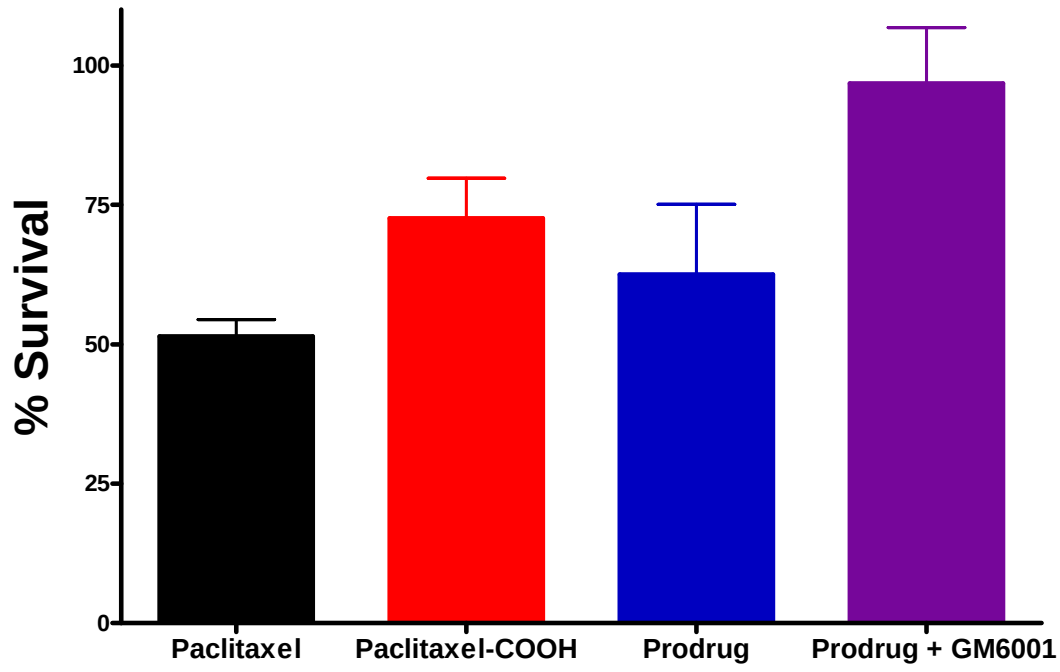

Figure 5.6. Cytotoxicity of PXL after 24 hours of treatment with: Paclitaxel (PXL, black), modified Paclitaxel (PXL-COOH, Red), Prodrug (Blue), Prodrug & GM6001 MMP inhibitor (Purple) in PyVT-R221A-Luc cells. All trials were treated with an equivalent of 50 nM PXL.

96 hours) it is about as toxic as PXL and PXL-COOH (Appendix A). A dramatic change in toxicity between the prodrug (PXL-Pep-Dendron) and the digestion product (PXL-AVRW) occur between 24 and 48 hours after the first dose. The cleaved product jumped from 109% survival to 44% survival between 24 hours (1 dose) and 48 hours (2 doses) while the prodrug does not increase in toxicity on the second day. Structural differences between PXL/PXL-COOH and PXL-AVRW could account for the difference, possibly making cellular internalization or microtubular binding slower with the bulkier PXL-AVRW. Alternatively, further enzymatic degradation of PXL-AVRW may be necessary prior to the onset of cytotoxic effects.

Next, toxicity data of the intact PXL-Pep-Dendron was obtained in which any MMPs released by the cells were blocked with GM6001, a general MMP inhibitor (Figure 5.6). The uninhibited prodrug displays toxicity similar to PXL and PXL-COOH, while the cells treated with GM6001 (a general MMP inhibitor) are not significantly affected by the prodrug (PXL-Pep-Dendron). The pre-cleaved prodrug (PXL-AVRW) produces similar cytotoxitiy as PXL and PXL-COOH in the PyVT-R221A-Luc cell line (Appendix A), again treating with 50 nM concentrations in PXL. Furthermore, PyVT-R221A-Luc cells treated with only GM6001 did not produce significant changes in proliferation compared to media or DMSO treated controls. Cytotoxicity experiments with multiple doses confirm the trend observed in Figure 5.6 (Appendix A). Additional studies using 5 μM concentrations of PXL produce the same trends observed above (Appendix A). In summary, the cytotoxicity data indicates that the PyVT-R221A-Luc cells are

sensitive to PXL compounds and the proteolyzed prodrug (PXL-AVRW) has similar toxicity to the PyVT-R221A-Luc cell as PXL and PXL-COOH. In addition, the data are consistent with the prodrug being cleaved *in vitro* by MMP9 present in the PyVT-R221A-Luc cells presumably by MMP9 expressed by these cells and with cleavage of the prodrug (and thus the cytotoxicity) being blocked by the addition of GM6001. The above observations indicate that the PXL-Pep-Dendron prodrug is not active until cleaved selectively by MMP9.

The measured cytotoxicity at five concentrations of the various PXL compounds, PXL-Pep-Dendron (**22**), PXL-AVRW, PXL-COOH and PXL, was used to calculate IC_{50} values. After 72 hours, the prodrug is significantly less toxic than the cleaved product, PXL-COOH and PXL with an IC_{50} of 3.1 μM, compared to 1.3, 0.58 and 1.1 for PXL-AVRW, PXL-COOH and PXL respectively. This 72 hour point indicates that the MMP9 activated prodrug has low toxicity to PyVT-R221A-Luc cells, while after 96 hours the prodrug toxicity is comparable with the active drugs. Given

Table 5.1 IC_{50} toxicity values of Paclitaxel compounds in PyVT-R221A-Luc.

Compound	IC_{50} (μM)
PXL-Pep-Dendron	
24 Hour	4.8±0.014
72 Hour	3.1 ±.0020
96 Hour	0.83±0.0033
PXL-AVRW	
24 Hour	3.0±0.0019
72 Hour	1.3±0.0022
96 Hour	0.79±0.0020
PXL-COOH	
24 Hour	4.2±0.0017
72 Hour	0.58±0.0019
96 Hour	0.85±0.0022
PXL	
24 Hour	3.6±0.0026
72 Hour	1.1±0.0017
96 Hour	1.2±0.0018

that the PyVT-R221A-Luc cells express MMP9, the difference in relative IC_{50} values from 3 to 4 doses likely relates to the time it takes to activate the prodrug.

To further examine the efficacy of the prodrug, its toxicity was studied in a human cell line (MDA-MB-231 breast cancer), PXL-Pep-Dendron (**22**), PXL-AVRW (digestion product of the prodrug), PXL-COOH and PXL were tested at 5

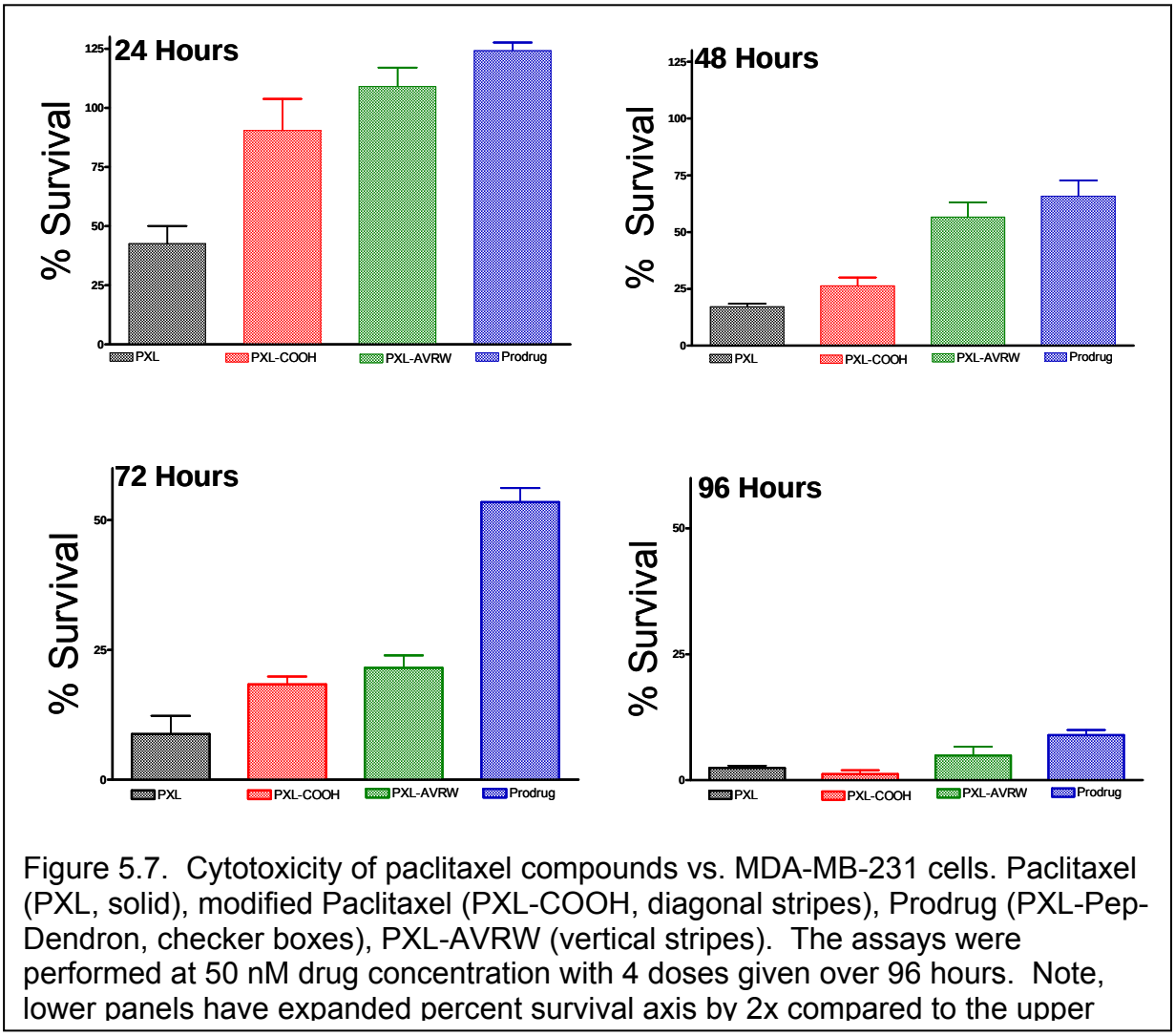

Figure 5.7. Cytotoxicity of paclitaxel compounds vs. MDA-MB-231 cells. Paclitaxel (PXL, solid), modified Paclitaxel (PXL-COOH, diagonal stripes), Prodrug (PXL-Pep-Dendron, checker boxes), PXL-AVRW (vertical stripes). The assays were performed at 50 nM drug concentration with 4 doses given over 96 hours. Note, lower panels have expanded percent survival axis by 2x compared to the upper

μM and 50 nM concentrations (in PXL) over the course of 4 doses and 96 hours (Figure 5.7 for 50 nM and Appendix A for 5 μM). Over the course of time, all compounds produced toxicity to the MDA-MB-231 cells; however, with the PXL-Pep-Dendron being the least toxic. The PXL-Pep-Dendron statistically differs from PXL after only 24 hours, PXL and PXL-COOH after 48 hours and PXL, PXL-COOH and PXL-AVRW after 72 hours (for statistical analysis see Appendix A). As with the PyVT-R221A-Luc cell line, PXL-AVRW has the same toxicity as the

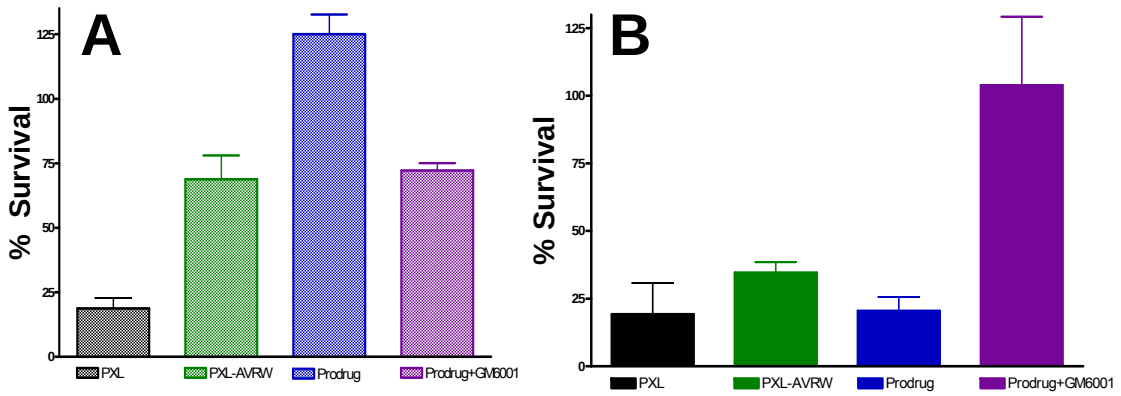

Figure 5.8. Cytotoxicity of prodrug with and without an MMP inhibitor versus PyVT-R221A-Luc cells (high MMP9 expressing). The data presented is the percent survival after 2 doses of compound over 48 hours. All paclitaxel treated cells were treated with an equivalent of 50 nM paclitaxel. The cytotoxicity is measured with respect to GM6001 and control. GM6001 is a general MMP inhibitor. (**A**) MMP9 negative cells (LLC-RSV) cytotoxicity of paclitaxel (PXL, solid), cleaved prodrug (PXL-AVRW, vertical stripes), prodrug (PXL-Pep-Dendron, boxes) and Prodrug + GM6001 (horizontal stripes) in. GM6001 enhanced the growth of cells by about 20% after 48 hours. (**B**) MMP9 positive cells (LLC-MMP9) cytotoxicity of paclitaxel (PXL, solid), cleaved prodrug (PXL-AVRW, vertical stripes), prodrug (PXL-Pep-Dendron, boxes) and Prodrug + GM6001 (horizontal stripes) in. GM6001 reduce the growth of LLC-MMP9 cells by about 40% after 48 hours.

prodrug over the first 48 hours, however after 72 hours there is a significant change in the toxicity between the two compounds (see Appendix A for statistical analysis). This supports the hypothesis that PXL-AVRW either needs extra time to enter the cell and interact with the microtubules or further cleavage from an unknown protease occurs in the cellular environment. If the latter is true, then this requirement would be seen in different cell lines and should not be affected by the MMP9 concentration in the cell.

To further study the *in vitro* effects of the prodrug on MMP9, two cell lines; one that contains a naturally low concentration of MMP9 (LLC-RSV) and another transfected with a vector to express high amounts of MMP9 (LLC-MMP9) were studied. As with the other two cell lines, prodrug (PXL-Pep-Dendron, **22**) yielded the highest levels of survival (Figure 5.8). In the MMP9 negative cell line, the prodrug proliferates statistically the same as the DMSO treated control cells, indicating no toxicity (Figure 5.8A). In the MMP9 positive cell line, the prodrug has toxicity statistically equivalent to PXL and PXL-AVRW, the MMP9 digested product (Figure 5.8B, statistical data can be found in Appendix A). When the MMP9 expressing cells are treated with GM6001 and prodrug, toxicity seen in cells treated with prodrug alone disappears. This data demonstrates that GM6001 inhibited protease activity is necessary for the prodrug to produce toxicity.

As a further comparison, the toxicity of the prodrug with and without GM6001 in MMP9 expressing and non-expressing cells is shown in Figure 5.8.

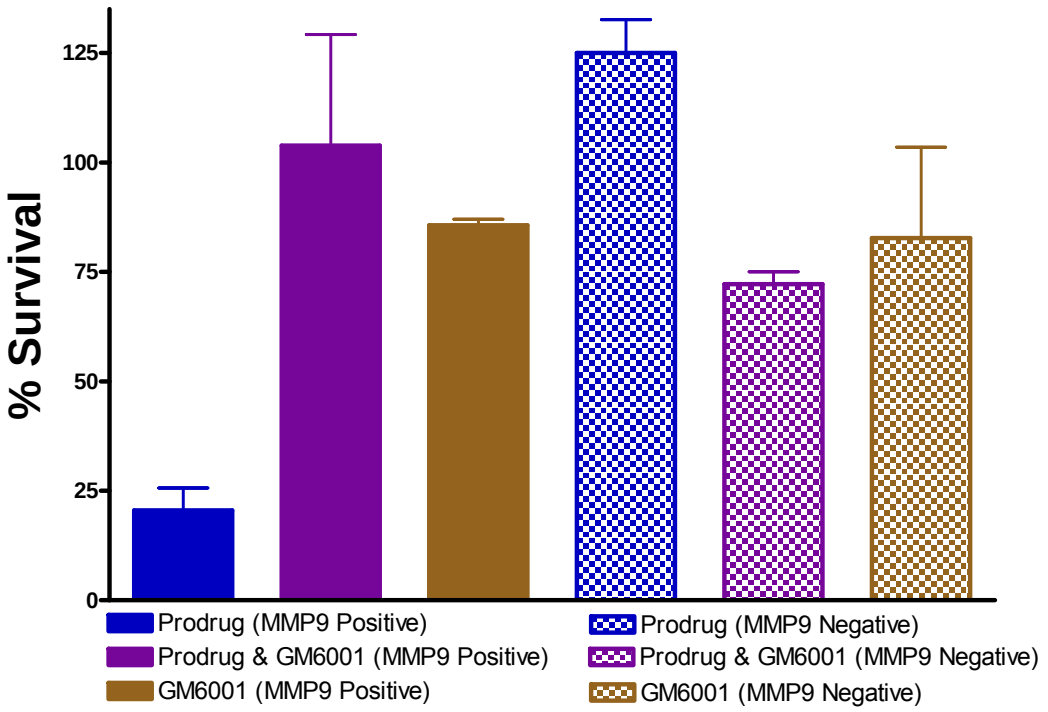

Figure 5.9. Cytotoxicity of prodrug with and without an MMP inhibitor versus PyVT-R221A-Luc cells (MMP9 expressing). The data presented is the percent survival after 2 doses of compound over 48 hours. All paclitaxel treated cells were treated with an equivalent of 50 nM paclitaxel. The cytotoxicity is measured with respect to GM6001 and control. GM6001 is a general MMP inhibitor. Cytotoxicity of prodrug (solid), Prodrug + GM6001 (horizontal stripes) and GM6001 (Diagonal checkers) in MMP9 positive cells (LLC-MMP9) and prodrug (white dots), Prodrug + GM6001 (diagonal stripes) and GM6001 (boxes) in MMP9 negative cells (LLC-RSV).

The LLC-MMP9 cells treated with intact prodrug have an 80% reduction in cell growth compared to the same cell line treated coincidently with prodrug and an MMP inhibitor (GM6001). The MMP9 negative cell line has the highest survival rate when treated with prodrug. All indications are that PXLPep-Dendron (**22**) is non-toxic until cleaved by MMP9 and therefore should interact preferentially with MMP9 expressing tissues such as in tumor rather than healthy tissues (which generally contain low levels of MMP9).

5.5 Conclusions

The MMP9 activated prodrug was synthesized by attaching a modified paclitaxel to the terminal amines on the H_2N-Pep-Dendron scaffold and MMP9 digestion to PXL-AVRW was confirmed. Using prodrug (PXL-Pep-Dendron) and digested prodrug (PXL-AVRW) cellular toxicity studies were completed to demonstrate the utility of the prodrug. The intact prodrug was shown to be toxic in cell lines that express MMP9 and have reduced toxicity in cell lines that are MMP9 negative. The broad spectrum MMP inhibitor, GM6001, diminished the cytotoxicity of PXL-Pep-Dendron versus the MMP9 expressing cell line PyVT-R221A-Luc and LLC-MMP9. The compound was significantly less effective versus LLC-RSV as compared with LLC-MMP9 cells (e.g. blocking the MMP9 in PyVT-R221A-Luc and LLC-MMP9 cells significantly reduced the toxicity of the prodrug). These data are consistent with the interpreted data, showing that MMP9 expression is necessary for toxicity and the drug has limited toxicity under the conditions tested until activated by MMP9. The progress described in this dissertation places the project in a position to test the *in vivo* efficacy of the prodrug in animals, leading to the eventual translation into use in humans.

5.7 Experimental Procedures

General Methods:

MDA-MB-231 cells were purchased from ATCC and cultured in DMEM, 10% FBS and gentamycin with 5% CO_2. PyVT-R221A-Luc cells were obtained

from the Matrisian laboratory and cultured in DMEM without L-glutamine, 10% FBS, gentamycin and puromycin with 5% CO_2. LLC-RSV and LLC-MMP9 cells were obtained from the Matrisian laboratory and cultured in DMEM, 10% FBS and gentamycin with 5% CO_2. The custom ordered peptides were purchased from Genscript™. The enzymes were purchased from Calbiochem. All other chemicals were purchased from Fisher Scientific or Aldrich Chemical companies and used as is unless otherwise indicated.

(2a,4a,5ß,7ß,10ß,13a)-4,10-bis(acetyloxy)-13-{[(2R,3S)-3-(benzoylamino)-2-oxobutanoic acid-3-phenylpropanoyl]oxy}-1,7-dihydroxy-9-oxo-5,20-epoxytax-11-en-2-yl benzoate (PXL-COOH):

This compound was made as described in [101]. Briefly, paclitaxel (77.61 mg, 0.091 mmols) was dissolved in methylene chloride (6 mL). Succinic anhydride (13.1 mg, 0.131 mmols) in 0.8 mL of methylene chloride was added followed by pyridine (27 μl). The reaction was stirred for 4 days. TLC (1:1 hexanes: ethyl acetate on silica gel) indicated 4 spots under a UV lamp and with potassium permanganate staining. Staining with bromo-cresol green indicated that the carboxylic acid was the last spot. The reaction was concentrated onto silica gel and purified with the Biotage™ SP1 system using a hexane/ ethylacetate gradiant followed by flushing with methanol to elute the product. After concentration the last peak eluted was 84.5 mg (97%) of desired product as confirmed by MS. MS $(ESI)^+$ Found: 954.30 Dalton $(M + H)^+$; calculated: 954.99 Da. ($C_{51}H_{56}NO_{17}$).

PXL-Pep-Dendron (22):

All glassware used in the reaction was flame dried and cooled in a desiccator prior to use. The solvents were anhydrous and all solid materials were dried under vacuum for more than 3 hours prior to use and exposed to anhydrous Ar(g) gas upon breaking the vacuum seal. First, PXL-COOH (8.51 mg, 0.0091 mmols) was dissolved in 0.5 mL DMF. Next, EDCI (5.00 mg, 0.026 mmols) and BOP (5 mg, 0.011 mmols) were added to the PXL-COOH solution followed by DIEA (180 μl). The reaction was stirred for 30 minutes prior to adding H_2N-Pep-Gly-Dendron (3.56 mg, 0.00068 mmols), dissolved in 0.5 mL DMF. The reaction was stirred under Ar(g) overnight with SEC spectra taken 5 minutes after H_2N-Pep-Gly-Dendron addition and after 15 hours. A notable change in the elution time of the first peak indicated coupling occurred. The reaction was concentrated under vacuum, and dissolved in DMSO. The product was purified by first using Amicon Centrifugation Diafiltration tubes (3,000 MWCO) to concentrate the high molecular weight compounds followed by three washings with DMSO to remove all the low molecular weight compounds. The remaining high molecular weight compounds were separated using SEC to provide 5.13 mg (85%) of pure $(PXL\text{-}Pep)_4$-Gly-Dendron. MADLI-TOF MS (CHCA) Found 2,121 Dalton (Fragment: PXL-[Ahx]-AVRWLLTA-[Ahx]-Gly + H)$^+$; calculated 2,119 Dalton ($C_{108}H_{148}N_{16}O_{28}$); Found 4,409 Dalton (Fragment: (PXL-[Ahx]-AVRWLLTA-[Ahx]-Gly)4-Dendron/4 + H)$^+$; calculated 4,408 Dalton ($C_{447}H_{609}N_{64}O_{121}$). SEC (55% 0.05% TFA in Acetonitrile/ 45% 0.065% TFA in water) elution time 7.7 minutes.

Cleavage of Peptide compounds with Enzymes:

The compound to be cleaved or tested for ability to cleave was dissolved in methanol at 10 mg/mL. Next, 100 μl of this solution was diluted with 900 μl of tricine buffer to make a 1 mg/mL solution. A 10 μL aliquot of solution was injected into the HPLC (C18 silica with 55% 0.05% TFA in Acetonitrile/ 45% 0.065% TFA in water) for a zero time point. Following HPLC, enzyme (either MMP9, MMP2 or Trypsin) was added to the reagent solution and the reaction mixture was incubated at 37 ^{o}C overnight. Again, analytical HPLC was used to determine what percentage of the sample had cleaved. For samples which produced solid, the solid was collected, dissolved in 100% methanol and injected into the HPLC. The samples were then characterized with ESI and MALDI-TOF MS to determine the cleavage products. The solid usually contained the cleaved product.

Toxicity studies

Cells were plated at 40,000 – 60,000 cells/mL into 24 well plates (0.5 mL/well) in appropriate culture medium. A separate plated was used for each time point measured in the assay (i.e. four plates were used to measure 4 time points). The cells were incubated overnight at 37 ^{o}C (usually 24 hours). After examination under the microscope to ensure the cells were attached and looked

healthy, the media was aspirated off each well (taking care to not disrupt the cells) and replaced with media containing the drug/ compound of interest or a control compound. The drug and control solutions were made fresh just prior to use. The cells were incubated 24 hours and then either redosed with fresh drug-media solutions or the cells were trypsinized and counted using trypan blue. For typsinization, the media was removed by aspiration and each well was washed with 0.5 mL of DPBS. The DPBS was removed and each well was treated with 200 μl of trypsin. The plate was incubated for 10 - 15 minutes and then agitated, either with a shaker or by hand. Finally, 40 μl of trypan blue was added to each well (typically 4 wells at a time) and the cells were counted with a hemocytometer. The dosing and counting was continued for the remaining time points so that the cells were given fresh drug every 24 hours until counted.

CHAPTER VI

CONCLUSIONS AND FUTURE DIRECTIONS

The research presented in this dissertation was intended to aid in advancing medical research by improving on molecular imaging and therapeutic delivery through the use of functionalized dendrimeric particles. Two projects: one developing TSPO targeted imaging agents and the other an MMP9 activatable prodrug was developed simultaneously that have several commonalities. These commonalities include: 1) the development of dendrimeric particles for biological purposes, 2) the functionalization of a dendrimer or dendron and 3) the use of targeting biomarkers to specifically delivery the dendrimeric particles to diseased cells.

The work in Chapter 2 was an expansion of previous work performed in the Bornhop laboratory that focused on developing new imaging agents for targeting TSPO. The project was transitioned from small molecules that can incorporate only a single imaging agent (and thus only a single imaging modality) per targeting ligand to a multifunctional, polyvalent species that incorporates multiple imaging/targeting modalities. Here, a G(4)-PAMAM dendrimer scaffold was modified to target TSPO and produce fluorescence and MRI signals on mitochondria of high TSPO expressing cells. Due to the desity of the gadolinium metal, EM imaging was investigated. Although the treated cells produced increased contrast compared to controls, the contrast was due to osmium

staining of the dendrimers post fixation. Regardless, the increase contrast on mitochondria in treated versus control cells shows that the dendrimers are targeting the mitochondria. Furthermore, this is proof-of-principle that EM can be used to study cellular processes at the molecular level. The EM studies are being further explored by Madeline Dukes in Dr. Niels De Jonge's laboratory along with the development of liquid STEM for live cell imaging.

Potential clinical uses of the TSPO targeted agents go beyond diagnostic agents to include applications as surgical tools and therapeutic efficacy monitoring. The most common cancers in which diagnostic imaging of TSPO expression would be useful are brain, breast, colorectal and prostate tumors since these cancers have been shown to have extremely high concentrations of the protein. As diagnostic agents, the MR signature is useful since it can be detected in deep tissue and is inherently sensitive; while the fluorescence agent has limited use. As surgical tools, the dual-modality of the agent is advantages because the fluorescence and MRI signatures can be used in conjunction. In particular, brain gliomas often need to be surgically removed and it is up to the surgeon's discretion as to which excised. Removing more tissue than necessary can lead to un-necessary loss of brain function; while leaving cancerous tissue can lead to tumor regrowth. Since gliomas (brain cancer) have high expression of TSPO, these dual-modal imaging dendrimers provide a method for in surgery cancer labeling. The dendrimer can be administered via pre-surgical injection or "splashed on" the exposed tissue during surgery. If injection is the method of delivery, then a pre-surgical MRI scan will reveal the location size and shape of

the tumor. The sensitive fluorescence signal then differentiates which tissue (or cells if surgical techniques become that accurate) needs to be removed. Post surgical success/failure can be monitored with the MRI agent on the dendrimer. The targeted MR agent is improved over the typical profusion agents for post surgical applications, since scar and other highly vascularized tissues produce increased contrast in the MRI are difficult to differentiate from re-emergence of the diseased tissue. The dendrimer imaging agents can be further applied to progression monitoring of therapeutics in TSPO associated diseases. During treatment imaging a patient's effected tissues provides insight into whether the cancer is spreading (therapy completely failing), maintaining size (therapy stopping or slowing growth) or disappearing (therapy is being successful). Targeted and sensitive imaging techniques, including better imaging agents, can also be used to detect early signs of metastases, which can be treated promptly for better patient outcome.

Although imaging to detect and follow the progression of disease and therapy is useful in minimizing the invasiveness of treatments. Nanoparticles can also be utilized to further reduce invasiveness by incorporating therapeutics. Chemical therapeutics limit invasive procedures such as surgical retraction while targeted clinical therapeutics reduce systemic toxicity and maximize positive patient outcomes. In the second project presented here, a series of MMP9 activated therapeutic dendrons were developed, which can then be coupled with other dendrons to form tailor made dendrimers with the desired properties.

Specifically, these MMP9 activated therapeutic dendrons are designed to target early tumor progression and the establishment of micro-metastatic lesions.

Rational design was implemented in developing the prodrug. Proteolytic cleavage of a peptide by MMP9 was incorporated as the method for delivering the active drug. Not only is MMP9 associated with early stages of tumor development of micro-metastatic lesions, but the peptide sequence AVRWLLTA has been shown to be specifically cleaved by the enzyme[186]. Incorporating this peptide into a dendron was intended to create a molecular carrying system that releases drug or imaging agent upon cleavage by MMP9. The focus of the work presented here was to incorporate a therapeutic molecule that would be released and produce toxicity to MMP9 associated cells. Initially doxorubicin (DOX) was investigated; however the attachment chemistry inactivated the drug. Following attempts with modified DOX conjugation, paclitaxel was attached to the scaffold and found to be more efficacious than DOX for this system.

Synthesizing an MMP9 cleavable therapeutic proved more of a challenge than initially anticipated. First, the coupling of the cleavable peptide to the dendron scaffold was difficult to characterize, both in determining that attachment had occurred and in determining the number of peptides per dendron that attached. After employing a variety of techniques including nuclear magnetic resonance (NMR), size exclusion chromatography (SEC) and a ninhydrin assay for primary amines, a matrix assisted laser desorption ionization time-of-flight mass spectrum (MALDI-TOF MS) of the product was finally obtained, the MALDI-TOF spectrum definitively confirmed that four peptides had attached to the

dendron. Attaching DOX to the H_2N-Pep-Dendron was an easier synthetic expedition, but unfortunately the drug was permanently inactivated due to unforeseen structural changes.

Two strategies were investigated to produce a working MMP9 activated prodrug molecule: a new peptide sequence that released LL-DOX (a toxic analogue of DOX) and attaching paclitaxel to the scaffold. The modified peptide, AVRWLL, was found to not be digested by MMP9. Nonetheless, preliminary cellular toxicity studies were performed on this compound with results indicating that these agents have some therapeutic efficacy. During the experiments to test therapeutic efficacy, a sub-population of DOX resistant, rapidly proliferating cells formed. More extensive investigation of these agents need to be performed to determine the usefulness of these agents.

Incorporating paclitaxel (PXL) onto the H_2N-Pep-Dendron in place of DOX was the most successful strategy for producing an MMP9 activated prodrug. The attachment of PXL was simple and accomplished quickly. The final product, PXL-Pep-Dendron, was tested in cells as both the intact prodrug and MMP9 cleaved products. The intact compound was also tested with inhibitors and in MMP9 positive and negative cell lines. The inhibitors increased survival in the MMP9 positive cell lines, indicating that the prodrug is cleaved *in vitro*, leading to the toxic effect observed. The combination of all the cell studies demonstrates that the MMP9 activated prodrug is non-toxic until activated by the protease.

Along with an MMP9 activable prodrug, other modules are necessary to produce a multifunctional dendrimer. The idea is that individual dendrons with

different functionalities will be coupled together to give "**mix and match**" dendrimers. Any number of dendrons can be synthesized to give optimal functionality for the desired effect in treating and/or imaging any disease. A complimentary dendron for the MMP9 prodrug, MMP9 activated molecular sensor, is being developed that produces fluorescence upon MMP9 cleavage. The prodrug dendron coupled with the molecular sensor dendron provides a dual matched MMP9 activatible dendrimers; where the sensor visualizes drug delivery. Other modules that can be incorporated include: (a) an imaging agent to track the dendrimer location before and after delivery, (b) a targeting ligand to specifically bind the disease site and (c) ADME agents to tune administration, distribution, metabolism and excretion properties of the dendrimers. The "**mix and match**" concept can be expanded to include a variety of drugs, imaging agents, sensors and ADME agents as well as to target any protease or receptor and treat and/or image any disease.

APPENDIX A

BIOLOGICAL DATA OF MMP9 ACTIVATED PRODRUGS

A.1 MMP9 Expression in Cells

To estimate the MMP9 expression of the four cell lines being used in toxicity studies, zymography was performed on the cell lysates and the media. Briefly, zymography was performed by taking the cell media and lysates from confluent T75 flasks were concentrating the solutions with 3,000 MWCO diafiltration tubes and tested the concentrated samples with a bicinchoninic acid assay for total protein content. Next, an acrylamide gel was ran using 10 μg of protein per well and HT1080 as a positive control. The results of the assay were quantified by detection of the Pro and active MMP9 bands on the gel as determined by the MW marker and HT1080 positive control (Table 5.1). As expected, the MMP9 content of the LLC-RSV cells was not detectable with this assay, indicating no enzyme present. The LLC-MMP9 cells have a high level of MMP9 in the media and low levels of MMP9 in the cell lysates. Since the enzyme is secreted from the cell into the surrounding area (cell media), it is expected to see more MMP9 in the media than the lysates. The media associated with PyVT-R221A-Luc cells also contained high levels of MMP9 with

none being detected in the lysates. Media from the MDA-MB-231 cells had only a very slight band in the gel and none was detected in the lysates. Overall, two cell lines, LLC-MMP9 and PyVT-R221A-Luc, were found to contain significant levels of MMP9.

Table A.1 MMP9 expression levels in the cells lines of interest.

Cell Line	MMP9 Detection Level
LLC-RSV Lysates	Not Detectable
LLC-RSV Media	Not Detectable
LLC-MMP9 Lysates	Low Levels
LLC-MMP9 Media	High Levels
PyVT-R221A-Luf Lysates	Not Detectable
PyVT-R221A-Luf Media	High Levels
MDA-MB-231 Lysates	Not Detectable
MDA-MB-231 Media	Barely Detectable

A.2 Toxicity Studies

The results of the initial toxicity study using PyVT-R221A-Luc cells were encouraging with the intact molecule being less toxic than the MMP9 cleaved product (Figure 5.4). The MMP9 cleaved compound also displayed toxicity similar to PXL-COOH and PXL after 72 and 96 hours (3 and 4 doses). One dose

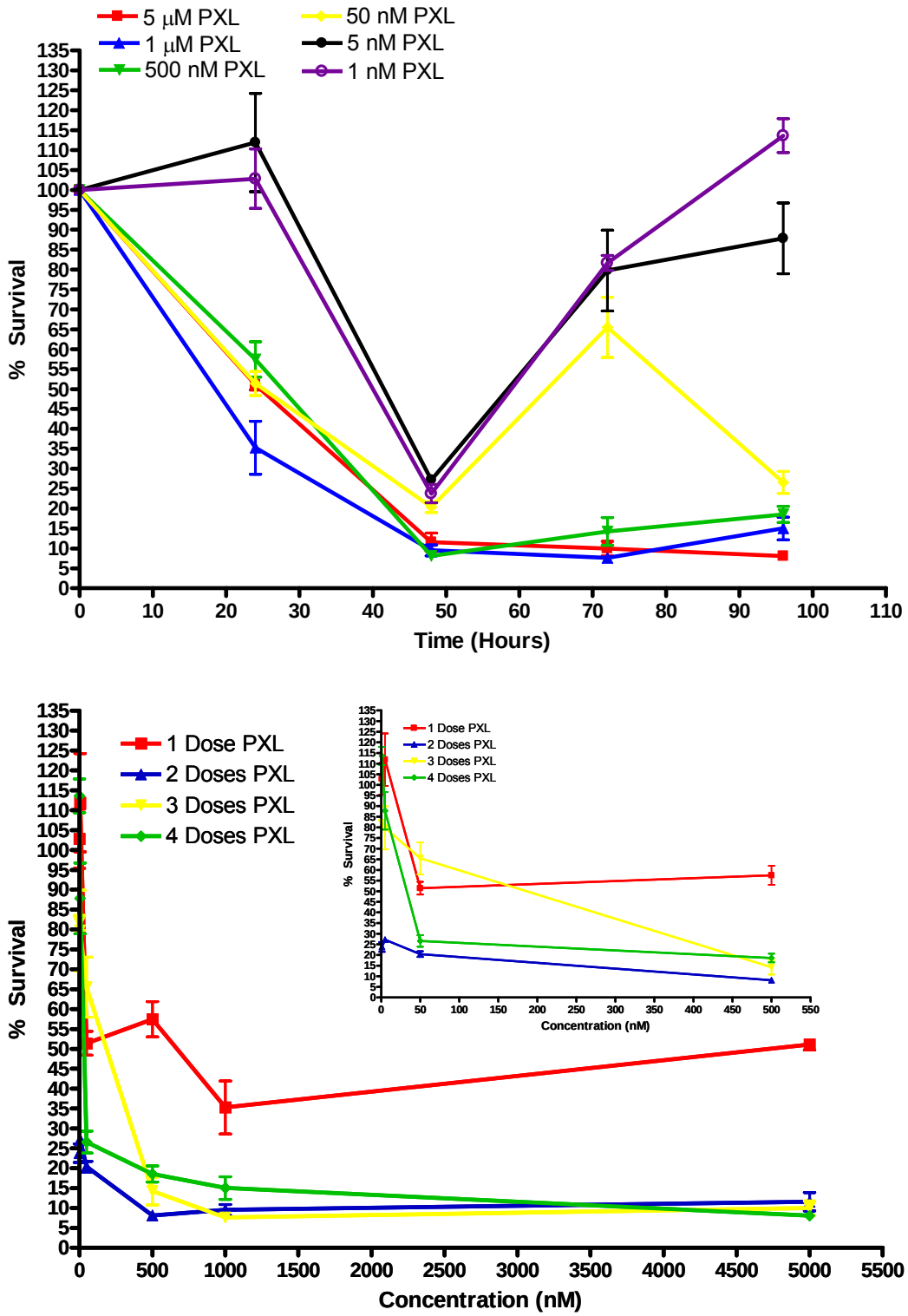

Figure A.1 Survival of Paclitaxel (PXL). Top % Survival versus Time at 5 μM, 1 υM, 500 nM, 50 nM, 5 nM and 1 nM . Bottom: % Survival versus Time at 24, 48, 72 and 96 hours in PyVT-R221A-Luf cells.

of PXL-Pep-Dendron (**22**) did not produce much toxicity in either the cleaved or intact molecules (Figure 5.4). A dramatic change in toxicity between the intact and cleaved PXL-Pep-Dendron (**22**) was seen between 24 and 48 hours after the first dose, when the cleaved molecule went from 109% of cells surviving compared to control at 24 hours (1 dose) to 44% at 48 hours (2 doses). Further studies were performed to 1) determine the difference in survival between the intact and cleaved PXL-Pep-Dendrons (**22**), 2) optimize the dosing range and time, 3) study the effect of an MMP inhibitor on the survival of cells treated with the intact prodrug, 4) study the affect of the prodrug in a human cell line and 5) study the effect of the drug (cleaved and intact) in MMP9 positive and null cell lines.

The complete toxicity studies included testing PXL, PXL-COOH and intact and cleaved PXL-Pep-Dendron (**22**) with 4 doses (over 96 hours) at concentrations from 1 nM to 5 μM in PXL. As shown in Figure A.1, PXL is toxic at the higher concentrations tested: 5 μM, 1 μM, 500 nM and 50 nM after 96 hours; but the 5 and 1 nM doses were effective against the PyVT-R221A-Luc cells only after 48 hours followed by proliferation at 72 and 96 hours. The proliferation at later doses (72 & 96 hour) could be due to ineffective technique when running the assay or to the development of PXL resistant cells. One dose of drug has the least effect on the cells, but still culminates in 50% survival of the cells treated with 5 μM.

As illustrated in Figure A.2, after two doses it is evident that there is an overall lower survival than the other time points. Possibilities for this observation

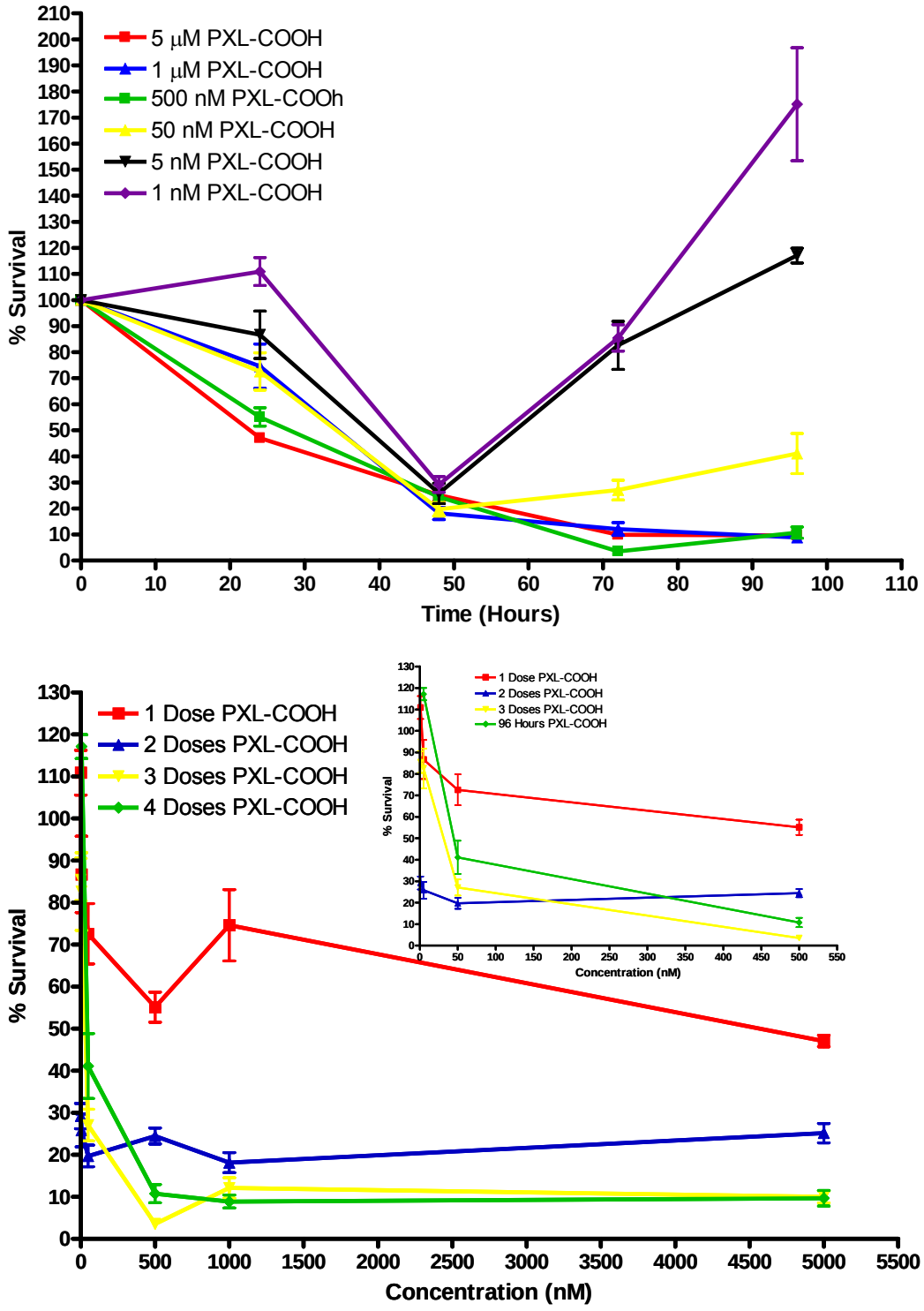

Figure A.2 Survival of Paclitaxel (PXL-COOH). Top % Survival versus Time at 5 υM, 1 υM, 500 nM, 50 nM, 5 nM and 1 nM . Bottom: % Survival versus Time at 24, 48, 72 and 96 hours in PyVT-R221A-Luf cells.

are that there was a technique error at this point or the cells have some PXL resistance that is overcome after 48 hours and the sub-culture of cells begins to proliferate. Repeating this experiment and trying to culture the potential sub-culture would conclude which possibility is occurring here. Doses 3 and 4 look promising, with only three doses, of drug needed to produce a toxic effect equal to PXL. At high concentrations 3 or 4 doses are equally as toxic.

The PXL-COOH toxicity indicate that there is little difference between the native drug (PXL) and the modified drug (PXL-COOH) when comparing Figure 5.5 to 5.6. Again, the cells dosed with the lower concentrations (5 and 1 nM) have a low survival rate at 48 hours and promptly make a come back after 72 and 96 hours. The highest three concentrations (5 μM, 1 μM and 500 nM) all produce a survival rate of 10% or below after 72 hours, which continues to the 96 hour (4 Doses) data. Over the number of doses given, the results follow a basic trend. When only one dose is given, there is a 60 – 80 % survival rate of cells, depending on the concentration given to the cells. Once 2 doses are given, that survival rate drops to 20 – 30 % of cells. At 3 and 4 doses the survival rate is more concentration dependent, with 1 and 5 nM concentrations having a survival rate of 80 – 110%. These points reflect the increased survival after 48 hours in the other graph (Figure 5.5 Top). After the two low concentrations, the 50 nM dose has a survival of 25 and 40 % for 3 and 4 doses respectively. Then, the higher concentrations of drug behave as expected and produce a mere 10% survival rate of cells after either 72 or 96 hours.

After looking at the toxicity data for PXL and PXL-COOH in PyVT-R221A-Luc cells, the data of the prodrug was analyzed (Figures A.1 and A.2). First, the intact PXL-Pep-Dendron (**22**) was graphed. From the percent survival versus time graph (Figure A.3, Top), the intact PXL-Pep-Dendron (**22**) has a 30 – 40 % survival after 96 hours (4 Doses) at higher concentrations of drug (5 μM, 1 μM, 500 nM and 50 nM). Compared to the approximate 10% survival that was observed after 72 and 96 hours for PXL and PXL-COOH at these concentrations, it appears that the intact PXL-Pep-Dendron (**22**) is less toxic, as desired for the development of the prodrug.

Analyzing that data from the percent survival versus concentration graph (Figure A.3, Bottom), it is clear that at high concentrations of intact PXL-Pep-Dendron (**22**) more doses is more efficacious. At a 500 nM concentration, 1 and 2 doses appear to have the same or better efficacy as subsequent doses. At lower concentrations, the survival rate ranges from 80 % for one dose to 35 % for 4 doses, indicating that the cells can tolerate a low dose of the intact prodrug without much effect. Since there are detectable levels of MMP9 in the cell line, there could be some cleavage that occurs *in vitro*. Overall, the intact PXL-Pep-Dendron (**22**) is not as toxic as the native PXL or the modified PXL-COOH. The toxicity of PXL has been reduced, although not completely inactivated. Inactivation was also observed with DOX-Pep-Dendron (**13**), so next, the toxicity

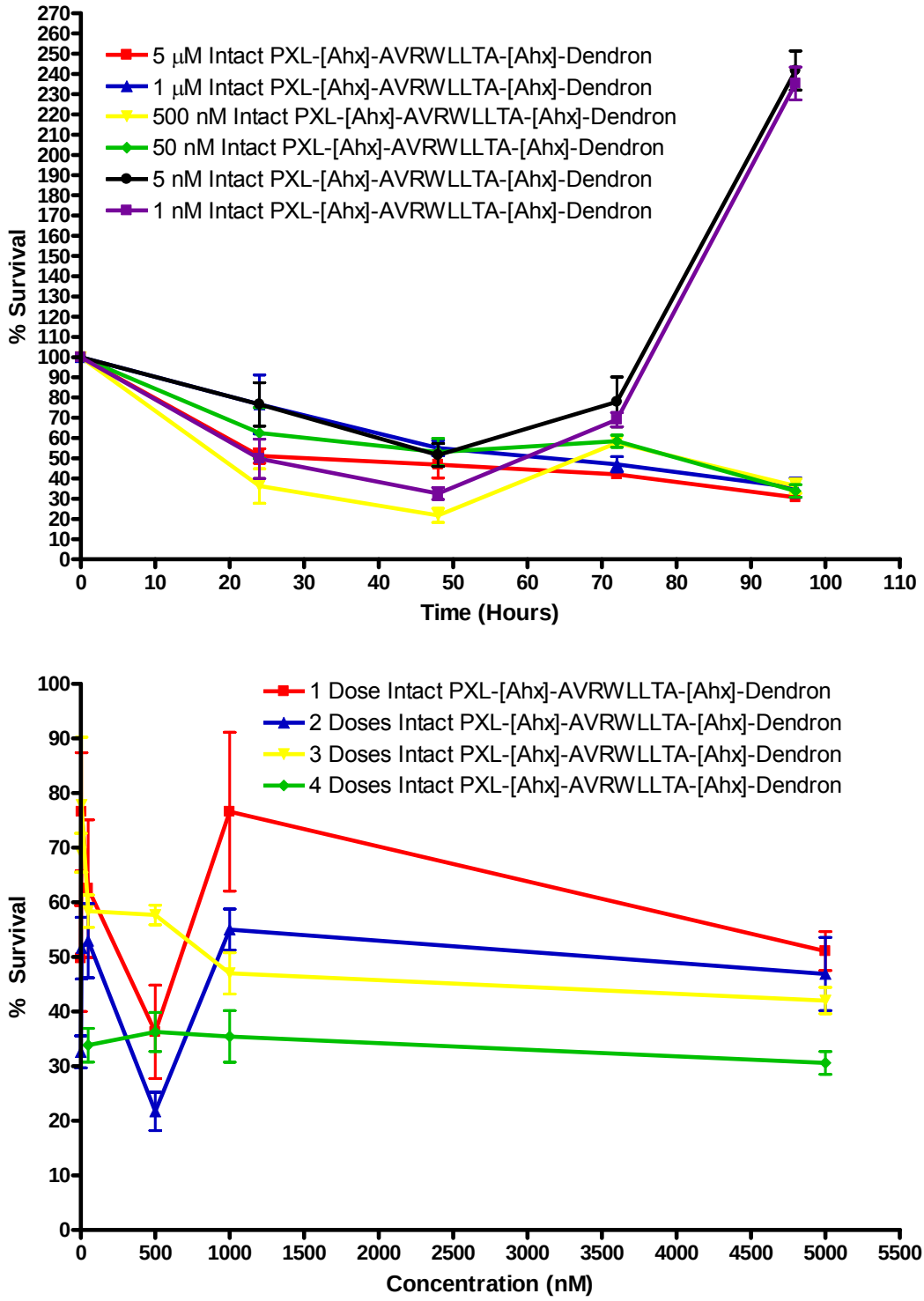

Figure A.3 Survival of Intact PXL-[Ahx]-AVRWLLTA-[Ahx]-Dendron (**22**). Top % Survival versus Time at 5 υM, 1 υM, 500 nM, 50 nM, 5 nM and 1 nM . Bottom: % Survival versus Time at 24, 48, 72 and 96 hours in PyVT-R221A-Luf Cells.

of the cleaved PXL- Pep-Dendron (**22**) was studied.

Ideally, the cleaved PXL-Pep-Dendron (**22**) would have the same or better efficacy as PXL and PXL-COOH or at least perform better than intact PXL-Pep-

Table A.2 96 Hour toxicity data of PXL, PXL-COOH, Cleaved and Intact in PXLPep-Dendron.

Compound	5 μM	1 μM	500 nM	50 nM	5 nM	1 nM
PXL	8	14	18	26	89	113
PXL-COOH	8	9	9	40	175	118
Cleaved PXL-[Ahx]-AVRWLLTA-[Axh]-Dendron	13	14	38	26	65	83
Intact PXL-[Ahx]-AVRWLLTA-[Axh]-Dendron	29	33	37	35	244	233

Dendron (**22**). At the lower concentrations, cleaved PXL-Pep-Dendron (**22**) performs better than intact PXL-Pep-Dendron (**22**) with survival rates of 83 and 65% at concentrations of 1 and 5 nM compared with 233 and 244% respectively for intact PXL-Pep-Dendron (**22**). The PXL-COOH has survival rates of 175 and 118 % for 5 and 1 nM concentration dosages while PXL has 113 and 89 % survival after 4 doses with 1 and 5 nM respectively. As seen in all the toxicity data, the 1 and 5 nM counts are off due to the cells becoming immune at low concentrations or errors in running the assay. Thus, the intact PXL-Pep-Dendron (**22**) compares well with that of PXL-COOH and PXL, however none of the drugs are efficacious at these concentrations. Looking at higher concentrations (500 nM and above), where PXL and PXL-COOH had survival rates of 8 -15% and intact PXL-Pep-Dendron (**22**) has survival rates of 22 – 35 %; the PXL-Pep-

Dendron (**22**) had survival rates between 11 and 25 %. Disregarding the 500 nM point for the cleaved dendron reduces the toxicity of the cleaved PXL-[Axh]-AVRWLLTA-[Ahx]-Dendron to approximately that observed for the PXL and PXL-COOH compounds. This indicates that the cleaved prodrug is more efficient at killing PyVT-R221A-Luc cells than the intact. Over the first three time points, intact PXL-Pep-Dendron (**22**) has a survival range of 27 – 89 %, cleaved PXL-Pep-Dendron (**22**) a range of 18 – 95 %, PXL-COOH a range of 2 – 111 % and PXL a range of 5 – 111 %. The lack of significant difference in the survival rates reflects the zymography results, which show PyVT-R221A-Luc cells express MMP9. Therefore, even intact molecule can be cleaved by the enzyme and produce toxicity to the cell through the expected mechanism. In looking at the data graphed as percent survival versus concentration, it's apparent that the more doses given of cleaved PXL-Pep-Dendron (**22**), the lower the survival rate. Furthermore, as the concentration of dose increases, the survival rate decreases as desired for the activated prodrug.

Next, toxicity data of the intact PXL-Pep-Dendron was obtained in which any MMPs produced by the cells were blocked with GM6001, a general MMP inhibitor (Figure A.4). Only 2 concentrations were tested for each molecule. As observed in Figure A.4, treatment of GM6001 not only improves the cell survival for intact prodrug, but also for the cleaved prodrug. The reason

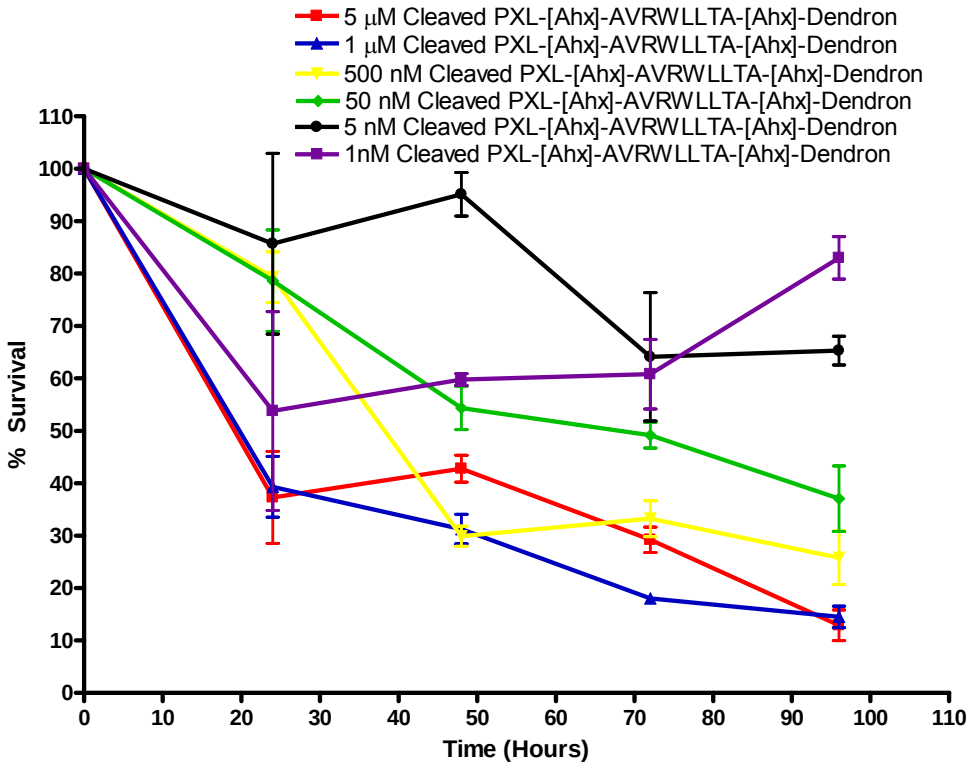

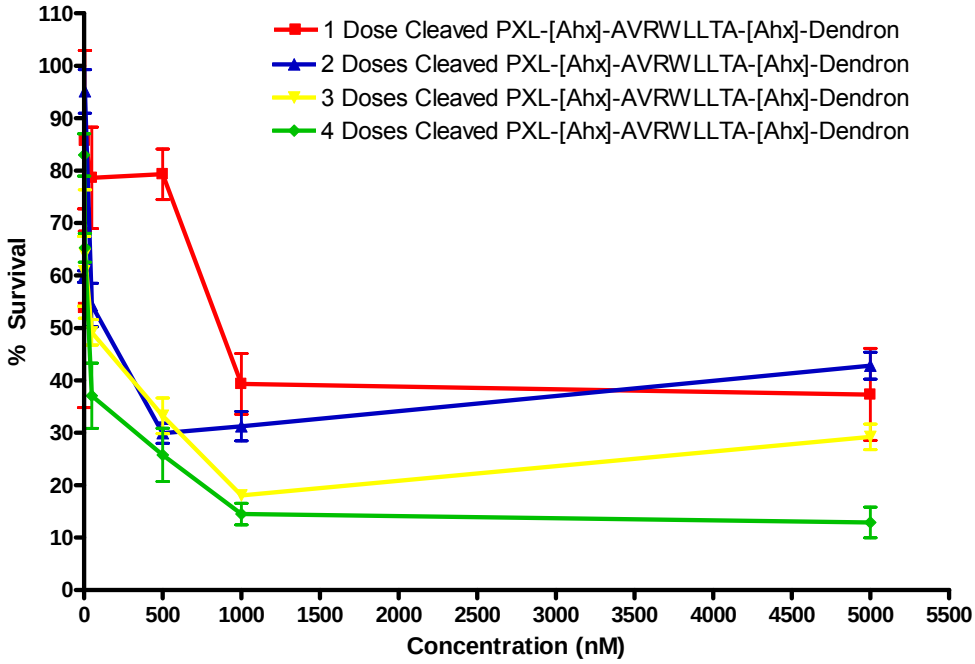

Figure A.4 Survival of Intact PXL-[Ahx]-AVRWLLTA-[Ahx]-Dendron (**22**). Top % Survival versus Time at 5 υM, 1 υM, 500 nM, 50 nM, 5 nM and 1 nM . Bottom: % Survival versus Time at 24, 48, 72 and 96 hours in PyVT-R221A-Luf Cells.

for this remains a mystery and needs further investigation; however it is possible that since GM6001 is a general MMP9 inhibitor some other mechanism could be blocked that is necessary for the cleaved product to be toxic. The other mechanism could include further cleavage by a different MMP or another enzyme (non-MMP) which is also blocked with GM6001.

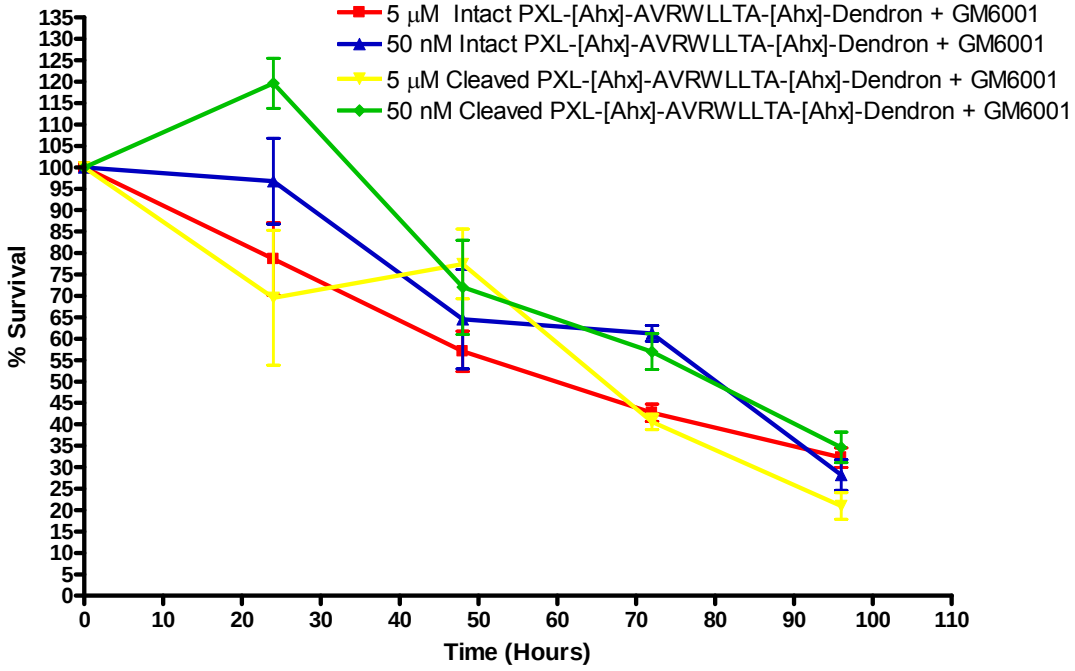

Figure A.5 Survival of Intact and Cleaved PXL-[Ahx]-AVRWLLTA-[Ahx]-Dendron (**22**) with 10 μM GM6001.

Finally, endpoint analysis for the cells dosed with 5 μM of drug or prodrug (cleaved and intact) are graphed as a bar graph for comparison (Figure A.6). Although the different doses and time points show the same general trend, the

96 hour (5 μM) time point is the most pronounced. The trends are as follows: 1) Intact PXL-Pep-Dendron (**22**) is less toxic than cleaved PXL-Pep-Dendron (**22**) by a factor of two; 2) GM6001 does not inhibit the activity of Intact PXL-Pep-Dendron (**22**), but does inhibit cleaved PXL-Pep-Dendron (**22**); and 3) PXL-COOH and PXL are slightly more toxic that cleaved PXL-Pep-Dendron (**22**). Overall the GM6001 inhibition data shows that PXL-Pep-Dendron (**22**) is working to some extent as a prodrug in the PyVT-R221A-Luc cells.

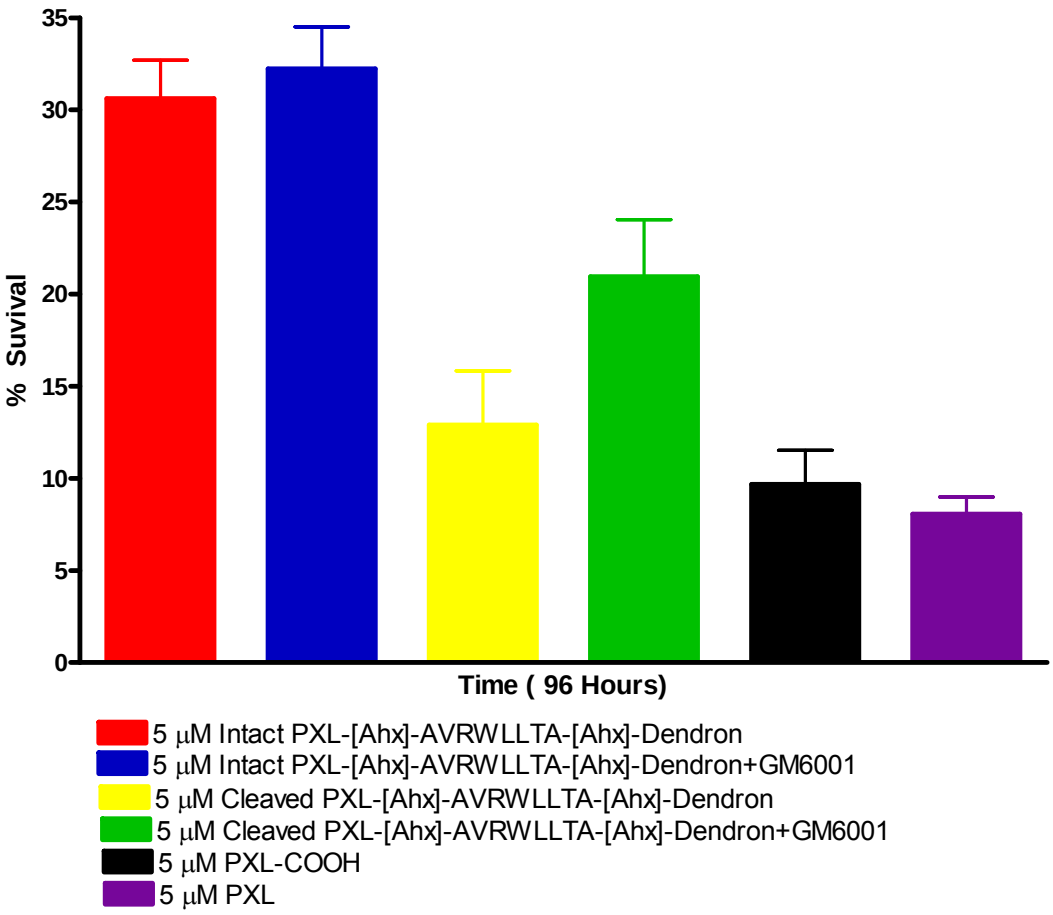

Figure A.6 Survival of Intact and Cleaved PXL-[Ahx]-AVRWLLTA-[Ahx]-Dendron (**22**) with and without 10 μM GM6001 as well as PXL-COOH and PXL after 4 doses (96 hours) at 5 μM concentration of compound in PyVT-R221A-Luf Cells.

To further examine the potential for these prodrugs, their toxicity was determined in a human cell line (MDA-MB-231 breast cancer). The studies were completed as described above, using both intact and cleaved PXL-Pep-Dendron (**22**), intact PXL-Pep-Dendron (**22**) with 10 μM GM6001 (a general MMP inhibitor), PXL-COOH and PXL at 5 μM and 50 nM concentrations. For both concentrations interrogated, the intact PXL-Pep-Dendron (**22**) is the least toxic followed by compound **22** with GM6001. Although it was not expected that GM6001 would be toxic to the cells, a follow-up experiment indicated that after 48 hours (2 Doses) the survival rate was 90% while after 96 hours (4 Doses) the survival rate dropped to 68%. As seen in Figure A.6, after 48 hours there is an 11% difference at 5 μM and a 10% difference at 50 nM between PXL-Pep-Dendron (**22**) and compound **22** co-incubated with GM6001. Not only does it appear that GM6001 is moderately toxic to the cells, but it also does not block activity of the intact prodrug. Possibilities for this observation include the prodrug being toxic or there is another mechanism of cleavage occurring that is not related to MMPs is therefore not blocked by GM6001. Since there was barely a detectable level of MMP9 in the cell media and none in the lysates, the prodrug is most likely not being cleaved by MMP9 to form the active cleavage product. Thus, the toxicity is likely due to the GM6001 or proteolytic activity by an enzyme other than MMP9.

Cleaved PXL-Pep-Dendron (**22**) is more toxic than intact **22** in a concentration dependent fashion. At 5 μM concentrations, cleaved PXL-Pep-Dendron (**22**) is 60% more toxic after 24 hours of treatment, before converging at

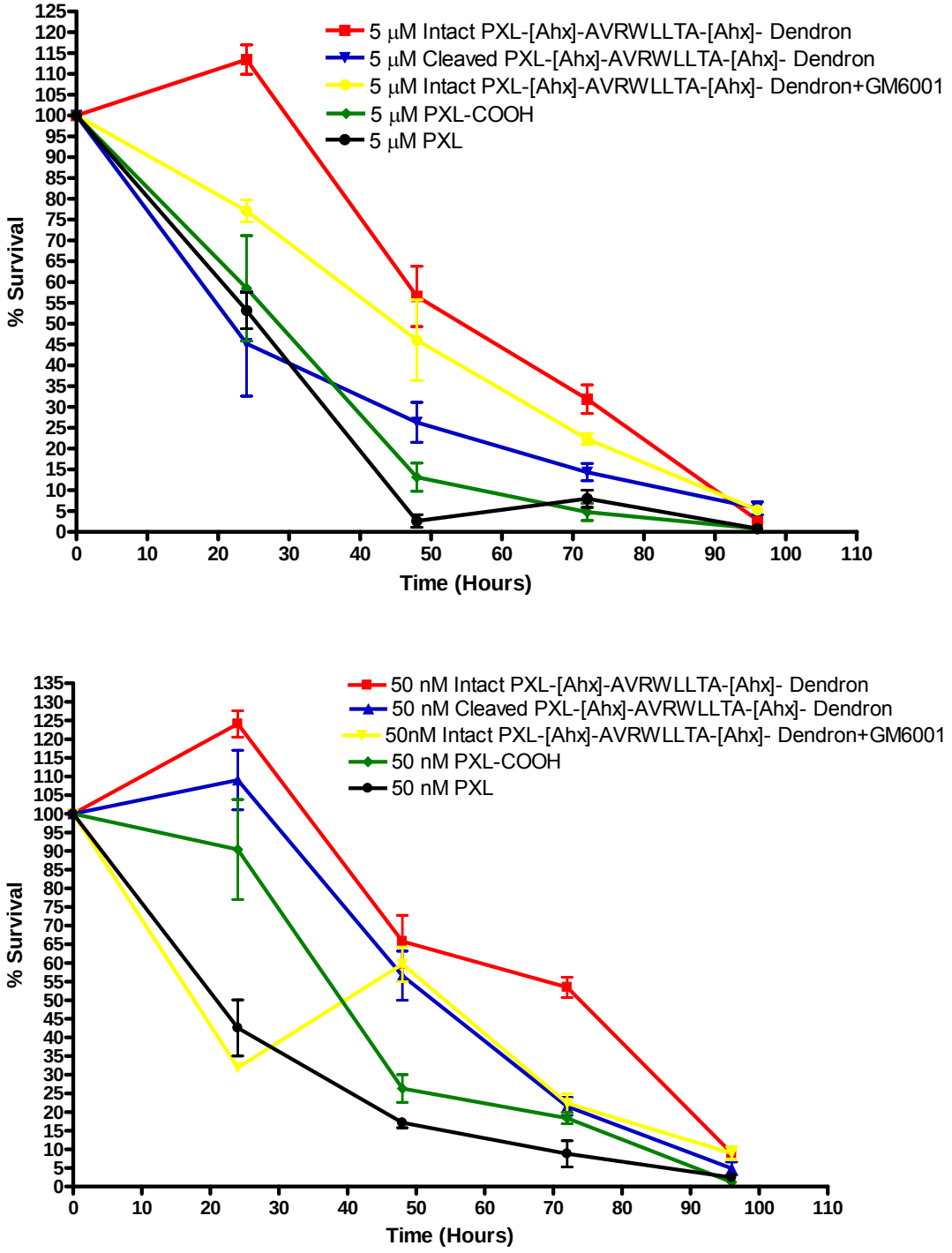

Figure A.7. Survival of Intact PXL-[Ahx]-AVRWLLTA-[Ahx]-Dendron (**22**) with and without10 μM GM6001, Cleaved PXL-[Ahx]-AVRWLLTA-[Ahx]-Dendron (**22**), PXL-COOH and PXL in MDA-MB-231 human breast cancer cells at 5 μM (Top) and 50 nM (Bottom) doses.

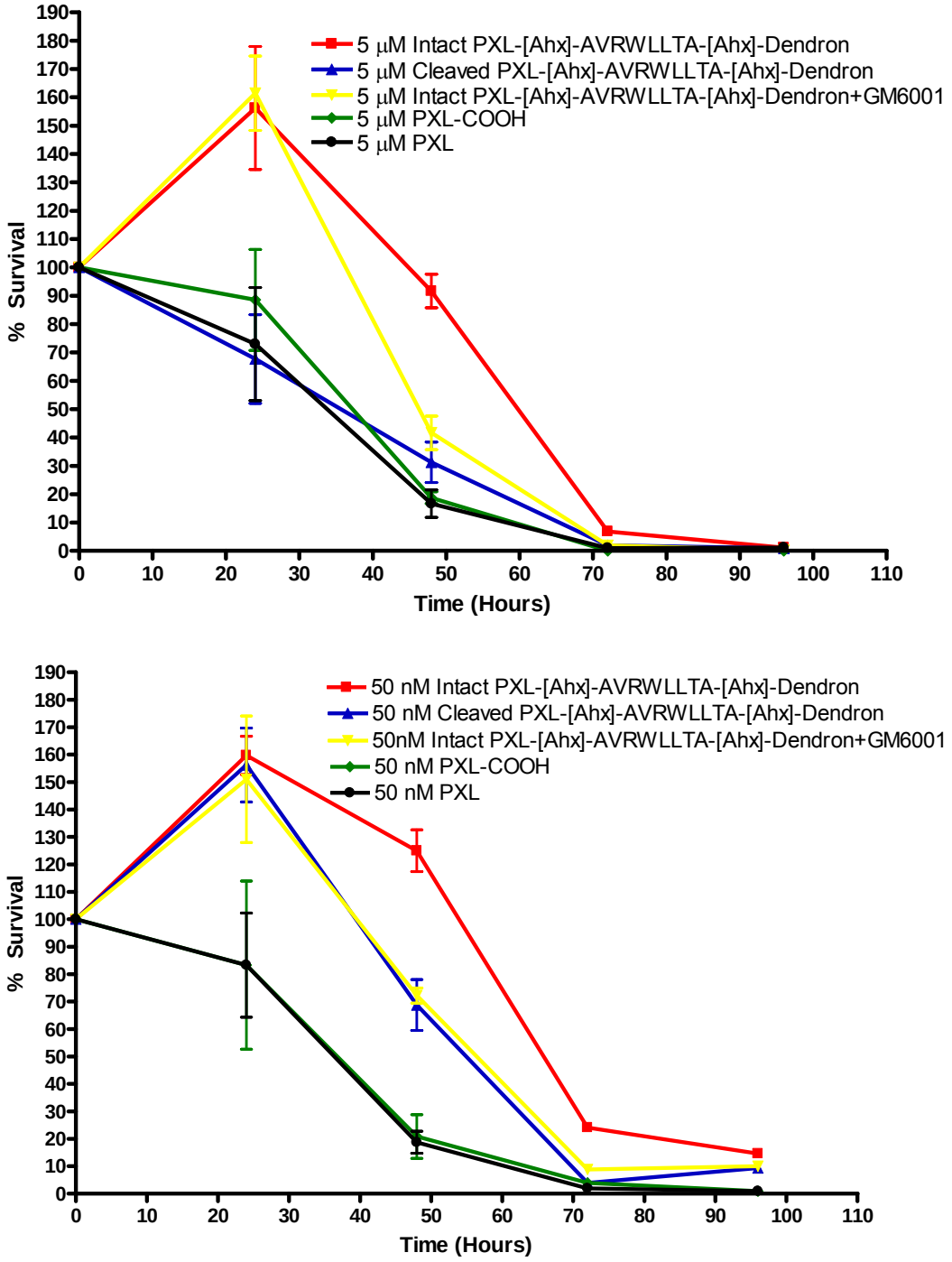

Figure A.8. Survival of Intact PXL-[Ahx]-AVRWLLTA-[Ahx]-Dendron (**22**) with and without10 μM GM6001, Cleaved PXL-[Ahx]-AVRWLLTA-[Ahx]-Dendron (**22**), PXL-COOH and PXL in LLC-RSV Lewis Lung Cancer cells at 5 μM (Top) and 50 nM (Bottom) doses.

about the same toxicity level after 96 hours. At 50 nM concentration, the cleaved product only kills about 17% more cells than intact **22** and again by 96 hours the two curves merge at 5 – 10% survival. Although this difference is not ideal, it provides the same trend as the PyVT-R221A-Luc cells.

Finally, the PXL-COOH and PXL have about the same toxicity at both concentrations tested and are the most toxic compounds tested in this study. The only exception is the 24 hour point at 50 nM dosing concentration where the PXL has a much lower survival rate. This could be due to reduced toxicity with the modification to paclitaxel or an error in the first dosing cycle. Overall, the MDA-MB-231 cells have the expected trend in which the prodrug is less toxic in the "inactive" form than in the "active" form.

To study the *in vitro* effect of MMP9, two last cell lines were studied: LLC-RSV and LLC-MMP9 which contain naturally low and transfected with high amounts of MMP9 respectively. As with the other two cell lines, intact PXL-Pep-Dendron (**22**) has the highest levels of survival (Figure A.7). Also, again including GM6001 with intact **22** lowered the survival of the cells at 48 and 72 hours. At 24 and 96 hours **22** and **22** + GM6001 were the same for both concentrations, indicating that there may be some increased toxicity due to GM6001. This observation was further confirmed with a follow-up study that showed that after 48 hours the percent survival of LLC-RSV cells treated with only GM6001 at 77%. Cleaved PXL-Pep-Dendron (**22**) proved to be more efficient at killing cells after 48 and 72 hours than the intact **22** at both concentrations (Figure A.9). The cleaved and intact **22** had a greater survival

difference with the 5 μM concentration with the 24 hour time point also offering a greater kill rate. Finally, the PXL-COOH and PXL were both more efficacious at killing the cells than either the intact or cleaved prodrug, but not by too much for some time points. Overall, intact prodrug, **22,** has little effect on the cells, while cleaved prodrug, **22,** has some effect, but not as much as native PXL or modified PXL-COOH.

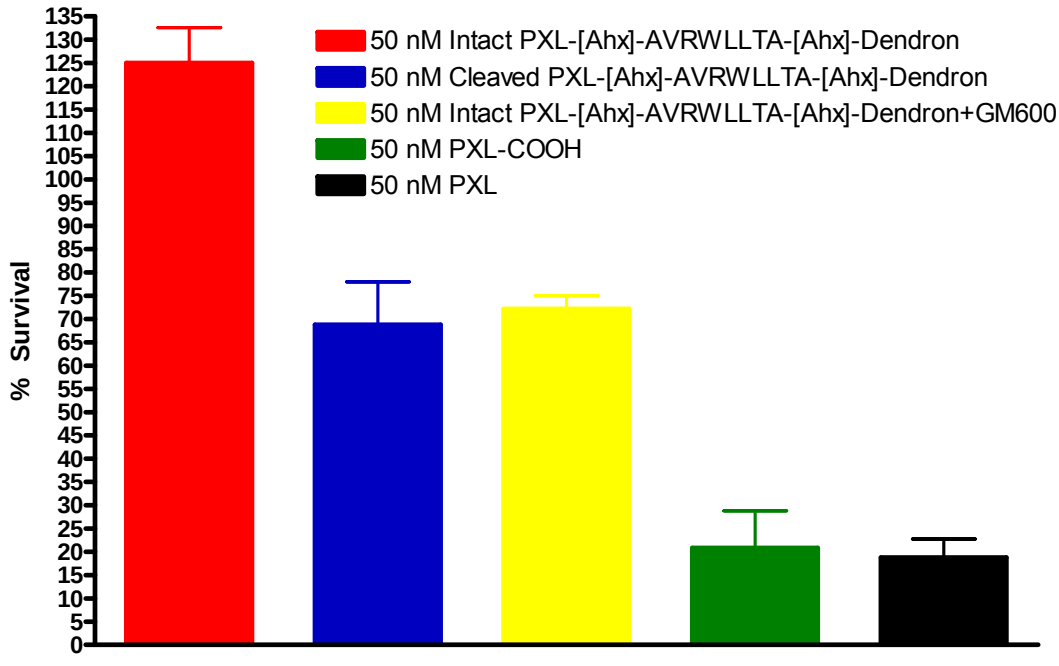

Figure A.9 Survival of Intact and Cleaved PXL-[Ahx]-AVRWLLTA-[Ahx]-Dendron (**22**) with and without 10 μM GM6001 as well as PXL-COOH and PXL after 2 doses (48 hours) at 50 nM concentration of compound in LLC-RSV cells.

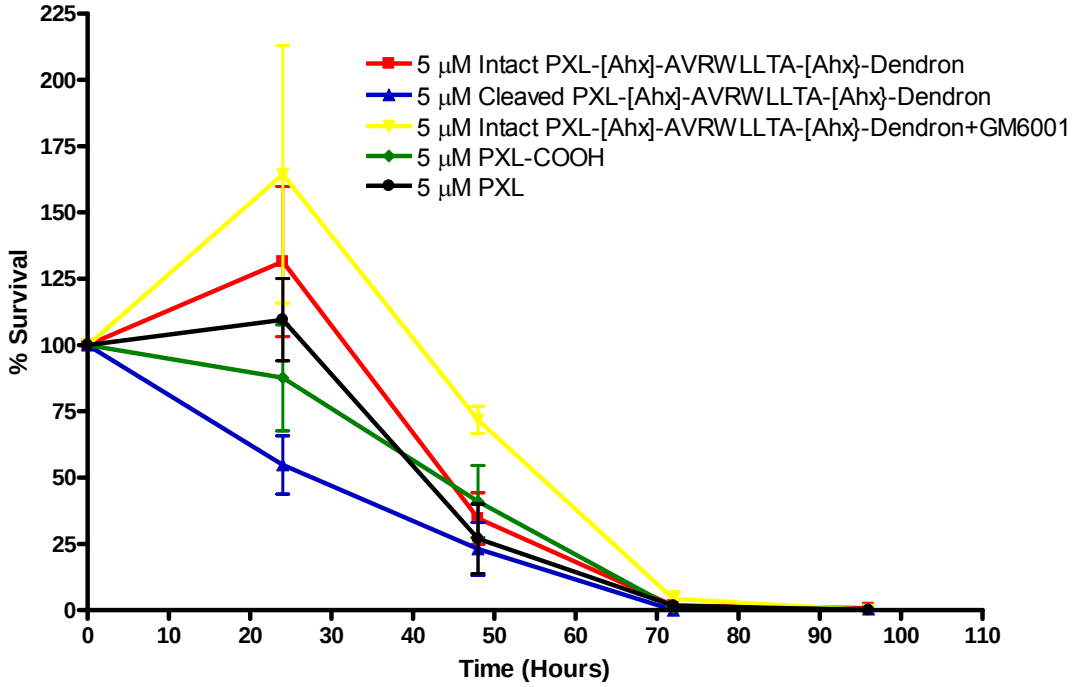

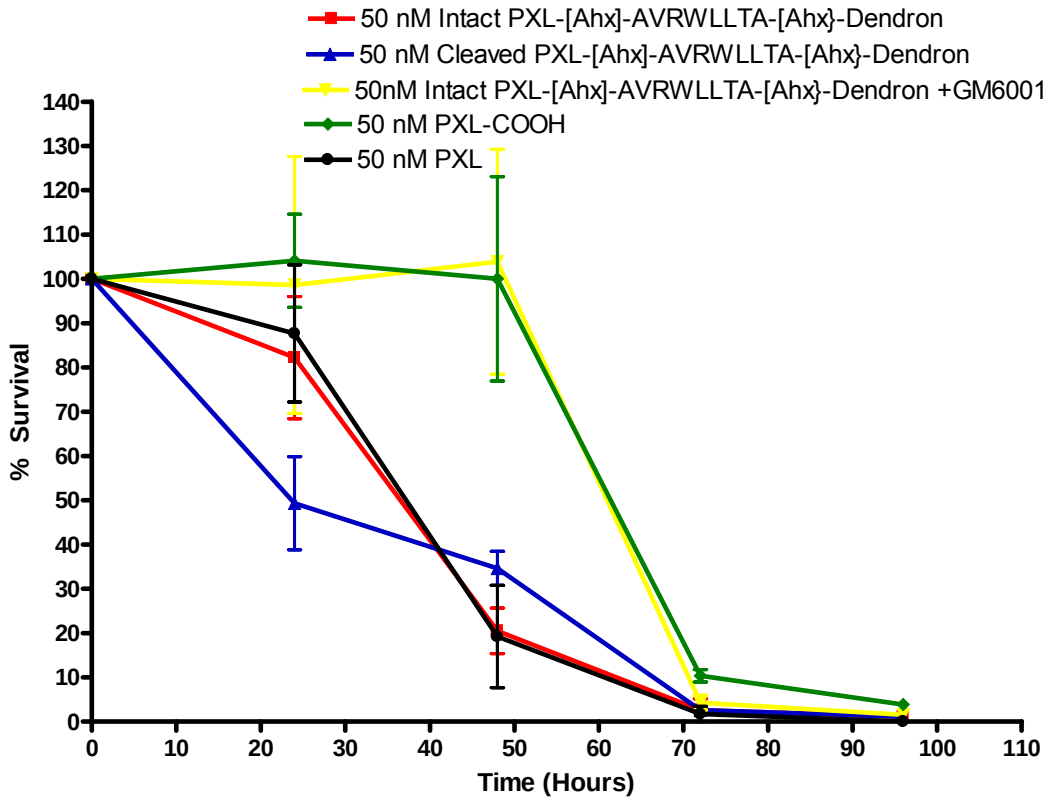

Figure A.10. Survival of Intact PXL-[Ahx]-AVRWLLTA-[Ahx]-Dendron (**22**) with and without10 μM GM6001, Cleaved PXL-[Ahx]-AVRWLLTA-[Ahx]-Dendron (**22**), PXL-COOH and PXL in LLC-MMP9 Lewis Lung Cancer cells at 5 μM (Top) and 50 nM (Bottom) doses.

Next, I studied the LLC-MMP9 cell line, which has been transfected with the gene for producing the enzyme and therefore has a high concentration of MMP9 (confirmed by the zymography). In the LLC-MMP9 cell line, the toxicity

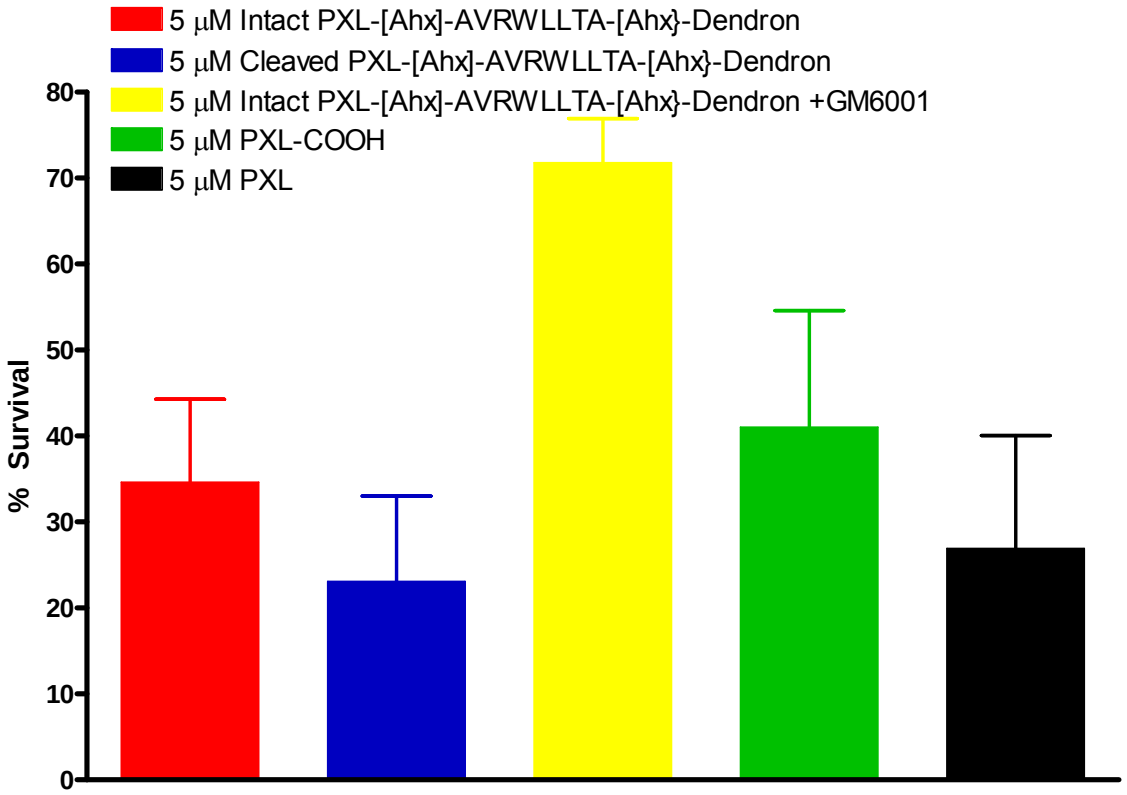

Figure A.11 Survival of Intact and Cleaved PXL-[Ahx]-AVRWLLTA-[Ahx}-Dendron (**22**) with and without 10 μM GM6001 as well as PXL-COOH and PXL after 2 doses (48 hours) at 50 nM concentration of compound in LLC-MMP9 cells.

studies reflect this high level of MMP9 and that the enzyme is necessary for toxicity of the prodrug. For both concentrations tested, the least toxic (highest

survival rate) is intact PXL-Pep-Dendron (**22**) with GM6001. Peculiarly, the PXL-COOH also has a high survival rate in this cell line. However, cleaved **22** appears to have the most cell death over both concentrations tested followed by the native PXL. Just slightly less toxic than the PXL is the intact PXLPep

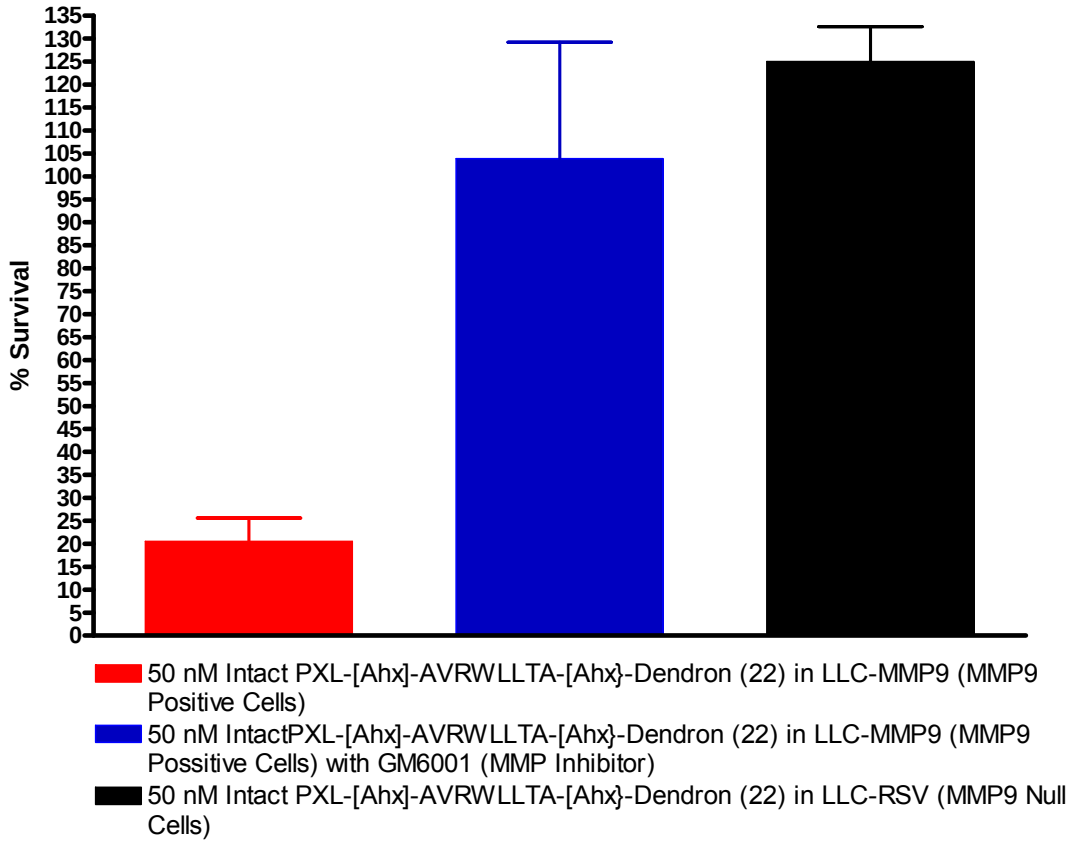

Figure A.12. Comparison of PXL-[Ahx]-AVRWLLTA-[Ahx]-Dendron (**22**) treated cells in MMP9 positive, MMP9 positive with GM6001 and MMP9 null cells.

-

Dendron (**22**), which presumably undergoes cleavage by MMP9 prior to inducing cell death.

As a further comparison, the toxicity of the cleaved and intact prodrugs in the LLC-RSV and LLC-MMP9 cell lines is graphed in Figure A.11. The LLC-MMP9 cells treated with intact prodrug have an 80% reduction in cell grown compared to the same cell line treated coincidently with intact prodrug and an MMP inhibitor. Finally, the MMP9 null cell line has the highest survival rate when treated with intact prodrug. All indications are that PXL-Pep-Dendron (**22**) is inactive until cleaved by MMP9.

A.3 Raw Data from Toxicity Studies

Table A.3. Cell count raw data from cytotoxicity experiments with DOX, Leu-DOX, Leu-Leu-DOX, and Paclitaxel after 24 hours in PyVT-R221A-Luc cells.

Compound & Concentration	Well 1	Well 2	Well 3	Well 4	Average	Average Cells/mL	Average # Cells
10 ug/mL DOX	1	2	0	0	0.75	1800	432
3 ug/mL DOX	4	0	0	1	1.25	3000	720
1 ug/mL DOX	1	3	0	1	1.25	3000	720
0.3 ug/mL DOX	2	1	2	1	1.5	3600	864
0.1 ug/mL DOX	2	3	2	0	1.75	4200	1008
0.3% DMSO			6	8	7	16800	4032
Media	3	2			2.5	6000	1440
15 ug/mL Leu-DOX	1	0	2	2	1.25	3000	720
10 ug/mL Leu-DOX	4	2	2	0	2	4800	1152
5 ug/mL Leu-DOX	2	2	0	0	1	2400	576
1 ug/mL Leu-DOX	4	3	2	3	3	7200	1728
0.1 ug/mL Leu DOX	1	5	1	6	3.25	7800	1872
0.3% DMSO			6	4	5	12000	2880
Media	2	5			3.5	8400	2016
15 ug/mL Leu-Leu-DOX	0	3	3	8	3.5	8400	2016
10 ug/mL Leu-Leu-DOX	5	4	1	1	2.75	6600	1584

5 ug/mL Leu-Leu-DOX	3	3	9	6	5.25	12600	3024
1 ug/mL Leu-Leu-DOX	0	0	0	3	0.75	1800	432
0.1 ug/mL Leu-Leu-DOX	3	4	1	5	3.25	7800	1872
0.3% DMSO			4	4	4	9600	2304
Media	4	4			4	9600	2304
10 ug/mL PXL EtOH	0	2	1	0	0.75	1800	432
10 ug/mL PXL - COOH EtOH/DMSO	0	0	0	1	0.25	600	144
10 ug/mL PXL DMSO	1	0	1	2	1	2400	576
10 ug/mL PXL-COOH DMSO	1	0	1	0	0.5	1200	288
0.3% EtOH	1	0	5	2	2	4800	1152
0.3% DMSO			4	3	3.5	8400	2016
Media	6	2			4	9600	2304
15 ug/mL PXL	0	1	0	1	0.5	1200	288
15 ug/mL PXL-COOH	0	2	1	0	0.75	1800	432
0.3% DMSO	4	9	4	4	5.25	12600	3024
0.3% DMSO	2	6	6	2	4	9600	2304
Media	3	1	3	3	2.5	6000	1440
Media	4	2	3	1	2.5	6000	1440

Table A.4 Cell count raw data from cytotoxicity experiments with DOX, Leu-DOX, Leu-Leu-DOX, and Paclitaxel after 48 hours in PyVT-R221A-Luc cells.

Compound and Concentration	Well 1	Well 2	Well 3	Well 4	Average	Average Cells/mL	Average # Cells
10 ug/mL DOX	0	0	0	0	0	0	0
3 ug/mL DOX	0	0	1	0	0.25	600	144
1 ug/mL DOX	0	0	0	1	0.25	600	144
0.3 ug/mL DOX	0	1	1	0	0.5	1200	288
0.1 ug/mL DOX	2	0	0	0	0.5	1200	288
0.3% DMSO			6	9	7.5	18000	4320
Media	9	5			7	16800	4032
15 ug/mL Leu-DOX	1	0	0	2	0.75	1800	432
10 ug/mL Leu-DOX	2	1	1	2	1.5	3600	864
5 ug/mL Leu-DOX	3	0	2	1	1.5	3600	864
1 ug/mL Leu-DOX	7	3	3	3	4	9600	2304
0.1 ug/mL Leu DOX	8	3	1	7	4.75	11400	2736
0.3% DMSO			2	1	1.5	3600	864
Media	2	2			2	4800	1152
15 ug/mL Leu-Leu-DOX	2	4	1	1	2	4800	1152
10 ug/mL Leu-Leu-DOX	1	2	5	9	4.25	10200	2448
5 ug/mL Leu-Leu-DOX	6	3	2	2	3.25	7800	1872
1 ug/mL Leu-Leu-DOX	2	1	0	1	1	2400	576
0.1 ug/mL Leu-Leu-DOX	1	7	4	0	3	7200	1728
0.3% DMSO			7	5	6	14400	3456
Media	4	8			6	14400	3456
10 ug/mL PXL EtOH	0	0	3	0	0.75	1800	432
10 ug/mL PXL -COOH EtOH/DMSO	1	0	3	0	1	2400	576
10 ug/mL PXL DMSO	0	1	1	0	0.5	1200	288
10 ug/mL PXL-COOH DMSO	2	1	2	2	1.75	4200	1008
0.3% EtOH	6	2	4	5	4.25	10200	2448
0.3% DMSO			1	3	2	4800	1152
Media	0	4			2	4800	1152
15 ug/mL PXL	1	0	1	1	0.75	1800	432
15 ug/mL PXL-COOH	0	1	0	0	0.25	600	144
0.3% DMSO	4	2	3	2	2.75	6600	1584
0.3% DMSO	6	8	1	1	4	9600	2304
Media	9	6	6	4	6.25	15000	3600
Media	2	4	2	0	2	4800	1152

Table A.5 Cell count raw data from cytotoxicity experiments with DOX, Leu-DOX, Leu-Leu-DOX, and Paclitaxel after 72 hours in PyVT-R221A-Luc cells.

Compound & Concentration	Well 1	Well 2	Well 3	Well 4	Average	Average Cells/mL	Average # Cells
10 ug/mL DOX	0	0	0	0	0	0	0
3 ug/mL DOX	0	0	0	0	0	0	0
1 ug/mL DOX	0	0	0	0	0	0	0
0.3 ug/mL DOX	1	0	0	0	0.25	600	144
0.1 ug/mL DOX	0	1	0	1	0.5	1200	288
0.3% DMSO			5	3	4	9600	2304
Media	6	16			11	26400	6336
15 ug/mL Leu-DOX	0	2	0	0	0.5	1200	288
10 ug/mL Leu-DOX	1	1	1	0	0.75	1800	432
5 ug/mL Leu-DOX	1	0	3	0	1	2400	576
1 ug/mL Leu-DOX	3	4	3	3	3.25	7800	1872
0.1 ug/mL Leu DOX	4	13	3	3	5.75	13800	3312
0.3% DMSO			10	6	8	19200	4608
Media	14	9			11.5	27600	6624
15 ug/mL Leu-Leu-DOX	1	0	5	0	1.5	3600	864
10 ug/mL Leu-Leu-DOX	3	0	2	1	1.5	3600	864
5 ug/mL Leu-Leu-DOX	4	4	1	1	2.5	6000	1440
1 ug/mL Leu-Leu-DOX	3	3	0	0	1.5	3600	864
0.1 ug/mL Leu-Leu-DOX	4	3	0	0	1.75	4200	1008
0.3% DMSO			5	5	5	12000	2880
Media	6	3			4.5	10800	2592
10 ug/mL PXL EtOH	0	0	0	1	0.25	600	144
10 ug/mL PXL -COOH EtOH/DMSO	0	1	0	0	0.25	600	144
10 ug/mL PXL DMSO	0	0	0	0	0	0	0
10 ug/mL PXL-COOH DMSO	0	0	0	1	0.25	600	144
0.3% EtOH	5	3	6	4	4.5	10800	2592
0.3% DMSO			8	7	7.5	18000	4320
Media	3	4			3.5	8400	2016
15 ug/mL PXL	0	0	0	1	0.25	600	144
15 ug/mL PXL-COOH	0	0	1	0	0.25	600	144
0.3% DMSO	1	4	4	0	2.25	5400	1296
0.3% DMSO	3	4	3	2	3	7200	1728
Media	5	3	6	7	5.25	12600	3024
Media	5	3	2	6	4	9600	2304

Table A.6 Cell count raw data from cytotoxicity experiments with DOX, Leu-DOX, Leu-Leu-DOX, and Paclitaxel after 96 hours in PyVT-R221A-Luc cells.

Compound & Concentration	Well 1	Well 2	Well 3	Well 4	Average	Average Cells/mL	Average # Cells
10 ug/mL DOX	0	0	0	0	0	0	0
3 ug/mL DOX	0	0	0	0	0	0	0
1 ug/mL DOX	0	0	0	0	0	0	0
0.3 ug/mL DOX	0	0	0	0	0	0	0
0.1 ug/mL DOX	0	1	0	0	0.25	600	144
0.3% DMSO			65	20	42.5	102000	24480
Media	10	34			22	52800	12672
15 ug/mL Leu-DOX	1	0	0	0	0.25	600	144
10 ug/mL Leu-DOX	1	0	0	0	0.25	600	144
5 ug/mL Leu-DOX	1	1	0	1	0.75	1800	432
1 ug/mL Leu-DOX	9	2	3	1	3.75	9000	2160
0.1 ug/mL Leu DOX	7	6	10	24	11.75	28200	6768
0.3% DMSO			21	7	14	33600	8064
Media	11	19			15	36000	8640
15 ug/mL Leu-Leu-DOX	3	5	0	1	2.25	5400	1296
10 ug/mL Leu-Leu-DOX	6	4	6	3	4.75	11400	2736
5 ug/mL Leu-Leu-DOX	5	6	5	4	5	12000	2880
1 ug/mL Leu-Leu-DOX	8	10	5	12	8.75	21000	5040
0.1 ug/mL Leu-Leu-DOX	13	8	10	4	8.75	21000	5040
0.3% DMSO			64	14	39	93600	22464
Media	24	47			35.5	85200	20448
10 ug/mL PXL EtOH	1	1	0	0	0.5	1200	288
10 ug/mL PXL -COOH EtOH/DMSO	0	0	1	0	0.25	600	144
10 ug/mL PXL DMSO	0	0	0	0	0	0	0
10 ug/mL PXL-COOH DMSO	0	0	0	0	0	0	0
0.3% EtOH	4	3	6	5	4.5	10800	2592
0.3% DMSO			21	22	21.5	51600	12384
Media	10	28			19	45600	10944
15 ug/mL PXL	1	1	0	0	0.5	1200	288
15 ug/mL PXL-COOH	0	0	0	0	0	0	0
0.3% DMSO	19	5	8	3	8.75	21000	5040
0.3% DMSO	10	8	22	1	10.25	24600	5904
Media	5	7	14	3	7.25	17400	4176
Media	13	7	17	7	11	26400	6336

Table A.7 Cell count raw data from cytotoxicity experiments with DOX, PXL and PXL-COOH after 24 hours in PyVT-R221A-Luc cells.

Compound & Concentration	Well 1	Well 2	Well 3	Well 4	Well 5	Well 6	Average	Average Cells/mL	Average # Cells
Media	5	7					6	14400	3456
0.1% DMSO			14	5			9.5	22800	5472
0.1 ng/mL DOX	20	8	4	7			9.75	23400	5616
1 ng/mL DOX	12	7	4	4			6.75	16200	3888
10 ng/mL DOX	6	16	8	0.3			7.575	18180	4363.2
100 ng/mL DOX	11	7	3	2			5.75	13800	3312
1000 ng/mL DOX	3	0	1	5			2.25	5400	1296
Media	29	22					25.5	61200	14688
0.1% DMSO			25	20			22.5	54000	12960
1 ng/mL PXL	17	14	13	17			15.25	36600	8784
10 ng/mL PXL	7	8	6	7			7	16800	4032
100 ng/mL PXL	8	5	4	7			6	14400	3456
1000 ng/mL PXL	8	1	2	1			3	7200	1728
10 ug/mL PXT	4	6	0	0			2.5	6000	1440
Media	20	36					28	67200	16128
0.1% DMSO			25	6			15.5	37200	8928
1 ng/mL PXL-COOH	44	11	17	13			21.25	51000	12240
10 ng/mL PXL-COOH	18	17	12	24			17.75	42600	10224
100 ng/mL PXL-COOH	4	5	4	2			3.75	9000	2160
1000 ng/mL PXL-COOH	6	4	2	2			3.5	8400	2016
10 ug/mL PXL-COOH	7	1	1	0			2.25	5400	1296
Media	13	29	18	14	15	14	17.16667	41200	9888
Media	16	13	24	12	22	34	20.16667	48400	11616
0.1% DMSO	19	19	11	9	6	10	12.33333	29600	7104
0.1% DMSO	6	8	8	6	9	9	7.666667	18400	4416

Table A.8 Cell count raw data from cytotoxicity experiments with DOX, PXL and PXL-COOH after 48 hours in PyVT-R221A-Luc cells.

Compound & Concentration	Well 1	Well 2	Well 3	Well 4	Well 5	Well 6	Average	Average Cells/mL	Average # Cells
Media	39	19					29	69600	16704
0.1% DMSO			30	53			41.5	99600	23904
0.1 ng/mL DOX	31	41	22	53			36.75	88200	21168
1 ng/mL DOX	26	18	33	38			28.75	69000	16560
10 ng/mL DOX	39	12	15	17			20.75	49800	11952
100 ng/mL DOX	6	5	7	6			6	14400	3456
1000 ng/mL DOX	0	0	0	1			0.25	600	144
Media	30	29					29.5	70800	16992
0.1% DMSO			58	13			35.5	85200	20448
1 ng/mL PXL	54	17	40	8			29.75	71400	17136
10 ng/mL PXL	19	35	19	3			19	45600	10944

100 ng/mL PXL	4	6	5	2			4.25	10200	2448
1000 ng/mL PXL	6	5	1	1			3.25	7800	1872
10 ug/mL PXT	6	3	4	3			4	9600	2304
Media	29	38					33.5	80400	19296
0.1% DMSO			54	22			38	91200	21888
1 ng/mL PXL-COOH	36	38	43	46			40.75	97800	23472
10 ng/mL PXL-COOH	20	19	26	20			21.25	51000	12240
100 ng/mL PXL-COOH	11	7	4	2			6	14400	3456
1000 ng/mL PXL-COOH	8	7	1	6			5.5	13200	3168
10 ug/mL PXL-COOH	1	2	5	1			2.25	5400	1296
Media	27	31	24	21	12	20	22.5	54000	12960
Media	28	33	50	25	24	13	28.83333	69200	16608
0.1% DMSO	36	44	44	26	20	15	30.83333	74000	17760
0.1% DMSO	25	55	21	10	13	6	21.66667	52000	12480

Table A.9 Cell count raw data from cytotoxicity experiments with DOX, PXL and PXL-COOH after 72 hours in PyVT-R221A-Luc cells.

Compound & Concentration	Well 1	Well 2	Well 3	Well 4	Well 5	Well 6	Average	Average Cells/mL	Average # Cells
Media	99	194					146.5	351600	84384
0.1% DMSO			97	43			70	168000	40320
0.1 ng/mL DOX	86	57	23	48			53.5	128400	30816
1 ng/mL DOX	44	81	36	18			44.75	107400	25776
10 ng/mL DOX	26	13	22	4			16.25	39000	9360
100 ng/mL DOX	3	3	2	2			2.5	6000	1440
1000 ng/mL DOX	0	0	0	0			0	0	0
Media	97	99					98	235200	56448
0.1% DMSO			70	13			41.5	99600	23904
1 ng/mL PXL	57	50	22	25			38.5	92400	22176
10 ng/mL PXL	2	12	7	1			5.5	13200	3168
100 ng/mL PXL	1	4	4	0			2.25	5400	1296
1000 ng/mL PXL	1	4	2	3			2.5	6000	1440
10 ug/mL PXT	1	3	0	1			1.25	3000	720
Media	88	249					168.5	404400	97056
0.1% DMSO			49	93			71	170400	40896
1 ng/mL PXL-COOH	57	69	38	27			47.75	114600	27504
10 ng/mL PXL-COOH	37	32	25	21			28.75	69000	16560
100 ng/mL PXL-COOH	2	1	1	2			1.5	3600	864
1000 ng/mL PXL-COOH	6	1	5	8			5	12000	2880
10 ug/mL PXL-COOH	4	1	5	4			3.5	8400	2016
Media	136	80	259	92	247	203	169.5	406800	97632
Media	42	79	34	18	18	9	33.33333	80000	19200
0.1% DMSO	15	34	45	78	124	17	52.16667	125200	30048

0.1% DMSO	22	43	27	68	13	23	32.66667	78400	18816

Table A.10 Cell count raw data from cytotoxicity experiments with DOX, PXL and PXL-COOH after 96 hours in PyVT-R221A-Luc cells.

Compound & Concentration	Well 1	Well 2	Well 3	Well 4	Well 5	Well 6	Average	Average Cells/mL
Media	36	25					30.5	73200
0.1% DMSO			42	21			31.5	75600
0.1 ng/mL DOX	72	52	116	9			62.25	149400
1 ng/mL DOX	56	102	36	2			49	117600
10 ng/mL DOX	18	15	14	0			11.75	28200
100 ng/mL DOX	3	2	1	0			1.5	3600
1000 ng/mL DOX	0	0	0	0			0	0
Media	61	69					65	156000
0.1% DMSO			40	27			33.5	80400
1 ng/mL PXL	36	24	28	17			26.25	63000
10 ng/mL PXL	16	12	5	3			9	21600
100 ng/mL PXL	7	0	1	2			2.5	6000
1000 ng/mL PXL	2	1	0	0			0.75	1800
10 ug/mL PXT	1	1	0	0			0.5	1200
Media	33	45					39	93600
0.1% DMSO			31	13			22	52800
1 ng/mL PXL-COOH	21	23	14	11			17.25	41400
10 ng/mL PXL-COOH	65	24	11	11			27.75	66600
100 ng/mL PXL-COOH	1	4	0	1			1.5	3600
1000 ng/mL PXL-COOH	5	1	1	0			1.75	4200
10 ug/mL PXL-COOH	0	0	0	0			0	0
Media	21	11	16	7	16	33	17.33333	41600
Media	32	22	27	18	14	12	20.83333	50000
0.1% DMSO	49	19	30	16	27	15	26	62400
0.1% DMSO	23	32	26	11	22	17	21.83333	52400

Table A.11 Cell count raw data from cytotoxicity experiments with preliminary PXL Prodrug compounds.

24 Hours	Well 1	Well 2	Well 3	Well 4	Average	Average Cells/mL	Average # Cells
PXL-AVRW	7	12	9	10	9.5	114000	57000
PXL-Pep-Dendron	14	9	6	13	10.5	126000	63000
PXL-COOH	6	2	6	7	5.25	63000	31500
PXL	4	5	4	5	4.5	54000	27000
0.1% DMSO/ 1% MeOH	11	5	11	8	8.75	105000	52500
Media	3	11	11	7	8	96000	48000
48 Hours	Well 1	Well 2	Well 3	Well 4			
PXL-AVRW	7	5	3	5	5	60000	30000
PXL-Pep-Dendron	11	8	9	15	10.75	129000	64500
PXL-COOH	0	6	5	4	3.75	45000	22500
PXL	3	2	2	5	3	36000	18000
0.1% DMSO/ 1% MeOH	15	13	7	11	11.5	138000	69000
Media	6	17	18	18	14.75	177000	88500
72 Hours	Well 1	Well 2	Well 3	Well 4			
PXL-AVRW	2	5	5	5	4.25	51000	25500
PXL-Pep-Dendron	7	6	15	13	10.25	123000	61500
PXL-COOH	3	3	1	3	2.5	30000	15000
PXL	2	0	1	4	1.75	21000	10500
0.1% DMSO/ 1% MeOH	9	15	31	36	22.75	273000	136500
Media	27	14	18	21	20	240000	120000

Table A.12 Cell count raw data from cytotoxicity experiments with PXL Prodrug compounds after 24 hours in PyVT-R221A-Luc cells..

24 Hours	Well 1	Well 2	Well 3	Well 4	Average	Average Cells/mL	Average # Cells

5 μM PXL-Pep-Dendron	14	29	13	11	16.75	40200	20100
1 μM PXL-Pep-Dendron	17	14	26	3	15	36000	18000
500 nM PXL-Pep-Dendron	9	6	6	15	9	21600	10800
50 nM PXL-Pep-Dendron	24	9	15	14	15.5	37200	18600
5 nM PXL-Pep-Dendron	16	13	23	24	19	45600	22800
1 nM PXL-Pep-Dendron	11	9	17	4	10.25	24600	12300
5 μM PXL-AVRW	10	15	5	7	9.25	22200	11100
1 μM PXL-AVRW	12	9	6	12	9.75	23400	11700
500 nM PXL-AVRW	19	18	22	6	16.25	39000	19500
50 nM PXL-AVRW	16	25	22	15	19.5	46800	23400
5 nM PXL-AVRW	30	25	20	10	21.25	51000	25500
1 nM PXL-AVRW	4	19	17	4	11	26400	13200
5 μM PXL-Pep -Dendron & GM6001	21	19	14	24	19.5	46800	23400
50 nM PXL-Pep-Dendron & GM6001	24	31	20	21	24	57600	28800
5 μM PXL-AVRW & GM6001	20	27	10	12	17.25	41400	20700
50 nM PXL-AVRW & GM6001	32	27	17	30	26.5	63600	31800
DMSO/ Media	30	42	23	17	28	67200	33600
Media	14	34	27	6	20.25	48600	24300
5 μM PXL-COOH	22	12	12	11	14.25	34200	17100
1 μM PXL-COOH	23	21	16	14	18.5	44400	22200
500 nM PXL-COOH	23	15	14	12	16	38400	19200
50 nM PXL-COOH	20	22	15	15	18	43200	21600
5 nM PXL-COOH	21	19	18	28	21.5	51600	25800
1 nM PXL-COOH	26	28	31	25	27.5	66000	33000
5 μM PXL	18	13	13	12	14	33600	16800
1 μM PXL	13	5	8	9	8.75	21000	10500
500 nM PXL	11	15	15	16	14.25	34200	17100
50 nM PXL	14	11	12	14	12.75	30600	15300
5 nM PXL	20	31	34	26	27.75	66600	33300
1 nM PXL	31	24	23	24	25.5	61200	30600
DMSO/Media	39	29	20	18	26.5	63600	31800
Media	32	42	35	37	36.5	87600	43800
DMSO/Media	24	14	23	19	28.16667	67600	33800
DMSO/Media	27	29	41	30			
DMSO/Media	24	22	34	17			
Media	36	34	33	24	31.83333	76400	38200
Media	31	33	35	34			
Media	29	28	34	31			

Table A.13 Cell count raw data from cytotoxicity experiments with PXL Prodrug compounds after 48 hours in PyVT-R221A-Luc cells..

48 Hours	Well 1	Well 2	Well 3	Well 4	Average	Average Cells/mL	Average # Cells
5 μM PXL-Pep-Dendron	22	21	13	13	17.25	41400	20700
1 μM PXL-Pep-Dendron	23	19	22	17	20.25	48600	24300
500 nM PXL-Pep-Dendron	11	5	7	9	8	19200	9600
50 nM PXL-Pep-Dendron	20	26	18	14	19.5	46800	23400
5 nM PXL-Pep-Dendron	23	16	7	18	16	38400	19200
1 nM PXL-Pep-Dendron	12	11	15	10	12	28800	14400
5 μM PXL-AVRW							
1 μM PXL-AVRW							
500 nM PXL-AVRW	17	13	16	17	15.75	37800	18900
50 nM PXL-AVRW	14	11	9	12	11.5	27600	13800
5 nM PXL-AVRW	10	10	11	13	11	26400	13200
1 nM PXL-AVRW	17	18	23	19	19.25	46200	23100
5 μM PXL-Pep -Dendron & GM6001	36	37	32	16	30.25	72600	36300
50 nM PXL-Pep-Dendron & GM6001	23	22	22	21	22	52800	26400
5 μM PXL-AVRW & GM6001							
50 nM PXL-AVRW & GM6001							
DMSO/ Media	21		18	24	15.75	37800	18900
Media	23	17	36	19	23.75	57000	28500
5 μM PXL-COOH	27	27	23	37	28.5	68400	34200
1 μM PXL-COOH	30	35	25	16	26.5	63600	31800
500 nM PXL-COOH	38	34	44	26	35.5	85200	42600
50 nM PXL-COOH	49	29	32	34	36	86400	43200
5 nM PXL-COOH							
1 nM PXL-COOH							
5 μM PXL	11	7	9	10	9.25	22200	11100
1 μM PXL	7	5	1	8	5.25	12600	6300
500 nM PXL	9	8	11	8	9	21600	10800
50 nM PXL	10	7	6	6	7.25	17400	8700
5 nM PXL	6	9	10	13	9.5	22800	11400
1 nM PXL	10	12	13	8	10.75	25800	12900
DMSO/Media							
Media							
DMSO/Media	5	6	4	2	4.25	10200	5100
DMSO/Media	4	0	3	1	2	4800	2400
DMSO/Media	3	4	2	3	3	7200	3600

Media	8	8	8	6	7.5	18000	9000
Media	11	9	10	10	10	24000	12000
Media	11	7	9	8	8.75	21000	10500

Table A.14 Cell count raw data from cytotoxicity experiments with PXL Prodrug compounds after 72 hours in PyVT-R221A-Luc cells.

72 Hours	Well 1	Well 2	Well 3	Well 4	Average	Average Cells/mL	Average # Cells
5 μM PXL-Pep-Dendron	17	14	13	15	14.75	35400	17700
1 μM PXL-Pep-Dendron	17	14	20	15	16.5	39600	19800
500 nM PXL-Pep-Dendron	22	20	20	19	20.25	48600	24300
50 nM PXL-Pep-Dendron	20	18	23	21	20.5	49200	24600
5 nM PXL-Pep-Dendron	36	9.75	23	23	22.9375	55050	27525
1 nM PXL-Pep-Dendron	27	21	24	25	24.25	58200	29100
5 μM PXL-AVRW							
1 μM PXL-AVRW							
500 nM PXL-AVRW	12	10	11	8	10.25	24600	12300
50 nM PXL-AVRW	13	6	7	6	8	19200	9600
5 nM PXL-AVRW	11	10	14	5	10	24000	12000
1 nM PXL-AVRW	19	18	15	17	17.25	41400	20700
5 μM PXL-Pep -Dendron & GM6001	30	28	21	11	22.5	54000	27000
50 nM PXL-Pep-Dendron & GM6001	25	17	22	7	17.75	42600	21300
5 μM PXL-AVRW & GM6001							
50 nM PXL-AVRW & GM6001							
DMSO/ Media	14	14	17	15	15	36000	18000
Media	22	23	21	20	21.5	51600	25800
5 μM PXL-COOH	13	16	14	14	14.25	34200	17100
1 μM PXL-COOH	23	17	18	22	20	48000	24000
500 nM PXL-COOH	51	42	55	13	40.25	96600	48300
50 nM PXL-COOH	31	26	35	2	23.5	56400	28200
5 nM PXL-COOH							
1 nM PXL-COOH							
5 μM PXL	4	2	4	4	3.5	8400	4200
1 μM PXL	5	4	6	2	4.25	10200	5100
500 nM PXL	2	1	1	1	1.25	3000	1500
50 nM PXL	11	12	6	9	9.5	22800	11400
5 nM PXL	35	32	29	20	29	69600	34800
1 nM PXL	32	33	30	25	30	72000	36000
DMSO/Media							
Media							

DMSO/Media	4	5	3	2	3.5	8400	4200
DMSO/Media	3	2	3	6	3.5	8400	4200
DMSO/Media	2	5	5	8	5	12000	6000
Media	24	27	18	12	20.25	48600	24300
Media	34	34	20	24	28	67200	33600
Media	30	28	28	21	26.75	64200	32100

Table A.15 Cell count raw data from cytotoxicity experiments with PXL Prodrug compounds after 96 hours in PyVT-R221A-Luc cells.

96 Hours	Well 1	Well 2	Well 3	Well 4	Average	Average Cells/mL	Average # Cells
5 μM PXL-Pep-Dendron	11	10	9	8	9.5	22800	11400
1 μM PXL-Pep-Dendron	12	7	14	11	11	26400	13200
500 nM PXL-Pep-Dendron	12	10	14	9	11.25	27000	13500
50 nM PXL-Pep-Dendron	9	11	9	13	10.5	25200	12600
5 nM PXL-Pep-Dendron	72	72	81	28	63.25	151800	75900
1 nM PXL-Pep-Dendron	71	78	70	16	58.75	141000	70500
5 μM PXL-AVRW							
1 μM PXL-AVRW							
500 nM PXL-AVRW	6	5	2	3	4	9600	4800
50 nM PXL-AVRW	5	3	6	4	4.5	10800	5400
5 nM PXL-AVRW	12	6	9	5	8	19200	9600
1 nM PXL-AVRW	16	13	10	7	11.5	27600	13800
5 μM PXL-Pep -Dendron & GM6001	22	21	20	18	20.25	48600	24300
50 nM PXL-Pep-Dendron & GM6001	29	25	26	23	25.75	61800	30900
5 μM PXL-AVRW & GM6001							
50 nM PXL-AVRW & GM6001							
DMSO/ Media	9	12	10	9	10	24000	12000
Media	10	8	11	6	8.75	21000	10500
5 μM PXL-COOH	5	9	7	5	6.5	15600	7800
1 μM PXL-COOH	14	10	10	9	10.75	25800	12900
500 nM PXL-COOH	105	33	50	37	56.25	135000	67500
50 nM PXL-COOH	52	37	48	29	41.5	99600	49800
5 nM PXL-COOH							
1 nM PXL-COOH							
5 μM PXL	3	4	0	2	2.25	5400	2700
1 μM PXL	4	3	2	2	2.75	6600	3300

500 nM PXL	8	4	2	4	4.5	10800	5400
50 nM PXL	7	11	15	18	12.75	30600	15300
5 nM PXL	36	52	38	35	40.25	96600	48300
1 nM PXL	142	67	52	44	76.25	183000	91500
DMSO/Media							
Media							
DMSO/Media	3	3	2	2	2.5	6000	3000
DMSO/Media	6	3	5	1	3.75	9000	4500
DMSO/Media	6	6	4	7	5.75	13800	6900
Media	6	10	8	9	8.25	19800	9900
Media	31	32	26	20	27.25	65400	32700
Media	39	35	33	34	35.25	84600	42300

Table A.16 Cell count raw data from cytotoxicity experiments with DOX Prodrug compounds after 24 hours in PyVT-R221A-Luc cells.

24 Hours	Well 1	Well 2	Well 3	Well 4	Average	Average Cells/mL	Average # Cells
5 uM AVRWLL-DOX	15	12	16	16	14.75	35400	17700
50 nM AVRWLL-DOX	20	14	21	17	18	43200	21600
5 uM Dendron-AVRWLL-DOX	7	13	7	15	10.5	25200	12600
50 nM Dendron-AVRWLL-DOX	17	11	15	13	14	33600	16800
5 uM Leu-Leu-DOX	5	9	7	7	7	16800	8400
50 nM Leu-Leu-DOX	5	24	15	19	15.75	37800	18900
5 uM Leu-DOX	28	22	22	15	21.75	52200	26100
50 nM Leu-DOX	40	38	19	42	34.75	83400	41700
5 uM DOX	11	12	10	5	9.5	22800	11400
50 nM DOX	33	29	17	31	27.5	66000	33000
DMSO/Media	39	29	20	18	26.5	63600	31800
Media	32	42	35	37	36.5	87600	43800
DMSO/Media	24	14	23	19	28.16667	67600	33800
DMSO/Media	27	29	41	30			
DMSO/Media	24	22	34	17			
Media	36	34	33	24	31.83333	76400	38200
Media	31	33	35	34			
Media	29	28	34	31			

Table A.17 Cell count raw data from cytotoxicity experiments with DOX Prodrug compounds after 48 hours in PyVT-R221A-Luc cells.

48 Hours	Well 1	Well 2	Well 3	Well 4	Average	Average Cells/mL	Average # Cells
5 uM AVRWLL-DOX	17	19	20	12	17	40800	20400
50 nM AVRWLL-DOX	18	16	12	16	15.5	37200	18600
5 uM Dendron-AVRWLL-DOX	7	4	12	9	8	19200	9600
50 nM Dendron-AVRWLL-DOX	19	12	16	10	14.25	34200	17100
5 uM Leu-Leu-DOX	5	5	7	9	6.5	15600	7800
50 nM Leu-Leu-DOX	7	6	8	8	7.25	17400	8700
5 uM Leu-DOX	3	5	4	3	3.75	9000	4500
50 nM Leu-DOX	8	6	5	5	6	14400	7200
5 uM DOX	0	0	0	0	0	0	0
50 nM DOX	3	2	6	2	3.25	7800	3900
DMSO/Media	46	40	41	28	38.75	93000	46500
Media	38	45	32	11	31.5	75600	37800
DMSO/Media	45	39	38	32	36.58333	87800	43900
DMSO/Media	39	44	31	32			
DMSO/Media	49	31	32	27			
Media	34	32	37	41	35.25	84600	42300
Media	40	33	31	31			
Media	30	43	35	36			

Table A.18 Cell count raw data from cytotoxicity experiments with DOX Prodrug compounds after 72 hours in PyVT-R221A-Luc cells.

72 Hours	Well 1	Well 2	Well 3	Well 4	Average	Average Cells/mL	Average # Cells
5 uM AVRWLL-DOX	28	26	26	16	24	57600	28800
50 nM AVRWLL-DOX	39	32	40	17	32	76800	38400
5 uM Dendron-AVRWLL-DOX	22	30	28	32	28	67200	33600
50 nM Dendron-AVRWLL-DOX	35	33	38	37	35.75	85800	42900
5 uM Leu-Leu-DOX	11	9	9	3	8	19200	9600
50 nM Leu-Leu-DOX	10	5	6	10	7.75	18600	9300
5 uM Leu-DOX	4	7	8	8	6.75	16200	8100
50 nM Leu-DOX	32	30	34	35	32.75	78600	39300
5 uM DOX	0	0	0	0	0	0	0
50 nM DOX	7	6	5	1	4.75	11400	5700
DMSO/Media	37	38	57	36	42	100800	50400
Media	45	46	36	33	40	96000	48000
DMSO/Media	25	52	40	41	34.66667	83200	41600
DMSO/Media	28	34	33	36			
DMSO/Media	28	30	39	30			

Media	41	46	28	38	32.58333	78200	39100
Media	34	24	45	22			
Media	50	28	16	19			

Table A.19 Cell count raw data from cytotoxicity experiments with DOX Prodrug compounds after 96 hours in PyVT-R221A-Luc cells.

96 Hours	Well 1	Well 2	Well 3	Well 4	Average	Average Cells/mL	Average # Cells
5 uM AVRWLL-DOX	31	37	35	29	33	79200	39600
50 nM AVRWLL-DOX	43	43	45	35	41.5	99600	49800
5 uM Dendron-AVRWLL-DOX	35	41	41	42	39.75	95400	47700
50 nM Dendron-AVRWLL-DOX	38	32	30	36	34	81600	40800
5 uM Leu-Leu-DOX	27	25	29	23	26	62400	31200
50 nM Leu-Leu-DOX	24	22	26	26	24.5	58800	29400
Plate 7							
5 uM Leu-DOX	7	1	5	1	3.5	8400	4200
50 nM Leu-DOX	49	51	43	50	48.25	115800	57900
5 uM DOX	0	0	0	0	0	0	0
50 nM DOX	20	22	15	13	17.5	42000	21000
DMSO/Media	141	80	98	60	94.75	227400	113700
Media	102	76	99	42	79.75	191400	95700
Plate 8							
DMSO/Media	29	32	34	27	28.5	68400	34200
DMSO/Media	21	29	31	29			
DMSO/Media	39	18	25	28			
Media	33	36	28	30	28.5	68400	34200
Media	25	30	31	27			
Media	16	27	32	27			

Table A.20 Cell count raw data from cytotoxicity experiments with Paclitaxel Prodrug compounds after 24 hours in MDA-MB-231, LLC-RSV and LLC-MMP9 cells.

24 Hours	Well 1	Well 2	Well 3	Well 4	Average	Average Cells/mL	Average # Cells
MDA-MB-231							
5 μM PXL-Pep-Dendron	11	4	10	11	9	21600	10800
50 nM PXL-Pep-Dendron	12	12	11	6	10.25	24600	12300

5 μM PXL-AVRW	6	6	1	4	4.25	10200	5100
50 nM PXL-AVRW	12	11	9	9	10.25	24600	12300
5 μM PXL-Pep-Dendron & GM6001	7	7	7	8	7.25	17400	8700
50 nM PXL-Pep-Dendron & GM6001	3	3	3	1	2.5	6000	3000
5 μM PXL-COOH	8	7	4	3	5.5	13200	6600
50 nM PXL-COOH	11	9	9	5	8.5	20400	10200
5 μM PXL	6	4	5	5	5	12000	6000
50 nM PXL	3	6	3	4	4	9600	4800
0.5 % DMSO	20	13	11	10	13.5	32400	16200
Media	8	6	10	6	7.5	18000	9000
0.5% DMSO	5	5	12	7	8	19200	9600
0.5% DMSO	10	4	3	5		0	0
0.5% DMSO	11	9	12	13		0	0
Media	12	10	12	9	11.66667	28000	14000
Media	12	9	10	9		0	0
Media	16	12	13	16		0	0
LLC-RSV							
5 μM PXL-Pep-Dendron	10	8	7	5	7.5	18000	9000
50 nM PXL-Pep-Dendron	14	8	7	8	9.25	22200	11100
5 μM PXL-AVRW	5	4	2	2	3.25	7800	3900
50 nM PXL-AVRW	7	8	6	9	7.5	18000	9000
5 μM PXL-Pep-Dendron & GM6001	8	9	8	6	7.75	18600	9300
50 nM PXL-Pep-Dendron & GM6001	10	8	6	5	7.25	17400	8700
5 μM PXL-COOH	6	2	4	5	4.25	10200	5100
50 nM PXL-COOH	5	7	4		5.333333	12800	6400
5 μM PXL	6	2	2	4	3.5	8400	4200
50 nM PXL	5	6	3	2	4	9600	4800
0.5 % DMSO	11	9	8	8	9	21600	10800
Media	2	2	0	1	1.25	3000	1500
0.5% DMSO	4	3	4	4	3.333333	8000	4000
0.5% DMSO	1	3	3	0		0	0
0.5% DMSO	7	5	4	2		0	0
Media	3	2	0	4	2.666667	6400	3200
Media	6	3	8	1		0	0
Media	0	4	1	0		0	0
LLC-MMP9							
5 μM PXL-Pep-Dendron	7	9	5	3	6	14400	7200
50 nM PXL-Pep-Dendron	5	2	4	4	3.75	9000	4500
5 μM PXL-AVRW	2	4	2	2	2.5	6000	3000
50 nM PXL-AVRW	3	1	3	2	2.25	5400	2700

5 μM PXL-Pep-Dendron & GM6001	13	5	9	3	7.5	18000	9000
50 nM PXL-Pep-Dendron & GM6001	3	2	5	8	4.5	10800	5400
5 μM PXL-COOH	5	6	3	2	4	9600	4800
50 nM PXL-COOH	4	6	5	4	4.75	11400	5700
5 μM PXL	6	3	6	5	5	12000	6000
50 nM PXL	5	4	5	2	4	9600	4800
0.5% DMSO	14	7	3	7	7.75	18600	9300
Media	1	3	7	1	3	7200	3600
0.5% DMSO	4	3	4	3	3.5	8400	4200
0.5% DMSO	6	2	3	3		0	0
0.5% DMSO	5	4	2	3		0	0
Media	4	4	2	3	4.916667	11800	5900
Media	5	4	4	3		0	0
Media	10	6	6	8		0	0

Table A.21 Cell count raw data from cytotoxicity experiments with Paclitaxel Prodrug compounds after 48 hours in MDA-MB-231, LLC-RSV and LLC-MMP9 cells.

48 Hours	Well 1	Well 2	Well 3	Well 4	Average	Average Cells/mL	Average # Cells
MDA-MB-231							
5 μM PXL-Pep-Dendron	9	14	8	12	10.75	25800	12900
50 nM PXL-Pep-Dendron	12	15	14	9	12.5	30000	15000
5 μM PXL-AVRW	7	4	6	3	5	12000	6000
50 nM PXL-AVRW	14	8	11	10	10.75	25800	12900
5 μM PXL-Pep-Dendron & GM6001	13	9	9	4	8.75	21000	10500
50 nM PXL-Pep-Dendron & GM6001	20	13	10	11	13.5	32400	16200
5 μM PXL-COOH	4	2	3	1	2.5	6000	3000
50 nM PXL-COOH	5	6	6	3	5	12000	6000
5 μM PXL	1	0	1	0	0.5	1200	600
50 nM PXL	4	3	3	3	3.25	7800	3900
0.5 % DMSO	20	21	19	18	19.5	46800	23400
Media	12	18	16	12	14.5	34800	17400
0.5% DMSO	20	22	14	18	18.83333	45200	22600
0.5% DMSO	40	18	17	3		0	0
0.5% DMSO	24	14	24	12		0	0
Media	21	11	21	12	13.66667	32800	16400

Media	21	11	12	5		0	0
Media	20	12	6	12		0	0
LLC-RSV							
5 μM PXL-Pep-Dendron	13	10	10	11	11	26400	13200
50 nM PXL-Pep-Dendron	16	13	14	17	15	36000	18000
5 μM PXL-AVRW	6	4	2	3	3.75	9000	4500
50 nM PXL-AVRW	7	11	9	6	8.25	19800	9900
5 μM PXL-Pep-Dendron & GM6001	7	5	4	4	5	12000	6000
50 nM PXL-Pep-Dendron & GM6001	14	9	8	9	10	24000	12000
5 μM PXL-COOH	2	2	2	3	2.25	5400	2700
50 nM PXL-COOH	0	4	4	2	2.5	6000	3000
5 μM PXL	3	3	1	1	2	4800	2400
50 nM PXL	3	1	3	2	2.25	5400	2700
0.5 % DMSO	19	8	6	2	8.75	21000	10500
Media	4	4	9	7	6	14400	7200
0.5% DMSO	20	9	14	12	13.08333	31400	15700
0.5% DMSO	14	21	4	1		0	0
0.5% DMSO	28	22	8	4		0	0
Media	6	5	7	9	6.5	15600	7800
Media	4	4	10	3		0	0
Media	11	9	5	5		0	0
LLC-MMP9							
5 μM PXL-Pep-Dendron	4	2	2	1	2.25	5400	2700
50 nM PXL-Pep-Dendron	2	0	1	1	1	2400	1200
5 μM PXL-AVRW	3	0	1	2	1.5	3600	1800
50 nM PXL-AVRW	2	2	2	3	2.25	5400	2700
5 μM PXL-Pep-Dendron & GM6001	10	5	5	4	6	14400	7200
50 nM PXL-Pep-Dendron & GM6001	11	6	7	3	6.75	16200	8100
5 μM PXL-COOH	4	3	1	0	2	4800	2400
50 nM PXL-COOH	9	9	5	3	6.5	15600	7800
5 μM PXL	1	4	2	0	1.75	4200	2100
50 nM PXL	3	0	2	0	1.25	3000	1500
0.5% DMSO	2	0	0	13	3.75	9000	4500
Media	9	1	3	8	5.25	12600	6300
0.5% DMSO	5	12	5	4	7.416667	17800	8900
0.5% DMSO	12	10	7	6		0	0
0.5% DMSO	12	5	6	5		0	0
Media	8	3	4	1	3.833333	9200	4600
Media	5	2	2	5		0	0

Media	1	2	10	3		0	0

Table A.22 Cell count raw data from cytotoxicity experiments with Paclitaxel Prodrug compounds after 72 hours in MDA-MB-231, LLC-RSV and LLC-MMP9 cells.

72 Hours	Well 1	Well 2	Well 3	Well 4	Average	Average Cells/mL	Average # Cells
MDA-MB-231							
5 μM PXL-Pep-Dendron	12	10	11	7	10	24000	12000
50 nM PXL-Pep-Dendron	19	17	16	15	16.75	40200	20100
5 μM PXL-AVRW	6	5	4	3	4.5	10800	5400
50 nM PXL-AVRW	8	8	6	5	6.75	16200	8100
5 μM PXL-Pep-Dendron & GM6001	6	7	8	7	7	16800	8400
50 nM PXL-Pep-Dendron & GM6001	7	5	7	9	7	16800	8400
5 μM PXL-COOH	2	0	1	3	1.5	3600	1800
50 nM PXL-COOH	7	5	5	6	5.75	13800	6900
5 μM PXL	2	3	1	4	2.5	6000	3000
50 nM PXL	2	6	2	1	2.75	6600	3300
0.5 % DMSO	39	31	23	25	29.5	70800	35400
Media	34	27	24	21	26.5	63600	31800
0.5% DMSO	35	38	31	14	30.08333	72200	36100
0.5% DMSO	40	39	29	10		0	0
0.5% DMSO	49	39	31	6		0	0
Media	31	9	5	7	16.5	39600	19800
Media	34	11	11	15		0	0
Media	26	29	15	5		0	0
LLC-RSV							
5 μM PXL-Pep-Dendron	3	4	4	3	3.5	8400	4200
50 nM PXL-Pep-Dendron	14	11	13	11	12.25	29400	14700
5 μM PXL-AVRW	1	1	1	1	1	2400	1200
50 nM PXL-AVRW	5	2	2	2	2.75	6600	3300
5 μM PXL-Pep-Dendron & GM6001	0	0	2	2	1	2400	1200
50 nM PXL-Pep-Dendron & GM6001	6	2	5	5	4.5	10800	5400
5 μM PXL-COOH	0	0	0	0	0	0	0
50 nM PXL-COOH	2	2	3	1	2	4800	2400
5 μM PXL	0	2	0	0	0.5	1200	600
50 nM PXL	1	1	1	1	1	2400	1200
0.5 % DMSO	29	22	26	23	25	60000	30000
Media	25	28	26	27	26.5	63600	31800

0.5% DMSO	50	51	50	13	39.66667	95200	47600
0.5% DMSO	53	45	46	4		0	0
0.5% DMSO	58	54	41	11		0	0
Media	20	2	11	12	11.91667	28600	14300
Media	22	9	9	9		0	0
Media	15	15	10	9		0	0
LLC-MMP9							
5 μM PXL-Pep-Dendron	1	0	0	1	0.5	1200	600
50 nM PXL-Pep-Dendron	3	0	0	0	0.75	1800	900
5 μM PXL-AVRW	0	0	0	0	0	0	0
50 nM PXL-AVRW	1	1	0	1	0.75	1800	900
5 μM PXL-Pep-Dendron & GM6001	0	3	2	0	1.25	3000	1500
50 nM PXL-Pep-Dendron & GM6001	2	1	0	2	1.25	3000	1500
5 μM PXL-COOH	0	0	1	0	0.25	600	300
50 nM PXL-COOH	3	4	3	2	3	7200	3600
5 μM PXL	1	1	0	0	0.5	1200	600
50 nM PXL	2	0	0	0	0.5	1200	600
0.5% DMSO	21	9	5	4	9.75	23400	11700
Media	5	5	0	3	3.25	7800	3900
0.5% DMSO	28	24	7	3	17.91667	43000	21500
0.5% DMSO	30	21	25	1		0	0
0.5% DMSO	29	46	1	0		0	0
Media	7	7	3	1	4.833333	11600	5800
Media	25	3	0	4		0	0
Media	3	3	2	0		0	0

Table A.23 Cell count raw data from cytotoxicity experiments with Paclitaxel Prodrug compounds after 96 hours in MDA-MB-231, LLC-RSV and LLC-MMP9 cells.

96 Hours	Well 1	Well 2	Well 3	Well 4	Average	Average Cells/mL	Average # Cells
MDA-MB-231							
5 μM PXL-Pep-Dendron	3	2	0	2	1.75	4200	2100
50 nM PXL-Pep-Dendron	5	6	7	4	5.5	13200	6600
5 μM PXL-AVRW	3	5	5	1	3.5	8400	4200
50 nM PXL-AVRW	6	3	2	1	3	7200	3600
5 μM PXL-Pep-Dendron & GM6001	3	5	2	3	3.25	7800	3900
50 nM PXL-Pep-Dendron & GM6001	6	5	8	3	5.5	13200	6600
5 μM PXL-COOH	0	1	1	0	0.5	1200	600

50 nM PXL-COOH	0	2	0	1	0.75	1800	900
5 μM PXL	1	0	0	1	0.5	1200	600
50 nM PXL	1	2	1	2	1.5	3600	1800
0.5 % DMSO	49	48	27	40	41	98400	49200
Media	32	29	13	12	21.5	51600	25800
0.5% DMSO	58	42	52	19	48.41667	116200	58100
0.5% DMSO	50	66	31	26		0	0
0.5% DMSO	61	65	69	42		0	0
Media	63	66	18	12	28.75	69000	34500
Media	57	18	10	18		0	0
Media	32	18	16	17		0	0
LLC-RSV							
5 μM PXL-Pep-Dendron	2	1	0	2	1.25	3000	1500
50 nM PXL-Pep-Dendron	16	12	16	17	15.25	36600	18300
5 μM PXL-AVRW	2	2	0	0	1	2400	1200
50 nM PXL-AVRW	12	10	10	10	10.5	25200	12600
5 μM PXL-Pep-Dendron & GM6001	1	0	0	0	0.25	600	300
50 nM PXL-Pep-Dendron & GM6001	12	13	11	9	11.25	27000	13500
5 μM PXL-COOH	0	0	0	0	0	0	0
50 nM PXL-COOH	1	2	0	1	1	2400	1200
5 μM PXL	0	2	3	0	1.25	3000	1500
50 nM PXL	2	2	0	0	1	2400	1200
0.5 % DMSO	114	29	38	23	51	122400	61200
Media	48	54	42	29	43.25	103800	51900
0.5% DMSO	117	127	107	103	111.9167	268600	134300
0.5% DMSO	109	90	125	116		0	0
0.5% DMSO	112	140	99	98		0	0
Media	60	64	55	7	39.75	95400	47700
Media	60	64	12	9		0	0
Media	55	36	44	11		0	0
LLC-MMP9							
5 μM PXL-Pep-Dendron	0	1	0	1	0.5	1200	600
50 nM PXL-Pep-Dendron	0	0	1	2	0.75	1800	900
5 μM PXL-AVRW	0	1	0	0	0.25	600	300
50 nM PXL-AVRW	1	1	0	1	0.75	1800	900
5 μM PXL-Pep-Dendron & GM6001	0	0	0	0	0	0	0
50 nM PXL-Pep-Dendron & GM6001	1	2	1	0	1	2400	1200
5 μM PXL-COOH	0	0	1	0	0.25	600	300
50 nM PXL-COOH	3	3	2	2	2.5	6000	3000

5 μM PXL	0	0	0	0	0	0	0
50 nM PXL	0	0	0	0	0	0	0
0.5% DMSO	14	9	3	11	9.25	22200	11100
Media	15	6	18	11	12.5	30000	15000
0.5% DMSO	69	31	50	38	60.5	145200	72600
0.5% DMSO	78	66	63	76		0	0
0.5% DMSO	67	59	64	65		0	0
Media	38	29	9	8	20.66667	49600	24800
Media	25	14	15	13		0	0
Media	26	31	22	18		0	0

Table A.24 Cell count raw data from cytotoxicity experiments with GM6001 after 48 and 96 hours in PyVT-R221A-Luc, MDA-MB-231, LLC-RSV and LLC-MMP9 cells.

PyVT 48 Hour	Well 1	Well 2	Well 3	Well 4	Average	Average Cells/mL	Average # Cells
5 uM GM6001		21	38	66	41.66667	100000	50000
50 nM GM6001	64	50		30	48	115200	57600
DMSO	69	59	30	25	45.75	109800	54900
Media	51	41	44		45.33333	108800	54400
PyVT 96 Hour							
5 uM GM6001	71	74	69	74	72	172800	86400
50 nM GM6001	58	49	55	48	52.5	126000	63000
DMSO	82	75	72		76.33333	183200	91600
Media	62	83	32		59	141600	70800
MDA 48 Hour							
5 uM GM6001	40	31	24	26	30.25	72600	36300
50 nM GM6001	23	24	17	16	20	48000	24000
DMSO	42	42	30	20	33.5	80400	40200
Media	32	21	19	42	28.5	68400	34200
MDA 96 Hour							
5 uM GM6001	33	30	29	27	29.75	71400	35700
50 nM GM6001	33	32	33	31	32.25	77400	38700
DMSO	45	50	41	37	43.25	103800	51900
Media	47	40	44	39	42.5	102000	51000
LLC-RSV 48 Hour							
5 uM GM6001		38	38	26	34	81600	40800
50 nM GM6001		29	55	26	36.66667	88000	44000
DMSO		59	44	30	44.33333	106400	53200
Media	45	62		32	46.33333	111200	55600
LLC-RSV 96 Hour							
5 uM GM6001	115	133	142	141	132.75	318600	159300
50 nM GM6001		189	183	170	180.6667	433600	216800
DMSO	75	74	88	76	78.25	187800	93900
Media		165	173	139	159	381600	190800

LLC-MMP9 48 Hour							
5 uM GM6001	23	17	18		19.33333	46400	23200
50 nM GM6001	44	37	43	32	39	93600	46800
DMSO	36		30	20	28.66667	68800	34400
Media	32	29	25		28.66667	68800	34400
LLC-MMP9 96 Hour							
5 uM GM6001	74	73	74	69	72.5	174000	87000
50 nM GM6001	65	62	72	65	66	158400	79200
DMSO	59	61	64	59	60.75	145800	72900
Media	85	88	81		84.66667	203200	101600

A.4 Cytotoxicity Graphs of Cellular Data

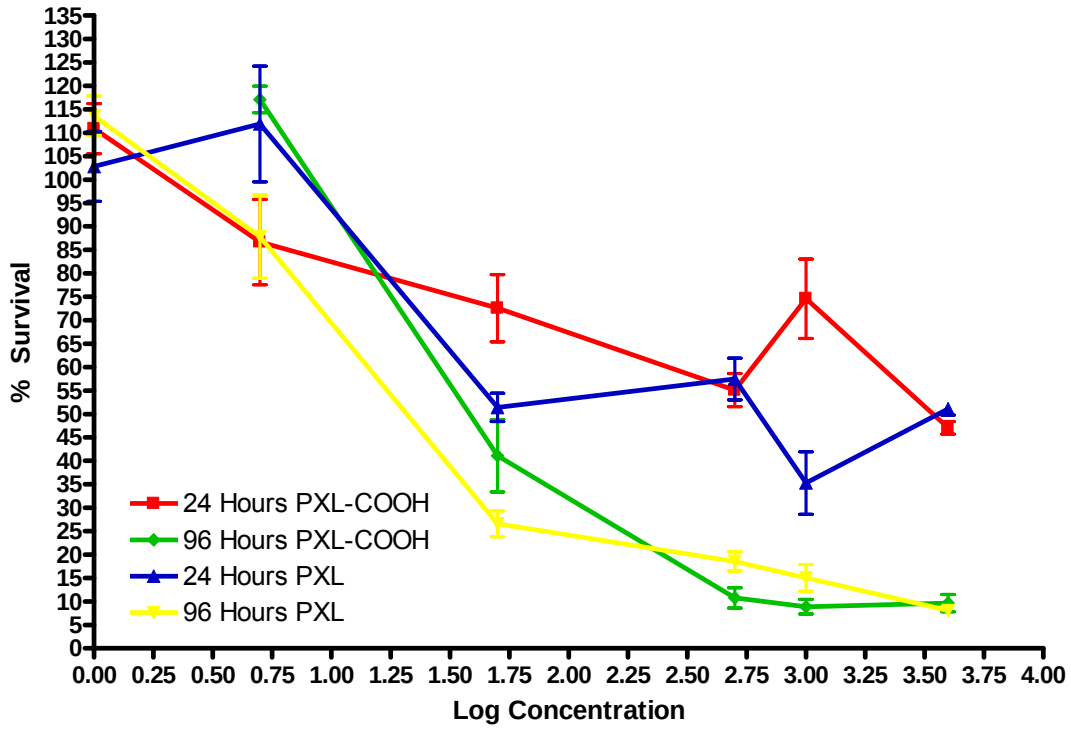

Figure A.13. Cytotoxicity versus Log Concentration (□M) in PyVT-R221A-Luc Cells

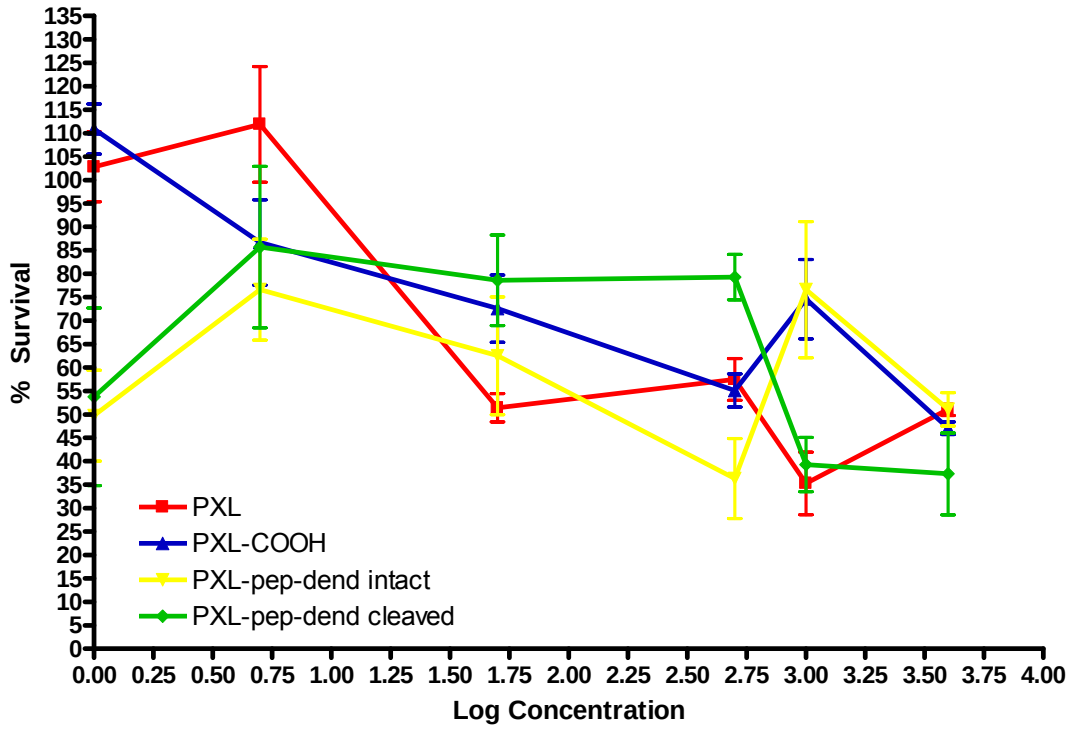

Figure A.14 Cytotoxicity versus Log Concentration (□M) in PyVT-R221A-Luc Cells after 24 Hours

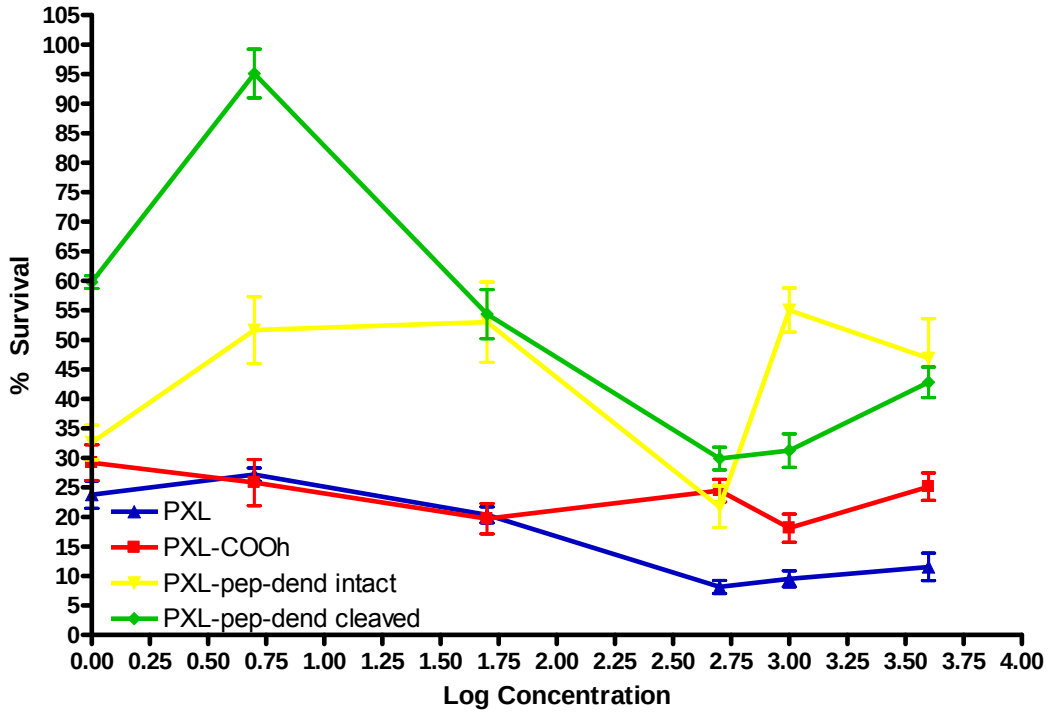

Figure A.15 Cytotoxicity versus Log Concentration (□M) in PyVT-R221A-Luc Cells after 48 Hours

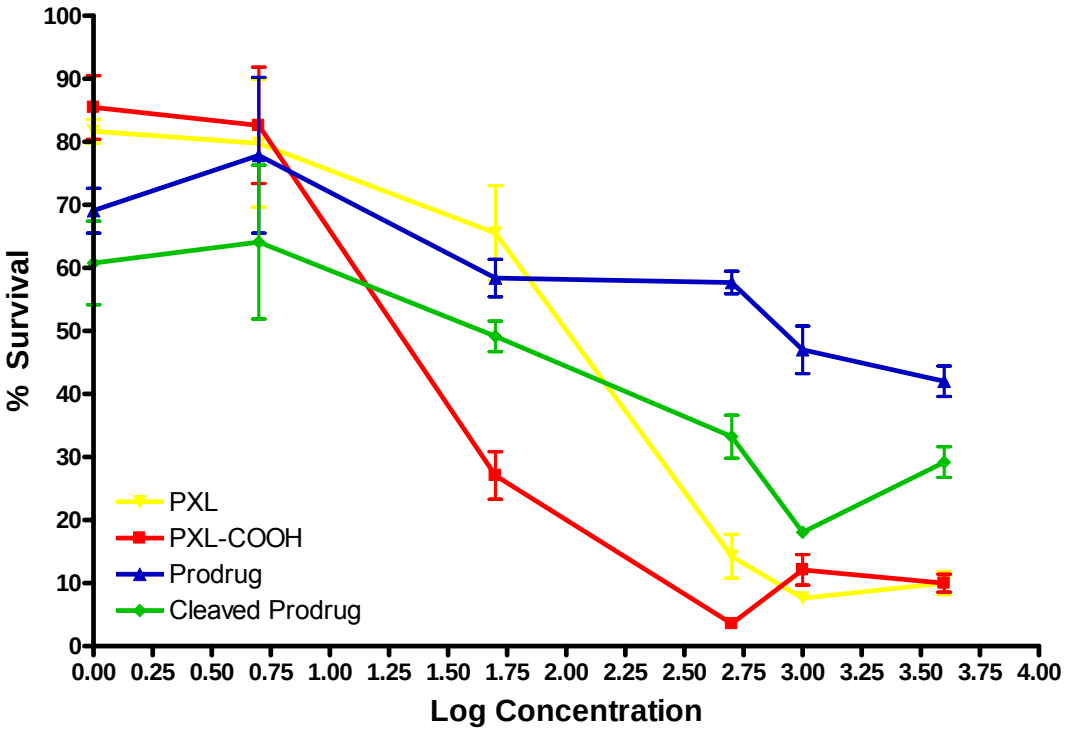

Figure A.16 Cytotoxicity versus Log Concentration (□M) in PyVT-R221A-Luc Cells after 72 Hours

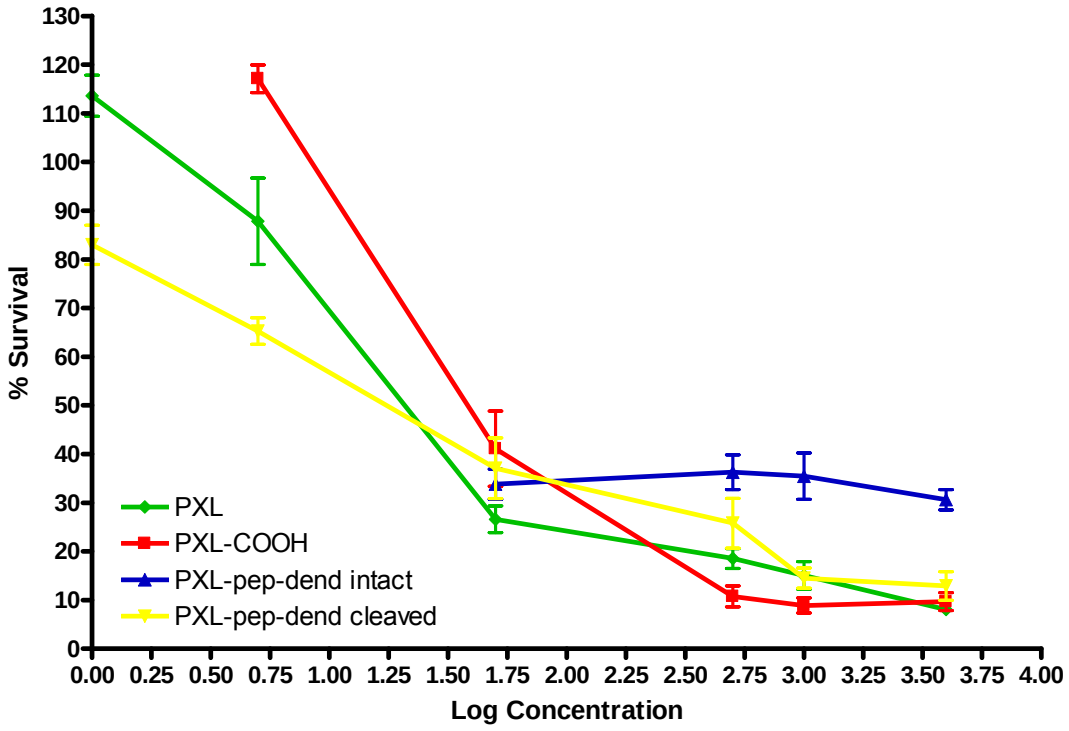

Figure A.17 Cytotoxicity versus Log Concentration (□M) in PyVT-R221A-Luc Cells after 96 Hours

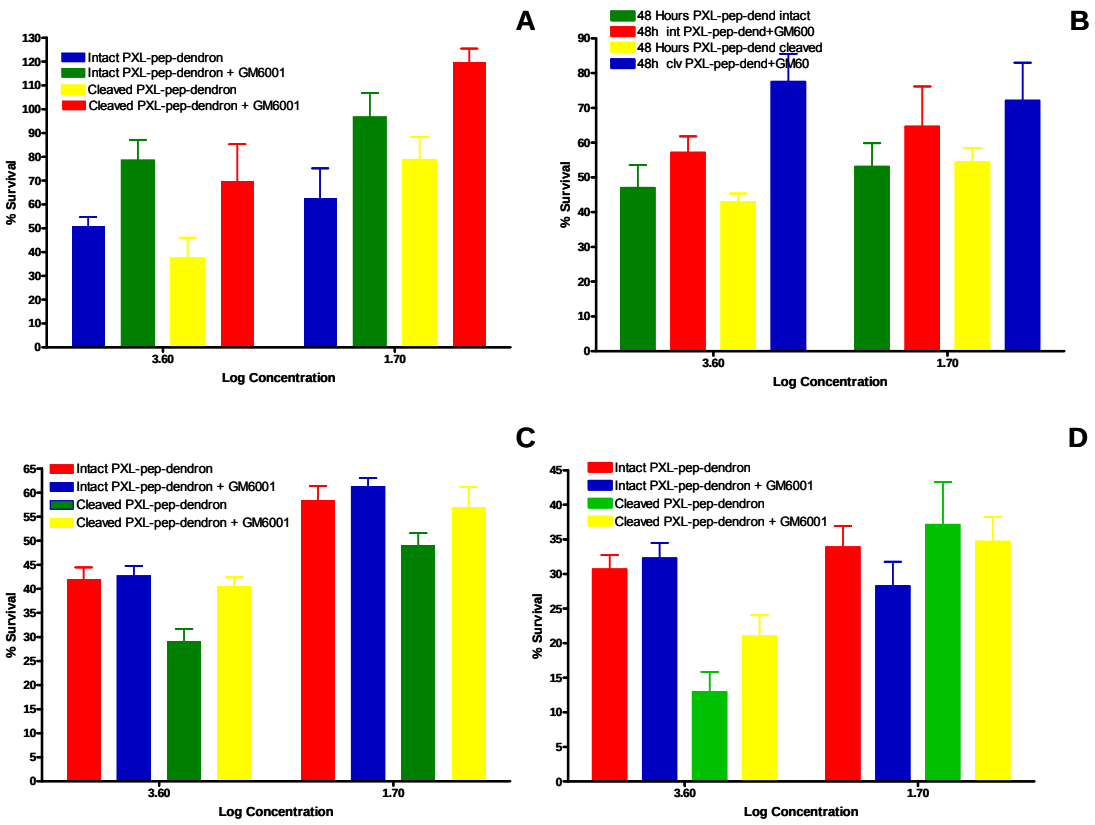

Figure A.18. Bar graph of cellular cytotoxicity versus Log Concentration in PyVT-R221A-Luc cells after (A) 24 Hours, (B) 48 Hours, (C) 72 Hours and (D) 96 Hours

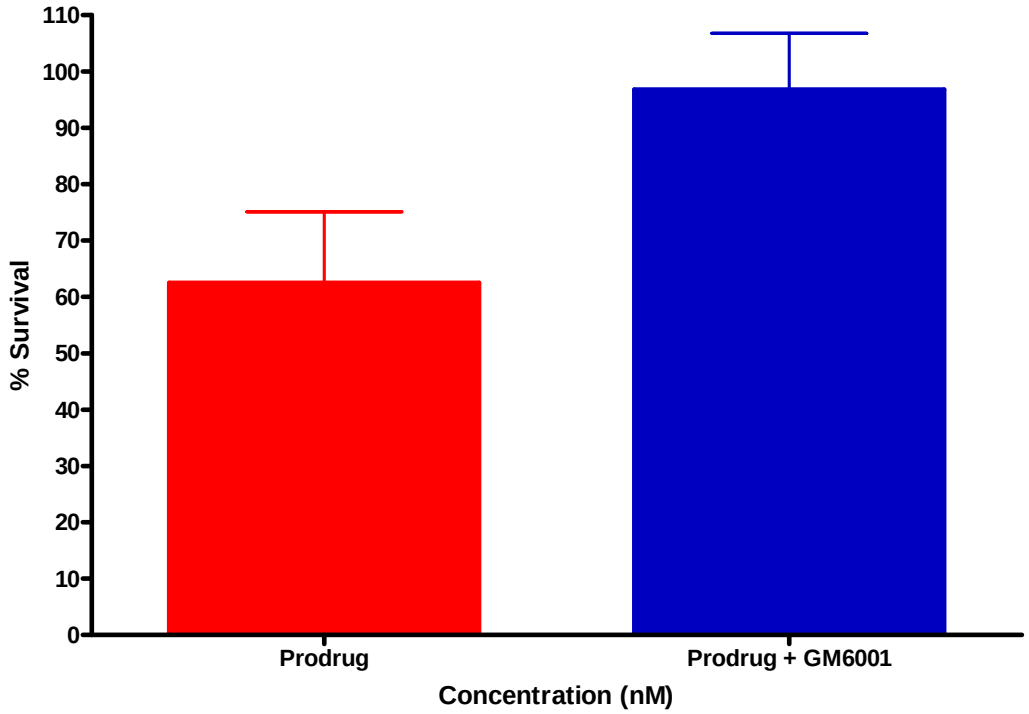

Figure A.19. Bar graph of cellular cytotoxicity versus Concentration in PyVT-R221A-Luc cells.

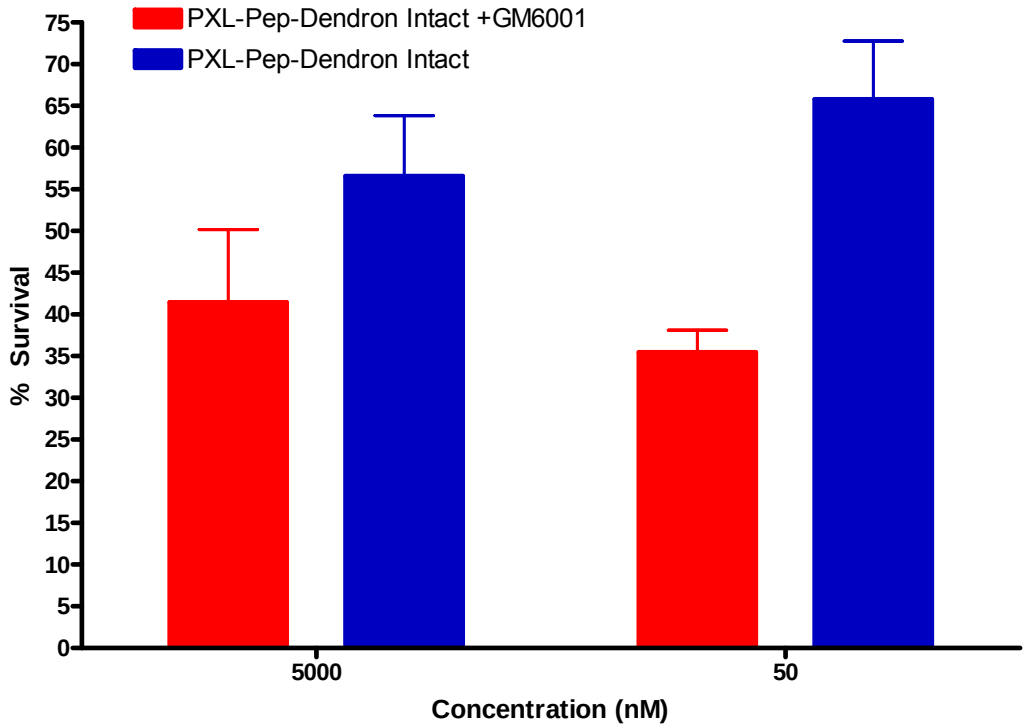

Figure A.20. Bar graph of cellular cytotoxicity versus Concentration MB-MDA-231 cells after 48 hours.

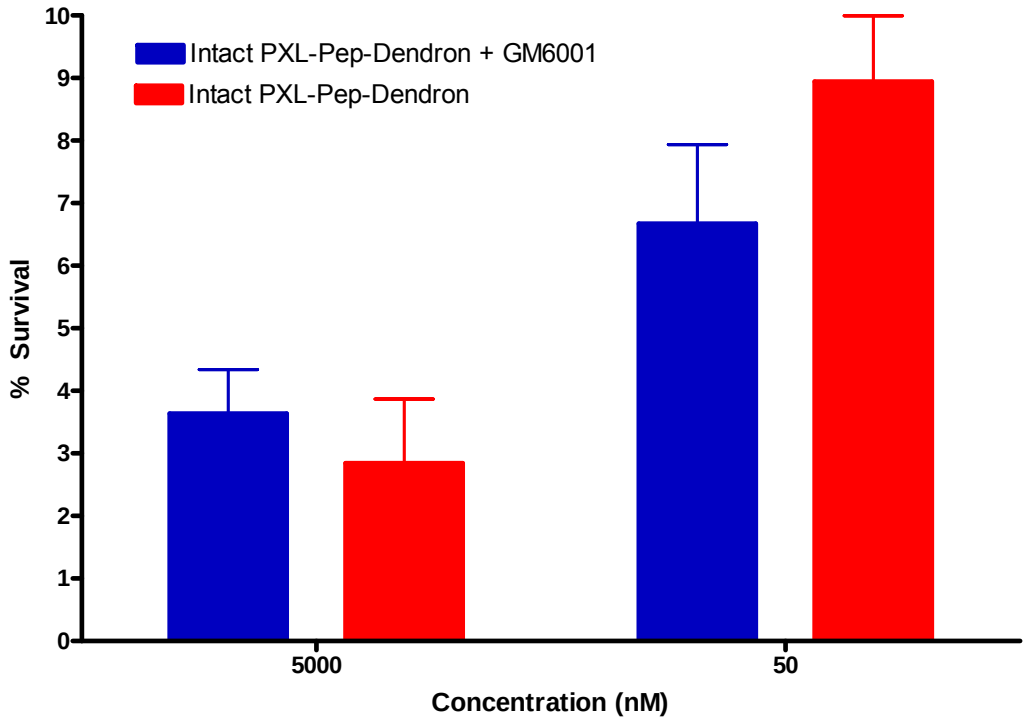

Figure A.21. Bar graph of cellular cytotoxicity versus Concentration MB-MDA-231 cells after 96 hours.

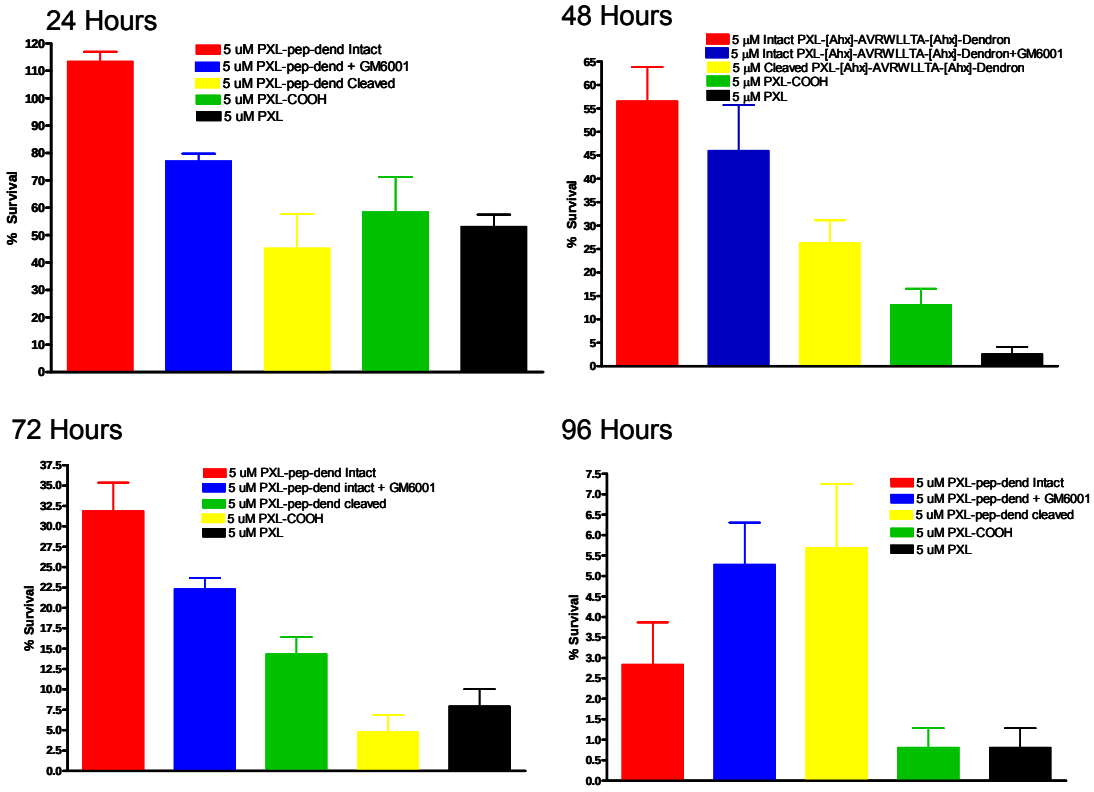

Figure A.22. Bar graph of cellular cytotoxicity at 5 μM in PXL MB-MDA-231 cells over 4 time points after 96 hours

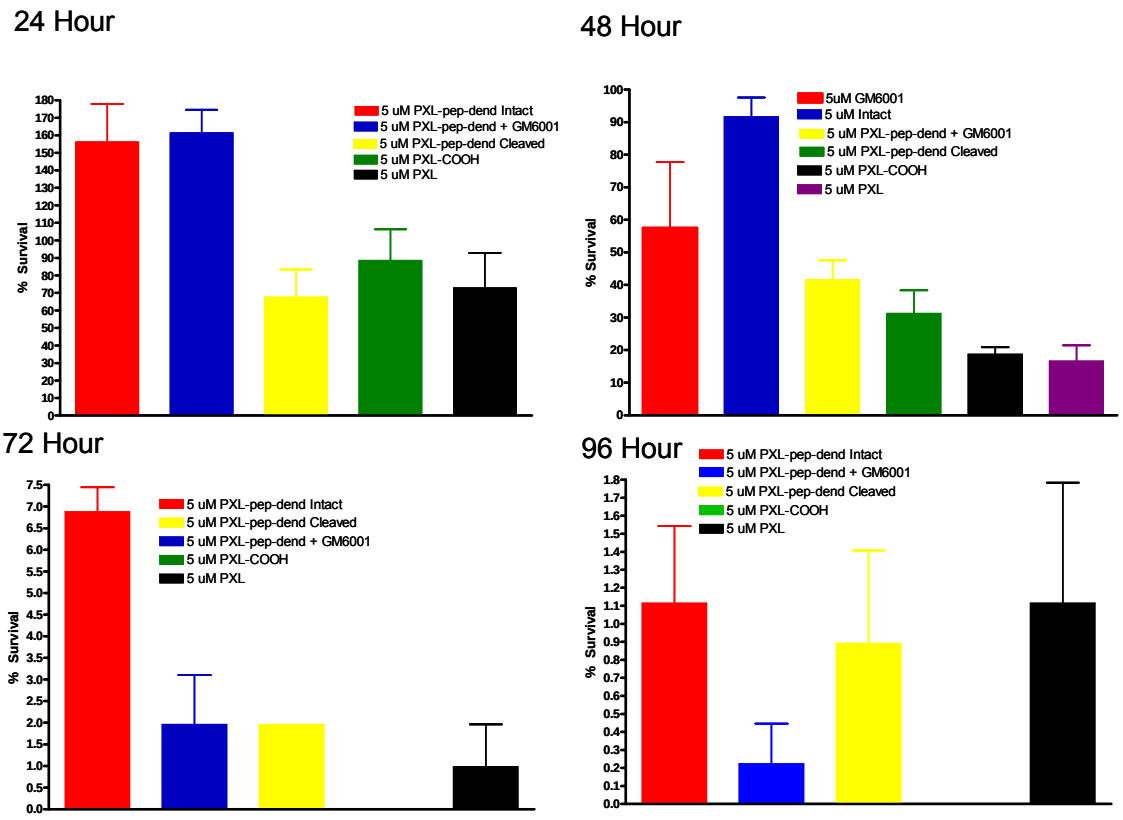

Figure A.23. Bar graph of cellular cytotoxicity at 5 μM in PXL LLC-RSV cells over 4 time points after 96 hours

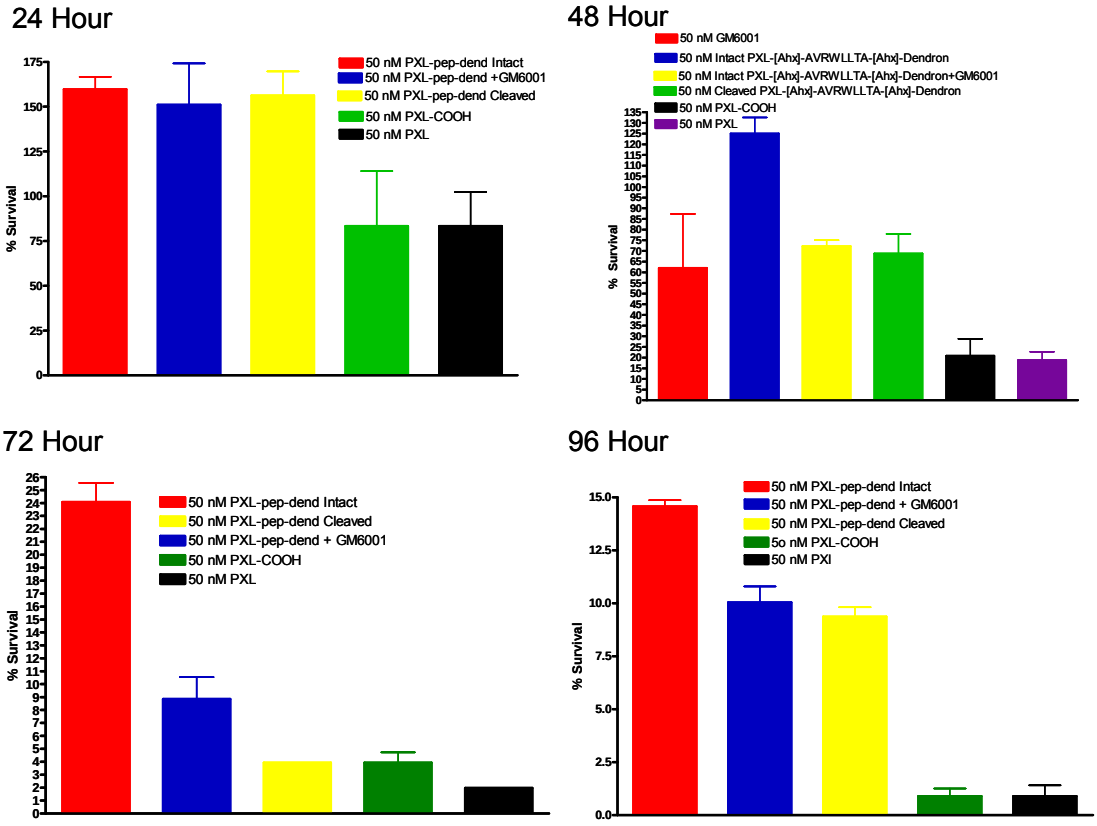

Figure A.24. Bar graph of cellular cytotoxicity at 50 nM in PXL LLC-RSV cells over 4 time points over 96 hours

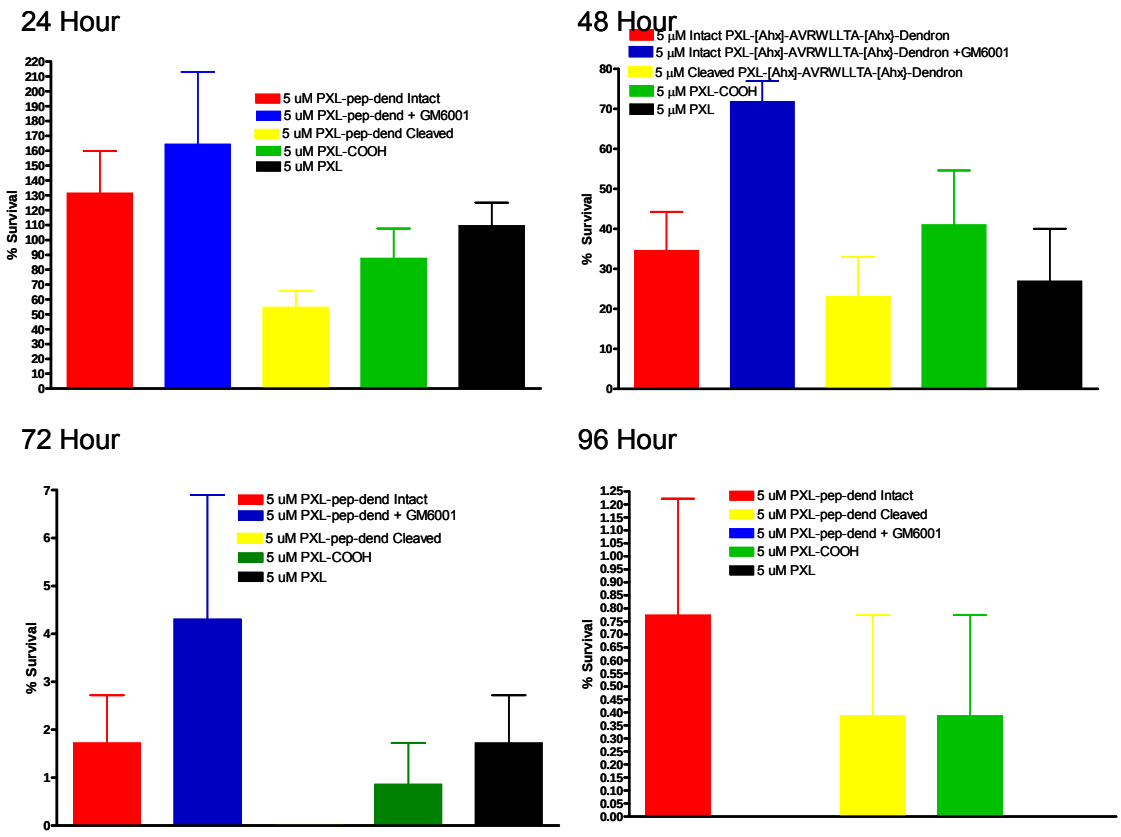

Figure A.25. Bar graph of cellular cytotoxicity at 5 μM in PXL LLC-MMP9 cells over 4 time points over 96 hours

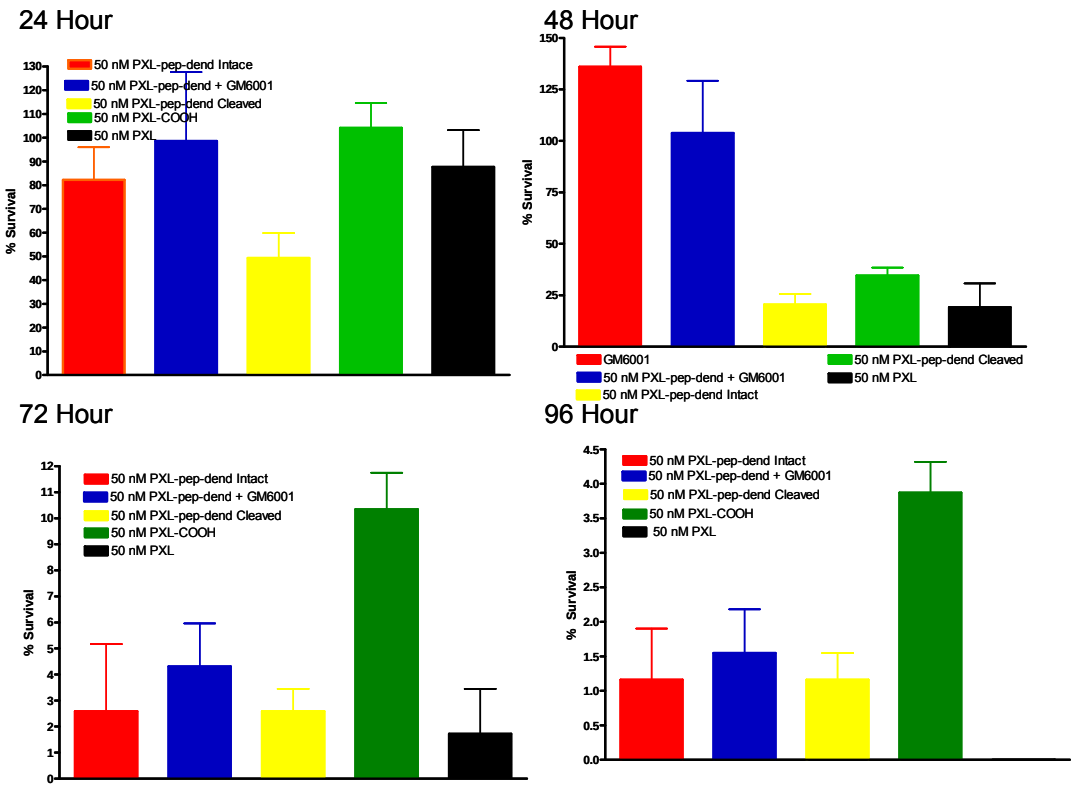

Figure A.26. Bar graph of cellular cytotoxicity at 50 nM in PXL LLC-MMP9 cells over 4 time points over 96 hours

APPENDIX B

SELECTED NMR SPECTRA

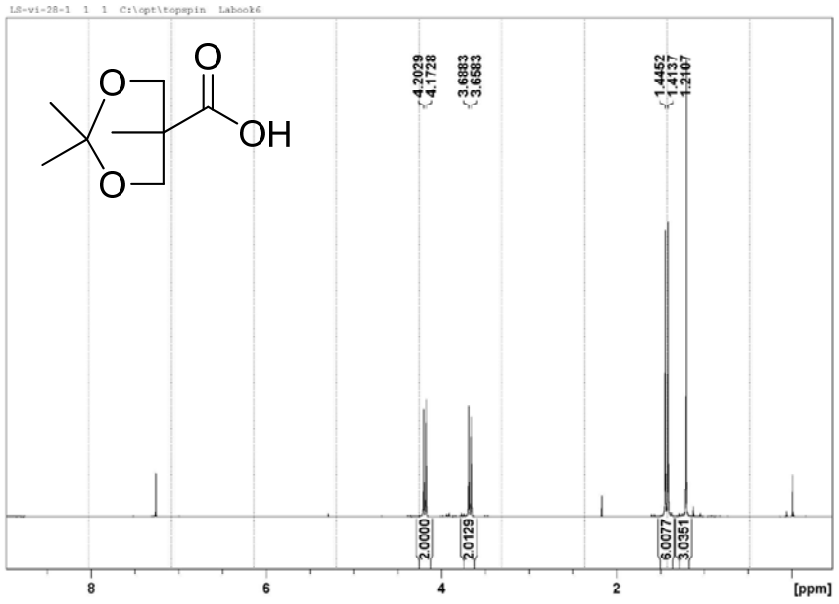

Figure B.1 NMR or Acetonide-Bis-MPA (2,2,5-trimethyl-1,3-dioxane-5-carboxylic acid).

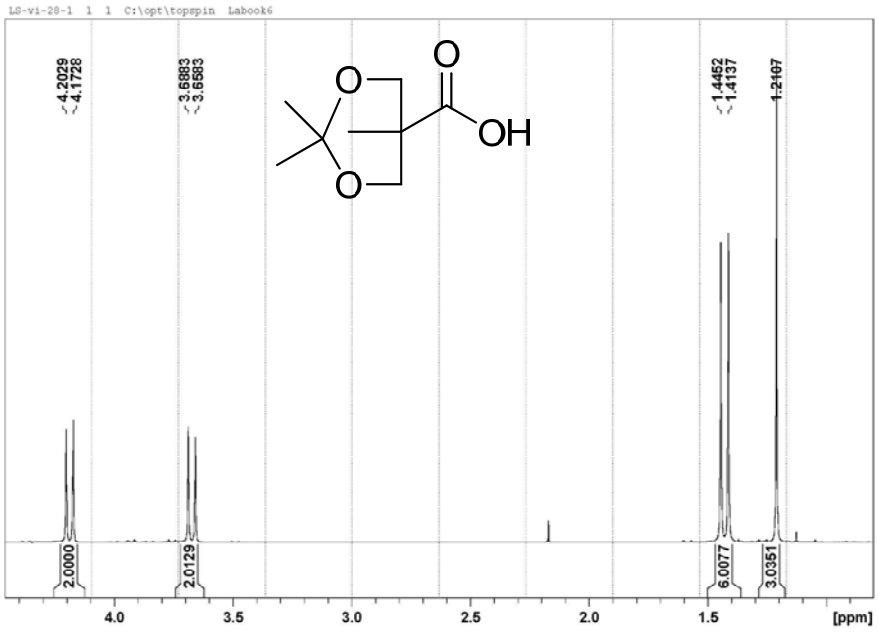

Figure B.2. Expanded NMR of Acetonide-Bis-MPA (2,2,5-trimethyl-1,3-dioxane-5-carboxylic acid).

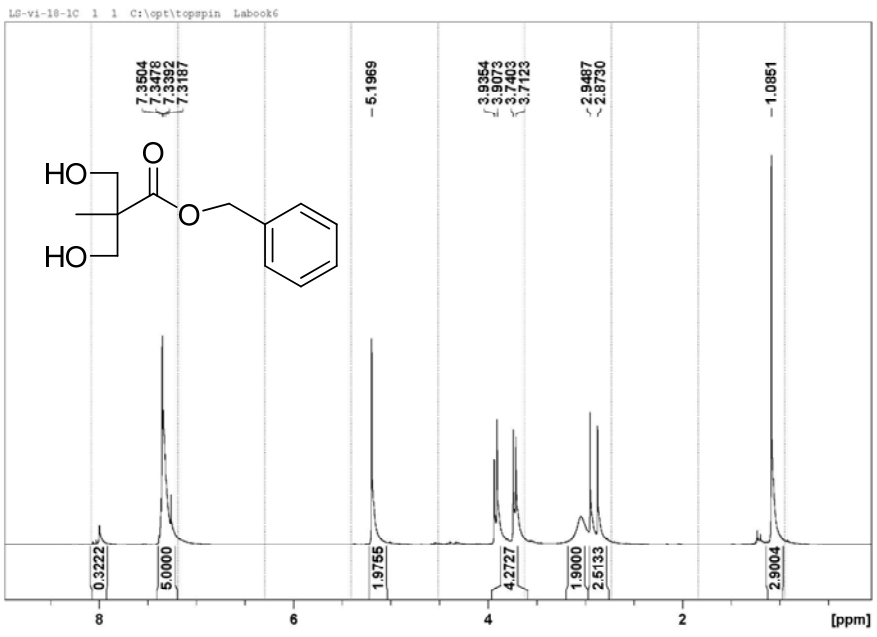

Figure B.3 NMR of Bis-MPA-Bn (benzyl 3-hydroxy-2-(hydroxymethyl)-2-methylpropanoate)

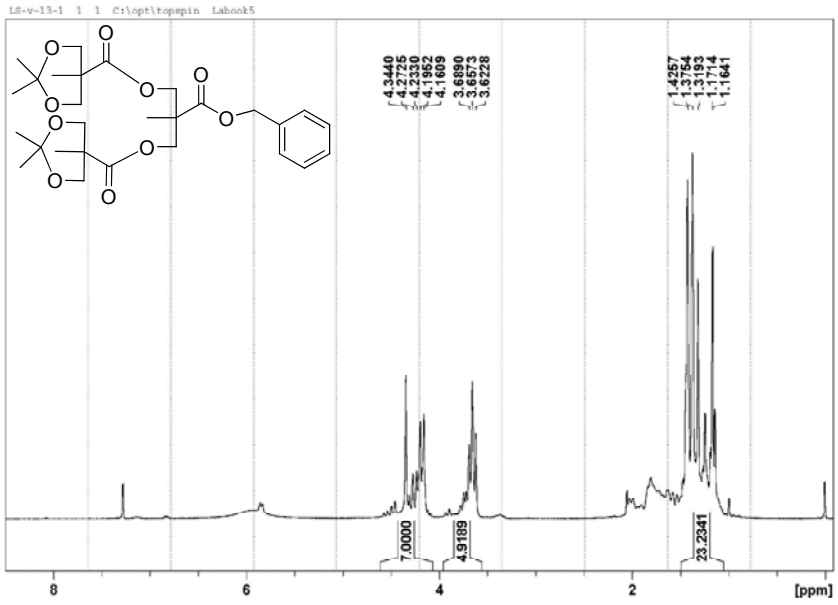

Figure B.4. NMR of Acetonide-G(1)-Dendron-Bn (2-(benzyloxycarbonyl)-2-methylpropane-1,3-diyl bis(2,2,5-trimethyl-1,3-dioxane-5-carboxylate).

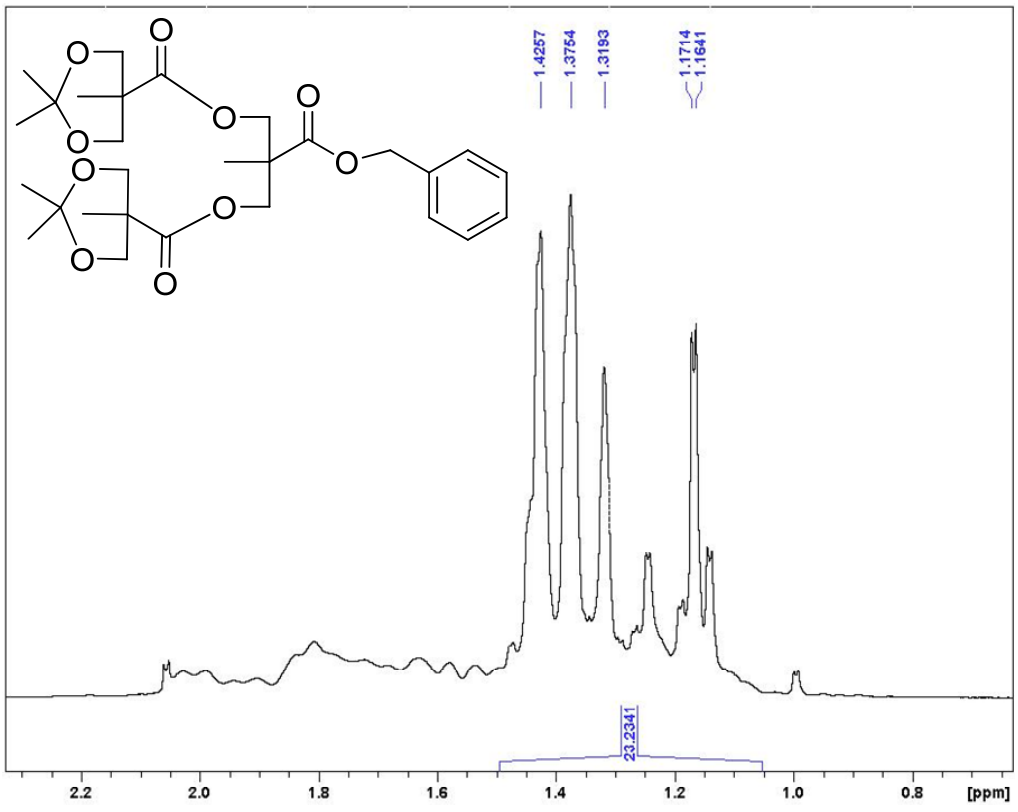

Figure B.5. Expanded NMR of Acetonide-G(1)-Dendron-Bn (2-(benzyloxycarbonyl)-2-methylpropane-1,3-diyl bis(2,2,5-trimethyl-1,3-dioxane-5-carboxylate).

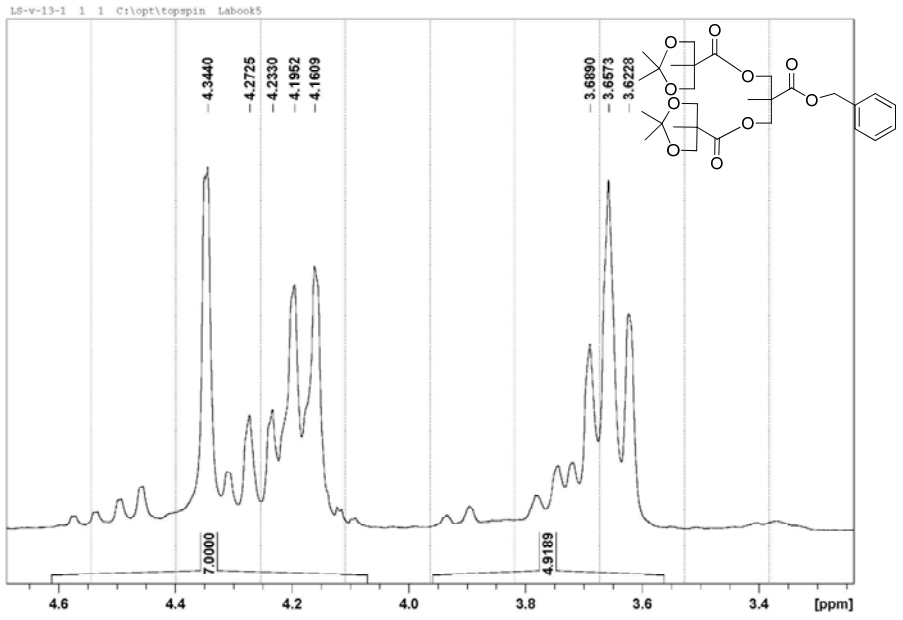

Figure B.6. Expanded NMR of Acetonide-G(1)-Dendron-Bn (2-(benzyloxycarbonyl)-2-methylpropane-1,3-diyl bis(2,2,5-trimethyl-1,3-dioxane-5-carboxylate).

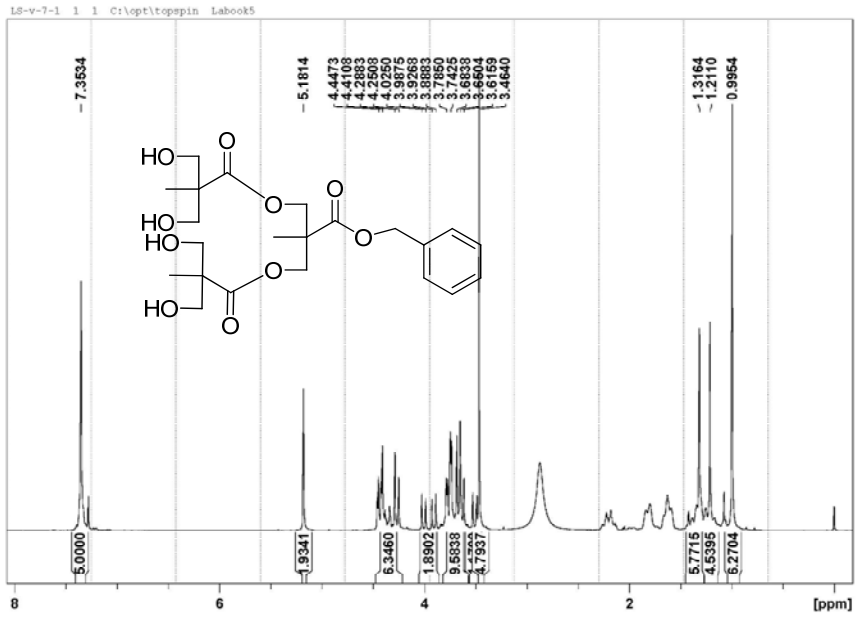

Figure B.7. NMR of G(1)-Dendron-Bn (2-(benzyloxycarbonyl)-2-methylpropane-bis(2,2,5-trimethyl-1,3-dioxane-5-carboxylate).

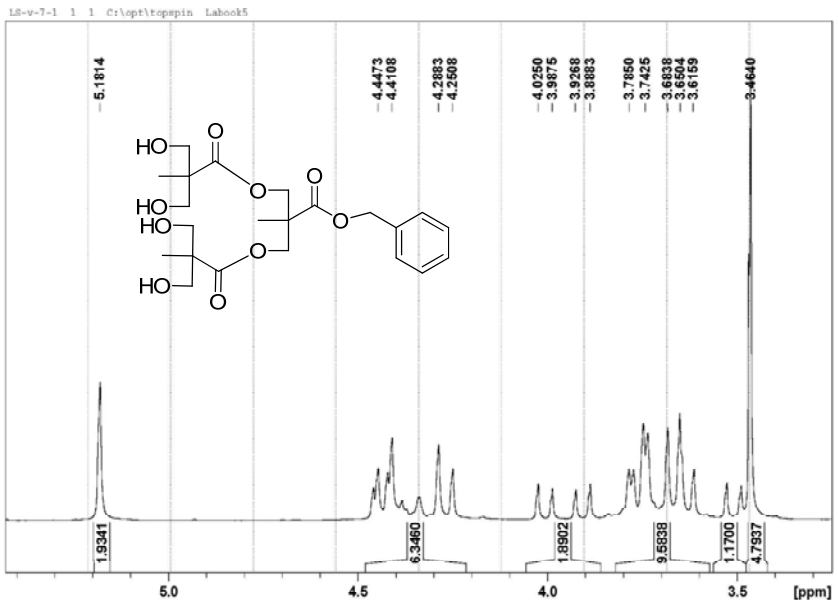

Figure B.8. NMR of G(1)-Dendron-Bn (2-(benzyloxycarbonyl)-2-methylpropane-bis(2,2,5-trimethyl-1,3-dioxane-5-carboxylate).

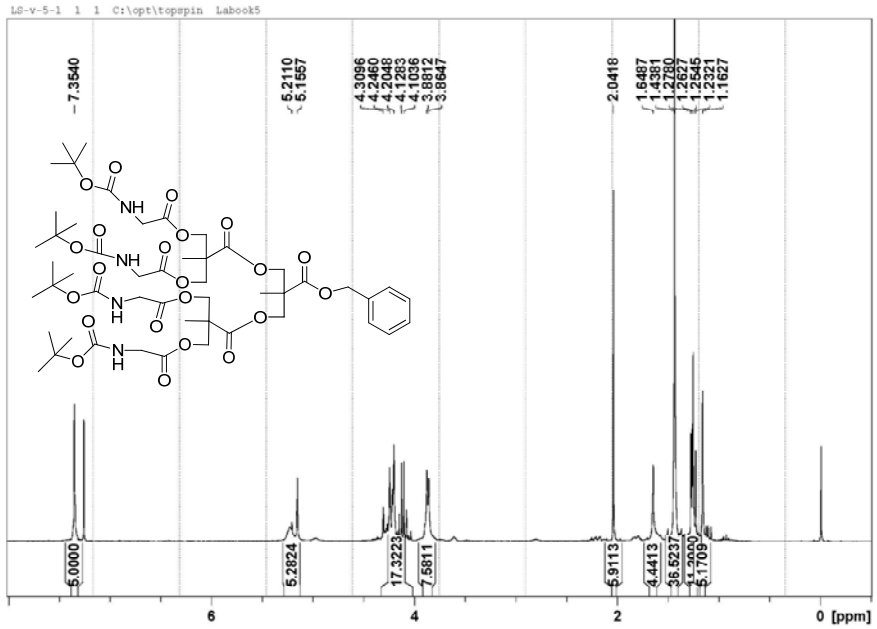

Figure B.9. NMR of Boc-Gly-Dendron-Bn (2-(benzyloxycarbonyl)-2-methylpropane-1,3-diyl bis[3-(2-tert-butoxycarbonylamino acetate)-2-((2-tert-butoxycarbonylamino acetate)-methyl)-2-methylpropanoate).

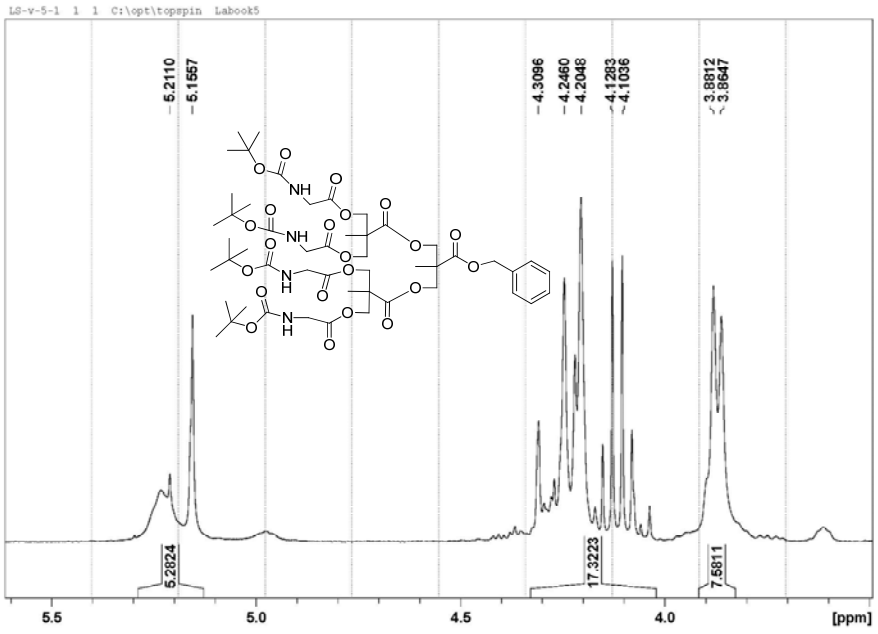

Figure B.10. Expanded NMR of Boc-Gly-Dendron-Bn (2-(benzyloxycarbonyl)-2-methylpropane-1,3-diyl bis[3-(2-tert-butoxycarbonylamino acetate)-2-((2-tert-butoxycarbonylamino acetate)-methyl)-2-methylpropanoate).

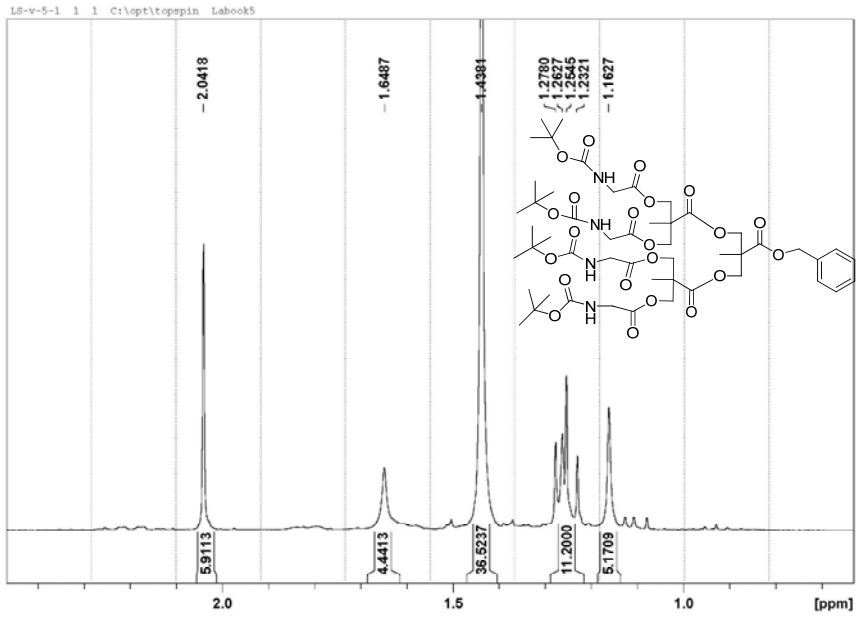

Figure B.11. Expanded NMR of Boc-Gly-Dendron-Bn (2-(benzyloxycarbonyl)-2-methylpropane-1,3-diyl bis[3-(2-tert-butoxycarbonylamino acetate)-2-((2-tert-butoxycarbonylamino acetate)-methyl)-2-methylpropanoate).

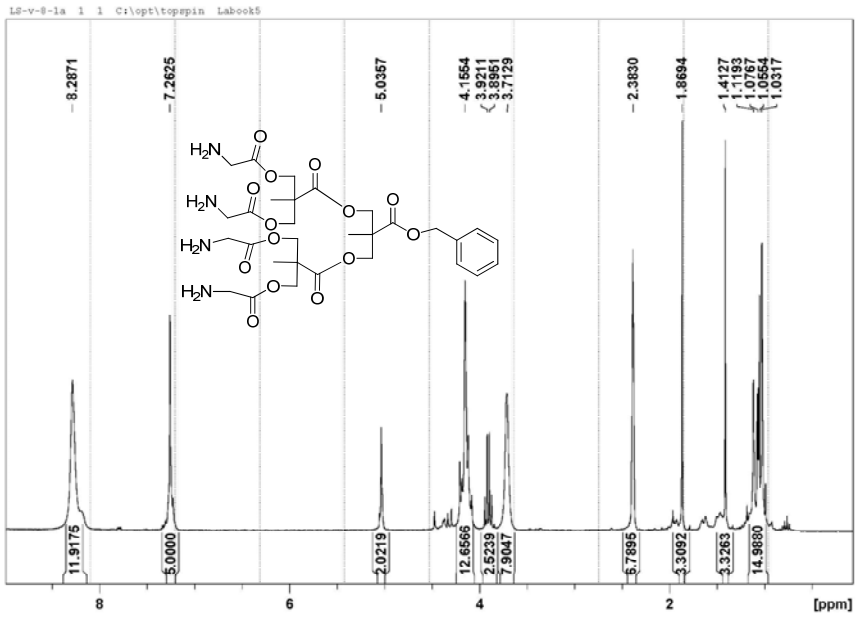

Figure B.12. NMR spectra of H_2N-Gly-Dendron-Bn (2-(benzyloxycarbonyl)-2-methylpropane-1,3-diyl bis[3-(2-amino acetate)-2-((2-amino acetate)-methyl)-2-methylpropanoate).

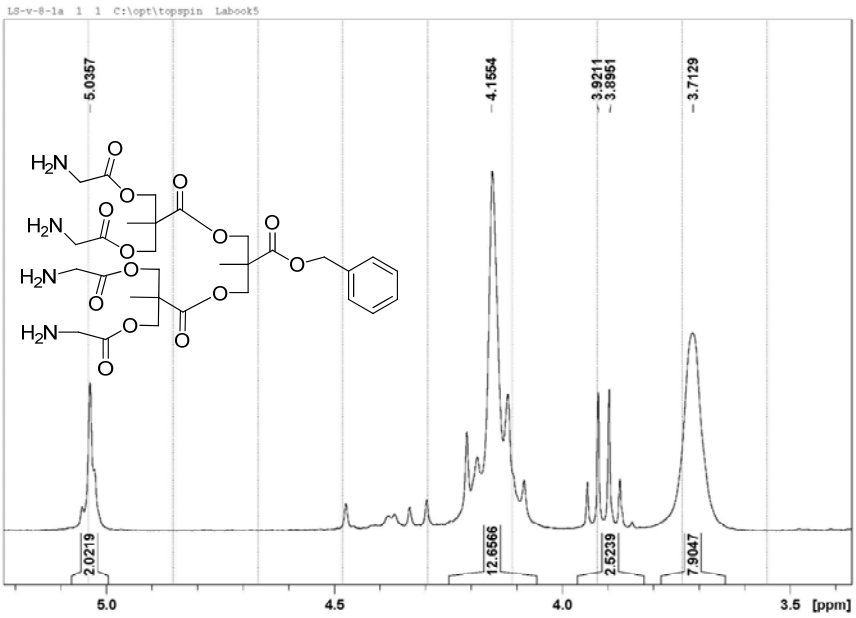

Figure B.13. Expanded NMR spectra of H_2N-Gly-Dendron-Bn (2-(benzyloxycarbonyl)-2-methylpropane-1,3-diyl bis[3-(2-amino acetate)-2-((2-amino acetate)-methyl)-2-methylpropanoate).

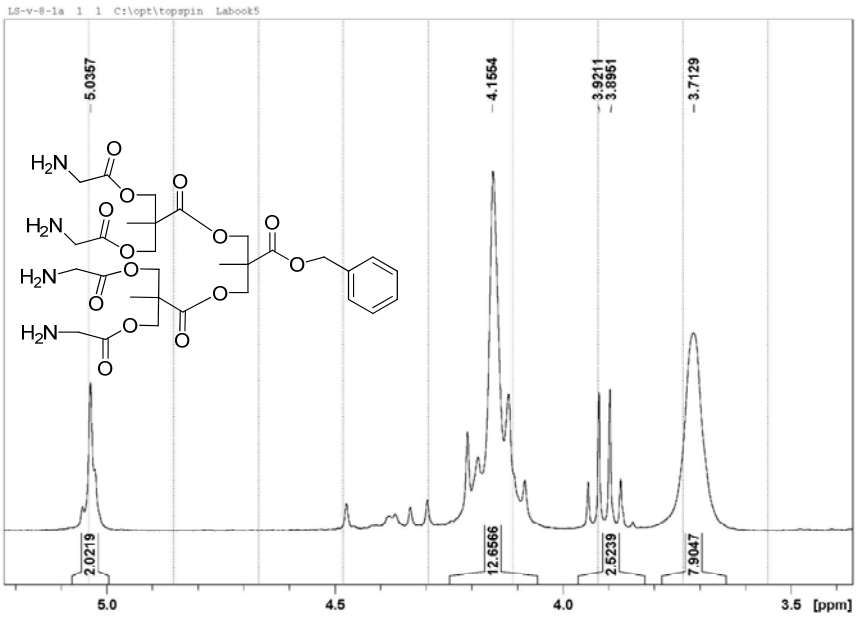

Figure B.14. Expanded NMR spectra of H_2N-Gly-Dendron-Bn (2-(benzyloxycarbonyl)-2-methylpropane-1,3-diyl bis[3-(2-amino acetate)-2-((2-amino acetate)-methyl)-2-methylpropanoate).

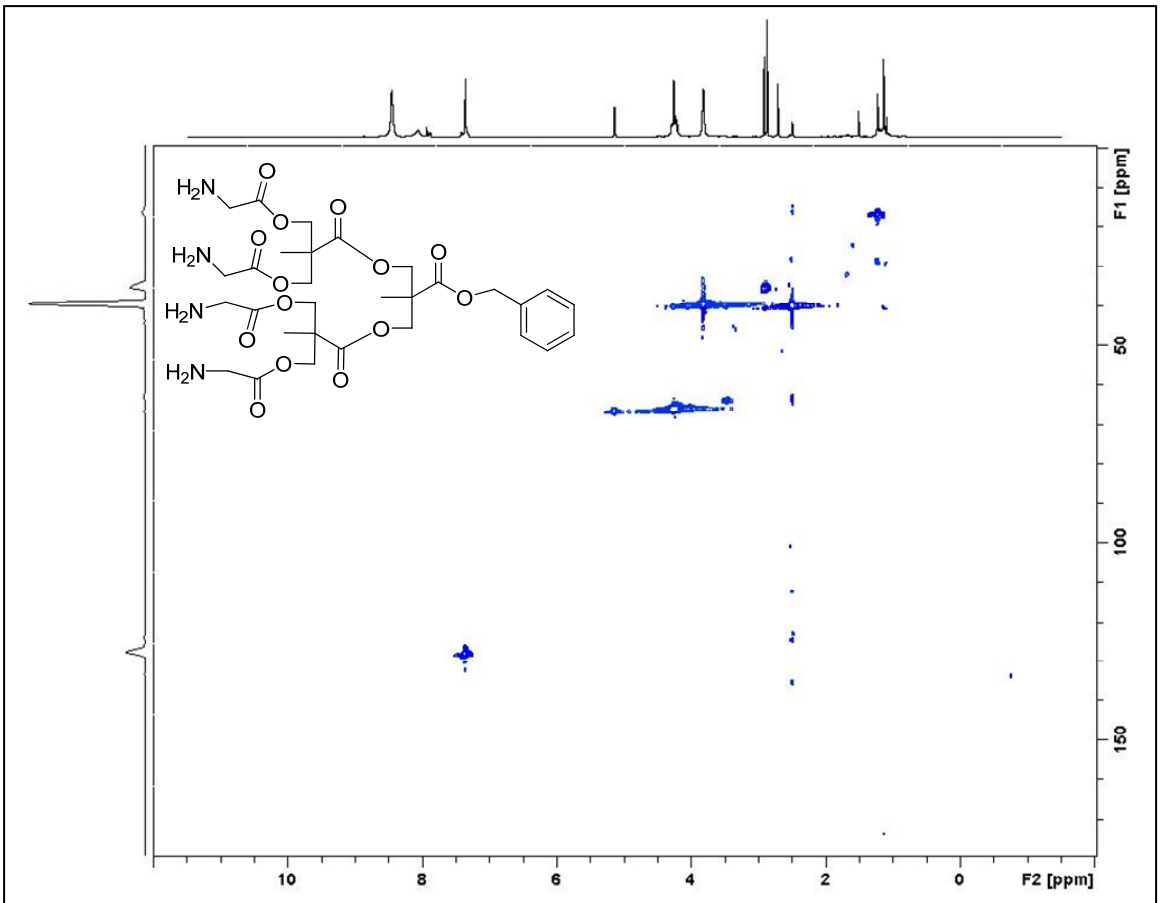

Figure B.15. HSQC NMR spectra of H_2N-Gly-Dendron-Bn (2-(benzyloxycarbonyl)-2-methylpropane-1,3-diyl bis[3-(2-amino acetate)-2-((2-amino acetate)-methyl)-2-methylpropanoate).

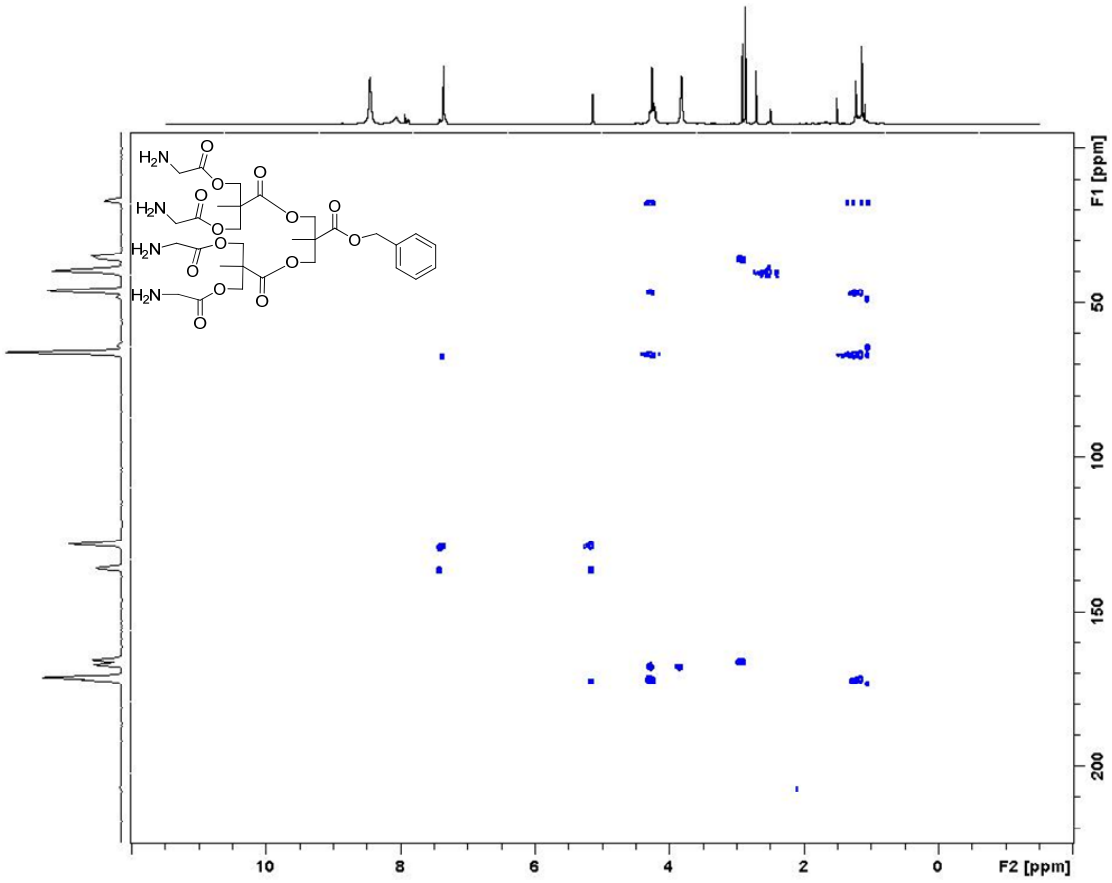

Figure B.16. HMBC NMR spectra of H_2N-Gly-Dendron-Bn (2-(benzyloxycarbonyl)-2-methylpropane-1,3-diyl bis[3-(2-amino acetate)-2-((2-amino acetate)-methyl)-2-methylpropanoate).

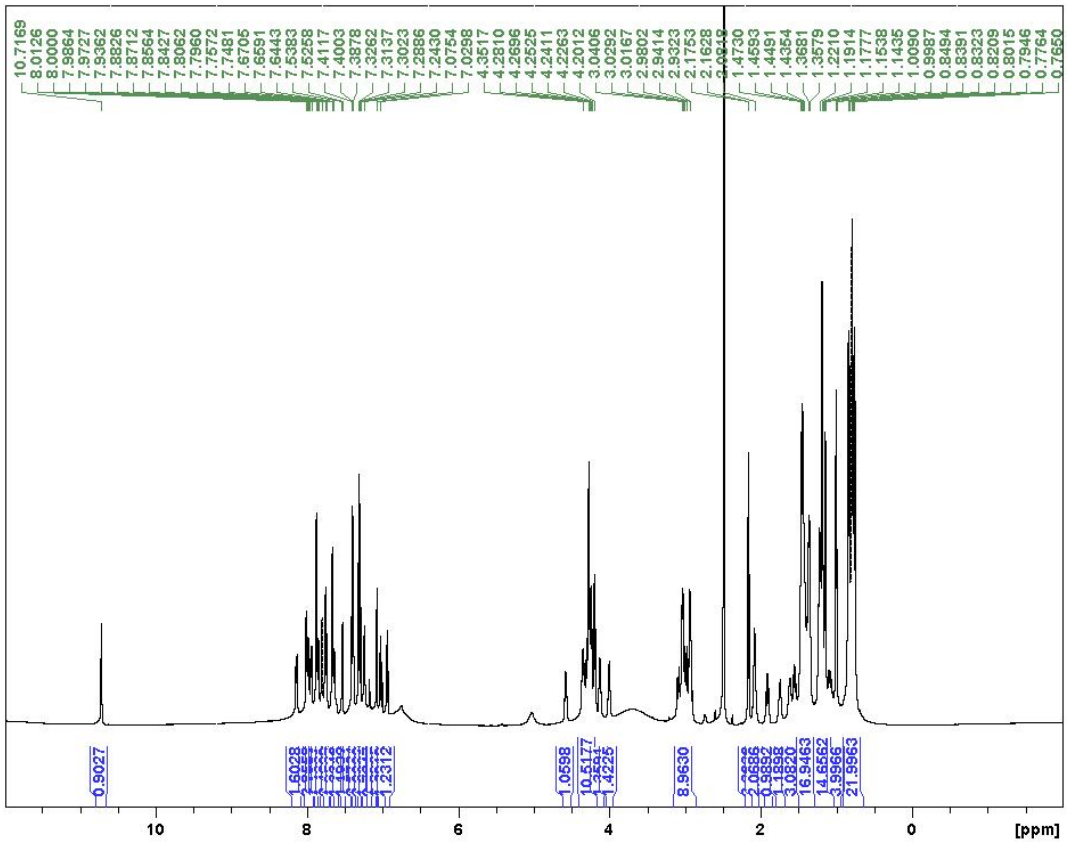

Figure B.17. ^{1}H NMR of Fmoc-AVRWLLTA.

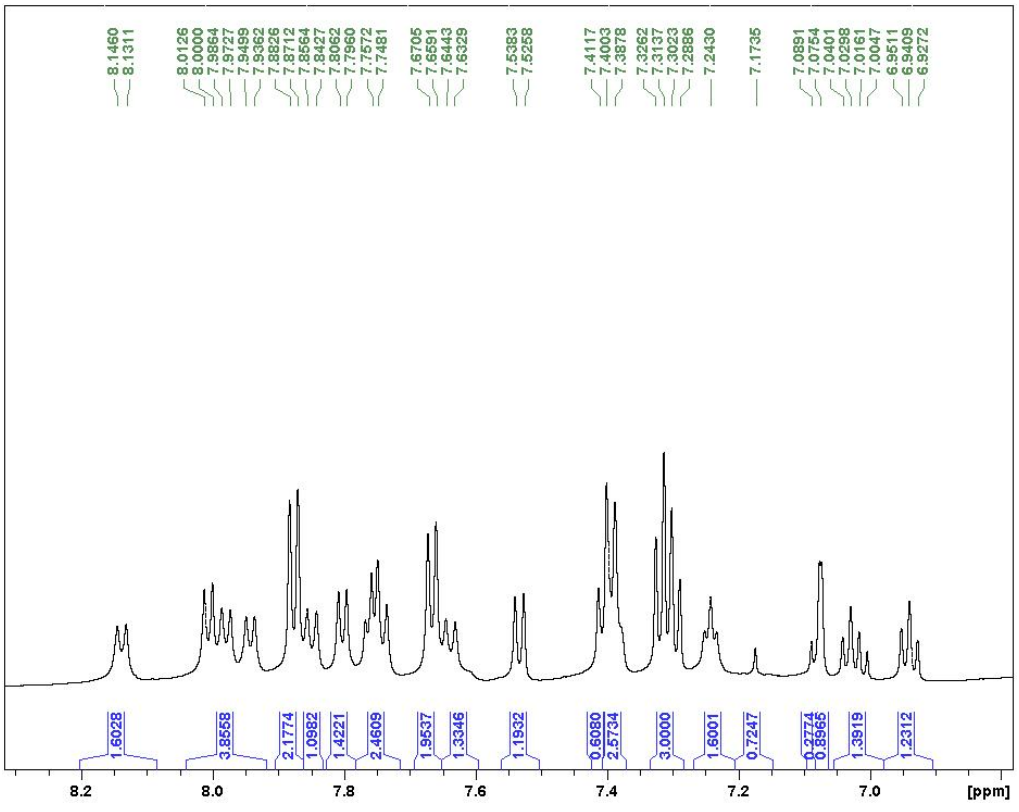

Figure B.18. Expanded ^{1}H NMR of Fmoc-AVRWLLTA.

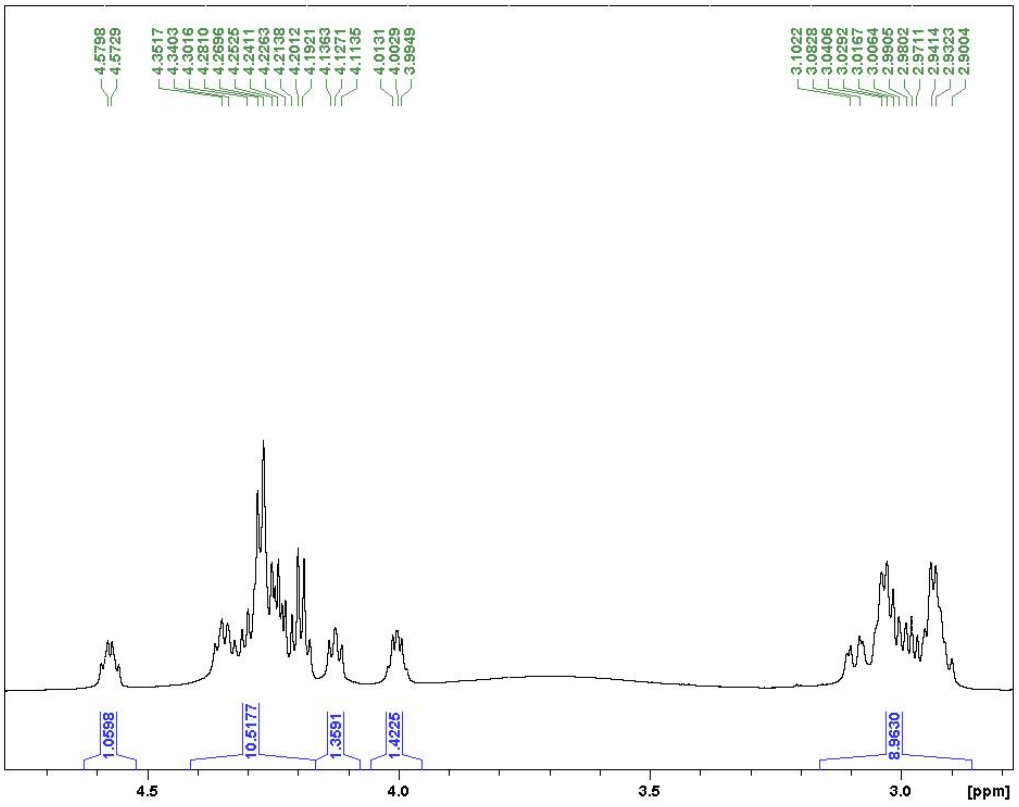

Figure B.19. Expanded ^{1}H NMR of Fmoc-AVRWLLTA.

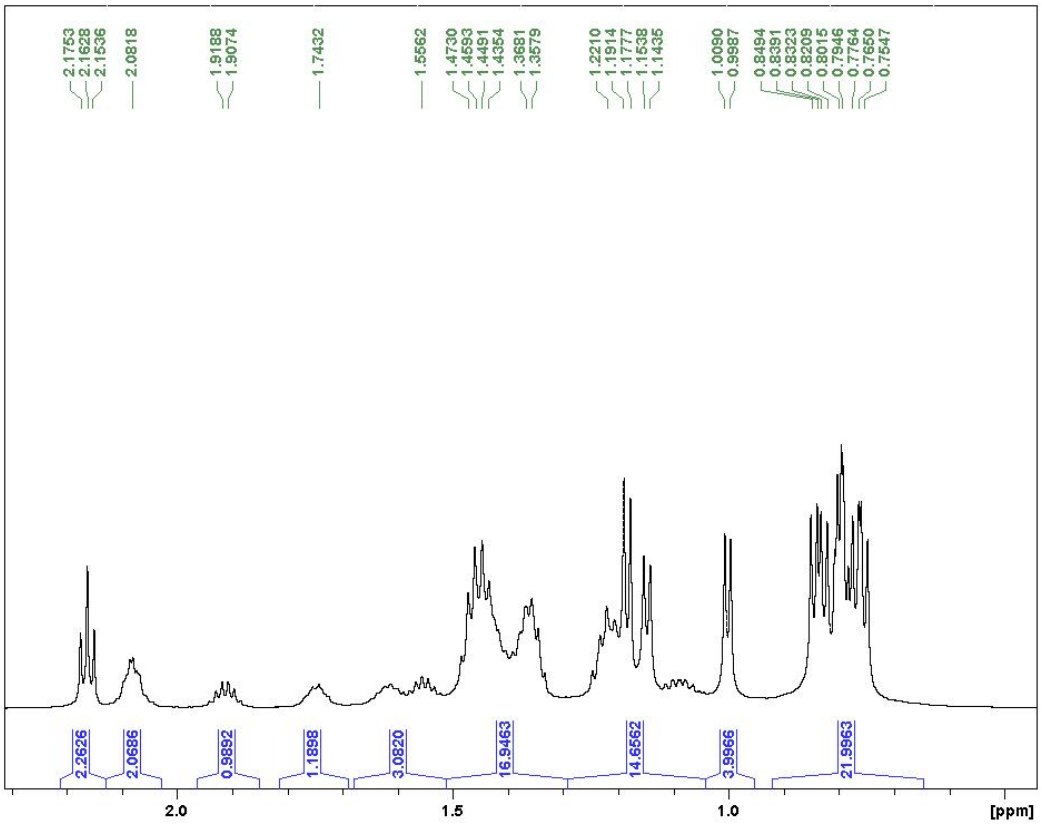

Figure B.20. Expanded ^{1}H NMR of Fmoc-AVRWLLTA.

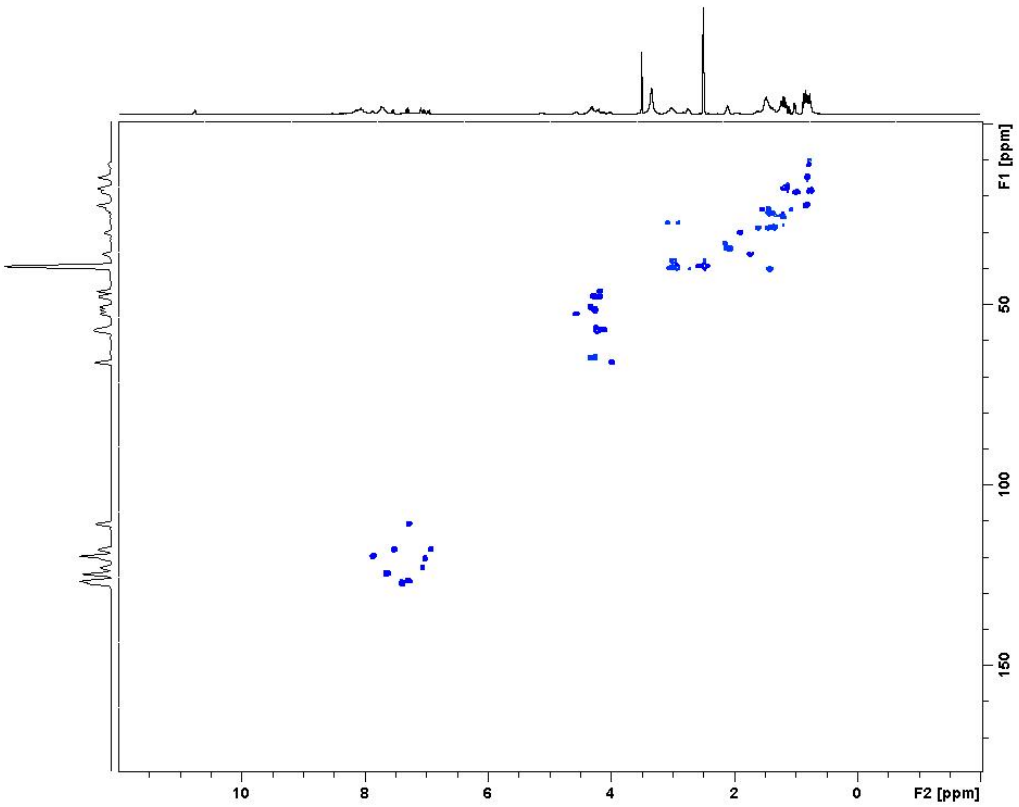

Figure B.21. HSQC NMR of Fmoc-AVRWLLTA.

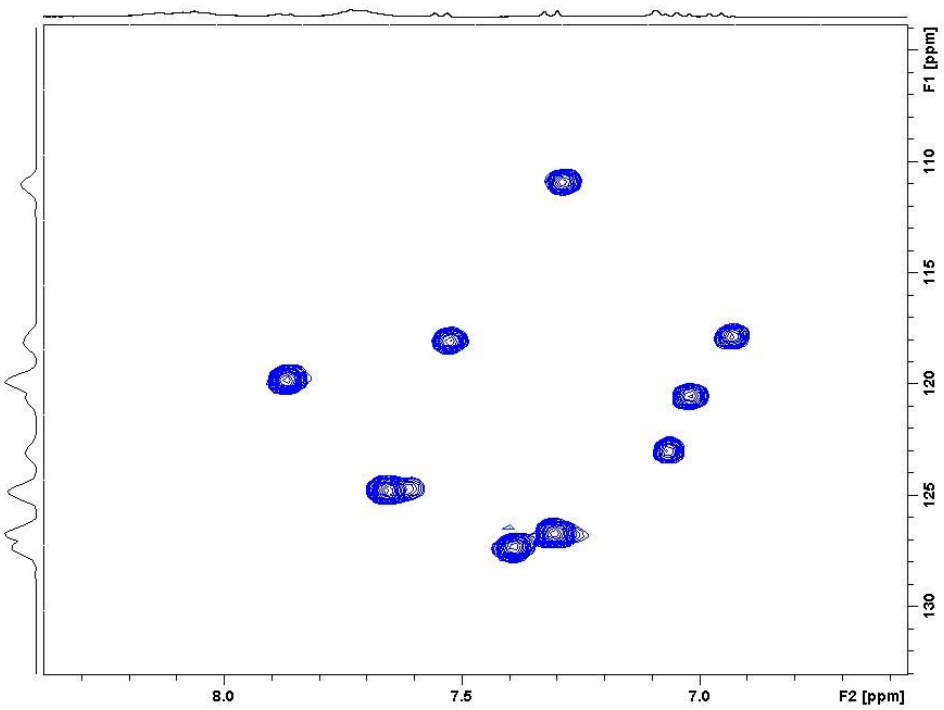

Figure B.22. Expanded HSQC NMR of Fmoc-AVRWLLTA.

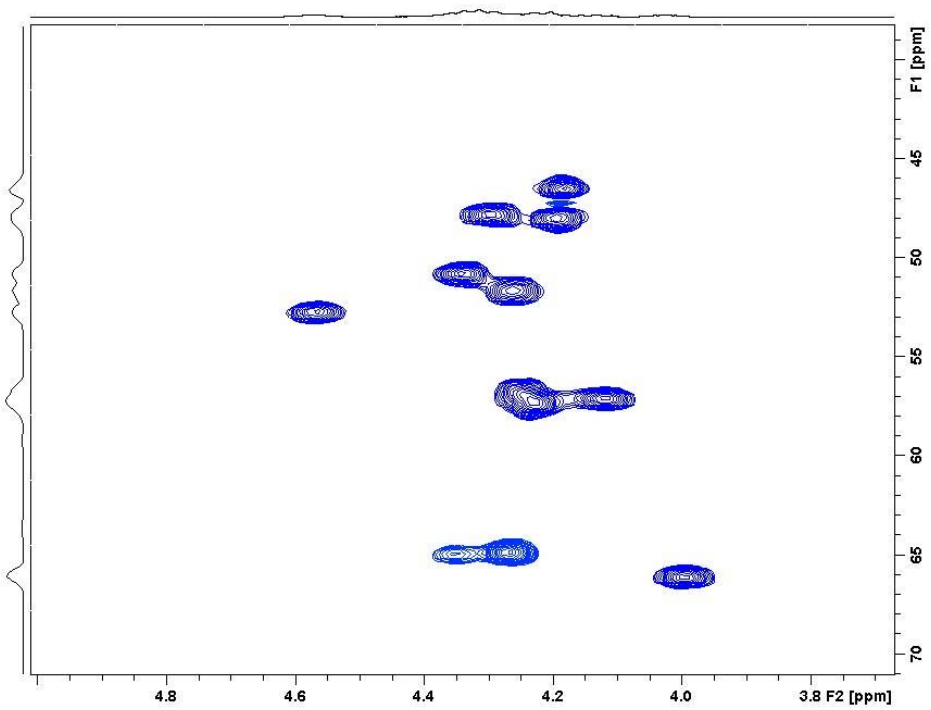

Figure B.23. Expanded HSQC NMR of Fmoc-AVRWLLTA.

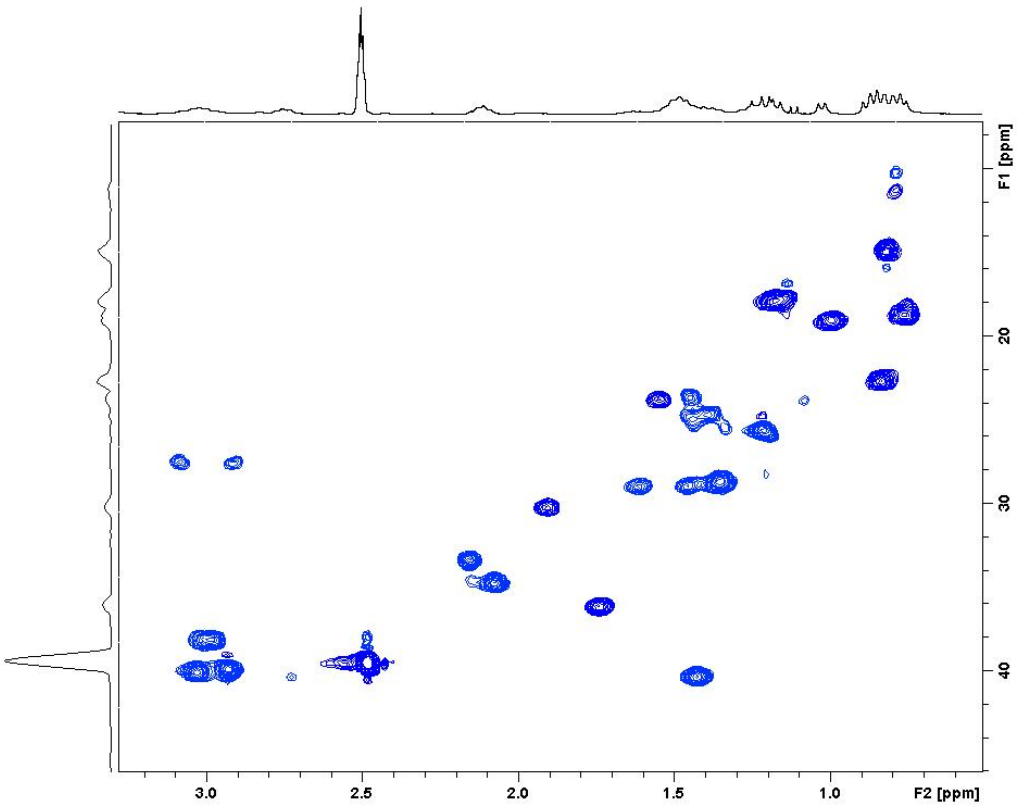

Figure B.24. Expanded HSQC NMR of Fmoc-AVRWLLTA

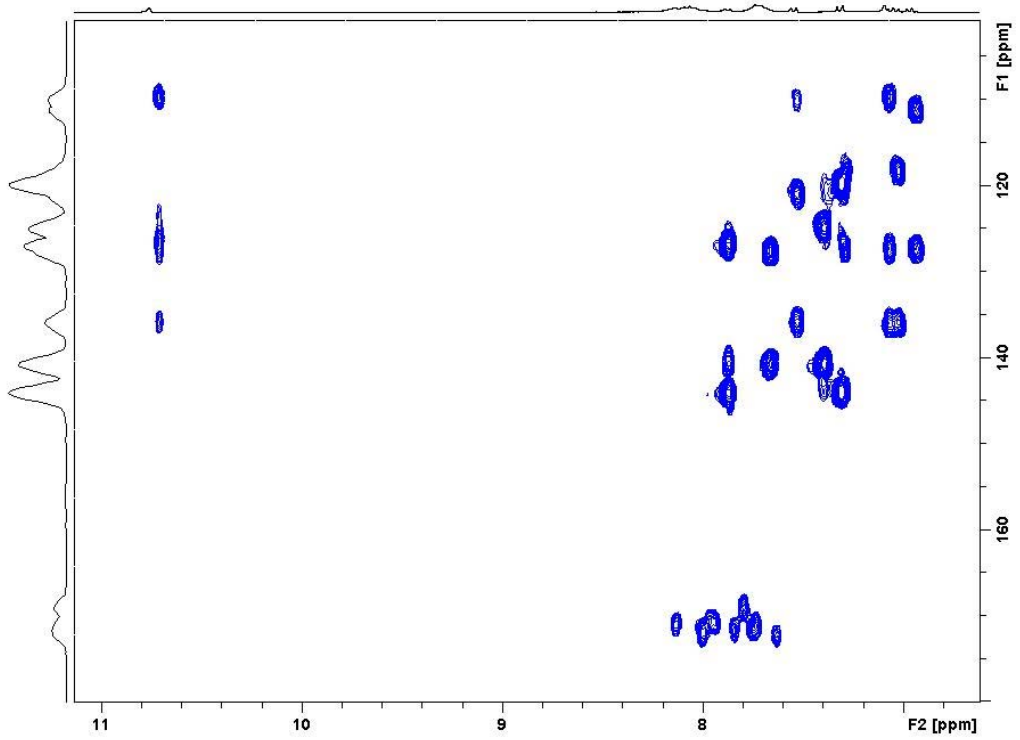

Figure B.25. Expanded HMBC NMR of Fmoc-AVRWLLTA

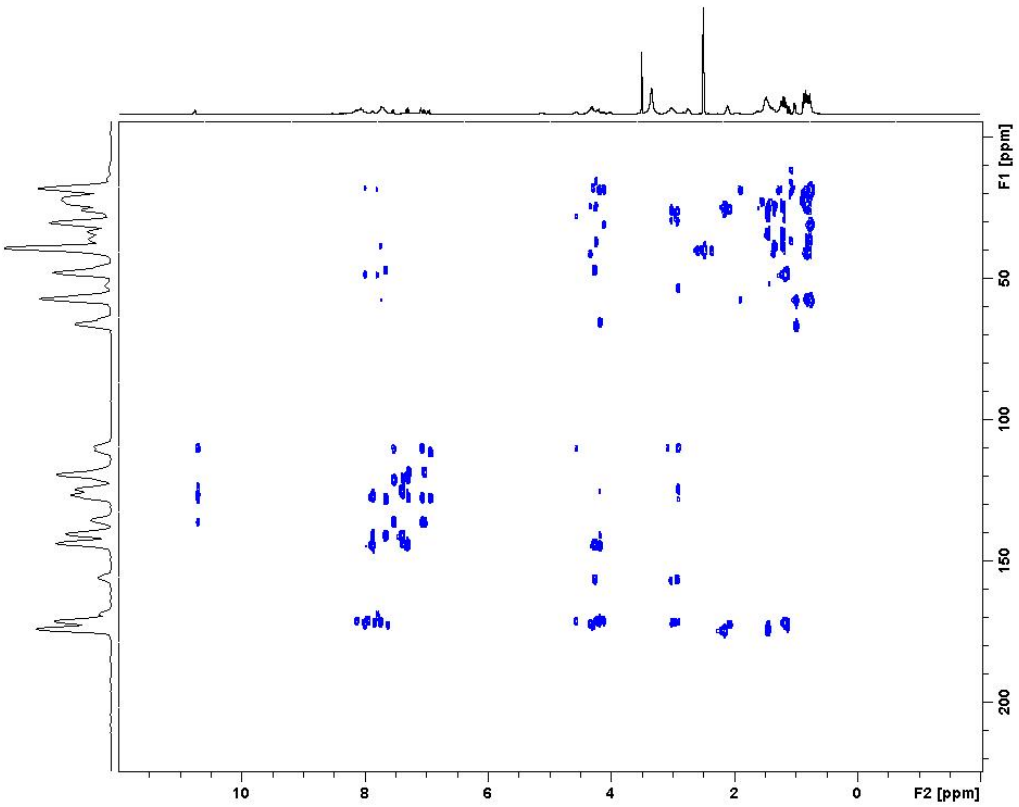

Figure B.26. HMBC NMR of Fmoc-AVRWLLTA

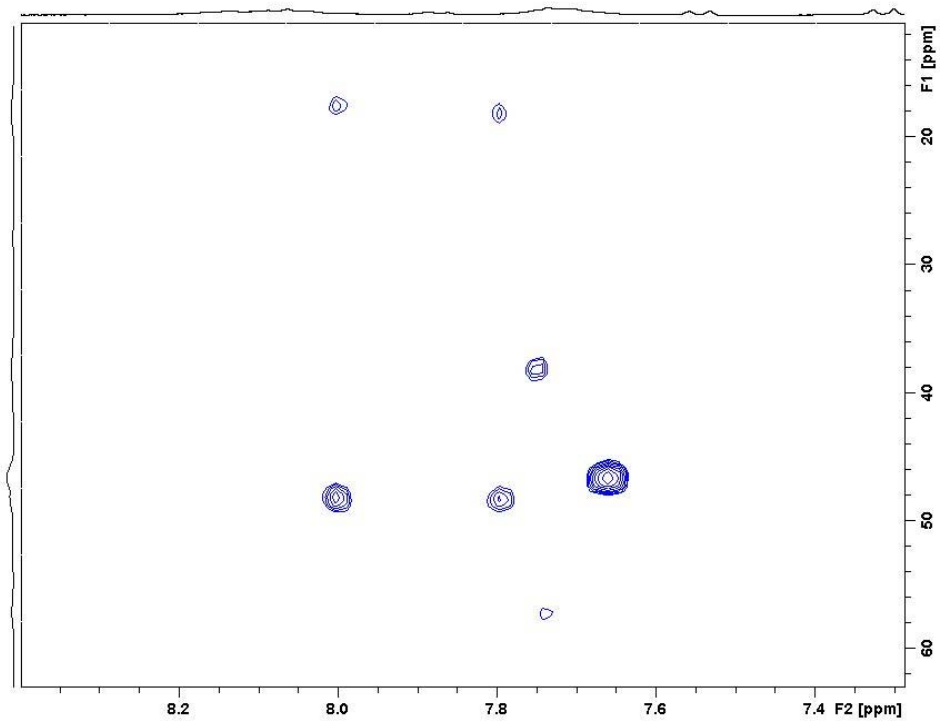

Figure B.27. Expanded HMBC NMR of Fmoc-AVRWLLTA

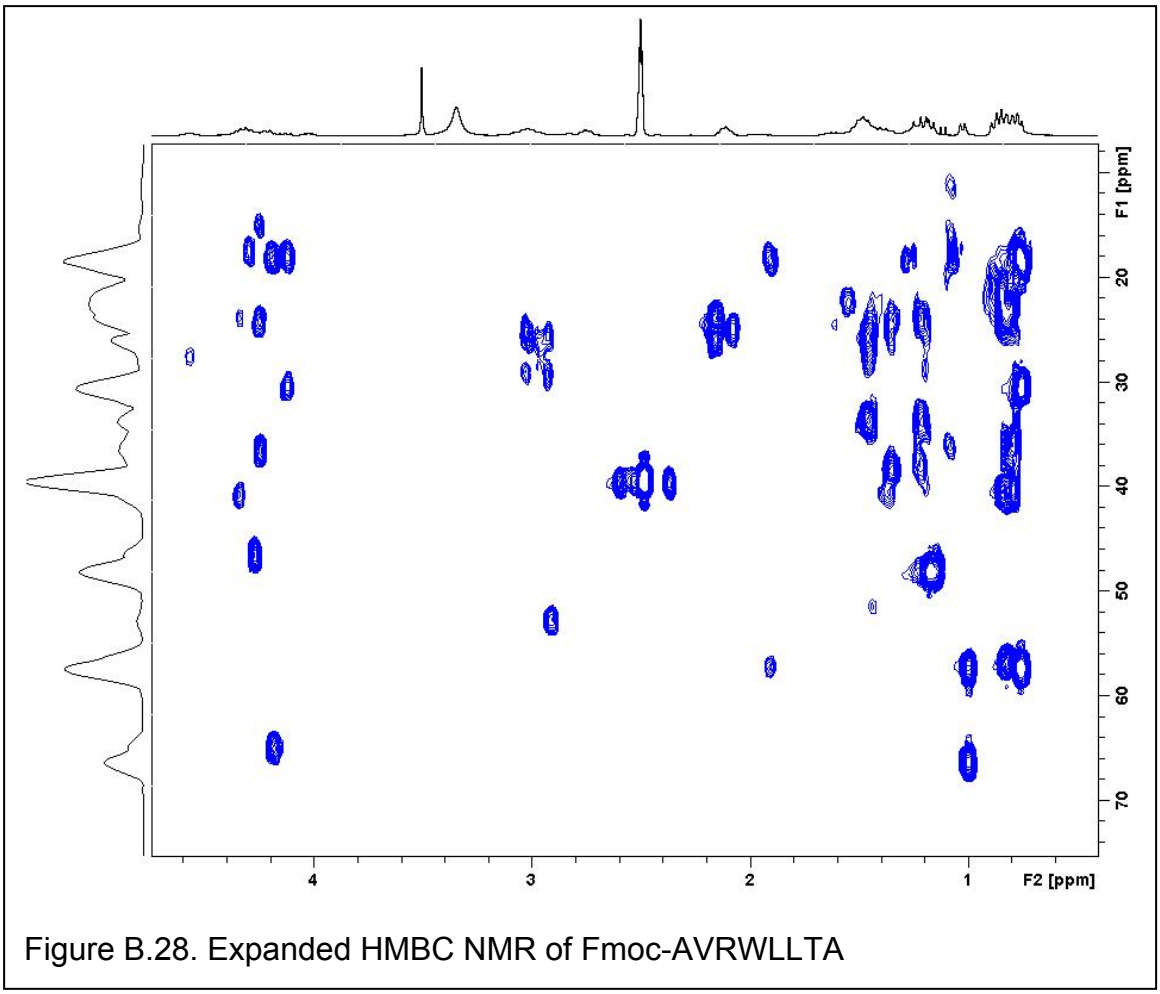

Figure B.28. Expanded HMBC NMR of Fmoc-AVRWLLTA

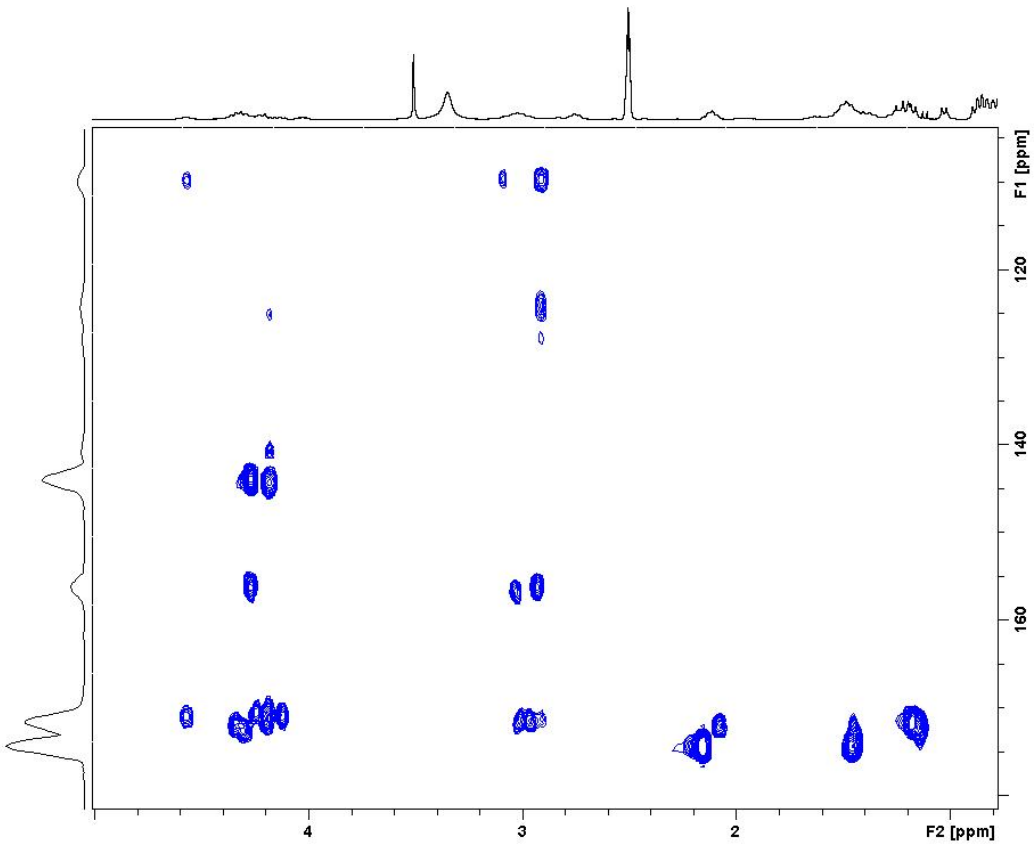

Figure B.29. Expanded HMBC NMR of Fmoc-AVRWLLTA

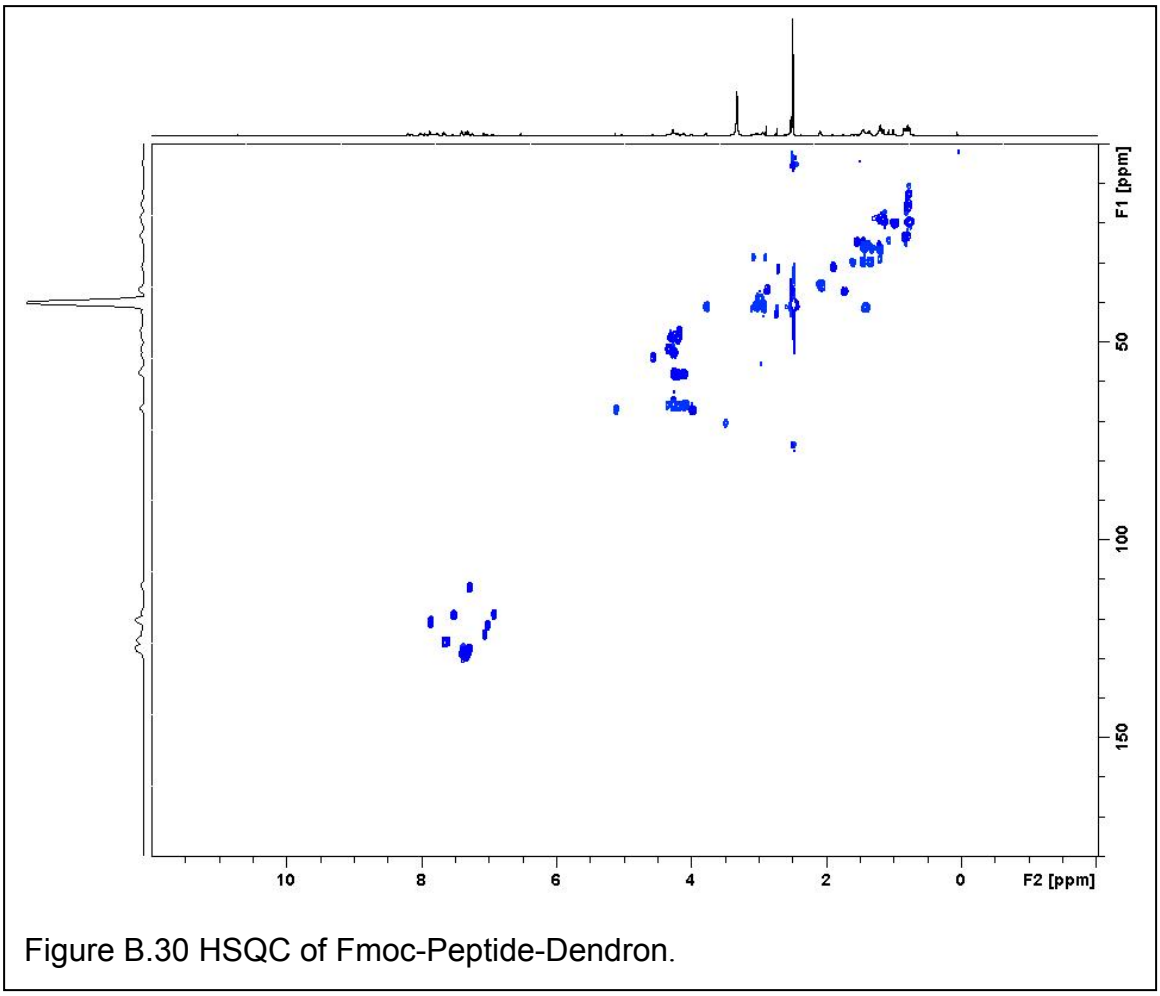

Figure B.30 HSQC of Fmoc-Peptide-Dendron.

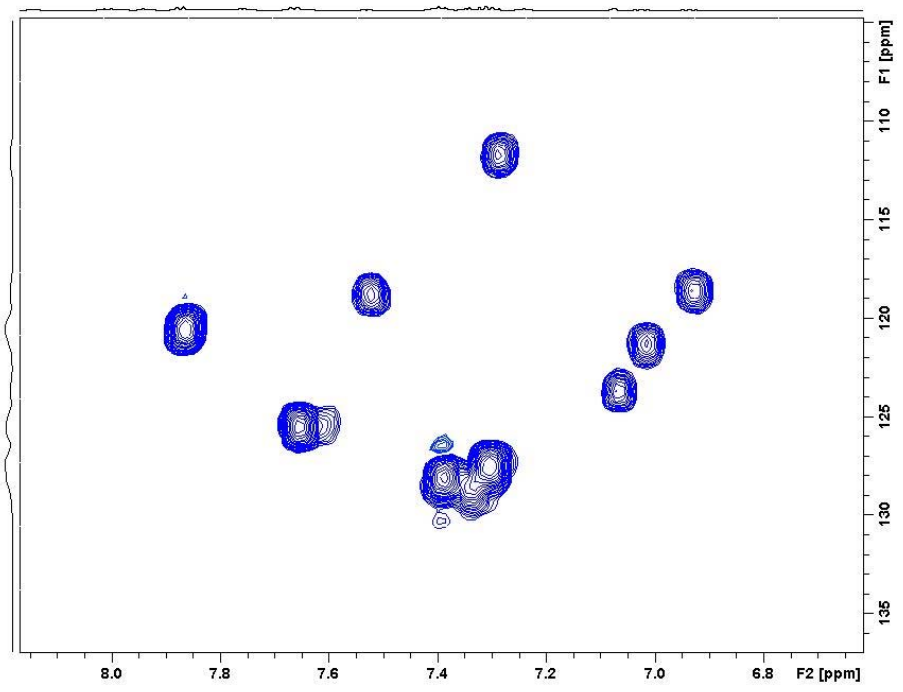

Figure B.31 Expanded HSQC of Fmoc-Peptide-Dendron

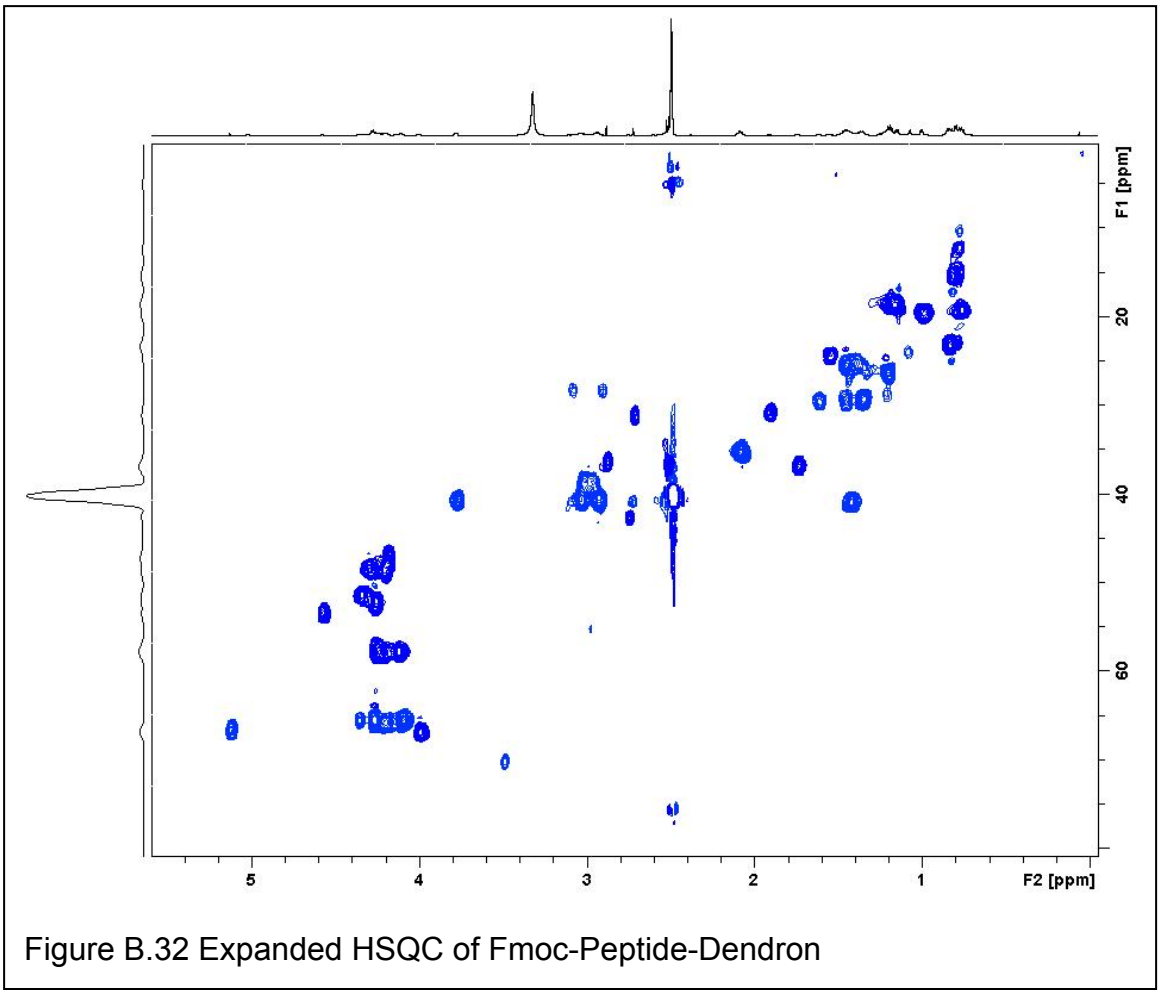

Figure B.32 Expanded HSQC of Fmoc-Peptide-Dendron

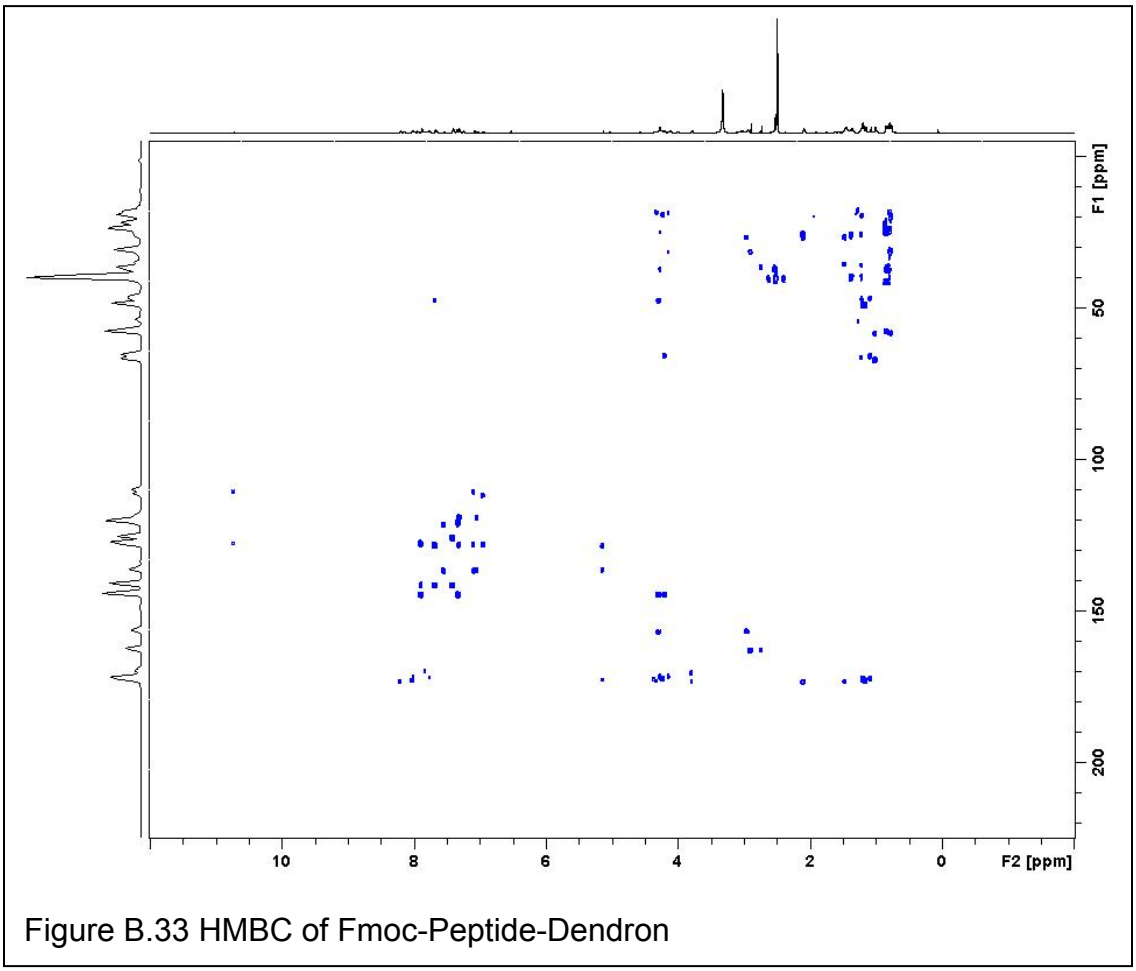

Figure B.33 HMBC of Fmoc-Peptide-Dendron

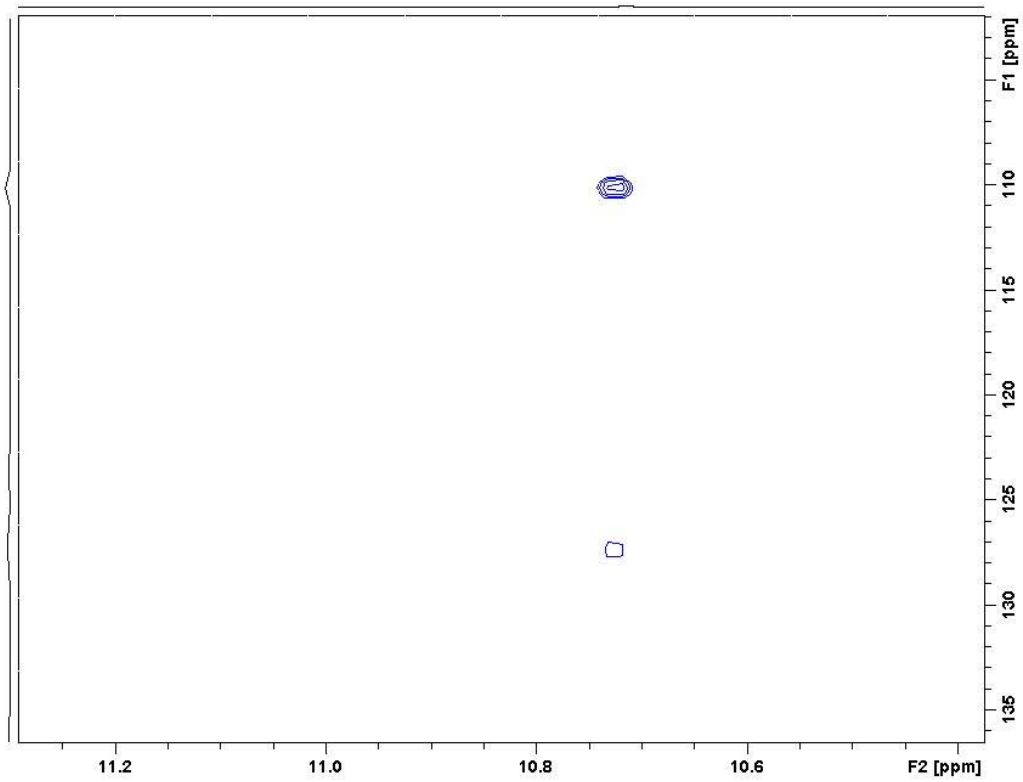

Figure B.34 Expanded HMBC of Fmoc-Peptide-Dendron

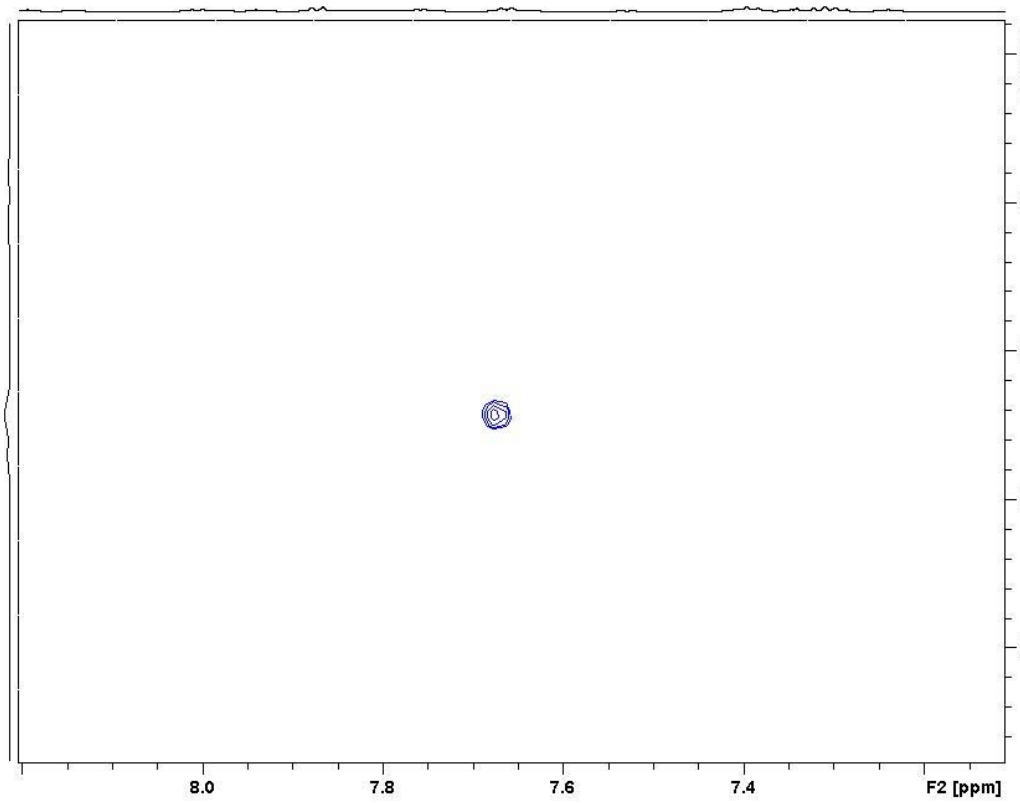

Figure B.35 Expanded HMBC of Fmoc-Peptide-Dendron

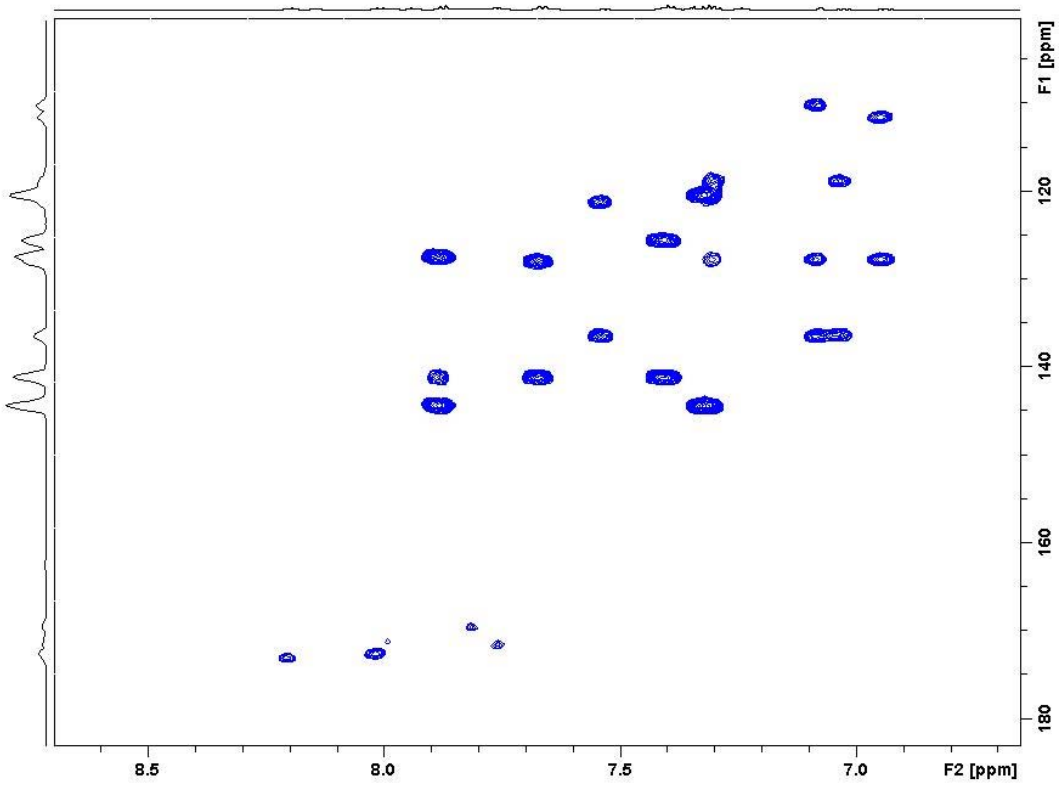

Figure B.36 Expanded HMBC of Fmoc-Peptide-Dendron

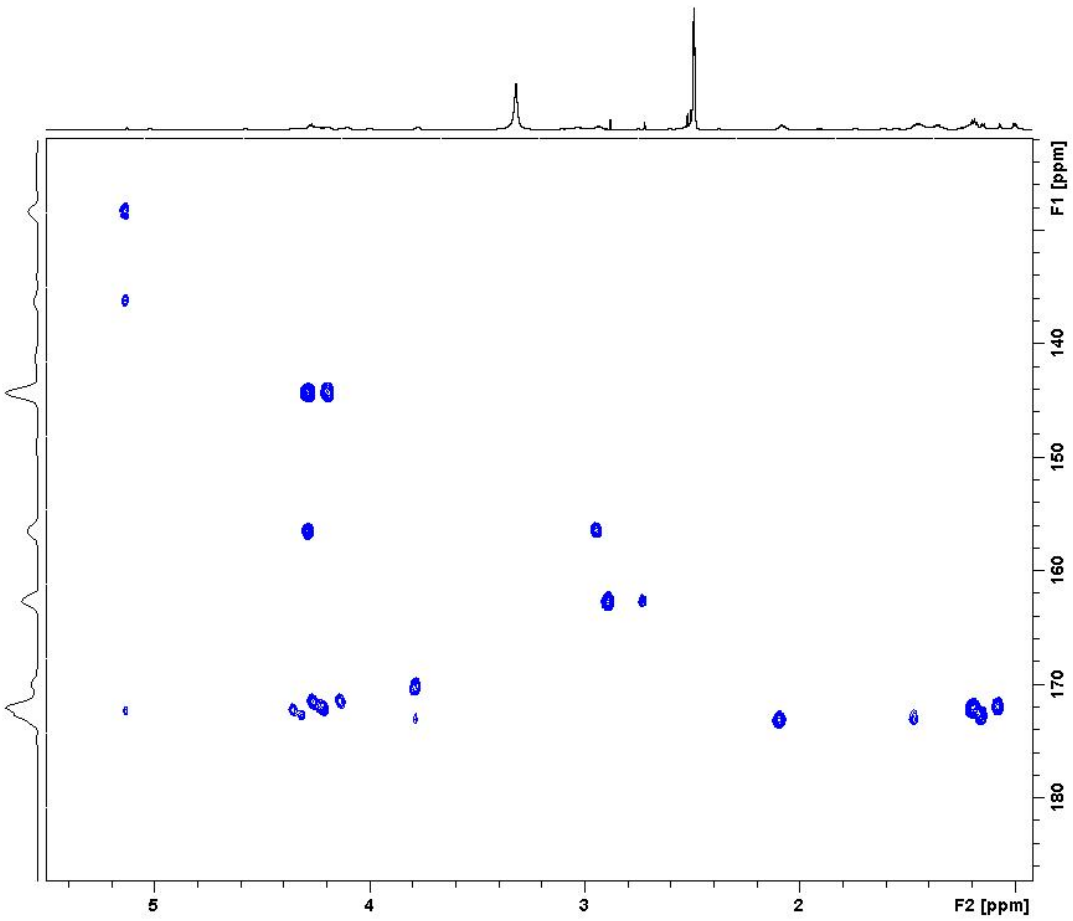

Figure B.37 Expanded HMBC of Fmoc-Peptide-Dendron

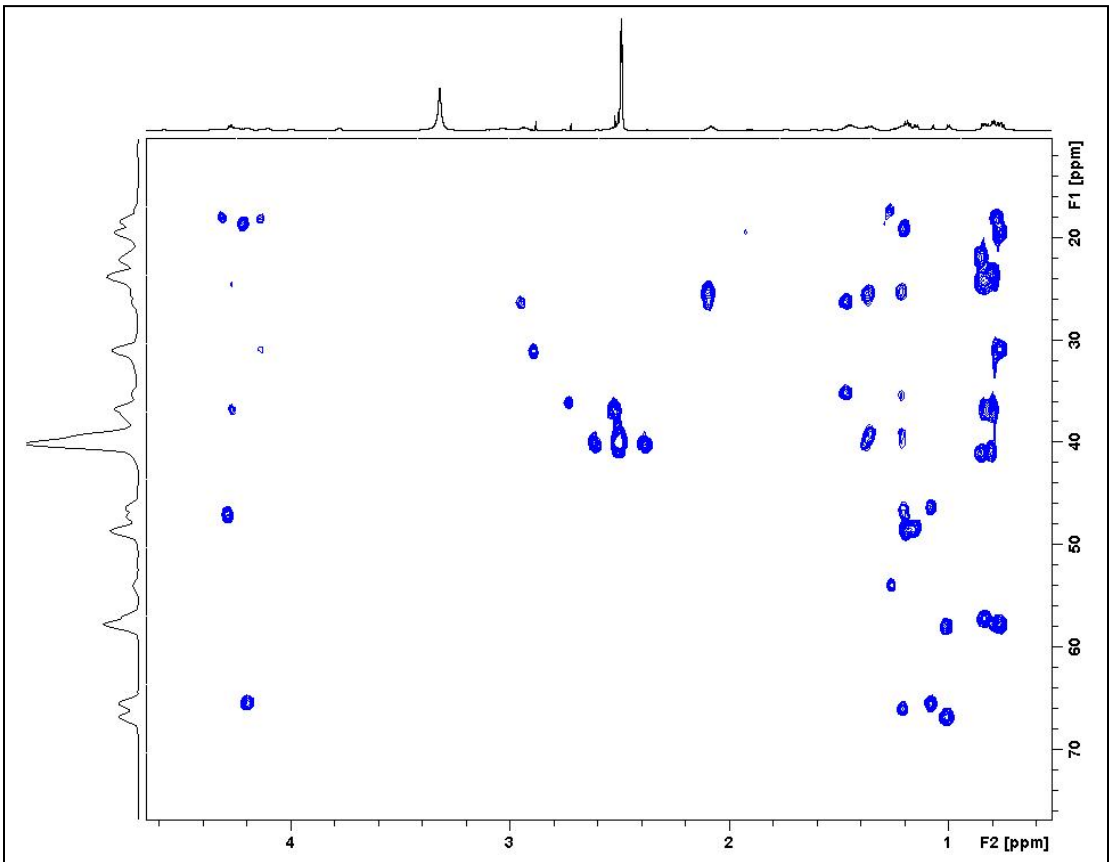

Figure B.38 Expanded HMBC of Fmoc-Peptide-Dendron

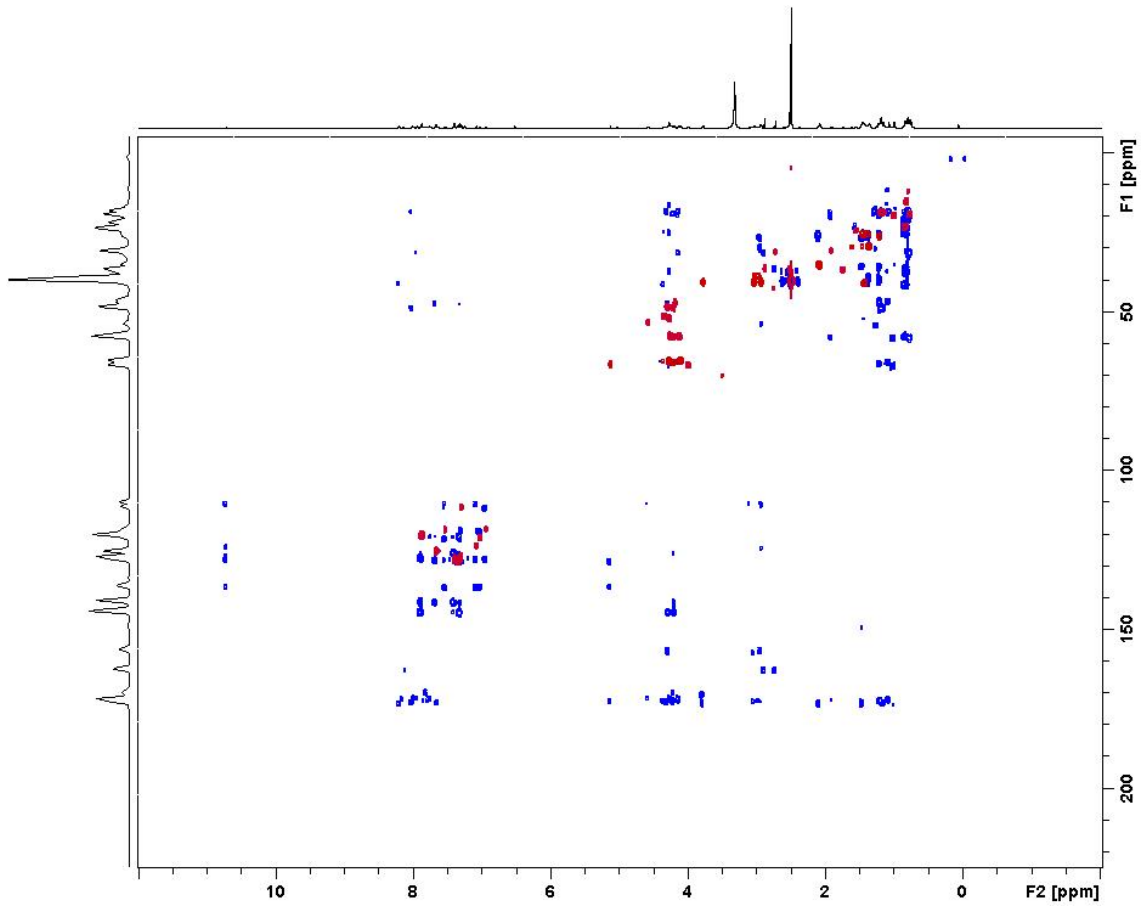

Figure B.39 HMBC & HSQC overlay of Fmoc-Peptide-Dendron.

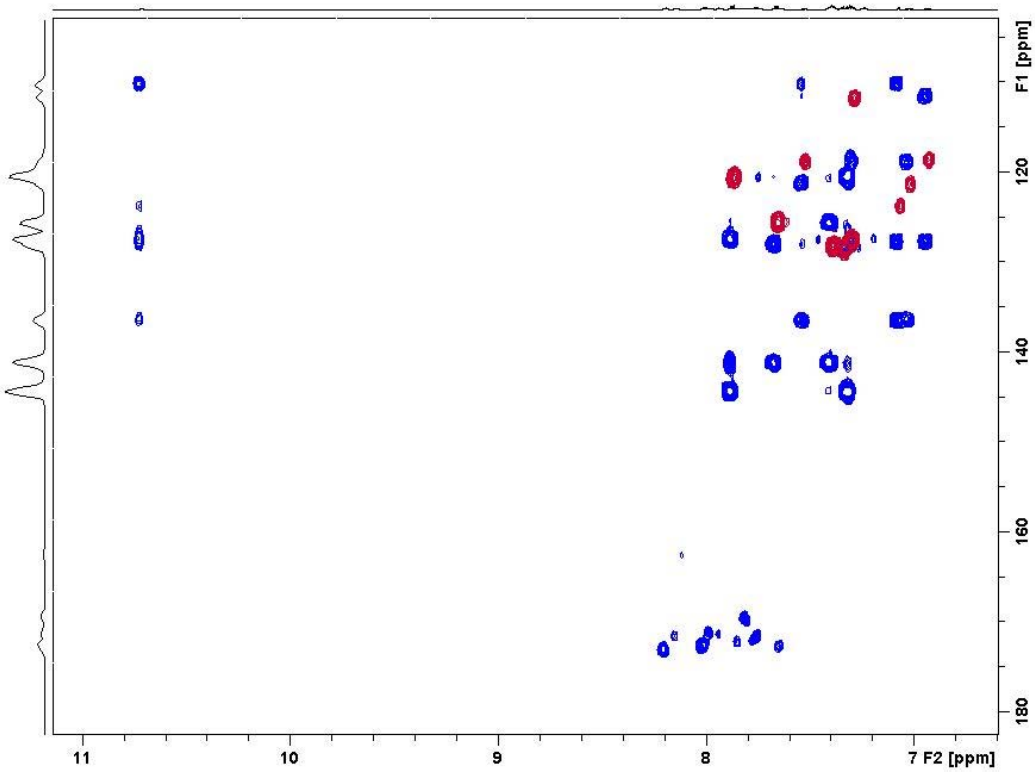

Figure B.40 Expanded HMBC & HSQC overlay of Fmoc-Peptide-Dendron.

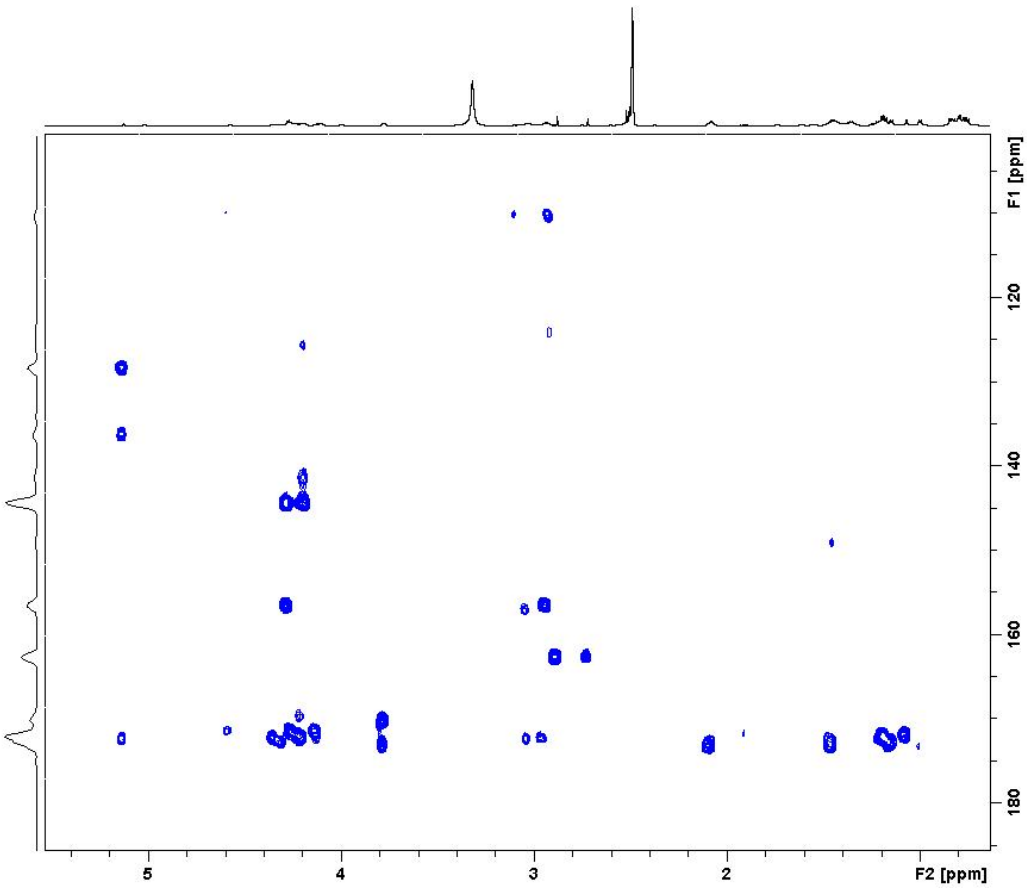

Figure B.41 Expanded HMBC & HSQC overlay of Fmoc-Peptide-Dendron.

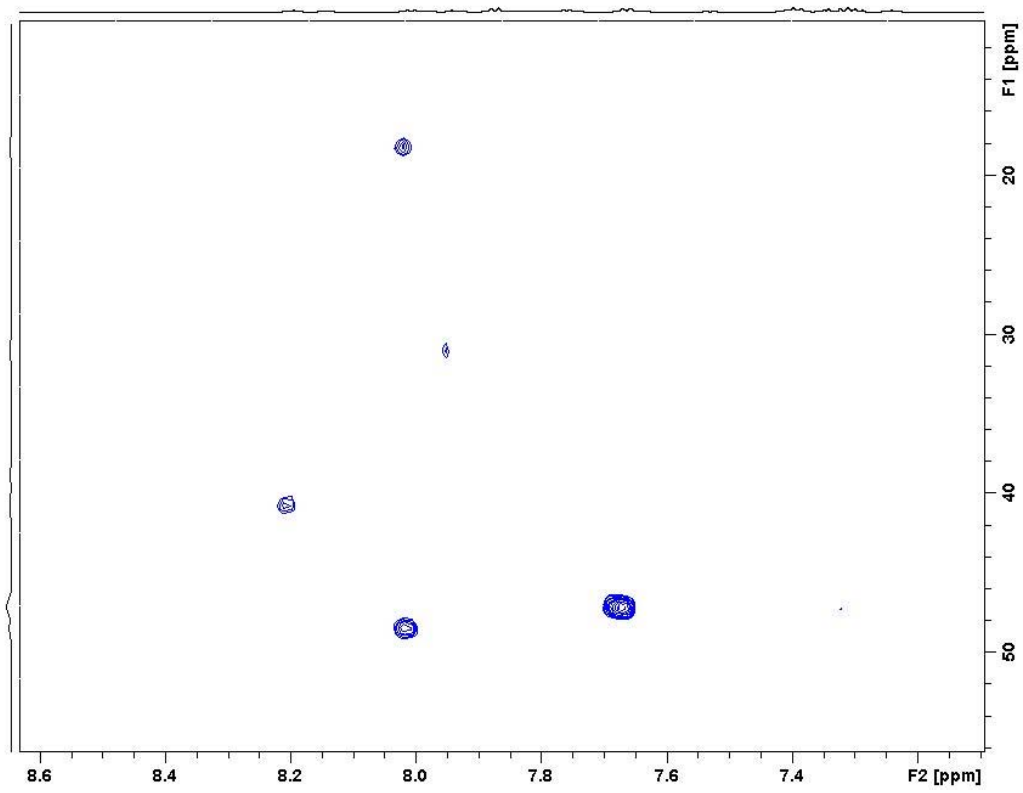

Figure B.42 Expanded HMBC & HSQC overlay of Fmoc-Peptide-Dendron.

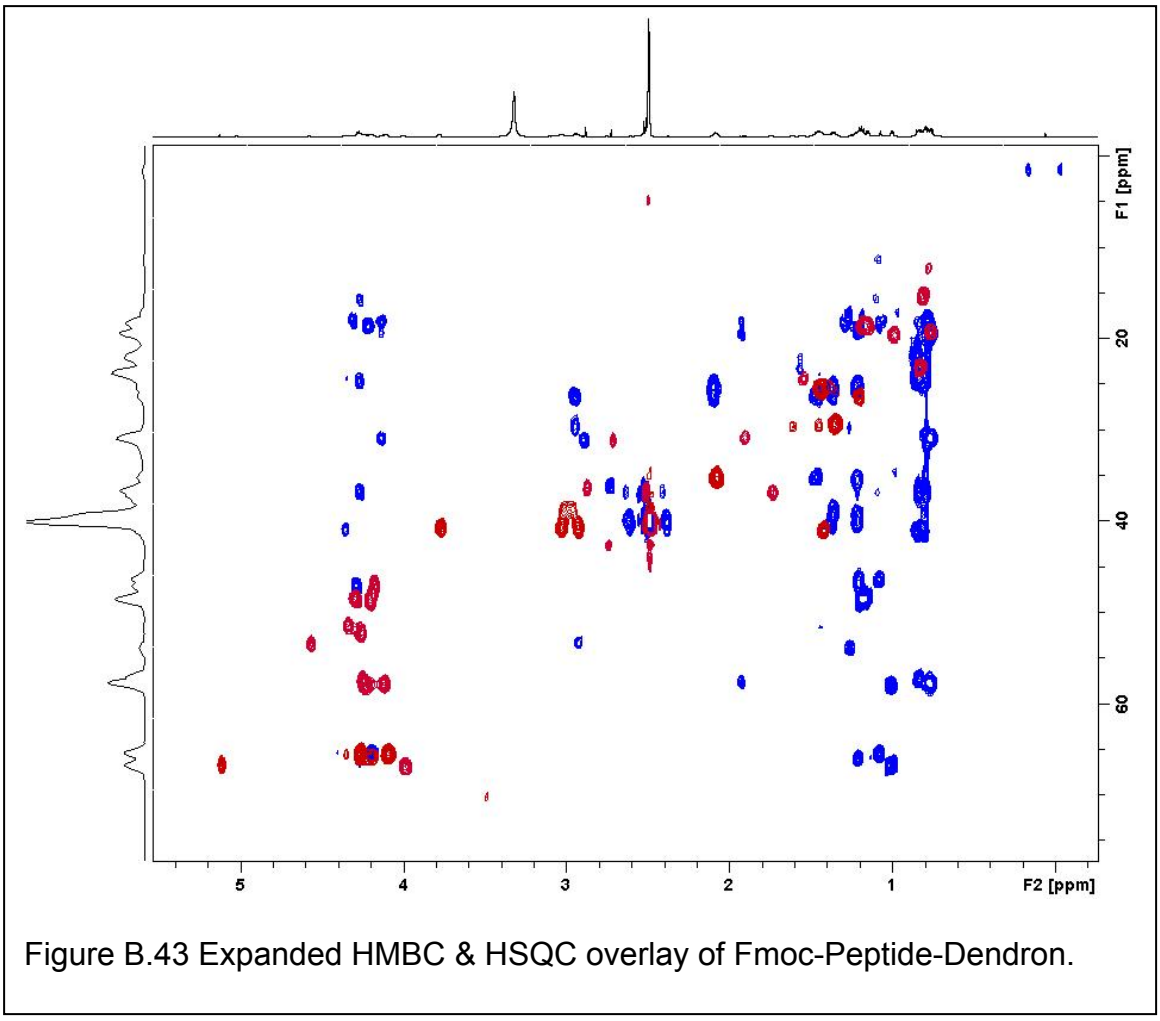

Figure B.43 Expanded HMBC & HSQC overlay of Fmoc-Peptide-Dendron.

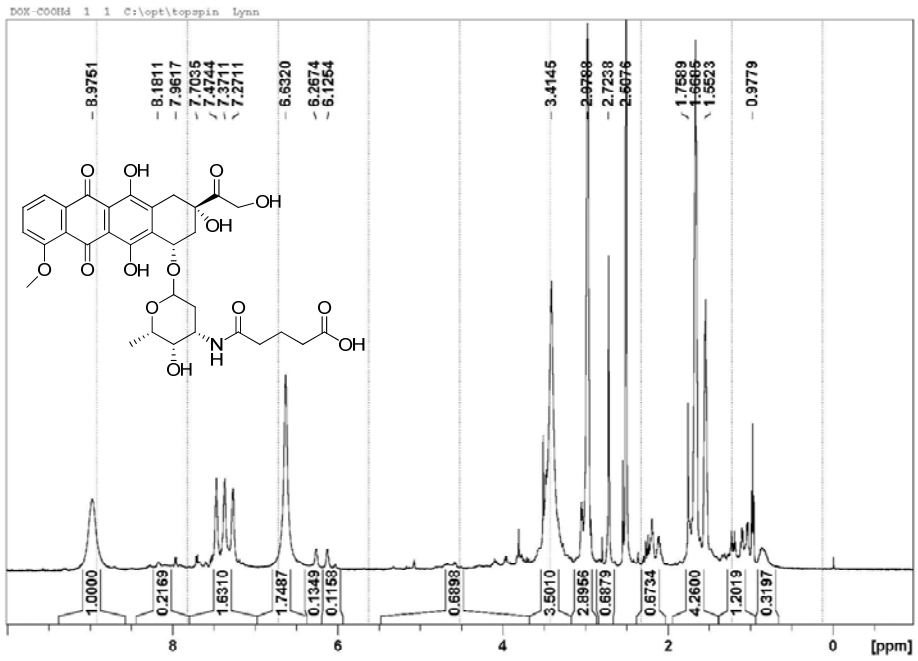

Figure B.44 ^{1}H NMR of DOX-COOH (5-(3-hydroxy-2-methyl-6-(3,5,12-trihydroxy-3-(2-hydroxyacetyl)-10-methoxy-6,11-dioxo-1,2,3,4,6,11-hexahydrotetracen-1-yl)tetrahydro-2H-pyran-4-ylamino)-5-oxopentanoic acid).

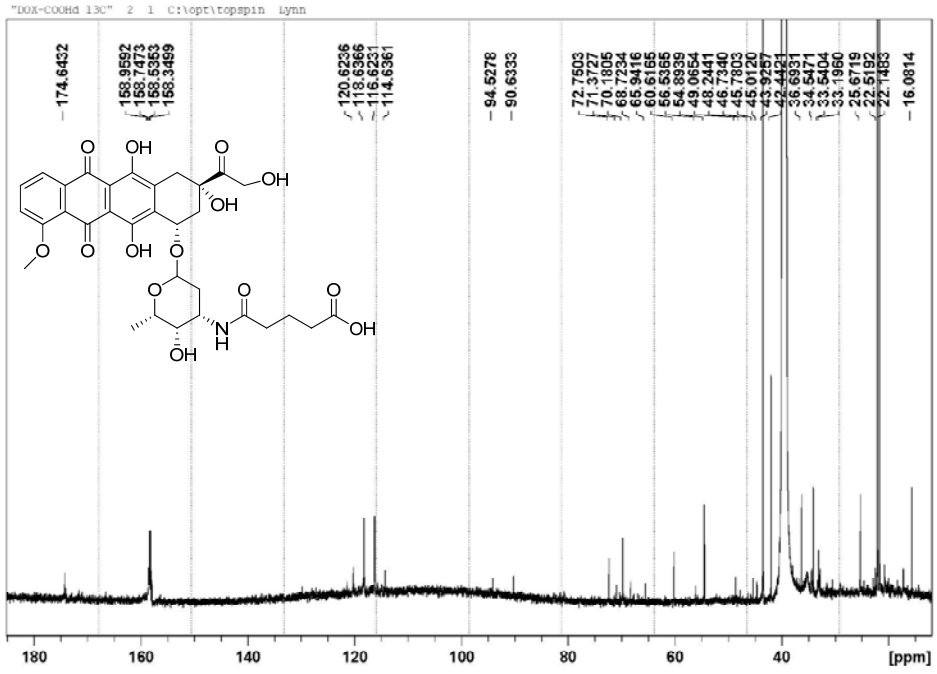

Figure B.45. ^{13}C NMR of DOX-COOH (5-(3-hydroxy-2-methyl-6-(3,5,12-trihydroxy-3-(2-hydroxyacetyl)-10-methoxy-6,11-dioxo-1,2,3,4,6,11-hexahydrotetracen-1-yl)tetrahydro-2H-pyran-4-ylamino)-5-oxopentanoic acid).

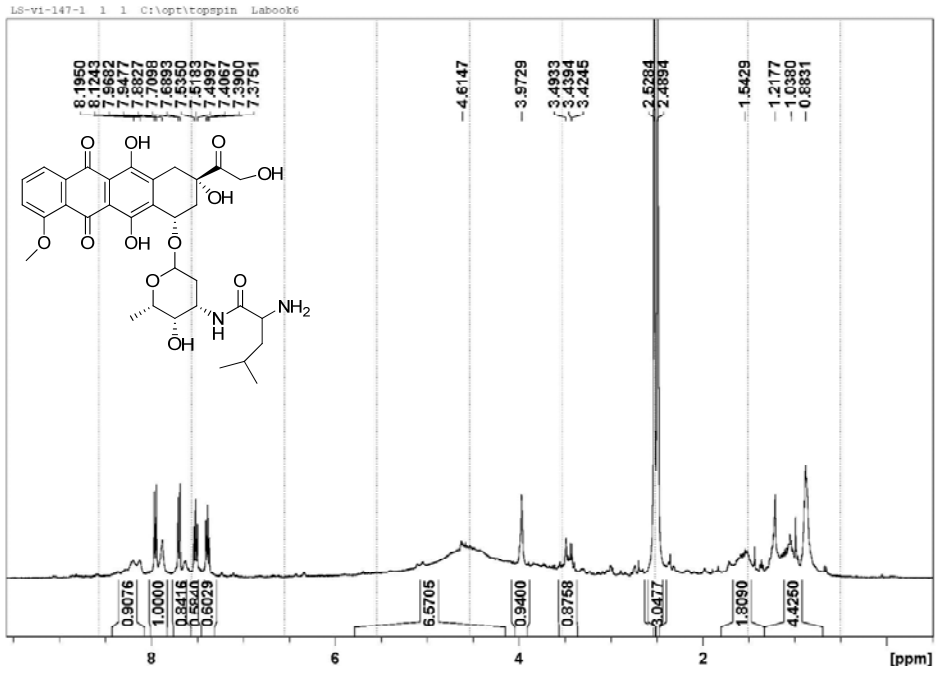

Figure B.46. ^{1}H NMR of Leu-DOX (2-amino-N-((2S,3S,4S)-3-hydroxy-2-methyl-6-((1S,3S)-3,5,12-trihydroxy-3-(2-hydroxyacetyl)-10-methoxy-6,11-dioxo-1,2,3,4,6,11-hexahydrotetracen-1-yloxy)tetrahydro-2H-pyran-4-yl)-4-methylpentanamide).

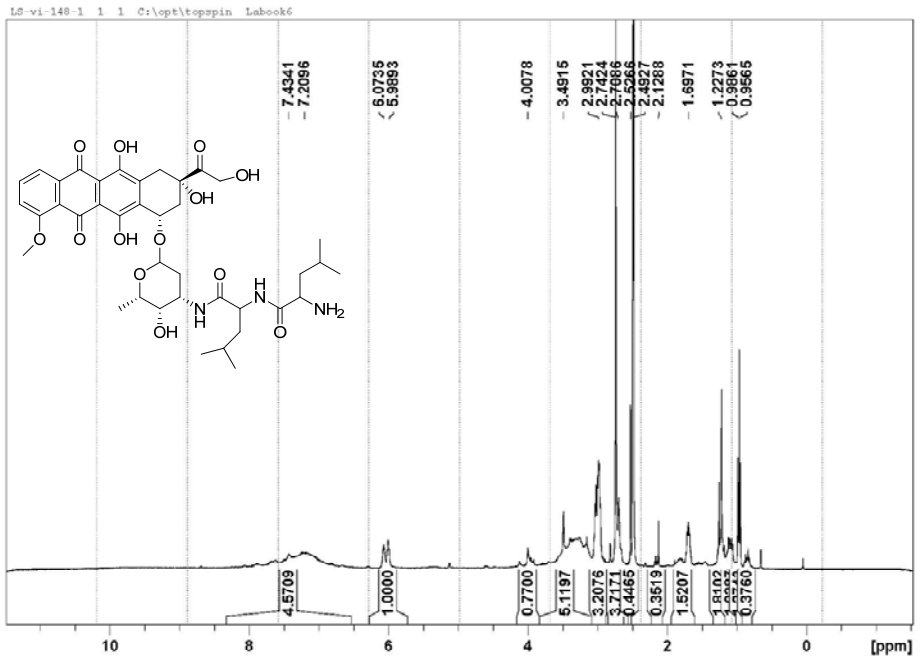

Figure B.47. ^{1}H NMR of Leu-DOX (2-amino-N-(1-((2S,3S,4S)-3-hydroxy-2-methyl-6-((1S,3S)-3,5,12-trihydroxy-3-(2-hydroxyacetyl)-10-methoxy-6,11-dioxo-1,2,3,4,6,11-hexahydrotetracen-1-yloxy)tetrahydro-2H-pyran-4-ylamino)-4-methyl-1-oxopentan-2-yl)-4-methylpentanamide)

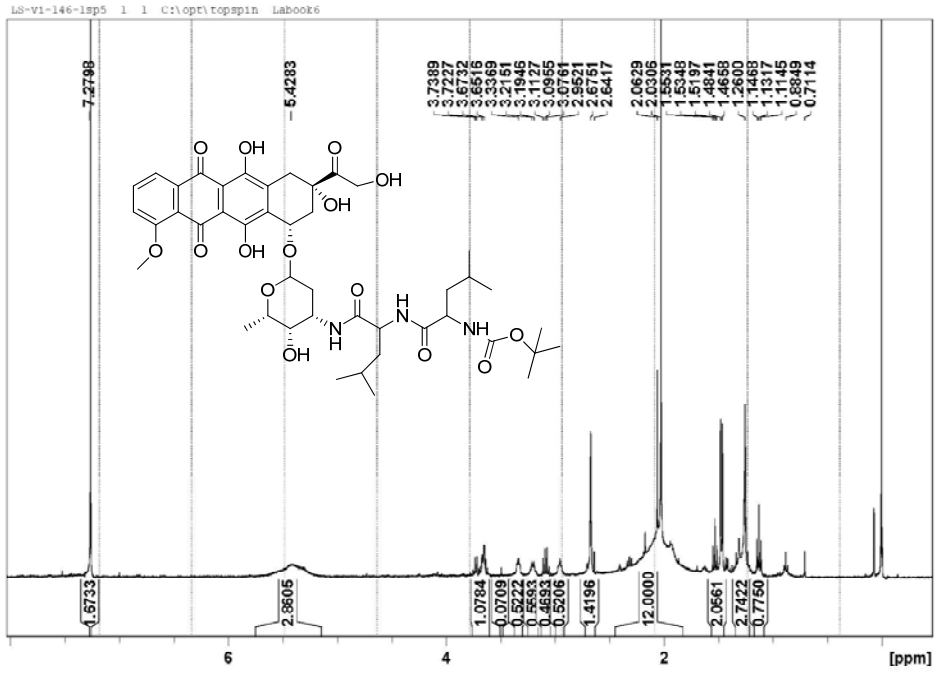

Figure B.48. ^{1}H NMR of Leu-Leu-DOX (tert-butyl 1-(1-((2S,3S,4S)-3-hydroxy-2-methyl-6-((1S,3S)-3,5,12-trihydroxy-3-(2-hydroxyacetyl)-10-methoxy-6,11-dioxo-1,2,3,4,6,11-hexahydrotetracen-1-yloxy)tetrahydro-2H-pyran-4-ylamino)-4-methyl-1-oxopentan-2-ylamino)-4-methyl-1-oxopentan-2-ylcarbamate).

REFERENCES CITED:

1) Brinckerhoff, C. E.; Matrisian, L. M., Matrix metallopreteinases: a tail of a frog that became a prince. *Nat. Rev. Mol. Cell Biol.* **2002,** 3, 207-214.

2) Martin, M. D.; Matrisian, L. M., Matrix metalloproteinases as prognostic factors for cancer. *Clinical Lab. Invest.* **2005,** 28, (6), 16-18.

3) Gillies, R. J., In vivo molecular imaging. *Journal of Cellular Biochemistry* **2002**, 231-238
.

4) Shah, K.; Jacobs, A.; Breakefield, X. O.; Weissleder, R., Molecular imaging of gene therapy for cancer. *Gene Therapy* **2004,** 11, (15), 1175-1187.

5) Weissleder, R.; Ntziachristos, V., Shedding light onto live molecular targets. *Nat Med* **2003,** 9, (1), 123-8.

6) Lee, C. C.; Yoshida, M.; Frechet, J. M. J.; Dy, E. E.; Szoka, F. C., In Vitro and in Vivo Evaluation of Hydrophilic Dendronized Linear Polymers. *Bioconjugate Chemistry* **2005,** 16, 535-541.

7) Kobayashi, H.; Kawamoto, S.; Choyke, P. L.; Sato, N.; Knopp, M. V.; Star, 5) A.; Waldmann, T. A.; Tagaya, Y.; Brechbiel, M. W., Comparison of dendrimer-based macromolecular contrast agents for dynamic micro-magnetic resonance lymphangiography. *Magnetic Resonance in Medicine* **2003,** 50, (4), 758-766.

8) Badjic, J. D.; Cantrill, S. J.; Grubbs, R. H.; Guidry, E. N.; Orenes, R.; Stoddart, J. F., The exclusivity of multivalency in dynamic covalent processes. *Angewandte Chemie-International Edition* **2004,** 43, (25), 3273-3278.
Lauffer, R., Paramagnetic Metal Complexes as Water Proton Relaxation Agents for NMR

9) Imaging: Theory and Design. *Chem. Rev.* **1987,** 87, 901-927.

10) Bremer, C.; Ntziachristos, V.; Weissleder, R., Optical-based molecular imaging: contrast agents and potential medical applications. *European Radiology* **2003,** 13, (2), 231-243.

11) Galande, A. K.; Hilderbrand, S. A.; Weissleder, R.; Tung, C.-H., Enzyme-Targeted Fluorescent Imaging Probes on a Multiple Antigenic Peptide Core. *J Med Chem* **2006,** 49, 4715-4720.

12) Funovics, M.; Weissleder, R.; Tung, C. H., Protease sensors for bioimaging. *Analytical and Bioanalytical Chemistry* **2003,** 377, (6), 956-963.

13) Pham, W.; Choi, Y. D.; Weissleder, R.; Tung, C. H., Developing a peptide-based near-infrared molecular probe for protease sensing. *Bioconjugate Chemistry* **2004,** 15, (6), 1403-1407.

14) Scherer, R. L.; McIntyre, J. O.; Matrisian, L. M., Imaging matrix metalloproteinases in cancer. *Cancer and Metastasis Reviews* **2008,** 27, (4), 679-690.

15) McIntyre, J. O.; Matrisian, L. M., Molecular imaging of proteolytic activity in cancer. *J. Cell Biochem.* **2003,** 90, (6), 1087-1097.

16) McIntyre, J. O.; Fingleton, B.; Wells, K. S.; Piston, D. W.; Lynch, C. C.; Gautam, S.; Matrisian, L. M., Development of a novel fluorogenic proteolytic beacon for in vivo detection and imaging of tumour-associated matrix metalloproteinase-7 activity. *Biochemical Journal* **2004,** 377, (3), 617-628.

17) Thomas, T. P.; Patri, A. K.; Myc, A.; Myaing, M. T.; Ye, J. Y.; Norris, T. B.; Baker, J. R., In vitro targeting of synthesized anti body-conjugated dendrimer nanoparticles. *Biomacromolecules* **2004,** 5, (6), 2269-2274.

18) Achilefu, S.; Jimenez, H. N.; Dorshow, R. B.; Bugaj, J. E.; Webb, E. G.; Wilhelm, R. R.; Rajagopalan, R.; Johler, J.; Erion, J. L., Synthesis, in vitro receptor binding, and in vivo evaluation of fluorescein and carbocyanine peptide-based optical contrast agents. *Journal of Medicinal Chemistry* **2002,** 45, (10), 2003-2015.

19) Hilderbrand, S. A.; Kelly, K. A.; Weissleder, R.; Tung, C. H., Monofunctional near-infrared fluorochromes for imaging applications. *Bioconjugate Chemistry* **2005,** 16, (5), 1275-1281.

20) Kelloff, G. J.; Krohn, K. A.; Larson, S. M.; Weissleder, R.; Mankoff, D. A.; Hoffman, J. M.; Link, J. M.; Guyton, K. Z.; Eckelman, W. C.; Scher, H. I.; O'Shaughnessy, J.; Cheson, B. D.; Sigman, C. C.; Tatum, J. L.; Mills, G. Q.; Sullivan, D. C.; Woodcock, J., The progress and promise of molecular imaging probes in oncologic drug development. *Clinical Cancer Research* **2005,** 11, (22), 7967-7985.

21) Josephson, L.; Kircher, M. F.; Mahmood, U.; Tang, Y.; Weissleder, R., Near-infrared fluorescent nanoparticles as combined MR/optical imaging probes. *Bioconjugate Chemistry* **2002,** 13, (3), 554-560.

22) Hogemann, D.; Ntziachristos, V.; Josephson, L.; Weissleder, R., High throughput magnetic resonance imaging for evaluating targeted nanoparticle probes. *Bioconjugate Chemistry* **2002,** 13, (1), 116-121.

23) Kobayashi, H.; Kawamoto, S.; Konishi, J.; Jo, S.; Brachbiel, M. W.; Star, R. A., Macromolecular MRI contrast agents with small dendrimer cores for functional kidney imaging. *Radiology* **2002,** 225, 237-237.

24) Yordanov, A. T.; Kobayashi, H.; English, S. J.; Reijnders, K.; Milenic, D.; Krishna, M. C.; Mitchell, J. B.; Brechbiel, M. W., Gadolinium-labeled dendrimers as biometric nanoprobes to detect vascular permeability. *Journal of Materials Chemistry* **2003,** 13, (7), 1523-1525.

25) Manning, H. C.; Goebel, T.; Marx, J. N.; Bornhop, D. J., Efficient Conjugation of a Trifunctional Lanthanide Chelate to a Peripheral Benzodiazepine Receptor Ligand. *Org. Lett.* **2002,** 4, (7), 1075-1078.

26) Griffin, J. M. M.; Skwierawska, A. M.; Manning, H. C.; Marx, J. N.; Bornhop, D. J., Simple, high yielding synthesis of trifunctional fluorescent lanthanide chelates. *Tetrahedron Letters* **2001,** 42, (23), 3823-3825.

27) Bornhop, D. J.; Griffin, J. M. M.; Goebel, T. S.; Sudduth, M. R.; Bell, B.; Motamedi, M., Luminescent lanthanide chelate contrast agents and detection of lesions in the hamster oral cancer model. *Applied Spectroscopy* **2003,** 57, (10), 1216-1222.

28) Manning, H. C.; Goebel, T.; Thompson, R. C.; Price, R. R.; Lee, H.; Bornhop, D. J., Targeted molecular imaging agents for cellular-scale bimodal imaging. *Bioconjugate Chemistry* **2004,** 15, (6), 1488-1495.

29) Bai, M.; Wyatt, S. K.; Han, Z.; Papadopoulos, V.; Bornhop, D. J., A novel conjugable translocator protein ligand labeled with a fluorescence dye for in vitro imaging. *Bioconjug Chem* **2007,** 18, (4), 1118-22.

30) Bai, M. F.; Sexton, M.; Stella, N.; Bornhop, D. J., MBC94, a conjugable ligand for cannabinoid CB2 receptor imaging. *Bioconjugate Chemistry* **2008,** 19, (5), 988-992.

31) Papadopoulos, V.; Lecanu, L.; Brown, R. C.; Han, Z.; Yao, Z.-X., Peripheral-Type Benzodiazepine Receptor in Neurosteroid Biosynthesis, Neuropathology and Neurological Disorders. *Neuroscience* **2006,** 138, 749-756.

32) Lacapere, J. J.; Papadopoulos, V., Peripheral-type benzodiazepine receptor: structure and function of a cholesterol-binding protein in steroid and bile acid biosynthesis. *Steroids* **2003,** 68, (7-8), 569-585.

33) Zhang, M. R.; Kida, T.; Noguchi, J.; Furutsuka, K.; Maeda, J.; Suhara, T.; Suzuki, K., [C-11]DAA1106: Radiosynthesis and in vivo binding to peripheral benzodiazepine receptors in mouse brain. *Nuclear Medicine and Biology* **2003,** 30, (5), 513-519.

34) Lockhart, A.; Davis, B.; Matthews, J. C.; Rahmoune, H.; Hong, G. Z.; Gee, A.; Earnshaw, D.; Brown, J., The peripheral benzodiazepine receptor ligand PK11195 binds with high affinity to the acute phase reactant alpha 1-acid glycoprotein: implications for the use of the ligand as a CNS inflammatory marker. *Nuclear Medicine and Biology* **2003,** 30, (2), 199-206.

35) Hardwick, M.; Fertikh, D.; Culty, M.; Li, H.; Vidic, B.; Papadopoulos, V., Peripheral-type benzodiazepine receptor (PBR) in human breast cancer: Correlation of breast cancer cell aggressive phenotype with PBR expression, nuclear localization, and PBR-mediated cell proliferation and nuclear transport of cholesterol. *Cancer Research* **1999,** 59, (4), 831-842.

36) Manning, H. C.; Goebel, T.; Marx, J. N.; Bornhop, D. J., Facile, efficient conjugation of a trifunctional lanthanide chelate to a peripheral benzodiazepine receptor ligand. *Organic Letters* **2002,** 4, (7), 1075-1078.

37) Newman, A. H.; Lueddens, H. W. M.; Skolnick, P.; Rice, K. C., Novel Irreversible Ligands Specific for Peripheral Type Benzodiazepine Receptors - (+/-) , (+) , and (-)-1-(2-Chlorophenyl)-N-(1-Methylpropyl)-N-(2-Isothiocyanatoethyl)-3-Isoquinolinecarboxamide and 1-(2-Isothiocyanatoethyl)-7-Chloro-1,3-Dihydro-5-(4-Chlorophenyl)-H-2-1,4-Benzodiazepin-2-One. *Journal of Medicinal Chemistry* **1987,** 30, (10), 1901-1905.

38) Manning, H. C.; Bai, M. F.; Anderson, B. M.; Lisiak, R.; Samuelson, L. E.; Bornhop, D. J., Expeditious synthesis of 'P'-protected macrocycles en route to lanthanide chelate metal complexes. *Tetrahedron Letters* **2005,** 46, (28), 4707-4710.

39) Manning, H. C.; Merchant, N. B.; Foutch, A. C.; Virostko, J. M.; Wyatt, S. K.; Shah, C.; McKinley, E. T.; Xie, J.; Mutic, N. J.; Washington, M. K.; LaFleur, B.; Tantawy, M. N.; Peterson, T. E.; Ansari, M. S.; Baldwin, R. M.; Rothenberg, M. L.; Bornhop, D. J.; Gore, J. C.; Coffey, R. J., Molecular imaging of therapeutic response to epidermal growth factor receptor blockade in colorectal cancer. *Clin Cancer Res* **2008,** 14, (22), 7413-22.

40) Deane, N. G.; Manning, H. C.; Foutch, A. C.; Washington, M. K.; Aronow, B. J.; Bornhop, D. J.; Coffey, R. J., Targeted imaging of colonic tumors in smad3-/- mice discriminates cancer and inflammation. *Mol Cancer Res* **2007,** 5, (4), 341-9.

41) Hughes, G. A., Nanostructure-mediated drug delivery. *Nanomedicine* **2005,** 1, (1), 22-30.

42) Delavoie, F.; Li, H.; Hardwick, M.; Robert, J.; Giatzakis, C.; Peranzi, G.; Yao, Z.; Maccario, J.; Lacapere, J.; Papadopoulos, V., In vivo and in vitro peripheral-

type benzodiazepine receptor polymerization: Functional significance in drug ligand and cholesterol binding. *Biochemistry* **2003,** 42, (15), 4506-4519.

43) Cho, K.; Wang, X.; Nie, S.; Chen, Z. G.; Shin, D. M., Therapeutic nanoparticles for drug delivery in cancer. *Clin Cancer Res* **2008,** 14, (5), 1310-6.

44) Lee, L. A.; Wang, Q., Adaptations of nanoscale viruses and other protein cages for medical applications. *Nanomedicine* **2006,** 2, (3), 137-49.

45) Hamoudeh, M.; Kamleh, M. A.; Diab, R.; Fessi, H., Radionuclides delivery systems for nuclear imaging and radiotherapy of cancer. *Advanced Drug Delivery Reviews* **2008,** 60, (12), 1329-1346.

46) Portney, N. G.; Ozkan, M., Nano-oncology: drug delivery, imaging, and sensing. *Analytical and Bioanalytical Chemistry* **2006,** 384, (3), 620-630.

47) Koo, O. M.; Rubinstein, I.; Onyuksel, H., Role of nanotechnology in targeted drug delivery and imaging: a concise review. *Nanomedicine* **2005,** 1, (3), 193-212.

48) Debbage, P.; Jaschke, W., Molecular imaging with nanoparticles: giant roles for dwarf actors. *Histochemistry and Cell Biology* **2008,** 130, (5), 845-875.

49) Kim, J. H.; Park, K.; Nam, H. Y.; Lee, S.; Kim, K.; Kwon, I. C., Polymers for bioimaging. *Progress in Polymer Science* **2007,** 32, (8-9), 1031-1053.

50) Platt, V. M.; Szoka, F. C., Anticancer therapeutics: Targeting macromolecules and nanocarriers to hyaluronan or CD44, a hyaluronan receptor. *Molecular Pharmaceutics* **2008,** 5, (4), 474-486.

51) Devalapally, H.; Chakilam, A.; Amiji, M. M., Role of nanotechnology in pharmaceutical product development. *Journal of Pharmaceutical Sciences* **2007,** 96, (10), 2547-2565.

52) Hughes, G. A., Nanostructure-mediated drug delivery. *Dm Disease-a-Month* **2005,** 51, (6), 342-361.

53) Minchin, R., Sizing up targets with nanoparticles. *Nature Nanotechnology* **2008,** 3, (1), 12-13.

54) Khosravi-Darani, K.; Pardakhty, A.; Honarpisheh, H.; Rao, V. S. N. M.; Mozafari, M. R., The role of high-resolution imaging in the evaluation of nanosystems for bioactive encapsulation and targeted nanotherapy. *Micron* **2007,** 38, (8), 804-818.

55) Murthy, N.; Robichaud, J. R.; Tirrell, D. A.; Stayton, P. S.; Hoffman, A. S., The design and synthesis of polymers for eukaryotic membrane disruption. *J Control Release* **1999,** 61, (1-2), 137-43.

56) Arun, R.; Ashok Kumar, C., Novel approaches on prodrug based drug design (vol 42, pg 677, 2008). *Pharmaceutical Chemistry Journal* **2009,** 43, (2), 123-123.

57) Lin, Y. K.; Pagel, L. M.; Axworthy, D.; Pantelias, A.; Hedin, N.; Press, O. W., A genetically engineered anti-CD45 single-chain antibody-streptavidin fusion protein for pretargeted Radioimmunotherapy of hematologic malignancies. *Cancer Research* **2006,** 66, (7), 3884-3892.

58) Gomes, P.; Vale, N.; Moreira, R., Cyclization-activated prodrugs. *Molecules* **2007,** 12, (11), 2484-2506.

59) Li, F. J.; Maag, H.; Alfredson, T., Prodrugs of nucleoside analogues for improved oral absorption and tissue targeting. *Journal of Pharmaceutical Sciences* **2008,** 97, (3), 1109-1134.

60) Lee, C. C.; Cramer, A. T.; Szoka, F. C.; Frechet, J. M. J., An intramolecular cyclization reaction is responsible for the in vivo inefficacy and apparent pH insensitive hydrolysis kinetics of hydrazone carboxylate derivatives of doxorubicin. *Bioconjugate Chemistry* **2006,** 17, (5), 1364-1368.

61) Kline, T.; Torgov, M. Y.; Mendelsohn, B. A.; Cerveny, C. G.; Senter, P. D., Novel antitumor prodrugs designed for activation by matrix metalloproteinases-2 and -9. *Mol Pharm* **2004,** 1, (1), 9-22.

62) Newkome, G. R.; Yao, Z. Q.; Baker, G. R.; Gupta, V. K., Micelles .1. Cascade Molecules - a New Approach to Micelles - a [27]-Arborol. *Journal of Organic Chemistry* **1985,** 50, (11), 2003-2004.

63) Tomalia, D. A.; Baker, H.; Dewald, J.; Hall, M.; Kallos, G.; Martin, S.; Roeck, J.; Ryder, J.; Smith, P., A New Class of Polymers - Starburst-Dendritic Macromolecules. *Polymer Journal* **1985,** 17, (1), 117-132.

64) Tomalia, D. A.; Baker, H.; Dewald, J.; Hall, M.; Kallos, G.; Martin, S.; Roeck, J.; Ryder, J.; Smith, P., Dendritic Macromolecules - Synthesis of Starburst Dendrimers. *Macromolecules* **1986,** 19, (9), 2466-2468.

65) Tomalia, D. A.; Hall, M.; Hedstrand, D. M., Starburst Dendrimers .3. The Importance of Branch Junction Symmetry in the Development of Topological Shell Molecules. *Journal of the American Chemical Society* **1987,** 109, (5), 1601-1603.

66) Tomalia, D. A.; Berry, V.; Hall, M.; Hedstrand, D. M., Starburst Dendrimers .4. Covalently Fixed Unimolecular Assemblages Reminiscent of Spheroidal Micelles. *Macromolecules* **1987,** 20, (5), 1164-1167.

67) Bosman, A. W.; Janssen, H. M.; Meijer, E. W., About dendrimers: Structure, physical properties, and applications. *Chemical Reviews* **1999,** 99, (7), 1665-1688.

68) Samuelson, L. E.; Sebby, K. B.; Walter, E. D.; Singel, D. J.; Cloninger, M. J., EPR and affinity studies of mannose-TEMPO functionalized PAMAM dendrimers. *Organic & Biomolecular Chemistry* **2004,** 2, (21), 3075-3079.

69) Bhadra, D.; Bhadra, S.; Jain, N. K., PEGylated peptide dendrimeric carriers for the delivery of antimalarial drug chloroquine phosphate. *Pharmaceutical Research* **2006,** 23, (3), 623-633.

70) Chandrasekar, D.; Sistla, R.; Ahmad, F. J.; Khar, R. K.; Diwan, P. V., The development of folate-PAMAM dendrimer conjugates for targeted delivery of anti-arthritic drugs and their pharmacokinetics and biodistribution in arthritic rats. *Biomaterials* **2007,** 28, (3), 504-512.

71) Chen, H. T.; Neerman, M. F.; Parrish, A. R.; Simanek, E. E., Cytotoxicity, hemolysis, and acute in vivo toxicity of dendrimers based on melamine, candidate vehicles for drug delivery. *Journal of the American Chemical Society* **2004,** 126, (32), 10044-10048.

72) Costantino, L.; Gandolfi, F.; Bossy-Nobs, L.; Tosi, G.; Gurny, R.; Rivasi, F.; Vandelli, M. A.; Forni, F., Nanoparticulate drug carriers based on hybrid poly(D,L-lactide-co-glycolide)-dendron structures. *Biomaterials* **2006,** 27, (26), 4635-4645.

73) D'Emanuele, A.; Attwood, D., Dendrimer-drug interactions. *Adv Drug Deliv Rev* **2005,** 57, (15), 2147-62.

74) D'Emanuele, A.; Jevprasesphant, R.; Penny, J.; Attwood, D., The use of a dendrimer-propranolol prodrug to bypass efflux transporters and enhance oral bioavailability. *Journal of Controlled Release* **2004,** 95, (3), 447-453.

75) Gurdag, S.; Khandare, J.; Stapels, S.; Matherly, L. H.; Kannan, R. M., Activity of dendrimer-methotrexate conjugates on methotrexate-sensitive and -resistant cell lines. *Bioconjugate Chemistry* **2006,** 17, (2), 275-283.

76) Jang, W. D.; Selim, K. M. K.; Lee, C. H.; Kang, I. K., Bioinspired application of dendrimers: From bio-mimicry to biomedical applications. *Progress in Polymer Science* **2009,** 34, (1), 1-23.

77) Kono, K.; Liu, M. J.; Frechet, J. M. J., Design of dendritic macromolecules containing folate or methotrexate residues. *Bioconjugate Chemistry* **1999,** 10, (6), 1115-1121.

78) Quintana, A.; Raczka, E.; Piehler, L.; Lee, I.; Myc, A.; Majoros, I.; Patri, A. K.; Thomas, T.; Mule, J.; Baker, J. R., Design and function of a dendrimer-based therapeutic nanodevice targeted to tumor cells through the folate receptor. *Pharmaceutical Research* **2002,** 19, (9), 1310-1316.

79) Svenson, S., Dendrimers as versatile platform in drug delivery applications. *European Journal of Pharmaceutics and Biopharmaceutics* **2009,** 71, (3), 445-462.

80) Tomalia, D. A.; Reyna, L. A.; Svenson, S., Dendrimers as multi-purpose nanodevices for oncology drug delivery and diagnostic imaging. *Biochemical Society Transactions* **2007,** 35, 61-67.

81) Paleos, C. M.; Tsiourvas, D.; Sideratou, Z., Molecular engineering of dendritic polymers and their application as drug and gene delivery systems. *Molecular Pharmaceutics* **2007,** 4, (2), 169-188.

82) Yang, H.; Lopina, S. T., In vitro enzymatic stability of dendritic peptides. *Journal of Biomedical Materials Research Part A* **2006,** 76A, (2), 398-407.

83) Agarwal, A.; Saraf, S.; Asthana, A.; Gupta, U.; Gajbhiye, V.; Jain, N. K., Ligand based dendritic systems for tumor targeting. *Int J Pharm* **2008,** 350, (1-2), 3-13.

84) Hardy, J. G.; Kostiainen, M. A.; Smith, D. K.; Gabrielson, N. P.; Pack, D. W., Dendrons with spermine surface groups as potential building blocks for nonviral vectors in gene therapy. *Bioconjugate Chemistry* **2006,** 17, (1), 172-178.

85) Kumar, P. V.; Asthana, A.; Dutta, T.; Jain, N. K., Intracellular macrophage uptake of rifampicin loaded mannosylated dendrimers. *Journal of Drug Targeting* **2006,** 14, (8), 546-556.

86) Svenson, S.; Tomalia, D. A., Dendrimers in biomedical applications--reflections on the field. *Adv Drug Deliv Rev* **2005,** 57, (15), 2106-29.

87) Takahashi, M.; Hara, Y.; Aoshima, K.; Kurihara, H.; Oshikawa, T.; Yamashita, M., Utilization of dendritic framework as a multivalent ligand: a functionalized gadolinium(III) carrier with glycoside cluster periphery. *Tetrahedron Letters* **2000,** 41, (44), 8485-8488.

88) Grayson, S. M.; Frechet, J. M. J., Synthesis and surface functionalization of aliphatic polyether dendrons. *Journal of the American Chemical Society* **2000,** 122, (42), 10335-10344.

89) Al-Jamal, K. T.; Ruenraroengsak, P.; Hartell, N.; Florence, A. T., An intrinsically fluorescent dendrimer as a nanoprobe of cell transport. *Journal of Drug Targeting* **2006,** 14, (6), 405-412.

90) Bielinska, A.; Eichman, J. D.; Lee, I.; Baker, J. R.; Balogh, L., Imaging {Au-0-PAMAM} gold-dendrimer nanocomposites in cells. *Journal of Nanoparticle Research* **2002,** 4, (5), 395-403.

91) Margerum, L. D.; Campion, B. K.; Koo, M.; Shargill, N.; Lai, J. J.; Marumoto, A.; Sontum, P. C., Gadolinium(III) DO3A macrocycles and polyethylene glycol coupled to dendrimers - Effect of molecular weight on physical and biological properties of macromolecular magnetic resonance imaging contrast agents. *Journal of Alloys and Compounds* **1997,** 249, (1-2), 185-190.

92) Yordanov, A. T.; Lodder, A. L.; Woller, E. K.; Cloninger, M. J.; Patronas, N.; Milenic, D.; Brechbiel, M. W., Novel iodinated dendritic nanoparticles for computed tomography (CT) imaging. *Nano Letters* **2002,** 2, (6), 595-599.

93) Woller, E. K.; Cloninger, M. J., Mannose functionalization of a sixth generation dendrimer. *Biomacromolecules* **2001,** 2, (3), 1052-1054.

94) Morgan, J. R.; Cloninger, M. J., Synthesis of carbohydrate-linked poly(polyoxometalate) poly(amido)amine dendrimers. *Journal of Polymer Science Part a-Polymer Chemistry* **2005,** 43, (14), 3059-3066.

95) Niederhafner, P.; Sebestik, J.; Jezek, J., Glycopeptide dendrimers. Part II. *Journal of Peptide Science* **2008,** 14, (1), 44-65.

96) Boysen, M. M. K.; Elsner, K.; Sperling, O.; Lindhorst, T. K., Glycerol and glycerol glycol glycodendrimers. *European Journal of Organic Chemistry* **2003**, (22), 4376-4386.

97) Wiener, E. C.; Auteri, F. P.; Chen, J. W.; Brechbiel, M. W.; Gansow, O. A.; Schneider, D. S.; Belford, R. L.; Clarkson, R. B.; Lauterbur, P. C., Molecular dynamics of ion-chelate complexes attached to dendrimers. *Journal of the American Chemical Society* **1996,** 118, (33), 7774-7782.

98) Bryant, L. H.; Brechbiel, M. W.; Wu, C. C.; Bulte, J. W. M.; Herynek, V.; Frank, J. A., Synthesis and relaxometry of high-generation (G = 5, 7, 9, and 10) PAMAM dendrimer-DOTA-gadolinium chelates. *Jmri-Journal of Magnetic Resonance Imaging* **1999,** 9, (2), 348-352.

99) Myc, A.; Majoros, I. J.; Thomas, T. P.; Baker, J. R., Dendrimer-based targeted delivery of an apoptotic sensor in cancer cells. *Biomacromolecules* **2007,** 8, (1), 13-18.

100) Majoros, I. J.; Myc, A.; Thomas, T.; Mehta, C. B.; Baker, J. R., PAMAM dendrimer-based multifunctional conjugate for cancer therapy: Synthesis, characterization, and functionality. *Biomacromolecules* **2006,** 7, (2), 572-579.

101) Majoros, I. J.; Thomas, T. P.; Mehta, C. B.; Baker, J. R., Poly(amidoamine) dendrimer-based multifunctional engineered nanodevice for cancer therapy. *Journal of Medicinal Chemistry* **2005,** 48, (19), 5892-5899.

102) Shi, X. Y.; Sun, K.; Balogh, L. P.; Baker, J. R., Synthesis, characterization, and manipulation of dendrimer-stabilized iron sulfide nanoparticles. *Nanotechnology* **2006,** 17, (18), 4554-4560.

103) Yamamoto, K.; Takanashi, K., Synthesis and functionality of dendrimer with finely controlled metal assembly. *Polymer* **2008,** 49, (19), 4033-4041.

104) Bernhardt, S.; Kastler, M.; Enkelmann, V.; Baumgarten, M.; Mullen, K., Pyrene as chromophore and electrophore: Encapsulation in a rigid polyphenylene shell. *Chemistry-a European Journal* **2006,** 12, (23), 6117-6128.

105) Knecht, M. R.; Garcia-Martinez, J. C.; Crooks, R. M., Synthesis, characterization, and magnetic properties of dendrimer-encapsulated nickel nanoparticles containing < 150 atoms. *Chemistry of Materials* **2006,** 18, (21), 5039-5044.

106) Diallo, M. S.; Christie, S.; Swaminathan, P.; Balogh, L.; Shi, X. Y.; Um, W.; Papelis, C.; Goddard, W. A.; Johnson, J. H., Dendritic chelating agents. 1. Cu(II) binding to ethylene diamine core poly(amidoamine) dendrimers in aqueous solutions. *Langmuir* **2004,** 20, (7), 2640-2651.

107) Oh, S. K.; Kim, Y. G.; Ye, H. C.; Crooks, R. M., Synthesis, characterization, and surface immobilization of metal nanoparticles encapsulated within bifunctionalized dendrimers. *Langmuir* **2003,** 19, (24), 10420-10425.

108) Nishiyama, N.; Stapert, H. R.; Zhang, G. D.; Takasu, D.; Jiang, D. L.; Nagano, T.; Aida, T.; Kataoka, K., Light-harvesting ionic dendrimer porphyrins as new photosensitizers for photodynamic therapy. *Bioconjugate Chemistry* **2003,** 14, (1), 58-66.

109) Nishiyama, N.; Jang, W. D.; Kataoka, K., Supramolecular nanocarriers integrated with dendrimers encapsulating photosensitizers for effective photodynamic therapy and photochemical gene delivery. *New Journal of Chemistry* **2007,** 31, (7), 1074-1082.

110) Maes, W.; Vanderhaeghen, J.; Smeets, S.; Asokan, C. V.; Van Renterghem, L. M.; Du Prez, F. E.; Smet, M.; Dehaen, W., Synthesis of multi(metallo)porphyrin dendrimers through nucleophilic aromatic substitution on meso-pyrimidinyl substituted porphyrins. *Journal of Organic Chemistry* **2006,** 71, (8), 2987-2994.

111) He, Z.; Ishizuka, T.; Jiangi, D. L., Dendritic architectures for design of photo- and spin-functional nanomaterials. *Polymer Journal* **2007,** 39, (9), 889-922.

112) Shcharbin, D.; Pedziwiatr, E.; Bryszewska, M., How to study dendriplexes I: Characterization. *Journal of Controlled Release* **2009,** 135, (3), 186-197.

113) Wu, P.; Feldman, A. K.; Nugent, A. K.; Hawker, C. J.; Scheel, A.; Voit, B.; Pyun, J.; Frechet, J. M. J.; Sharpless, K. B.; Fokin, V. V., Efficiency and fidelity in a click-chemistry route to triazole dendrimers by the copper(I)-catalyzed ligation of azides and alkynes. *Angewandte Chemie-International Edition* **2004,** 43, (30), 3928-3932.

114) Vrasidas, I.; de Mol, N. J.; Liskamp, R. M. J.; Pieters, R. J., Synthesis of lactose dendrimers and multivalency effects in binding to the cholera toxin B subunit. *European Journal of Organic Chemistry* **2001**, (24), 4685-4692.

115) Dichtel, W. R.; Hecht, S.; Frechet, J. M. J., Functionally layered dendrimers: A new building block and its application to the synthesis of multichromophoric light-harvesting systems. *Organic Letters* **2005,** 7, (20), 4451-4454.

116) Bernhardt, S.; Baumgarten, M.; Wagner, M.; Mullen, K., Multiple functionalization of benzophenones inside polyphenylene dendrimers - Toward entrapped ions and radicals. *Journal of the American Chemical Society* **2005,** 127, (35), 12392-12399.

117) Langereis, S.; Dirksen, A.; Hackeng, T. M.; van Genderen, M. H. P.; Meijer, E. W., Dendrimers and magnetic resonance imaging. *New Journal of Chemistry* **2007,** 31, (7), 1152-1160.

118) Xu, H.; Regino, C. A. S.; Koyama, Y.; Hama, Y.; Gunn, A. J.; Bernardo, M.; Kobayashi, H.; Choyke, P. L.; Brechbiel, M. W., Preparation and preliminary evaluation of a biotin-targeted, lectin-targeted dendrimer-based probe for dual-modality magnetic resonance and fluorescence Imaging. *Bioconjugate Chemistry* **2007,** 18, (5), 1474-1482.

119) Cardona, C. M.; Alvarez, J.; Kaifer, A. E.; McCarley, T. D.; Pandey, S.; Baker, G. A.; Bonzagni, N. J.; Bright, F. V., Dendrimers functionalized with a single fluorescent dansyl group attached "off center": Synthesis and

photophysical studies. *Journal of the American Chemical Society* **2000,** 122, (26), 6139-6144.

120) McIntyre, J. O.; Matrisian, L. M., Optical proteolytic beacons for in vivo detection of matrix metalloproteinase activity. *Methods Mol Biol* **2009,** 539, 155-74.

121) Wolinsky, J. B.; Grinstaff, M. W., Therapeutic and diagnostic applications of dendrimers for cancer treatment. *Advanced Drug Delivery Reviews* **2008,** 60, (9), 1037-1055.

122) Tekade, R. K.; Kumar, P. V.; Jain, N. K., Dendrimers in Oncology: An Expanding Horizon. *Chemical Reviews* **2009,** 109, (1), 49-87.

123) Stiriba, S. E.; Frey, H.; Haag, R., Dendritic polymers in biomedical applications: From potential to clinical use in diagnostics and therapy. *Angewandte Chemie-International Edition* **2002,** 41, (8), 1329-1334.

124) Acuff, H. B.; Carter, K. J.; Fingleton, B.; Gorden, D. L.; Matrisian, L. M., Matrix metalloproteinase-9 from bone marrow-derived cells contributes to survival but not growth of tumor cells in the lung microenvironment. *Cancer Research* **2006,** 66, (1), 259-266.

125) Martin, M. D.; Matrisian, L. M., Matrix metalloproteinases as prognostic factors for cancer. *Clinical Lab. Invest.* **2005,** 28, 16-18.

126) Martin, M. D.; Carter, K. J.; Jean-Philippe, S. R.; Chang, M.; Mobashery, S.; Thiolloy, S.; Lynch, C. C.; Matrisian, L. M.; Fingleton, B., Effect of ablation or inhibition of stromal matrix metalloproteinase-9 on lung metastasis in a breast cancer model is dependent on genetic background. *Cancer Res* **2008,** 68, (15), 6251-9.

127) Chen, X.; Su, Y.; Fingleton, B.; Acuff, H.; Matrisian, L. M.; Zent, R.; Pozzi, A., An orthotopic model of lung cancer to analyze primary and metastatic NSCLC growth in integrin alpha1-null mice. *Clin Exp Metastasis* **2005,** 22, (2), 185-93.

128) Martin, M. D.; Matrisian, L. M., The other side of MMPs: protective roles in tumor progression. *Cancer Metastasis Rev* **2007,** 26, (3-4), 717-24.

129) Chen, J. Q.; Tung, C. H.; Allport, J. R.; Chen, S.; Weissleder, R.; Huang, P. L., Near-infrared fluorescent Imaging of matrix metalloproteinase activity after myocardial infarction. *Circulation* **2005,** 111, (14), 1800-1805.

130) Kline, T.; Torgov, Y.; Mendelsohn, B. A.; Cerveny, C. G.; Senter, P. D., Novel Antitumor Prodrugs Designed for Activation by Matrix Metalloproteinases-2 and -9, Molecular Pharmaceutices. *Molecular Pharmaceutices* **2004,** 1, 9-22.

131) Garsky, V. M.; Lumma, P. K.; Feng, D. M.; Wai, J.; Ramjit, H. G.; Sardana, M. K.; Oliff, A.; Jones, R. E.; DeFeo-Jones, D.; Freidinger, R. M., The synthesis of a prodrug of doxorubicin designed to provide reduced systemic toxicity and greater target efficacy. *Journal of Medicinal Chemistry* **2001,** 44, (24), 4216-4224.

132) Brinckerhoff, C. E.; Matrisian, L. M., Timeline - Matrix metalloproteinases: a tail of a frog that became a prince. *Nature Reviews Molecular Cell Biology* **2002,** 3, (3), 207-214.

133) Wassermann, R.; Zwelling, L. A.; Mullins, T. D.; Silberman, L. E.; Andersson, B. S.; Bakic, M.; Acton, E. M.; Newman, R. A., Effects of 3'-Deamino-3'-(3-cyano-4-morpholinyl)doxorubicin and Doxorubicin on the Survival, DNA Integrity, and Nucleolar Morphology of Human Leukemia Cells in Vitro. *Cancer Research* **1986,** 46, 4041-4046.

134) Denmeade, S. R.; Nagy, A.; Gao, J.; Lilja, H.; Schally, A. V.; Isaacs, J. T., Enzymatic Activation of a Doxorubicin-Peptide Prodrug by Prostate-Specific Antigen. *Cancer Research* **1998,** 58, 2537-2540.

135) Murdter, T. E.; Sperker, B.; Kivisto, K. T.; McClellan, M.; Fritz, P.; Friedel, G.; Linder, A.; Bosslet, K.; Toomes, H.; Dierkesmann, R.; Kroemer, H. K., Enhanced Uptake of Doxorubicin into Bronchial Carcinoma: @-Glucuronidase Mediates Release of Doxorubicin from a Glucuromde Prodrug (HMR 1826) at the Tumor Site. *Cancer Research* **1997,** 57, 2440-2445.

136) Bernstein, B. J., Docetaxel as an alternative to paclitaxel after acute hypersensitivity reactions. *Ann Pharmacother* **2000,** 34, (11), 1332-5.

137) Orr, G. A.; Verdier-Pinard, P.; McDaid, H.; Horwitz, S. B., Mechanisms of Taxol resistance related to microtubules. *Oncogene* **2003,** 22, (47), 7280-95.

138) Mekhail, T. M.; Markman, M., Paclitaxel in cancer therapy. *Expert Opin Pharmacother* **2002,** 3, (6), 755-66.

139) Cabral, F.; Barlow, S. B., *Faseb Journal* **1989,** 3, 1593-1599.

140) Cabral, F. R.; Brady, R. C.; Schibler, M. J., *Ann N Y Acad Sci* **1986,** 466, 745-756.

141) WB, D.; L., W.; MA., J., *Biochemistry* **1995,** 34, 2203-2211.

142) Wilson, L.; Jordan, M. A., *Chemical Biology* **1995,** 2, 569-573.
Goncalves, A.; Braguer, D.; Kamath, K.; Martello, L.; Briand, C.; Horwitz, S.;

143) L.Wilson; M.A.Jordan, *Proc Natl Acad Sci* **2001,** 98, 11737-11742.

144) Gradishar, W. J., Albumin-bound paclitaxel: a next-generation taxane. *Expert Opin Pharmacother* **2006,** 7, (8), 1041-53.

145) Foote, M., Using nanotechnology to improve the characteristics of antineoplastic drugs: improved characteristics of nab-paclitaxel compared with solvent-based paclitaxel. *Biotechnol Annu Rev* **2007,** 13, 345-57.

146) Sharkey, R. M.; Cardillo, T. M.; Rossi, E. A.; Chang, C. H.; Karacay, H.; McBride, W. J.; Hansen, H. J.; Horak, I. D.; Goldenberg, D. M., Signal amplification in molecular imaging by pretargeting a multivalent, bispecific antibody. *Nature Medicine* **2005,** 11, (11), 1250-1255.

147) Mulder, W. J. M.; Strijkers, G. J.; van Tilborg, G. A. F.; Griffioen, A. W.; Nicolay, K., Lipid-based nanoparticles for contrast-enhanced MRI and molecular imaging. *Nmr in Biomedicine* **2006,** 19, (1), 142-164.

148) Morawski, A. M.; Winter, P. M.; Crowder, K. C.; Caruthers, S. D.; Fuhrhop, R. W.; Scott, M. J.; Robertson, J. D.; Abendschein, D. R.; Lanza, G. M.; Wickline, S. A., Targeted nanoparticles for quantitative imaging of sparse molecular epitopes with MRI. *Magnetic Resonance in Medicine* **2004,** 51, (3), 480-486.

149) Li, K. C. P.; Bednarski, M. D., Vascular-targeted molecular imaging using functionalized polymerized vesicles. *Journal of Magnetic Resonance Imaging* **2002,** 16, (4), 388-393.

150) Gillies, E. R.; Frechet, J. M. J., Dendrimers and dendritic polymers in drug delivery. *Drug Discovery Today* **2005,** 10, (1), 35-43.

151) Wickline, S. A.; Neubauer, A. M.; Winter, P.; Caruthers, S.; Lanza, G., Applications of nanotechnology to atherosclerosis, thrombosis, and vascular biology. *Arteriosclerosis Thrombosis and Vascular Biology* **2006,** 26, (3), 435-441.

152) Sinha, R.; Kim, G. J.; Nie, S. M.; Shin, D. M., Nanotechnology in cancer therapeutics: bioconjugated nanoparticles for drug delivery. *Molecular Cancer Therapeutics* **2006,** 5, (8), 1909-1917.

153) Papadopoulos, V.; Baraldi, M.; Guilarte, T. R.; Knudsen, T. B.; Lacapere, J. J.; Lindemann, P.; Norenberg, M. D.; Nutt, D.; Weizman, A.; Zhang, M. R.; Gavish, M., Translocator protein (18 kDa): new nomenclature for the peripheral-type benzodiazepine receptor based on its structure and molecular function. *Trends in Pharmacological Sciences* **2006,** 27, (8), 402-409.

154) Decaudin, D.; Castedo, M.; Nemati, F.; Beurdeley-Thomas, A.; De Pinieux, G.; Caron, A.; Pouillart, P.; Wijdenes, J.; Rouillard, D.; Kroemer, G.; Poupon, M. F., Peripheral benzodiazepine receptor ligands reverse apoptosis resistance of cancer cells in vitro and in vivo. *Cancer Research* **2002,** 62, (5), 1388-1393.

155) Casellas, P.; Galiegue, S.; Basile, A. S., Peripheral benzodiazepine receptors and mitochondrial function. *Neurochemistry International* **2002,** 40, (6), 475-486.

156) Olson, J. M.; Mcneel, W.; Young, A. B.; Mancini, W. R., Localization of the Peripheral-Type Benzodiazepine Binding-Site to Mitochondria of Human Glioma-Cells. *Journal of Neuro-Oncology* **1992,** 13, (1), 35-42.

157) Chen, J. W.; Breckwoldt, M. O.; Aikawa, E.; Chiang, G.; Weissleder, R., Myeloperoxidase-targeted imaging of active inflammatory lesions in murine experimental autoimmune encephalomyelitis. *Brain* **2008,** 131, (Pt 4), 1123-33.

158) Nahrendorf, M.; Sosnovik, D.; Chen, J. W.; Panizzi, P.; Figueiredo, J. L.; Aikawa, E.; Libby, P.; Swirski, F. K.; Weissleder, R., Activatable magnetic resonance imaging agent reports myeloperoxidase activity in healing infarcts and noninvasively detects the antiinflammatory effects of atorvastatin on ischemia-reperfusion injury. *Circulation* **2008,** 117, (9), 1153-60.

159) Hammoud, D. A.; Endres, C. J.; Chander, A. R.; Guilarte, T. R.; Wong, D. F.; Sacktor, N. C.; McArthur, J. C.; Pomper, M. G., Imaging glial cell activation with [C-11]-R-PK11195 in patients with AIDS. *Journal of Neurovirology* **2005,** 11, (4), 346-355.

160) Khandare, J.; Minko, T., Polymer-drug conjugates: Progress in polymeric prodrugs. *Progress in Polymer Science* **2006,** 31, (4), 359-397.

161) Satchi-Fainaro, R.; Duncan, R.; Barnes, C. M., Polymer therapeutics for cancer: Current status and future challenges. *Polymer Therapeutics Ii: Polymers as Drugs, Conjugates and Gene Delivery Systems* **2006,** 193, 1-65.

162) Winter, P. M.; Cai, K. J.; Chen, J.; Adair, C. R.; Kiefer, G. E.; Athey, P. S.; Gaffney, P. J.; Buff, C. E.; Robertson, J. D.; Caruthers, S. D.; Wickline, S. A.; Lanza, G. M., Targeted PARACEST nanoparticle contrast agent for the detection of fibrin. *Magnetic Resonance in Medicine* **2006,** 56, (6), 1384-1388.

163) Kolonko, E. M.; Kiessling, L. L., A polymeric domain that promotes cellular internalization. *Journal of the American Chemical Society* **2008,** 130, (17), 5626-+.

164) Kitchens, K. M.; Foraker, A. B.; Kolhatkar, R. B.; Swaan, P. W.; Ghandehari, H., Endocytosis and interaction of poly (amidoamine) dendrimers with Caco-2 cells. *Pharmaceutical Research* **2007,** 24, (11), 2138-2145.

165) Giepmans, B. N. G., Bridging fluorescence microscopy and electron microscopy. *Histochemistry and Cell Biology* **2008,** 130, (2), 211-217.

166) Koster, A. J.; Klumperman, J., Electron microscopy in cell biology: integrating structure and function. *Nature Cell Biology* **2003**, Ss6-Ss10.

167) de Jonge, N.; Peckys, D. B.; Kremers, G. J.; Piston, D. W., Electron microscopy of whole cells in liquid with nanometer resolution. *Proc Natl Acad Sci U S A* **2009**.

168) Hummelen, J. C.; vanDongen, J. L. J.; Meijer, E. W., Electrospray mass spectrometry of poly(propylene imine) dendrimers - The issue of dendritic purity or polydispersity. *Chemistry-a European Journal* **1997,** 3, (9), 1489-1493.

169) Kozikowski, A. P.; Kotoula, M.; Ma, D. W.; Boujrad, N.; Tuckmantel, W.; Papadopoulos, V., Synthesis and biology of a 7-nitro-2,1,3-benzoxadiazol-4-yl derivative of 2-phenylindole-3-acetamide: A fluorescent probe for the peripheral-type benzodiazepine receptor. *Journal of Medicinal Chemistry* **1997,** 40, (16), 2435-2439.

170) Starostarubinstein, S.; Ciliax, B. J.; Penney, J. B.; Mckeever, P.; Young, A. B., Imaging of a Glioma Using Peripheral Benzodiazepine Receptor Ligands. *Proceedings of the National Academy of Sciences of the United States of America* **1987,** 84, (3), 891-895.

171) Sehgal, I.; Sibrian-Vazquez, M.; Vicente, M. G. H., Photoinduced cytotoxicity and biodistribution of prostate cancer cell-targeted porphyrins. *Journal of Medicinal Chemistry* **2008,** 51, (19), 6014-6020.

172) Sacchi, S.; Bernasconi, M.; Martineau, M.; Mothet, J. P.; Ruzzene, M.; Pilone, M. S.; Pollegioni, L.; Molla, G., pLG72 modulates intracellular D-serine levels through its interaction with D-amino acid oxidase - Effect on schizophrenia susceptibility. *Journal of Biological Chemistry* **2008,** 283, (32), 22244-22256.

173) Bozzola, J. J.; Russel, L. D., Specimen Staining and Contrast Methods for Transmission Electron Microscopy. In *Microscopy: Principles and Techniques for Biologists*, 2nd ed.; 'Ed.'^'Eds.' Jones and Bartlett Publishers: Boston, **1999**; 'Vol.' p^pp 121-147.

174 Bozzola, J. J.; Russel, L. D., Specimen Preparation for Transmission Electron Microscopy. In *Electron Microscopy: Principles and Techniques for*

Biologists, ed.; 'Ed.'^'Eds.' Jones and Bartlett Publishers: Boston, **1999**; 'Vol.' p^pp 303.

175) Li, G. L.; Graham, A.; Chen, Y. H.; Dobhal, M. P.; Morgan, J.; Zheng, G.; Kozyrev, A.; Oseroff, A.; Dougherty, T. J.; Pandey, R. K., Synthesis, comparative photosensitizing efficacy, human serum albumin (Site II) binding ability, and intracellular localization characteristics of novel benzobacteriochlorins derived from vic-dihydroxybacteriochlorins. *Journal of Medicinal Chemistry* **2003,** 46, (25), 5349-5359.

176) Garnier, M.; Dimchev, A. B.; Boujrad, N.; Price, J. M.; Musto, N. A.; Papadopoulos, V., In-Vitro Reconstitution of a Functional Peripheral-Type Benzodiazepine Receptor from Mouse Leydig Tumor-Cells. *Molecular Pharmacology* **1994,** 45, (2), 201-211.

177) Short, B. G., Safety evaluation of ocular drug delivery formulations: techniques and practical considerations. *Toxicol Pathol* **2008,** 36, (1), 49-62.

178) Kridel, S. J.; Chen, E.; Kotra, L. P.; Howard, E. W.; Mobashery, S.; Smith, J. M., Substrate hydrolysis by matrix metalloproteinase-9. *Journal of Biological Chemistry* **2001,** 276, (23), 20572-20578.

179) Scherer, R. L.; McIntyre, J. O.; Matrisian, L. M., Imaging matrix metalloproteinases in cancer. *Cancer Metastasis Rev* **2008,** 27, (4), 679-90.

180) Lee, S.; Park, K.; Lee, S. Y.; Ryu, J. H.; Park, J. W.; Ahn, H. J.; Kwon, I. C.; Youn, I. C.; Kim, K.; Choi, K., Dark quenched matrix metalloproteinase fluorogenic probe for imaging osteoarthritis development in vivo. *Bioconjugate Chemistry* **2008,** 19, (9), 1743-1747.

181) Ihre, H.; Hult, A.; Soderlind, E., Synthesis, characterization, and H-1 NMR self-diffusion studies of dendritic aliphatic polyesters based on 2,2-bis(hydroxymethyl)propionic acid and 1,1,1-tris(hydroxyphenyl)ethane. *Journal of the American Chemical Society* **1996,** 118, (27), 6388-6395.

182) Horton, D.; Priebe, W.; Varela, O., Synthesis and Antitumor-Activity of 3'-Deamino-3'-Hydroxydoxorubicin - a Facile Procedure for the Preparation of Doxorubicin Analogs. *Journal of Antibiotics* **1984,** 37, (8), 853-858.

183) Arcomone, F.; Casazza, A.; Cassinellie, G.; Di Marco, A.; Penco, S., Doxorubicin and related compounds. II. Structure-activity consideration. *Developments in oncology* **1982,** 10, 179-189.

184) Bergers, G.; Brekken, R.; McMahon, G.; Vu, T. H.; Itoh, T.; Tamaki, K.; Tanzawa, K.; Thorpe, P.; Itohara, S.; Werb, Z.; Hanahan, D., Matrix

metalloproteinase-9 triggers the angiogenic switch during carcinogenesis. *Nature Cell Biology* **2000,** 2, (10), 737-744.

185) Albright, C. F.; Graciani, N.; Han, W.; Yue, E.; Stein, R.; Lai, Z.; Diamond, M.; Dowling, R.; Grimminger, L.; Zhang, S. Y.; Behrens, D.; Musselman, A.; Bruckner, R.; Zhang, M.; Jiang, X.; Hu, D.; Higley, A.; Dimeo, S.; Rafalski, M.; Mandlekar, S.; Car, B.; Yeleswaram, S.; Stern, A.; Copeland, R. A.; Combs, A.; Seitz, S. P.; Trainor, G. L.; Taub, R.; Huang, P.; Oliff, A., Matrix metalloproteinase-activated doxorubicin prodrugs inhibit HT1080 xenograft growth better than doxorubicin with less toxicity. *Mol Cancer Ther* **2005,** 4, (5), 751-60.

186) Chen, E. I.; Li, W. Z.; Godzik, A.; Howard, E. W.; Smith, J. W., A residue in the S-2 subsite controls substrate selectivity of matrix metalloproteinase-2 and matrix metalloproteinase-9. *Journal of Biological Chemistry* **2003,** 278, (19), 17158-17163.